Ferhat Abbas Sétif-1 University
Faculty of Technology
Processing Engineering Department

UNIVERSITÀ DEGLI STUDI DI GENOVA

In a co-tutoring program with:

GENOA University
School of Mathematical, Physical and Natural Sciences
PhD School in Science and Technology of Chemistry and Materials

Doctoral Thesis

Crystallization of Polylactic acid – Based immiscible blends and Nanocomposites

Presented by: **Seif Eddine FENNI**

Supervisor: Nacerddine HADDAOUI
Co-supervisor: Dario CAVALLO

Jury members

Prof. Djafer BENACHOUR	*President*	UFAS-1
Prof. Nacerddine HADDAOUI	*Supervisor*	UFAS-1
Dr. Dario CAVALLO	*Co-supervisor*	University of Genoa
Prof. Davide COMORETTO	*Examiner*	University of Genoa
Prof. Melia GUESSOUM	*Examiner*	UFAS-1
Prof. Fabrizio BARBERIS	*Examiner*	University of Genoa

Defended on: 08 April 2019

ACKNOWLEDGEMENTS

I thank all who, in one way or another, contributed in the completion of this thesis. First, I give thanks to God for protection and ability to do work.

I would like to express here thanks to my advisors, Professor Nacerddine Haddaoui and Doctor Dario Cavallo who provided me the opportunity to do such a research during the last three years;

To Prof. Haddaoui for the scientific supervision and for being very patient and receptive to all my thoughts, suggestions, and projects. For all his administrative support and for being like a father during my PhD period.

To Dr. Dario Cavallo for all his scientific and financial support, patience, and encouragement throughout all the period that I spent either in Italy or Spain. It is not often that one finds an advisor and colleague that always find the time for listening to the little problems and roadblocks that unavoidably crop up in the Ph.D course. His technical and editorial advices were essential to the completion of this work and have taught me innumerable lessons and insights on the workings of academic research in general.

I wish to thank professors Nacerddine Haddaoui, Dario Cavallo, Djafer Benachour, Lahcene Bencheikh, Rachida Doufnoune, Moncef Khitas, family and friends for the moral and administrative support that I received from them in 2015. I say it strongly, frankly and gratefully, thank you for giving me the opportunity to revive my Ph.D career.

I also owe my special thanks to:

- Prof Alejandro S. Müller for his perfect supervision and collaboration during my internship in the University of the Basque Country.

- Prof. Rachida Doufnoune for the nice collaboration.

- Prof. Orietta Monticelli for the nice collaboration and for offering to us the different materials.

- Lucia and Paola from CNR-Genoa, for the nice collaboration.

- My colleagues from the group of Genoa; Enrico, Filippo, Giulio, Jacopo, Luidji, Omar, Kun, Andrea, Francesca, Kasha and especially Bao.

- My second group in San Sebastian; Jon, Jorge, Idoia, Nerea, Irma, Eider, Leire, and especially Ricardo and Maryam.

- Professors; Davide Comoretto, Fabrizio Barberis, Djafer Benachour, and Melia Guessoum for being part of the commission of my thesis defense.

- Prof. Nadia Lotti from the University of Bologna and Prof. Kallay-Menyhard Alfred from the University of Budapest for reviewing my work and my thesis.

- Prof. Wahab from the Hospital of Sétif.

And finally, I would like to express my full thanks to my parent and my family and friends from Sétif, especially Djamel, Bassout, Oussama Kolli, Zohir Rahem, Abederrahemen Belhaoues, Lhadi Othmani, Hichem Rouagh, Ahmed Mezeheri, Belkacem Chemakh, and Mouaz Fellahi.

I would like also to acknowledge funding by:

1. The BIODEST project ((RISE) H2020-MSCA-RISE-2017-778092).
2. ALFA/ARSEL Liguria.

TABLE OF CONTENTS

Experimental Part

Chapter IV

Chapter V

Chapter VIII

LIST OF TABLES

LIST OF FIGURES

LIST OF ABBREVIATIONS

PLA	Poly (lactic acid)
PLLA	Poly (L-lactic acid)
PDLA	Poly (D-lactic acid)
PBS	poly (butylene succinate)
PCL	poly (caprolactone) or poly (ϵ-caprolactone)
PHB	Poly (hydroxybutyrate)
PEBA	Polyether block amide
PE	Polyethylene
PA	Polyamide
PA6	Polyamide-6
PS	Polystyrene
iPP	Isotactic Polypropylene
PVDF	Poly(vinylidene fluoride)
PMMA	Poly(methyl methacrylate)
LDPE	Low density polyethylene
PU	Polyurethane
PBSL	Poly(butylene succinate-co-l-lactate)
PHBV	Poly(hydroxybutyrate-cohydroxyvalerate)
PEG	Poly (ethylene glycol)
PPO	Poly(phenylene oxide)
PGA	Polyglycolide
ATBC	Acetyl(tributyl citrate)
LIM	D-limonene
Lapol	polyester plasticizer
EGMA	Poly(ethylene-glycidyl methacrylate)
E-AE-GMA	ethylene-co-acrylic ester-co-glycidyl methacrylate
EMAA–Zn	Zinc ionomers of the ethylene methyacrylic acid copolymer
EBA–GMA	Elastomeric ethylene-butyl acrylate–glycidyl methacrylate terpolymer
PGSMA	Poly(glycerol succinate-co-maleate)

HDI	Hexamethylene diisocyanate
CNC	Cellulose nanocrystals
DCP	Dicumyl peroxide
GO	Graphene oxide
GOs	Graphene oxide nanosheets
rPBSL	Random poly(butylene succinate-co-lactic acid)
PLLA-g-MA	Maleic-anhydride-grafted PLLA
PBS-g-MA	Maleic-anhydride-grafted PBS
NPCC	Nano-sized calcium carbonate
SB	Sodium benzoate
TiO_2	Titanium dioxide
PBS-g-CNC	PBS-g-cellulose nanocrystal
s-CNC	Surfactant modified cellulose nanocrystals
PEG-PPG	block copolymer of poly(ethylene glycol) and poly(propylene glycol
PLA-b-PC	Poly(L-lactide-block-carbonate)
P(LA-ran-CL)LMw	Poly(lactide-ran-caprolactone) Low molecular weight
P(LA-ran-CL)HMw	Poly(lactide-ran-caprolactone) High molecular weight
PLLA-PCL-PLLA	Triblock PLLA-PCL-PLLA copolymer
EC-bp	Ethyl cellosolve blocked polyisocyanate
POSS	Ad hoc functionalized polyhedral oligomeric silsesquioxane
POSS-oib	Octaisobutyl polyhedral oligomeric silsesquioxane
GNP	Graphite nanoplatelets
LDI	L-lysine-diisocyanate
LTI	L-lysine-triisocyanate
DMF	N,N-Dimethylformamide
THF	Tetrahydrofuran
DSC	Differential scanning calorimetry
TGA	Thermogravimetric analysis
SEM	Scanning electron microscopy
FE-SEM	Field-emission Scanning electron microscopy
PLOM	Polarized Light Microscopy
POM	Polarized Optical Microscopy

TEM	Transmission electron microscopy
XRD	X-ray diffraction
WAXD	Wide angle X-ray diffraction
WAXS	Wide Angle X-ray Scattering
FTIR	Fourier-transform infrared spectroscopy
MFR	Melt flow rate
NPs	Nanoparticles
MDs	Micro domains
NE	Nucleating efficiency
SN	Self-nucleation
T_s	Self-nucleation temperature
Vc	Relative volumetric transformed fraction
n	Avrami index or Avrami exponent
k	Overall crystallization rate
n_n	Factor represents the time dependence of the nucleation
n_d	Factor represents the dimensionality of the growing crystals
T_g	Glass transition temperature
wt%	Weight percentage
T_{cc}	Cold crystallization temperature
T_c	Crystallization temperature
T_m	Melting temperature
Xc	Crystallinity degree
ΔH_m	Melting enthalpy
$\Delta H_m°$	Equilibrium Melting enthalpy
ΔH_c	Crystallization enthalpy
ΔH_{cc}	Cold crystallization enthalpy
W_f	Weight fraction
G	Growth rate
Ta	Annealing temperature
τ (50%)	Crystallization half time
GPa	Giga Pascal
MPa	Mega Pascal

ISO	International organization of standardization
Dn	Number average
Dv	Volume average
DI	Domain I
DII	Domain II
DIII	Domain III
µm	Micro meter
T 5	Temperature of 5% of mass loss
T end	Temperature of 100% of mass loss

Introduction

Chapter I

Preface and objectives

New properties, specific characteristics for specific applications, lower prices and reuse of polymers, are needed to meet demands and requirements of today's society and, therefore, of the polymer industry. Numerous strategies have been applied to design tuned-property materials. Some of them include new synthetic routes and architectures, copolymerization, polymer blending, grafting, functionalization, and polymers mixing with nanoparticles and fillers. Among them, polymer blending is the most convenient strategy, and involves the presence and coexistence of at least two polymer phases.

In principle, this method can combine the best individual features of at least two polymers, provided that a proper interaction between the phases exists, or can be induced by additives or other strategies. The large part of these multiphasic materials and blends used in everyday life, are composed of semicrystalline polymers.

The crystalline features of pure polymers, such as morphology, crystal structure, thermal transitions and crystallization kinetics, are different from those exhibited when they are blended with other crystalline or amorphous components. Those crystalline features and structure will greatly affect the mechanical properties and the physical performance of the final material. The relation between structure and properties in semi-crystalline polymers is more complex with respect to that one of amorphous polymers, due to the contribution of both amorphous phase and crystals to the final mechanical behavior.

Therefore, the potential use of multi-crystalline polymeric systems requires a detailed understanding of the relationships between the polymer itself, its processing and the end-use properties of the product. Moreover, a deep comprehension of how the involved phases interact at the microscale, as in a polymer blend, and at the nanoscale, as in polymer nanocomposites, is mandatory.

Poly(L-lactic acid) (PLLA) is an excellent environmental friendly plastic, due to its high rigidity, biocompatibility and biodegradability which give it a large range of applications such as biomedical, agronomy, 3D printing, and food packaging applications. However, PLLA

suffer from slow nucleation/crystallization rate and high brittleness and cost, which limits the possibility of its application as a commodity polymer. Consequently, modification of the polymer to achieve suitable properties, has been a major topic during the last decade.

The work of this thesis is focused on two main topics; in a first part, the morphology, crystallization behavior, and properties of multiphasic polymeric materials, with two or more crystalline phases, were studied. Blends and blend nanocomposites of different semi-crystalline polymers, with different morphologies, were prepared, and the crystallization behavior of the various semi-crystalline polymers was studied, with a special emphasis on the nucleation and crystallization kinetics of PLA. In a second part, the chemical modification of PLA by reactive blending with the aim of improving the material toughness, was attempted. The resulting mechanical performance and crystallization behavior of the chemically modified PLA was investigated.

Summary

In this thesis, the morphology, crystallization behavior, thermal and mechanical properties of polymer blends and nanocomposites based on poly(L-lactide) (PLLA) were studied. With the aim of improving PLLA crystallization kinetics and mechanical properties (i.e., reducing PLLA brittleness), novel materials were prepared by the addition of other polymers immiscible with PLLA, or a solid phase (nanoparticles).

Bio-based blend nanocomposites of poly(L-lactic acid) (PLLA) and poly(butylene succinate) (PBS), with different concentrations (from 0.1 to 0.5 wt%) of graphene oxide (GO), were prepared via solution dispersion of PBS/GO followed by melt blending with PLLA in a 70/30 PLLA/PBS weight ratio. Scanning and Transmission Electron Microscopy revealed micron-sized droplets of PBS in the PLLA matrix with the nanofillers preferentially found in the PBS phase, at least partially located at the interface with PLLA. The GOs acts as nucleating agent for both semicrystalline polymers. A value of nucleating efficiency (NE) of around 80% is determined for GO towards PBS, among the highest NEs ever reported for this polymer. On the other hand, the efficiency in nucleating PLLA is equal to a modest 15%, also due to the unequal distribution of the nanofiller in the two polymers. A close relationship between the nanocomposite complex morphology and crystallization behavior of the two different polymers is thus established.

A second part of the work, focused on the morphology, nucleation, and crystallization behavior of binary and ternary blends, based on triple-crystalline polymers (PLLA, PBS and polycaprolactone (PCL)). Blends were prepared via melt-mixing, and morphological analysis revealed the occurrence of sea-island morphology in all the binary blends, while a "partial wetting" morphology was observed in all ternary blends. This morphology consists of droplets of the minor phase located and self-assembled at the interface between the other two major components. DSC analysis shows the occurrence of some common crystallization phenomena in immiscible polymer blends such us fractionated crystallization and coincident crystallization. DSC heating scans revealed the nucleating effect of crystalline PCL and PBS droplets on PLA from the glassy state during the heating process. PLOM analysis highlighted the existence of interface-induced nucleation phenomena: nucleating effect of (i) molten PCL and PBS on PLA phase and (ii) crystalline PLA on PBS phase were observed. In ternary blends, PCL was found to have a higher nucleating efficiency than PBS towards PLA.

Further investigation of binary and ternary blends based on PLA, PCL, and PBS was performed and the Self-nucleation analysis (SN) was investigated as a third part of the work. SN is found to be a good way to induce the crystallization of different polymer and to overcome fractionated crystallization and coincident crystallization. Results from SN allows us to deduce that production of self-nuclei is mainly determined by the melt temperature with only a slight influence of the blend morphology and content of the polymers under study.

In the last part of the work, dynamic vulcanization of fatty acid based polyester polyol with glycerol and PLLA in the presence of hexamethylene diisocyanate (HDI), was performed, with the aim of sustainably toughen PLLA. The dynamic vulcanization took place in a Brabender internal mixer, leading to the formation of a PLLA/PU biobased blend. Melt torque, FTIR, and gel fraction analysis demonstrated the successful formation of vulcanized PU inside the PLLA matrix. SEM analysis shows that the PLLA/PU blends exhibit sea-island morphology. Solubility tests revealed the formation of a rubbery phase, insoluble in chloroform, inside the PLLA matrix. FTIR analysis of the insoluble part shows the appearance of absorption band centred at 1758 cm^{-1} related to the crystalline carbonyl vibration of PLLA units, thus suggesting the partial involvement of the PLLA chains in the reaction. The content of PU in the blends played an important influence on the mechanical properties, thermal stability, and crystallization behaviours of the formed PLLA/PU blends. The overall crystallization rate of PLA was noticeably decreased by incorporation of PU while PLOM analysis revealed that presence of PU network inside PLLA resulted in faster PLLA nucleation. The mechanical properties were enhanced after formation of PU network, leading to higher impact strength and lower Young's modulus. However, the thermal stability of the blends was slightly reduced compared to neat PLLA.

Outline of the thesis

The introduction part of the present thesis is composed into three chapters, in which *chapter 1* displays the big lines of the thesis and the aim behind the present work, giving a brief summary of the works investigated in the experimental part.

In *Chapter 2*, some general concepts on crystallization of polymers, including nucleation and growth steps are described. A brief introduction on PLA, PCL, PBS and GO is also given, for the aim of facilitating the comprehension of the present thesis.

Chapter 3 describes the crystallization behavior of immiscible biodegradable polyester blends, with a special emphasis on the kinetics aspects. In particular, several aspects, as the influence of blending on nucleation, the phenomenon of fractionated crystallization, and the effects of composition on the morphology, will be highlighted,

The different parts of the experimental work of this thesis are separately treated in three chapters;

in *Chapter 4*, the blending of PLLA and PBS for enhancing the mechanical performance and crystallization kinetics will be discussed. The literature on PLA/PBS blends and their compatibilization, as well as recent applications and use of GO in the field of polymer blend reinforcing and compatibilization, are first reviewed. The main part of the chapter describes the effect of addition of graphene oxide (GO) nanofillers as a compatibilizer for the system. The morphology – crystallization behavior relationship will be discussed in details highlighting the role of GO nanosheets in nucleating the system.

Chapter 5 will present the study of morphology, nucleation and crystallization kinetics of immiscible binary and ternary blends based on PLA, PCL and PBS. A brief introduction on morphology of immiscible binary and ternary blends with a special focus on ternary blends, partial and complete wetting morphologies will be given. The morphology of binary and ternary blends will be investigated. The crystallization behavior of different phases in the various blends will be studied by means of DSC (non-isothermal and isothermal conditions) and PLOM with emphasis on PLA nucleation in contact with PCL and PBS.

Chapter 6 deals with the self-nucleation behavior of the PLA, PCL, and PBS phases in their binary and ternary blends. At first, a brief definition and theory about SN and its

applications in polymer characterization will highlighted, then the effect of melt blending, morphology and composition on the self-nucleation behavior will be investigated in details.

Chapter 7 discusses the chemical modification of PLLA by reactive blending. An overview on the previous works on chemical modification of PLA is then followed by the investigation of dynamic vulcanization of polyester polyol, glycerol, and PLLA in the presence of hexamethylene diisocyanate (HDI). In particular, the influence of such modification on the morphology, thermal and crystallization behavior, and mechanical performance will be discussed.

The most important achievements of the whole investigation, together with some perspectives for future work, are summarized in *Chapter 8*.

General aspects on polymer crystallization and investigated materials

Chapter II

General aspects on polymer crystallization and investigated materials

Since the main focus of this thesis is on the morphology and crystallization behavior of polyesters in their blends, therefore some basic concepts on polymer crystallization will be briefly introduced. Also, a short overview on the main materials on which we will focus, i.e., poly(lactide) (PLA), poly(caprolactone) (PCL), poly(butylene succinate) (PBS), and graphene oxide (GO) will be given.

2.1. Crystallization of polymers

Crystallization of polymers is a first-order phase transformation of a supercooled liquid [1,2]. Unlike low molecular weight molecules, which crystallize immediately when cooled below the equilibrium melting point, polymers only start to crystallize at a considerable supercooling. First slowly, then more rapidly, and finally slowly again as the crystallization temperature is further decreased [2]. This behavior is the result of two competing effects. Polymer crystallization takes place at temperatures between the melting temperature (T_m) and the glass transition temperature (T_g). As the temperature decreases, the crystallization rate increases due to the thermodynamic forces that drive the phase transformation. But a further increase of the supercooling leads to a decrease of the molecular segments' mobility, which in turns reduces the crystallization rate due to kinetics hindration. This effect becomes more significant as the temperature approaches the glass transition. Hence, the crystallization rate of polymers follows a bell shape trend as a function of temperature, with a maximum in the crystallization rate [3].

Polymer crystallization always involves primary crystallization, secondary crystallization and in some cases crystal reorganization or perfection. During primary crystallization two steps can be distinguished: primary nucleation and secondary nucleation or crystal growth [2,3].

2.1.1. Nucleation

Crystal formation in a polymer melt starts with the nucleation step. It involves the formation of a nucleus of supercritical size. This step is controlled by the free enthalpy change due to the phase transformation. At the nucleus critical size, the enthalpy barrier required to allow the nucleus growth is surpassed [3]. There is a critical size separating those clusters of crystallizable segments whose free energy of formation increases during growth from those whose energy decreases. If the size of an "embryo" surpasses this critical value, it turns into the nucleus of a growing crystal. Otherwise, it re-dissolves again in the melt. The nucleation step is thus associated with a free energy barrier to be overcome [4,5]. The formation of the nuclei may occur in the bulk phase (homogeneous nucleation) or on preexisting surfaces or heterogeneities (heterogeneous nucleation).

In the case of homogeneous nucleation, clusters with an enhanced inner order (or embryos) are formed in the melt due to thermal fluctuations. For very small clusters, the decrease in free energy due to the phase transition is exceeded by the increase in interfacial free energy.

The free energy barrier for primary homogeneous nucleation is higher than that required for heterogeneous nucleation. That is because homogeneous nucleation involves the formation of six new surfaces, while heterogeneous nucleations involve fewer surfaces. For that reason, a true primary homogeneous nucleation hardly ever occurs since it would typically require a supercooling of 50-100°C unless the polymer is pure. Instead, in practice, nucleation mostly occurs on the surface of foreign heterogeneities [6].

The mechanism of nucleation may change also as a function of temperature. As the supercooling increases, the thermodynamic driving force for the phase transformation also increases, and as a result the critical size of the nucleus and the free-enthalpy barrier decrease. [2] Thus, an increase in the nucleation rate is observed. But with a further increase in the supercooling a maximum in the nucleation rate, is also observed.

2.1.2. Crystal growth

After nucleation, crystal growth occurs by secondary and tertiary nucleation. The initial step is the formation of a secondary nucleus, which is followed by a series of tertiary nucleation events [6,7]. Many lamellar crystallites develop simultaneously and the growing crystal can show a quasi-spherical symmetry from the very beginning [4]. The formation of spherulites is

the typical semicrystalline morphology observed in many polymers. The size of the spherulites in general is in the range of micrometers.

The spherulitic growth rate (*G*) trend with temperature is similar to that of the primary nucleation. It involves two factors: the transport (diffusion) term and the secondary nucleation term. Because these terms have an opposite temperature dependence, the growth rate exhibits a maximum and follows a bell shape curve as a function of the crystallization temperature (or the supercooling). At high supercooling (left side of the bell shape curve), the molecular transport is the dominant term. The diffusion of the macromolecules to the growing front becomes very difficult as the temperature reaches the glass transition and the growth rate decreases to zero. At high crystallization temperatures (right side of the bell shape curve), the growth rate is controlled by the energy barrier due to secondary nucleation (see Figure 2.1) [8]. The growing lamella keeps a constant thickness. Crystal growth takes place in the lateral direction only, i.e., it is two-dimensional. There is practically no growth in chain direction perpendicular to the layer surface [4].

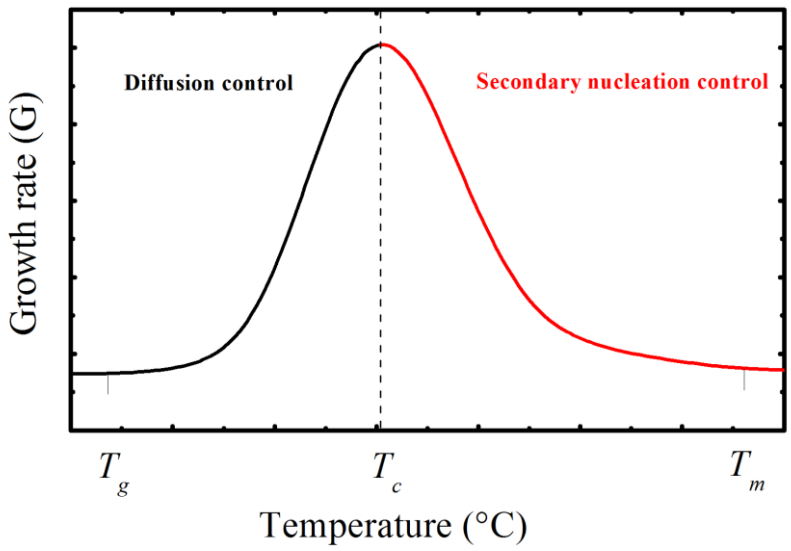

Figure 2.1. Crystal growth rate (*G*) as a function of the isothermal crystallization temperature.

2.1.3. Further stages of crystallization

After the crystal growth is completed and the sperulites are impinged, a secondary crystallization process may take place inside the intraspherulitic regions. Additionally, crystal reorganization and perfection of crystals can be induced under particular conditions such as, among others, long crystallization times and annealing at specific temperatures prior to melting. Thermodynamically more stable crystals can be obtained by internal rearrangements,

crystalline phase transitions, lamellar thickening, or removal of lattice defects. Crystal reorganization prior to melting occurs at a local scale. It typically involves melting of unstable crystals; recrystallization into more stables ones, and subsequent remelting [2].

2.1.4. Polymer crystallization theory

The attainment of high levels of crystallinity in polymers is not possible, not even for homopolymers with regular structure. High levels of crystallinity can only be achieved at crystallization temperatures close to the melting temperature but that requires excessively long times [8]. Since the crystalline phase only develops, at reasonable rates, at temperatures well below the equilibrium melting temperature, the final state is a non-equilibrium one that is a result of the competition between the thermodynamic and kinetic factors involved in the transformation [9].

Besides the supercooling, the primary nucleation might be affected by the density of heterogeneities or the presence of nucleating agents [8].

Polymer crystallization theories can take into consideration the overall crystallization kinetics, which includes both primary nucleation and crystal growth contributions [5], or the secondary nucleation (crystal growth) exclusively.

2.1.5. The Avrami equation

The Avrami equation was developed by Evans, Kolmogoroff, Johnson and Mehl, and Avrami during the 1930s and 1940s. The fundamentals of the model assumed that crystallization starts randomly at different locations and propagates outwards from the nucleation sites [6]. Certain limitations and special considerations regarding the Avrami analysis for polymers are [6]:

1. The solidified polymer is always semicrystalline only.

2. The volume of the system changes during crystallization.

3. The nucleation is seldom either simply athermal or simple thermal. A mixture of the two is common (see later).

4. Crystallization often follows two stages: (a) primary crystallization, characterized by radial growth of spherulites or axialites; (b) secondary crystallization, i.e., the slow increase in

crystallinity behind the crystal front caused by crystal thickening, formation of subsidiary crystal lamellae and crystal perfection. Secondary crystallization is slow and the initial rapid crystallization is usually dominated by primary crystallization.

The simplest form of the Avrami equation, considering a constant nucleation rate and constant linear growth, can be expressed as [5,8]:

$$1 - \nu_c = exp(-Kt^n) \qquad (1)$$

where *Vc* is the relative volumetric transformed fraction, *n* is the Avrami index and *k* the overall crystallization rate constant, which includes contributions from both nucleation and growth.

The Avrami index (*n*) is an integer whose value depends on the mechanism of nucleation and on the form of crystal growth. It is composed of two terms:

$$n = n_d + n_n \qquad (2)$$

where n_n represents the time dependence of the nucleation and n_d represents the dimensionality of the growing crystals. The nucleation can be purely instantaneous ($n_n = 0$) or purely sporadic ($n_n = 1$). The dimensionality term n_d can be 1, 2 or 3. In polymers, the possible dimensions of the growing crystal are 2 or 3. They represent axialites (two dimensional lamellar aggregates) and spherulites (superstructural three dimensional aggregates), respectively. Because the nucleation may not be completely sporadic or completely instantaneous, non-integer contributions to the Avrami index are obtained. For instance, when the growth of spherulites is not linear with time, the crystallization process may be governed by diffusion and n_n can have a value of 0.5, which indicates the Fickian dependence of growth with the square root of time [8,10,11].

The constant *k* can be used to provide a quantitative evaluation of the rate of crystallization evolution, since it includes the contribution of both nucleation and crystal growth events. It is directly related with the overall rate of crystallization $\tau_{1/2}^{-1}$ (the inverse of the half of the crystallization time, where$\tau_{1/2}$ corresponds to the time needed to achieve 50% of the overall crystallinity).

Through the Avrami equation, the isothermal crystallization data can be analyzed. There are several different kinds of experimental methods that are commonly used to measure the

overall crystallization rate. All of them follow a change in a property that is sensitive to crystallinity, for instance it could be the density or the specific volume. Other frequently used techniques include small-angle x-ray scattering, vibrational spectroscopy, nuclear magnetic resonance, polarized light microscopy and differential scanning calorimetry (DSC). Each method has a characteristic and different sensitivity to crystallinity. Particularly, the spherulitic growth rate is measured by either polarized light microscopy or small angle light scattering [9].

Among the aforementioned techniques, DSC is one of the most popularly used ones to follow the crystallization kinetics. That is due to the simplicity by which the data can be fitted with the Avrami Equation [8,10]. However, two factors are crucial in order to get a good fit: the relative volumetric conversion range chosen and the correction for the induction time [8,10].

2.2 Poly(Lactide), poly(ε-caprolactone) and poly(butylene succinate)

Recently, much attention has been given to polyesters obtained from sustainable resources, to biodegradable polymers and their blends, as their properties can be comparable with those of polymers derived from oil resources, but they are more environmentally benign. Among these bio-based and biodegradable polymers, Poly (lactic acid) (PLA), Poly (ε-caprolactone) (PCL), and poly (butylene succinate) (PBS) are the most studied and employed.

2.2.1 Poly (lactide) (PLA)

The increased scientific and industrial interest [12,13] on PLA relies on its remarkable biodegradability and good processability. It can be processed by extrusion, injection molding, thermoforming, blow molding, film blowing and melt spinning [14]. PLLA is bioresource and renewable and, compared to other bioplastics, it has relatively low price and commercial availability with the chemical formula [$(C_3H_4O_2)_n$]. Currently, it has been used in many different applications in the agricultural, medical, surgical and pharmaceutical fields, as well as in tissue engineering, film packaging, injection molding products, fabrics, fibers, bottles, cups and disposable food-contact materials and 3D applications [14].

PLA is a linear aliphatic polyester synthesized by ring-opening polymerization of lactide or by polymerization of lactic acid. The lactide monomer is a chiral molecule that exists in two optically active forms; L-lactide and D-lactide [15]. Therefore, the PLA properties are influenced by the stereochemistry. It can be either semicrystalline or amorphous depending on the thermal history and optical purity, i.e., the ratio of L to D enantiomer. To be crystalline, the

L-lactide content should be higher than 93%; otherwise the polymer is usually amorphous [14]. The crystallization degree of PLA, typically around 35 %, also depends on molecular weight and processing conditions [15].

Semicrystalline PLA is completely biodegradable and compostable under controlled conditions. It undergoes hydrolytic degradation by the random scission of the ester backbone. It has good thermal and barrier properties, high modulus (approximately 4.8 GPa) and good tensile strength [15]. Despite those features, PLA is brittle at room temperature, has a poor elongation at break and it is susceptible of suffering both hydrolysis and pyrolysis at high processing temperatures. For this reason, commercial PLA is typically stabilized against thermal degradation. It has also high rigidity and low impact resistance, with a difficult control of its crystallinity and hydrolysis rate. To overcome these drawbacks different approaches, that include copolymerization and blending with other biodegradable polymers, plasticizers and fillers, have been used [14].

Mechanical performance, degradation behavior, barrier and optical properties of PLLA are strictly related with the polymer crystallinity. Therefore, the understanding of its crystallization behavior is of relevance [16]. PLA displays different crystalline structures depending on the crystallization conditions. The α-form is the most common crystal type for PLA. Moreover, a less dense packing α'-form has been detected. The other structures include β and γ-form crystals. The superstructural morphology of PLLA typically consists on non-banded spherulites. However, others morphologies such as banded spherulites and axialites can be obtained by changing the thermal history, the crystallization conditions (supercooling) or the molecular weight. The glass transition temperature of PLLA is close to 60 ºC and its melting temperatures near 175 ºC [15]. The melting transition temperature of PLLA depends on the molecular weight as well as the optical purity. At lower molecular weight and increased D-lactide content, the melting temperature is decreased. In addition, the cold crystallization and glass transition is also affected by the content of D- enantiomer [16].

In general, the overall crystallization kinetics of PLLA is slow. The crystallization kinetics of PLA is strongly dependent on the optical purity. The degree of crystallinity, nucleation rate, and spherulite growth rate reduce substantially as the optical purity decreases [17]. PLA has the highest rate of crystallization (expressed as the inverse of half-crystallization time), between 100° and 130°C, but it displays a discontinuity at around 118 ºC. Also, the crystallization rate decreases as the molecular weight increases. To overcome the retarded crystallization, the addition of nucleating agents and small amounts of stereocomplex crystals

(crystals form by the co-crystallization of the two enantiomeric polylactides) has been effective. Commonly, it is reported that PLA crystallization takes place from an instantaneous nucleation into a spherulitic 3D dimension. However, Avrami exponent values ranging from 2 to 3.5 have been reported after fitting the isothermal crystallization data to the Avrami equation [16]. The size of the spherulites changes dramatically whether PLLA is isothermally crystallized from the melt or from a quenched glassy state [17].

2.2.2 Poly(ε-caprolactone)

PCL is one of the earliest biopolymers, as it was synthesized in 1930 [18]. It is a hydrophobic, biodegradable and biocompatible polyester that can be synthesized by ring-opening polymerization of the ε-caprolactone monomer via anionic, cationic or co-ordination catalysts. The repetitive molecular unit of PCL consists of five nonpolar methylene groups and a single relatively polar ester group [19,20].

PCL has a good solubility in a wide range of organic solvents (such as N,N-Dimethylformamide, tetrahydrofuran, dichloromethane, acetone, chloroform), high crystallinity (up to 70% depending on the molecular weight) [20], low melting point, tailored degradation kinetics and mechanical properties, easy processability, and good blend-compatibility. PCL has the following chemical composition [$(C_6H_{10}O_2)_n$]. As semicrystalline polymer, PCL exhibits a glass transition around –60 ºC and a melting temperature ranging between 59 and 64 ºC [15,19,21]. Because of these, PCL can be easily processed at relatively low temperatures into wide range of forms such as nanospheres, nanofibers and foams [19]. Due to its very low glass transition temperature, PCL is a very flexible and elastic polymer, with high elongation at break (> 700 %) but low tensile strength (around 23 MPa) [15].

Extensive research has been focused towards the biodegradation features [22] and potential biomedical applications of PCL. In that field, PCL has a proven use in controlled drug-delivery, medical devices (sutures, wound dressing, fixation devices) and tissue engineering (scaffolds fabrication for bone, cardiovascular, tendon, blood vessel, skin, nerve and cartilage engineering) [19].

PCL can undergo hydrolysis through the labile aliphatic ester bond. Despite that, the hydrolytic degradation rate is slower than that of other biopolymers such as PLA. For comparison, the degradation times of analogous parts can reach up to 3 or 4 years for PCL, while only few weeks or months for PLA and PGA. For that reason, it has been copolymerized

with monomers of highly degradable polylactide and polyglycolide [15,19,21]. Functionalization reactions have also been conducted on PCL to increase cell adhesion and improve hydrophilicity and biocompatibility. Blends of PCL with other polymers have been made to improve stress crack resistance, mechanical performance, dyeability and adhesion. Compatibility in PCL polymer blends depends on composition. PCL biodegradation proceeds under outdoor conditions by living organisms but to a lesser extent inside the body environment (in vivo) [19].

Early studies on the crystallization behavior of PCL have adopted dilatometry and optical microscopy. The crystalline growth of PCL was spherulitic and the crystallization exhibited a time dependent nucleation [23]. Clear Maltese cross has been observed for PCL at low supercooling. But as the crystallization temperature decreases, spherulites with banding are formed for low molecular weight PCL.

The crystallization behavior of PCL also depends on the molecular weight and the structural topology of chains. For instance, Pérez et al. [24,25] demonstrated that linear PCL nucleates and grows slower than analogous cyclic ones. Besides, as the molecular weight increases, the overall crystallization kinetics reached a maximum. Applying the Avrami fitting to the crystallization kinetics data predicted a 3D dimensional growth with instantaneous nucleation, since the Avrami index of PCLs were around 3.

2.2.3 Poly (butylene succinate)

Poly (butylene succinate) (PBS) is a biodegradable aliphatic polyester with the chemical formula $[(C_8H_{12}O_4)_n]$, commercially available since 1993. It is a polymer of wide industrial interest, used for production of mulching films, compostable bags, nonwoven sheets and textiles, as well as catering products and foams. PBS is a "green" polymer, generally synthesized through polycondensation of 1,4-butanediol and succinic acid, with both monomers produced from short-term renewable sources. Succinic acid can be attained from carbohydrates through fermentation with consumption of carbon dioxide, advantageously contributing to carbon sequestration, and 1,4-butanediol can be produced through hydrogenation and reduction of succinic acid. PBS can also be synthesized via a "greener" route like enzymatic catalysis, using a lipase catalyst, Candida Antarctica, physically adsorbed within a macroporous resin [26,27].

Biodegradability and compostability also contribute to the attractiveness of PBS. Biodegradation of PBS chains is initiated by hydrolysis of ester bonds, leading to the formation of water-soluble fragments. These short PBS chain segments can be assimilated by microorganisms and finally changed into eco-friendly products, that is, carbon dioxide, water and biomass. Given the many interesting properties of PBS, as for example a melting point similar to low density polyethylene, tensile strength close to polypropylene, stiffness between low density and high density polyethylene, and the variety of possible applications, including the production of biomedical/bioresorbable materials, biodegradable agricultural film, packaging, etc., it can be predicted that PBS resins will constitute a large market in few years [26,27].

PBS is a crystallizable polymer with a crystallization ability (X_c) in the range 35–45%. As such, its properties strongly depend on the crystal fraction and morphology. Crystallization from the relaxed melt leads to growth of α-crystals, which transform to β-crystals upon application of stress. Both crystal modifications have a monoclinic unit cell that includes two repeating units. The crystallization kinetics and crystal morphology of the α-form were widely studied. Crystal growth usually occurs via heterogeneous nucleation, but can also be initiated by homogeneous nucleation at temperatures below 7°C. Experimental data on both the nucleation and crystallization kinetics of PBS are available in a wide temperature range, from the glass transition temperature T_g around −35°C to temperatures close to the melting point. The melting behavior of PBS has also received attention, due to the presence of multiple endotherms, which arise from melting of crystals of low stability and subsequent recrystallization of the unstable melt occurring during heating. The equilibrium melting temperature, $T_m°$, was estimated to be 127.5°C if determined with the Hoffman-Weeks approach, and 146.5°C if calculated with Gibbs-Thomson equation [26-28].

Molecular weight and the morphology found to have a strong effect on PBS crystallization behavior as well. Applying the Avrami fitting to the crystallization kinetics data predicted a 3D dimensional growth with instantaneous nucleation, since the Avrami index of PBS oscillated around 3 [28-30].

2.3 Graphene oxide

Graphene is one single layer of graphite, in which the carbon atoms are sp2-bonded in a honeycomb lattice. Graphene and other materials that are based on graphene have attracted

research attention because of their unique properties, such as large surface area and great electrical, thermal and chemical properties. This reveals a huge potential in different applications [31-36].

Graphene can be obtained by using different techniques, one of the most common being Hummers' method. In this method the graphite is oxidized by using a solution of potassium permanganate in sulfuric acid. This process results to graphite oxide, which can be further exfoliated. Graphite oxide has a similar layered structure to graphite, but there are oxygen-containing groups, like hydroxyl and epoxy, at the plane of carbon atoms. These oxygen groups expand the interlayer distance and make the atomic-thick layers hydrophilic. There are also other oxygenated functional groups, like carbonyl and carboxyl, at the edges of the structure [31-36]. Hummers' method can be followed by ultrasonication, which causes the oxidized layers to be exfoliated in water. This modification of Hummers' method leads to graphene oxide (GO), a highly oxidized version of graphene [31].

GO-based polymer composites can be produced with several technics such as solution blending, in situ polymerization, and melt blending. In this last, the polymers are usually processed in pellet form. In this method, the polymers are melted with the help of high processing temperature, which leads to a viscous liquid. High shear forces of the process are utilized to disperse the nanofillers in the polymer matrix.

Good thing about this method is that it is cost effective. This is also a good technique for industrial applications, since it is highly compatible with the processes adopted at the industrial scale. It also does not require solvents for the dispersion process thus making the process simple, compared to other methods [31-36].

Recently, graphene oxide has been investigated as nanocompatibilizer and nano-reinforcement in polymer blends. Several paper reported the effect of GO nanosheets in enhancing the mechanical performance of polymer composites and blends. GO also prove high efficiency in compatibilizing immiscible polymer such as the works of nylon-6/PVDF, PA/PPO, and PMMA/PS [37-39].

2.4 References

1. Wunderlich B (Ed) (1977) Macromolecular physics, vol 2: Crystal nucleation, growth, annealing. Elsevier, Academic Press, New York

2. Schick C, Androsch R (2016) New Insights into Polymer Crystallization by Fast Scanning Chip Calorimetry. In Schick C, Mathot V (eds) Fast Scanning Calorimetry. Springer International Publishing, p 463-535
3. Sbirrazzuoli N, Guigo N, Vyazovkin S (2016) Isoconversional Kinetics by Fast Scanning Calorimetry. In Schick C, Mathot V (eds) Fast Scanning Calorimetry. Springer International Publishing, p 237-257
4. Strobl G (Ed) (2007) The Physics of Polymers. Springer, Verlag Berlin Heidelberg
5. Van Krevelen DW, Te Nijenhuis T (2009) Properties of polymers, 4 ed. Elsevier B.V, Amsterdam
6. Gedde UW (1995) Polymer Physics. Chapman & Hall, London
7. Di Lorenzo ML (2003) Spherulite growth rates in binary polymer blends. Prog. Polym. Sci. 28:663-689
8. Müller AJ, Michell RM, and Lorenzo AT (2016) Isothermal Crystallization Kinetics of Polymers. In Guo Q (Ed) Polymer Morphology: Principles, Characterization, and Processing, Ed. John Wiley & Sons, Inc, Hoboken, NJ, USA, p 181-203
9. Mandelkern L (2004) Crystallization of Polymers: Volume 2, Kinetics and Mechanisms. Cambridge University Press, UK
10. Lorenzo AT, Arnal ML, Albuerne J, Müller AJ (2007) DSC isothermal polymer crystallization kinetics measurements and the use of the Avrami equation to fit the data: Guidelines to avoid common problems. Polym. Test. 26:222-231
11. Schultz JM (Ed) (2001) Polymer Crystallization: The Development of Crystalline Order in Thermoplastic Polymers. Oxford University Press, UK
12. Jimenez A, Peltzer M, Ruseckaite R (Eds) (2015) Poly(lactic acid) Science and Technology: Processing, Properties, Additives and Applications. The Royal Society of Chemistry, Cambridge, UK
13. Auras R, Lim LT, Selke SEM, Tsuji H (2010) Poly(lactic acid). Synthesis, Structures, Properties, Processing, and Applications. John Wiley & Sons, Hoboken, NJ, USA
14. Fiori S (2015) Industrial Uses of PLA. In Jimenez A, Peltzer M, Ruseckaite R (Eds) Poly(lactic acid) Science and Technology: Processing, Properties, Additives and Applications, vol.12. RSC Polymer Chemistry Series. The Royal Society of Chemistry, Cambridge, UK
15. Nair LS, Laurencin CT (2007) Biodegradable polymers as biomaterials. Prog. Polym. Sci. 32:762-798

16. Müller AJ, Avila M, Saenz G, Salazar J (2015) Crystallization of PLA-based Materials. In Jimenez A, Peltzer M, Ruseckaite R (Eds) Poly(lactic acid) Science and Technology: Processing, Properties, Additives and Applications, vol.12. RSC Polymer Chemistry Series. The Royal Society of Chemistry, Cambridge, UK
17. Henton DE, Gruber P, Lunt J, Randall J (2005) Polylactic Acid Technology. In Mohanty AK, Misra M, Drzal LT (Eds) Natural Fibers, Biopolymers, and Biocomposites. Taylor & Francis, Boca Raton, Florida, USA
18. Natta FJV, Hill JW, Carothers WH (1934) Studies of Polymerization and Ring Formation. XXIII.1 ε-Caprolactone and its Polymers. J. Am. Chem. Soc. 56:455-457
19. Woodruff MA, Hutmacher MW (2010) The return of a forgotten polymer—Polycaprolactone in the 21st century. Progress in Polymer Science. 35:1217-1256
20. Perrin DE, English JP (1997) Polycaprolactone. In Domb AJ,Kost J, Wiseman DM, (Eds) Handbook of Biodegradable Polymers. CRC Press, USA
21. Sisson AL, Ekinci D, Lendlein A (2013) The contemporary role of ε-caprolactone chemistry to create advanced polymer architectures. Polymer.54:4333-4350
22. Chandra R, Rustgi R (1998) Biodegradable polymers. Prog. Polym. Sci. 23:1273-1335
23. Chynoweth KR, Stachurski ZH (1986) Crystallization of poly(ε-caprolactone). Polymer. 27:1912-1916
24. Pérez RA, Córdova ME, López JV, Hoskins JN, Zhang B, Grayson SM, Müller AJ (2014) Nucleation, crystallization, self-nucleation and thermal fractionation of cyclic and linear poly(ε-caprolactone)s. React. Funct. Polym. 80:71-82
25. Jordana KPG (2017) Multi-Crystalline Polymer Systems: Biodegradable Triblock Terpolymers and Nanostructured Blends. Morphology, Crystallization and Properties. Ph.D. thesis. University of the Basque Country, San Sebastian, Spain
26. Gumede TP, Luyt AS, Müller AJ (2018) Review on PCL, PBS, and PCL/PBS blends containing carbon nanotubes. eXPRESS Polym. Lett. 12:505-529
27. Huang Z, Qian L, Yin Q,Yu N, Liu T, Tian D (2018) Biodegradability studies of poly(butylene succinate) composites filled with sugarcane rind fiber. Polym. Test. 66:319-326
28. Yarici T, Kodal M, Ozkoc G (2018) Non-isothermal crystallization kinetics of Poly(Butylene succinate) (PBS) nanocomposites with different modified carbon nanotubes. Polymer. 146:361-377

29. Di Lorenzo ML, Androsch R, Righetti MC (2017) Low-temperature crystallization of poly(butylene succinate). Eur. Polym. J. 94 :384-391

30. Papageorgiou DG, Zhuravlev E, Papageorgiou GZ, Bikiaris D, Chrissafis K, Schick C (2014) Kinetics of nucleation and crystallization in poly(butylene succinate) nanocomposites. Polymer. 55:6725-6734

31. Marcano DC et al. (2010) Improved Synthesis of Graphene Oxide. ACS Nano. 4:4806-4814

32. Chen D, Feng H, Li J (2012) Graphene Oxide: Preparation, Functionalization, and Electrochemical Applications. Chem. Rev. 112:6027-6053

33. Ahmad H, Fan M, Hui D (2018) Graphene oxide incorporated functional materials: A review. Composites Part B. 145:270-280

34. Zhu Y, Murali S, Cai W, Li X, Suk JW, Potts JR, Ruoff RS (2010) Graphene and Graphene Oxide: Synthesis, Properties, and Applications. Adv. Mater. 22:3906-3924

35. Chabot V, Higgins D, Yu A, Xiao X, Chen Z, Zhang J (2014) A review of graphene and graphene oxide sponge: material synthesis and applications to energy and the environment. Energy Environ. Sci. 7:1564-1596

36. Wang Y, Li Z, Wang J, Li J, Lin Y (2011) Graphene and graphene oxide: biofunctionalization and applications in biotechnology. Trends Biotechnol. 29:205-212

37. Yang J, Feng C, Dai J, Zhang N, Huang T, Wang Y (2013) Compatibilization of immiscible nylon 6/poly(vinylidene fluoride) blends using graphene oxides. Polym. Int. 62:1085–1093

38. Cao Y, Zhang J, Feng J, Wu P (2011) Compatibilization of immiscible polymer blends using graphene oxide sheets. J. Am. Chem. Soc. Nano. 5 :5920–5927

39. Ye S, Cao Y, Feng J, Wu P (2013) Temperature-dependent compatibilizing effect of graphene oxide as a compatibilizer for immiscible polymer blends. RSC Adv. 3:7987–7995

Immiscible blends of semicrystalline polymers

Partially reproduced from: S.E. Fenni et al. "Nucleation and crystallization in bio-based immiscible polyester blends". Book chapter in: Di Lorenzo ML, Androsch R (Eds) Advances in Polymer Sciences: Thermal Properties of Bio-based Polymers. Chapter 48 https://doi.org/10.1007/12_2019_48

Chapter III

Immiscible blends of semicrystalline polymers

Polymer blending has been extensively used to prepare new polymeric materials with an attractive combination of properties that combine those of the pure components. However, given that most polymers are immiscible, because of their unfavorable enthalpy of mixing, they form phase-separated systems. Depending on interfacial tension, composition, rheological properties and processing conditions, immiscible polymer blends exhibit different morphologies, such as sea-island or co-continuous. Immiscible blends are characterized by poor mechanical properties coming from weak interfacial adhesion between the phases and/or stress concentrations at interface boundaries. [1-4] Several strategies have been employed to overcome this and improve blend compatibility, such as chemical modifications, addition of block copolymers, plasticizers, nanofillers and reactive blending [5-7].

If one or both components are semi-crystalline, the superstructure and the crystallization behavior of each material may be affected by blending. The detailed knowledge of how blending impacts crystallization is important since most polymer properties, such as optical, thermal, mechanical and barrier properties, will also be affected.

3.1 Morphological features

The final morphology of immiscible blends is affected both by intrinsic features of the materials, such as interfacial tension between the two polymers and melt viscosity ratio, and by preparation method, i.e., shear rate and blend composition. The two most typical morphologies are: i) droplets of the minor component, with sizes between 0.1 and 10 μm, dispersed in a continuous matrix of the other polymer (i.e., a sea-island morphology), and ii) co-continuous morphology, usually obtained for symmetric compositions, characterized by two continuous phases with similar characteristic sizes that are strongly interpenetrated [1-4]. Co-continuous morphologies in immiscible polymer blends have many advantages in comparison with sea-island morphologies, in particular regarding synergy in the mechanical properties and selective permeability, which provide opportunities for a wide range of technological applications.

Clear relationships have been found between blend morphology and the crystallization of immiscible polymers [8-13]. We have selected an example from the literature, even if the

reported blends are not biobased or biodegradable, because it can clearly illustrate the large changes produced by different morphologies on the nucleation and crystallization of the phases.

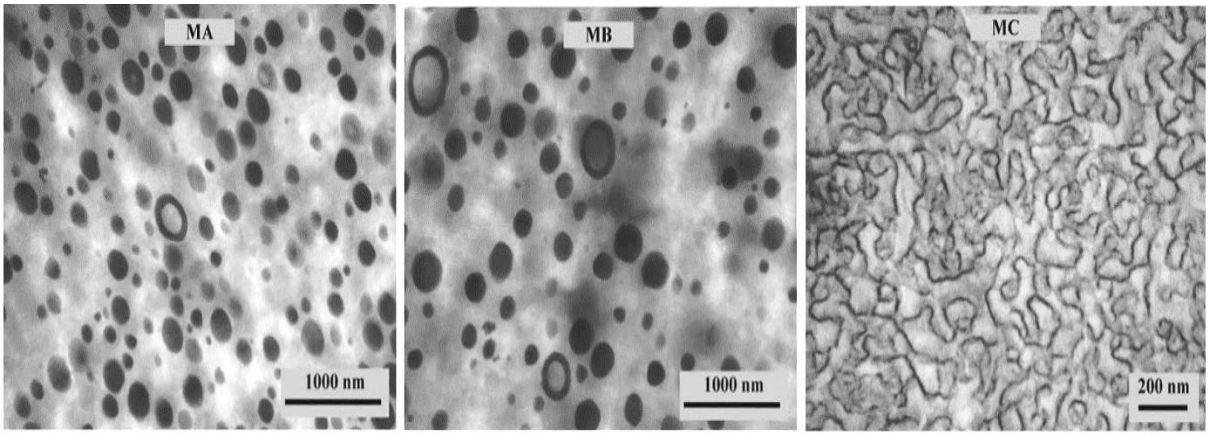

Figure 3.1. TEM micrographs of three PE/PA blends prepared by reactive extrusion, showing sea-island (MA and MB) and co-continuous morphologies (MC). Adapted from [9].

Figure 3.1 shows Transmission electron microscopy (TEM) images of polyethylene/polyamide (PE/PA) blends prepared by reactive extrusion. Depending on the composition and compatibilizer content, it was possible to produce two types of morphologies: (i) droplets of polyamide in a polyethylene matrix (samples MA and MB in Figure 3.1), (ii) co-continuous morphology of the two polymers (sample MC, Figure 3.1) [9]. The kinetics of crystallization of PA in PE/PA immiscible blends changed from classical sigmoidal-type (typical of heterogeneously nucleated polymers with Avrami indexes of 3-4), in the blend with the co-continuous morphology, to first-order kinetics in the blends MA with sea-island morphology with sub-micron PA droplets (typical of a crystallization process initiated by surface nucleation or homogeneous nucleation [8,9,12]). In the MC blend, the nucleation was found to be heterogeneous at lower supercooling, while in MA and MB blends, the nucleation became homogeneous or induced by the polymer-polymer interface, and crystallization occurred at extremely large supercooling. On the other hand, crystallization of the PE phase was enhanced in all blends, due to the nucleation effect of the PA, previously crystallized at higher temperature [9]. The relationship between immiscible blend morphology and crystallization behavior of bio-based polyester blends will be analyzed in detail below.

3.2 Crystallization behavior in immiscible blends

The polymers in an immiscible blend can be either amorphous or semicrystalline. Thus, amorphous/amorphous, crystalline/amorphous or crystalline/crystalline final blends can be prepared.

In principle, phase separation of the components is expected, therefore, in the case of two semicrystalline components, the crystallization of each polymer takes place independently from one another. As such, the crystalline features (melting temperature (T_m), lamellar thickness, and growth rate (G)) are expected to be similar to the ones of pure components . The same does not obviously hold for miscible blends, where dilution effects on crystallization can be appreciated. [10,11,13].

However, the crystallization kinetics of a given polymer in an immiscible blend can be substantially different from that of the pure component, since peculiar nucleation effects can arise. Nucleation could be enhanced and thus the overall crystallization kinetics is accelerated. Indeed, nucleation is commonly encountered at foreign surfaces, and it can thus be increased due to impurities/heterogeneities migration between the different phases during the blending process or to the presence of polymer/polymer interfaces. [1,2,10,13-17]. The opposite situation, i.e., a decrease of crystallization kinetics, is also commonly observed whenever the crystallizable polymers are separated in a "sufficiently high" number of individual domains. In these cases, the phenomenon is addressed as *fractionated crystallization*, as detailed in the following section.

3.2.1 Fractionated crystallization

The term "fractionated crystallization" was introduced by Frensch et al. [18]. This crystallization mechanism is observed in polymer blends, when a minor crystallizable component is dispersed in droplets with very small average diameter. The fractionated crystallization appears when the number of droplets or micro domains (MDs) is of the same order of magnitude, or larger, than the number of the active heterogeneities which act as primary nuclei for crystallization in the bulk polymer. For statistical reasons, different droplets ensembles will result, containing heterogeneities with varying nucleating ability, or even free of foreign particles. Therefore, upon cooling from the melt, the different fractions of droplets will crystallize at distinct supercoolings, from low to high depending on the nucleating efficiency of the contained heterogeneities. Ideally, "clean" droplets will solidify at the

maximum achievable supercooling (close to the glass transition temperature) by a homogeneous nucleation mechanism. Heterogeneity free droplets can also crystallize by interfacial nucleation at high supercoolings, but not as high as in the case of homogeneous nucleation, since the energy barrier for nucleation is lower when the interface between the two phases is able to nucleate the droplets. The different nucleation events are reflected in multiple exothermic peaks detected by a differential scanning calorimetry (DSC) cooling scan [10,12,13, 19-29].

The above outlined concept is described schematically in Figure 3.2. The most active nucleating impurities are represented with the letter A, while B indicated less active heterogeneities. After blending, the heterogeneities will be randomly distributed among the droplets. The micro domains containing type A heterogeneities crystallize at lower supercooling (exothermic peak 1 in the DSC of Figure 3.2), while droplets with type B impurities nucleate at lower temperatures (DSC peak 2). Impurities-free polymer droplets reach the largest supercooling for the given cooling conditions (exothermic peak 3).

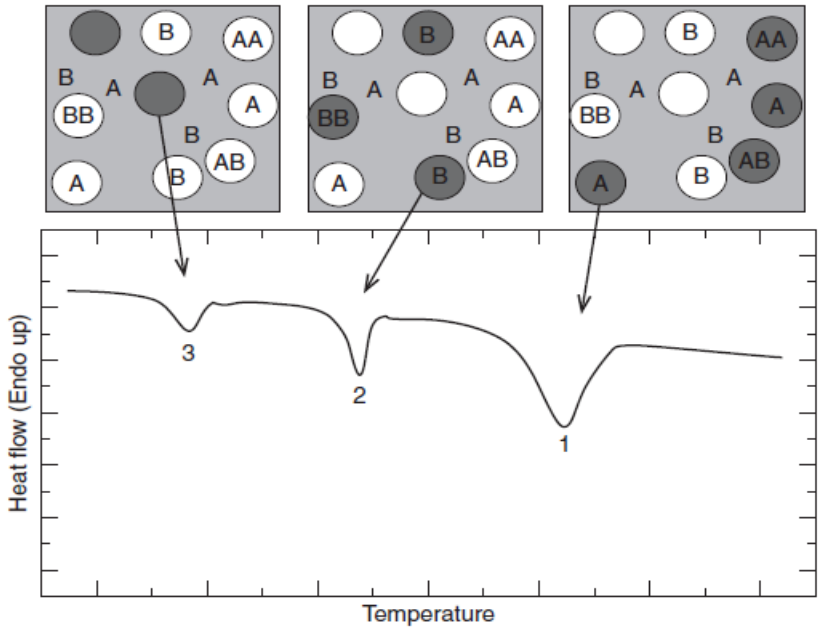

Figure 3.2. A schematic illustration of the fractionated crystallization of polymer droplets dispersed in an immiscible polymer matrix, as measured by DSC [19].

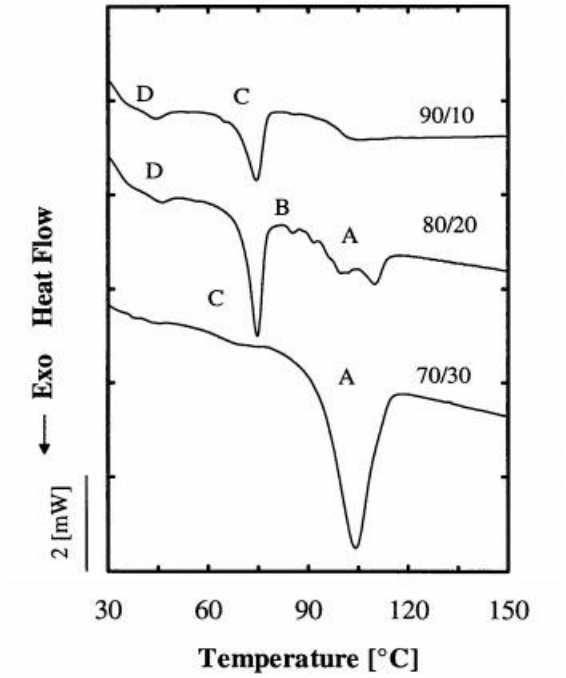

Figure 3.3. DSC cooling curves at 10°C/min for PS/iPP blends with the indicated compositions. [21].

Figure 3.3 shows a real example of fractionated crystallization in immiscible blends, and the effect of blend composition on its occurrence, for the system isotactic polypropylene/polystyrene. For a 70/30 wt% composition, isotactic Polypropylene (iPP) droplets have an average diameter of 7-9 µm and they mostly crystallize at low supercooling (peak A) while a small fraction of the droplets can be supercooled to a larger extent (peak C). By decreasing the amount of iPP to 20 %, the average droplet size decreases to around 1-2 µm, and a clear fractionated crystallization is observed: since four distinct crystallization exotherms (A-D) are revealed. These correspond to different types of heterogeneities (A-C) and to nucleation at the interface with polystyrene (PS) or via a homogenous route in pure iPP droplets (D). When iPP content is only 10 wt%, the average droplets size is less than 1 µm. The concentration of droplets thus increases well above the content of the heterogeneities which cause nucleation at low supercoolings (peaks A through C). In fact, the high temperatures nucleation events (A and B) disappear and the crystallization can only occur at lower temperatures, in exotherms C and D. If a compatibilizer is used in the blend, even smaller droplets are produced and exotherm C disappears, indicating that the only event associated with heterogeneity free droplets is the exothermic peak at maximum supercooling (D) which could be started by surface nucleation or homogeneous nucleation. As the glass transition temperature (T_g) temperature of iPP is close to 0 ºC and the crystallization peak (D) is at around 40 ºC, it may be possible that a homogeneous nucleation process could have triggered the nucleation of

these clean droplets. [8,10,12,21,23,24] In general, the fractionated crystallization leads to lower crystallinity and slightly lower melting temperatures, due to the decrease of lamellar thickness at those supercoolings [8,11,13,26,27]. For more details on fractionated crystallization, the reader is referred to the reviews of Müller et al. [12,21,25]

3.2.2 Nucleation at polymer/polymer interfaces

Several papers have reported the nucleation effect of one polymer on another in immiscible blends. The phenomenon is commonly indicated as interface-induced nucleation or interface-assisted crystallization, and can be typically visualized directly by Polarized Light Microscopy PLOM [30-37].

For example, Figure 3.4 shows some PLOM micrographs of the area near the phase boundary between poly(L-lactide) (PLLA) and poly(vinylidene fluoride) (PVDF). The two polymers were sequentially crystallized for a suitable time at 150°C and 140°C. At 150°C, only the PVDF phase is able to crystallize within the given time (Figure 3.4b), while after cooling to 140°C, PLLA can also crystallize. At 140°C, PLLA nucleates first at the interface with previously crystallized PVDF. A transcrystalline structure is produced due to the high (linear) nucleation density, which forces the spherulites to grow perpendicular to the interface (Figures 2.4c and 2.4d). We can note that, during the same crystallization time, only few PLLA spherulite nucleate within the bulk phase, away from the PVDF interface [33].

In a similar experiment on PVDF/PCL blends, the nucleation of the PCL phase after isothermal crystallization of PVDF was shown to occur at the interface with PVDF crystals, giving rise again to a transcrystalline PCL layer. The nucleation effect of PVDF on PCL could also be detected by non-isothermal differential scanning calorimetry, as a meaningful shift of PCL crystallization exotherm to higher temperature in a 70/30 wt% PVDF/PCL blend [34].

The nucleation of a given polymer on the surface of pre-existing crystals of a different polymer might not seem surprising, and can be possibly attributed to the existence of epitaxial relationship between the two crystalline structures. However, even if less documented, the nucleation of a semicrystalline polymer at the interface with an amorphous polymer in their immiscible blend is also possible. Figure 3.5 shows a polarized optical micrographs of isotactic polypropylene/poly(methyl methacrylate) (PP/PMMA) immiscible blend crystallized at 130ºC. iPP transcrystalline growth layer around the PMMA domains can be observed. It should be

noted that iPP crystallization takes place above the glass transition temperature of PMMA, thus the nucleation effectively occurs at the interface with a viscous liquid [35].

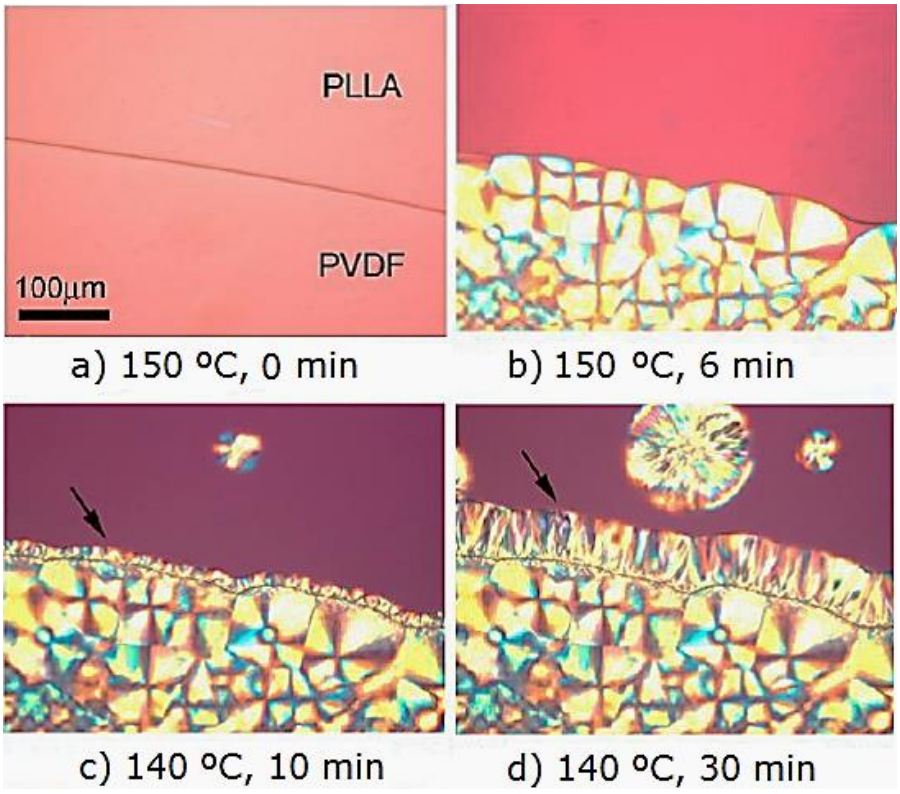

Figure 3.4. PLOM micrographs of PLLA and PVDF near their interface, during a sequential crystallization at 150 and 140°C. The upper and lower sides of the micrographs are PLLA and PVDF, respectively. Adapted from ref. [33].

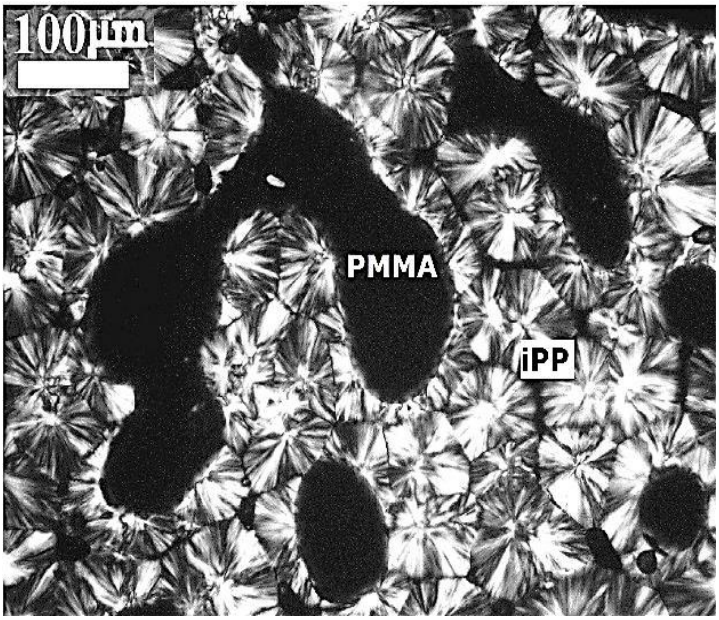

Figure 3.5. PLOM micrograph for an iPP/PMMA blend after the sample was crystallized at 130°C for 30 min. Adapted from reference [35].

3.2.3 Crystallization in presence of compatibilizers and nanoparticles

Usually, the addition of small amounts of "compatibilizer" (i.e., block-copolymers, graft copolymers, nanoparticles, etc.) results in large decrease in the size of the dispersed phase, in comparison with the non-compatibilized blend. The addition of a copolymer-based compatibilizer, in general, has remarkable influence on the crystallization behavior of the blend components as well, because of the large effect on the morphology of the system, which results either in a decrease in the size of the dispersed phase or in the formation of a percolated/co-continuous morphology [8,13,16,38,39]. Tol et al. [26], Yordanov and Minkova [28], studied the reactive compatibilization of the immiscible blends polystyrene/polyamide 6 (PS/PA6) and Low density polyethylene/polystyrene (LDPE/PS), using different kind of copolymer compatibilizers. They found a decrease in the droplet sizes and large increase in the droplets concentration. As a consequence, the nucleation mechanism of the crystalline polymer changed from heterogeneous to homogeneous/surface-induced. In the case of PA6, the increased supercooling favored the crystalline γ phase with respect to the α phase which develops in neat blends [26].

Another commonly used compatibilization method is "reactive blending", in which a molecule which can react with one or both phases is added during the extrusion process. During the reactive compatibilization, different kind of interactions among the polymers can develop, leading to hydrogen, ionic, or covalent bonding, depending on the specific functional groups involved. Typically, a co-continuous morphology can be obtained. In the case of reactive compatibilization, when some specific reagent is employed, the crystallization behavior of the final blend can be affected as a result of chain scission or reduction of chain mobility due to cross-linking. In general, reactive compatibilization reduces the degree of crystallinity and induces fractionated crystallization [1,2,5,11,13,21,27,28, 39-42].

Wang et al. [41] reported that the addition of dicumyl peroxide (DCP) at different concentrations to PLA/PBS 80/20 immiscible blend hinders the crystallization of both components, i.e., it decreases the crystallinity of both PBS and PLA and the cold crystallization rate of PLA by reducing its nucleation density. Reactive blending in this case is creating new covalent bonds randomly distributed in between the two polymers. Such new covalent bonds interrupt the linear crystallizable sequences creating molecular defects that need to be rejected to the amorphous phases, thereby reducing the crystallization ability of the components.

The addition of nanoparticles (NPs) or nanofillers to immiscible polymer blends can have an effect on the mechanical, thermal, optical and gas properties. NPs in immiscible blends could be located at the interface between the components, dispersed preferentially in one component, or dispersed in non-equivalent way in both components. Generally, and depending on their locations, NPs affect the crystallization behavior of the crystallizable components by enhancing the primary nucleation, thus acting as heterogeneous nucleants. [13, 43-45]. Examples can be found for instance for PLLA/PBS blends mixed with graphene oxide (GO) and cellulose nanocrystals (CNC) [44,45].

3.3 Crystallization in different immiscible bio-based polyester blends

3.3.1 Poly (lactic acid) / poly (butylene succinate) blends

This section presents a short review on previous research about PLA/PBS blends in which the effect of addition of PBS on different properties of the PLA matrix is studied with the aim of improving mechanical properties, gas barrier behavior etc. PLA is a biobased polyester that has high rigidity, biocompatibility and biodegradability. However, it presents slow crystallization and brittleness. PBS on the other hand, is a biodegradable polyester with good processability. The commonly observed thermal transitions of the two materials are summarized in the following. PLA partially crystallizes on cooling around 100°C and vitrifies at the glass transition temperature (T_g ≈60°C). Upon subsequent heating it might show cold crystallization above T_g (typically at ≈100°C) and melting with a peak temperature of ≈170°C. On the other hand PBS crystallizes on cooling at ≈75°C, has a low glass transition temperature (≈-35°C) and melts slightly above 116°C. We recall that for PLA the crystallization and melting temperatures are controlled by the relative contents of D- and L- isomer of lactide in the chain [46-48].

Several authors investigated the effect of cooling and heating rates, blend composition and addition of compatibilizers, nanoparticles and nucleating agents on the thermal and crystallization behavior of PLA/PBS blends [15,41,45,49-56]. Both non-isothermal with varying cooling rates and isothermal crystallization behavior were investigated, using differential scanning calorimetry (DSC) and polarized optical microscopy (PLOM). The main works performed on PLA/PBS based systems are schematically summarized in Table 3.1.

Table 3.1. Reported experimental works on PLA/PBS based blends, with emphasis on the aspects related to nucleation and crystallization.

Sample	Publication year	Composition wt%	Crystallization/nucleation conditions and technics	T_{cc} of PLA (°C)	T_c of PLA (°C)	T_c of PBS (°C)	Crystallization/nucleation outcomes	Reference
PLLA/PBS	2006	Neat PLLA	Isothermal and non-isothermal DSC at various cooling rates.	124.0	-	-	PBS accelerates the cold crystallization of PLA, but is less effective in melt crystallization. *Xc* increases with PBS content.	51
		99/1		113.3	-	-		
		95/5		96.7	-	-		
		90/10		94.8	-	-		
PLLA/ PBSL	2006	Neat PLLA	Non-isothermal DSC at various cooling rates; Isothermal DSC	124.0	-	-	Molten PBSL enhances the isothermal and non-isothermal PLLA crystallization during the cooling process and accelerates T_{cc} during the heating process. *Xc* was found to increase with the addition of PBSL.	51
		99/1		102	-	-		
		95/5		90.2	-	-		
		90/10		95.6	-	-		
PLA/PBS	2008	0-20 wt% of PBS.	DSC and PLOM : cooling from 180°C at 2°C/min.	-	-	-	Addition of PBS accelerates the crystallization rate of PLA during both cooling and heating scans and the PBS domains act as nuclei for PLA.	49
PLA/PBS/DCP	2009	Neat PLA	DSC non-isothermal crystallization PLOM isothermal crystallization X-Ray Diffraction	122.4	-	-	The addition of PBS accelerates the cold crystallization of PLA, while addition of DCP hinders both PLA and PBS crystallization. PBS acts as a nucleating agent for PLA but the effect is reduced after reaction with DCP.	41
		80/20		-	-	-		
		80/20/0.05		-	-	-		
		80/20/0.1		120.1	-	-		
		80/20/0.15		122.6	-	-		
		80/20/0.2		124.2	-	-		

PLLA/PBS	2012	Neat PLLA	DSC non-isothermal crystallization	132.5	-	-	Presence of PBS accelerates remarkably the cold crystallization of PLA, but no effect was recorded during the cooling process from the melt. PLA domains does not affect the crystallization behavior of PBS.	52
		Neat PBS		116.2	-	83.8		
		50/50		-	-	84.4		
		20/80		-	-	84.7		
PLA/PBS/PLLA-*g*-MA And PLA/PBS/PBS-*g*-MA	2014	0-100 wt% of PBS. With 0-4 wt% of PLLA-g-MA or PBS-g-MA	Non-isothermal DSC	-	-	-	PBS enhances the cold crystallization of PLA. The size and number of the dispersed PBS particles (droplets) has a significant influence on the crystallization rate of PLA (the smallest and highest number of dispersed PBS droplets resulted in higher nucleation effect). Addition of compatibilizer produced additional increases in the crystallinity of the blend.	53
PLA/PBS/TiO2 nanoparticles	2014	90/10	Non-isothermal DSC	95.7	-	-	DSC analysis showed that addition of TiO_2 promoted the crystallization of PLA. PBS has lower nucleating effect as compared with TiO_2.	54
		90/10/1		96.8	-	-		
		90/10/2		98.4	-	-		
		90/10/3		107.9	-	-		
		90/10/5		94.7	-	-		
PLA/PBS	2015	0-100 wt% of PBS	DSC and PLOM non-isothermal crystallization at a scan rate of 10°C/min.	-	-	-	After blending, crystallinity of both PLA and PBS increased. Addition of 20 wt% of PBS gave the largest increase in the crystallinity of PLA	15

PLA/PBS/ rPBSL	2016	80/20 wt% with 0-5 phr of rPBSL	DSC non-isothermal crystallization PLOM isothermal crystallization at 80°C.	-	-	-	Addition of rPBSL to 80/20 PLA/PBS blend affects nucleation and crystallization, since the compound acts as a nucleating agent and plasticizer.	50
PLA/PBS/DCP/PBS-*g*-CNC	2016	70/70 wt% with DCP/PBS-g-CNC = 0/0, 0/2, 0.2/0, 0.2/0.5, 0.2/1 and 0.2/2.	Non-isothermal DSC, WAXD	-	-	-	DCP and PBS-*g*-CNC have a strong contribution to the formation of PLA α form and low effect on PBS crystallization. In addition, PBS-*g*-CNC increases the crystallinity degree of the PLA/PBS system and affects the crystal size of both PLA and PBS. Addition of DCP restricts the crystallization.	55
PLLA/PBS/GO	2018	Neat PLLA	DSC in isothermal and non-isothermal conditions	97	101.6	-	In the neat blend, fractionated crystallization of PBS phase and slight increase in T_c of PLLA was observed Addition of GOs enhance the crystallization rate of both PLA and PBS.	45
		Neat PBS		-	-	77		
		70/30		91	105.2	73		
		70/30/0.1		-	103.7	92		
		70/30/0.3		-	105.5	92		
		70/30/0.5		-	105.5	92		

In the case of PLA/PBS blends, the crystallization and melting temperatures of the two polymers in the blends remains in the same range of that of the pure components, confirming the immiscibility between the two polyesters. The melting processes are sufficiently apart to be distinguished upon heating.

The crystallization rate of PLA is rather slow, so that often the structuring process is not completed during cooling, and an exothermic cold-crystallization peak is usually observed during the second heating scan. Several works have reported an acceleration of PLA cold crystallization rate by the addition of PBS [15,41,45,49,51-55]. Figure 3.6 presents a collection of the reported cold-crystallization temperatures of PLA in its blends with PBS, as a function of PBS content. The data has been normalized by using the difference between the cold-crystallization temperature of neat PLA and of the PLA component in the blend. The more negative the value of ΔT_{cc} is, the larger the nucleation effect upon heating from the glassy state.

Notwithstanding the differences in the absolute values of cold-crystallization temperatures, which might attributed to material (molar mass, D-lactide content) or measurement (heating rate) parameters, a clear shift of the cold-crystallization events towards lower temperature can be appreciated, especially upon the addition of a minor content of PBS (in the range 1-30 wt%). The largest nucleation effect can be approximately found for PBS content between 5 and 15 wt%. This is interpreted as the result of a decrease in the PBS droplets diameter, which lead to an increase in the PLA/PBS interfacial area.

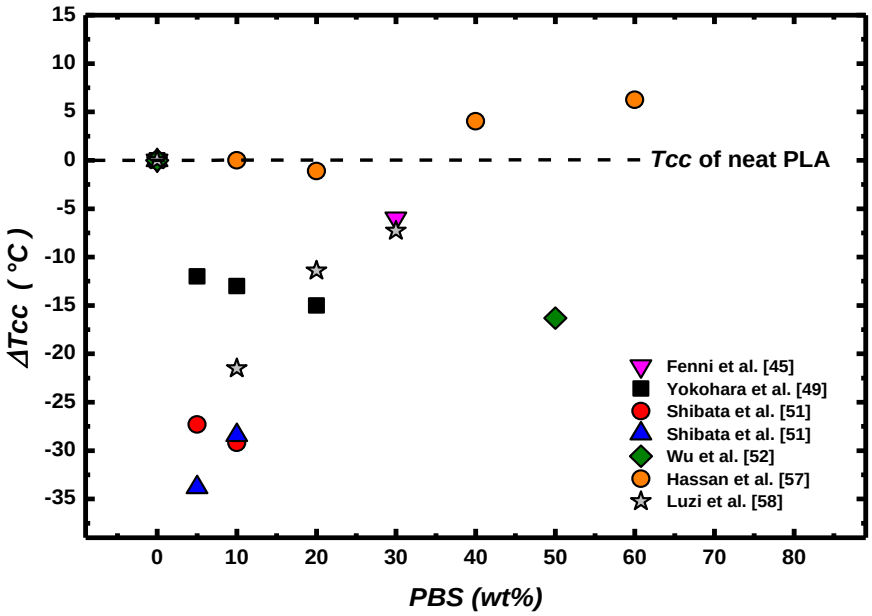

Figure 3.6. Difference in cold-crystallization temperature between neat PLA and blended sample (ΔT_{cc}) as a function of PBS content in different PLA/PBS blends reported in literature.

Although several works attributed this change in cold-crystallization rate to a certain miscibility between PLLA and PBS [50,58] at least on a local scale, this could not be sustained by any meaningful change in the glass transitions or morphology, while the growth rate is mostly unexplored. More probably, the enhancement of PLLA cold-crystallization can be well described as a heterogeneous nucleation phenomenon at the interface between the two polymer phases, thanks to the PBS crystals formed upon cooling. The possibility of impurities transfer between two melts cannot be ruled-out, but is not required to account for the observations.

On the other hand, only a limited number of works reported the effect of molten PBS in nucleating PLA during the cooling process or melt-crystallization [15,45,49,51]. For example, Yokohara and Yamaguchi [49] found that the addition of small amount of PBS largely increases the number of PLA nuclei, as observed by PLOM, and even enables the crystallization of the polymer during cooling at around 90°C. It should be noted that the melt crystallization of PLA necessarily occurs in a temperature range in which PBS is in the molten state. Therefore, the lower nucleating efficiency of the liquid-liquid contact surface could be expected.

Few studies have paid attention to the effect of the presence of PLA on PBS phase crystallization. Deng and Thomas [15] reported that blending PLA and PBS resulted in an increase in PBS crystallinity degree, which was tentatively attributed to a nucleating effect of PLA crystals. Differently, Hassan et al. [57], reported a decrease in the degree of crystallinity of PBS when it constitutes the minority phase in blends with PLA, as a consequence of fractionated crystallization and hindrance to the crystallization process exerted by the solidified PLA matrix. Another paper [45], also reported the appearance of fractionated crystallization of PBS phase and a large slowing down of its crystallization kinetics compared to pure PBS in PLA/PBS 70/30 wt% immiscible blend.

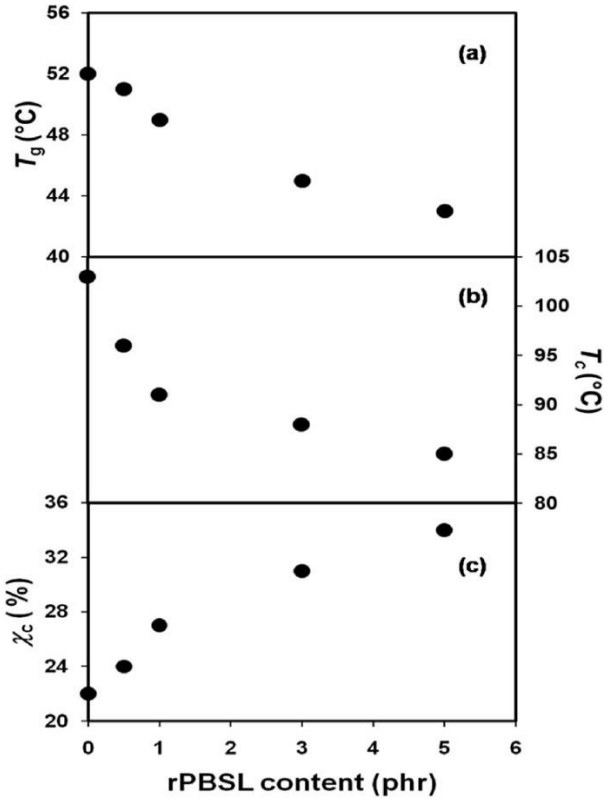

Figure 3.7. Glass transition (a), cold-crystallization temperature (b) and crystallinity (c) of PLA in PLA/PBS (80/20) blends with different contents of rPBSL [50].

Lastly, the effect of compatibilization, according to different strategies, on PLA/PBS blend crystallization can be analyzed. Wang et al. [41] employed dicumyl peroxide (DCP) with a content of 0-0.2 wt% to compatibilize an 80/20 wt% PLA/PBS blend. In the neat blend, PBS acted as nucleating agent for PLA, both during the heating process or during isothermal conditions below its melting point. A reduction in PBS crystallization and PLLA cold crystallization ability with increase of DCP content was observed, and attributed to the increase in the viscosity of system. However, the interruption of crystallizable chain sequences was not considered. Also, the decrease in PBS crystallinity could be related to the decrease in domains size with increase of DCP content and the appearance of fractionated crystallization phenomena.

Supthanyakul et al. [50], used a random poly (butylene succinate-*ran*-lactic acid) (rPBSL) copolymer as compatibilizer between PLA and PBS 80/20 wt% blends. The random copolymer was partially miscible with PLA, as deduced from the plasticization effect, with the glass transition temperature dropping about 10°C for 5 phr of rPBSL (see Figure 3.7a). The enhanced PLA mobility favored cold crystallization, which occurred much earlier on heating and lead to higher crystallinity (Figure 3.7b and 2.7c). The interpretation of the accelerated

crystallization to molecular mobility is supported by the measured increased in PLA growth rate, and decrease in spherulite induction time with increasing rPBSL content.

3.3.2 Poly (lactic acid) / poly (ε-caprolactone) blends

PLA/PCL immiscible blends have been extensively investigated, given the possible attractive combination of properties resulting from the mixture of these two components. PCL is a biodegradable polyester with a very flexible chain, characterized by a low glass transition temperature (≈ -60°C), although the melting and crystallization also occur in the low-temperature range at around 60 and 30°C, respectively. In this section, the main works dealing with the crystallization behavior of these blends, including the effect of composition and additives, are summarized [16,31,32,36,38,59-78]. Table 3.2 provides a compendium of the related studies.

Table 3.2. Main experimental works on PLA/PCL based blend, with emphasis on the aspects related to crystallization and nucleation.

Sample	Publication year	Composition wt%	Crystallization/nucleation conditions and technics	T_{cc} of PLA (°C)	T_c of PLA (°C)	T_c of PCL (°C)	Crystallization/nucleation outcomes	Reference
PLA/PCL/ PLLA-PCL-PLLA	2001	Neat PLA	PLOM isothermal crystallization; Isothermal and non-isothermal DSC	115	-	-	Addition of PCL promotes the crystallization of PLA from the glassy state regardless of PCL and PLLA-PCL-PLLA content. The PLLA spherulites growth rate kept constant in all compositions.	59
		90/10		100	-	-		
		80/20		100	-	-		
		70/30		100	-	-		
PDLA/PCL	2006	0-100 wt% of PCL	DSC non-isothermal crystallization PLOM isothermal measurements	-	-	-	The crystallization of PDLA was enhanced by PCL resulting in an increase of PDLA *Xc* in the 80/20 PDLA/PCL.	63
PLA/PCL /talc	2010	Neat PLA	DSC non-isothermal crystallization	109	-	-	40/60 PLA/PCL blend: Increase in PCL T_c during cooling process and slight decrease in PLA T_{cc} during subsequent heating process. Addition of talc results in remarkable increase in both PCL and PLA crystallization temperature.	44
		Neat PCL		-	-	30		
		40/60		106	-	39		
		70/30/1		-	110	36		
		Neat PCL		-	-	-		
		80/20		102.1	-	-		
		50/50		105.9	-	-		
		20/80		103.2	-	-		
		80/20		121.2	-	-		
		80/20/2.5		114.4	-	-		
		80/20/7.5		98.1	-	-		

PLA/PCL/ EC-bp	2013	Neat PLA	DSC non-isothermal crystallization. WAXD	126.8	-	-	Addition of PCL accelerates the cold crystallization of PLA and Xc increases. EC-bp plays the role of cross-linking agent, thus decreasing the crystallization rate of PLA.	60
		Neat PCL		-	-	-		
		90/10		121.6	-	-		
		80/20		119.6	-	-		
		70/30		115.5	-	-		
		70/30/0.5		121	-	-		
		70/30/1		124.2	-	-		
		70/30/2		128.7	-	-		
		90/10		90.52	-	-		
		80/20		90.09	-	-		
		70/30		90.39	-	-		
PLA/PCL/POSS	2014	70/30 wt% with 2% of different kind of POSS	DSC non-isothermal crystallization	-	-	-	The addition of PCL and Octaisobutyl-POSS results in slight changes in PLA crystallization. The presence of POSS limits PCL crystallization.	61
PLA/PCL/TiO_2	2015	30-70 wt% of PCL with 1-5 wt% of TiO_2.	DSC non-isothermal crystallization	-	-	-	PCL crystallinity kept constant and do not change in the blends (despite the presence of PLA, TiO_2 or PLA+TiO_2).	62
PLA/PCL/ P(LA-ran-CL)LMw	2016	Neat PLA	PLOM isothermal crystallization of PLA, Isothermal and non-isothermal DSC analysis.	128.1	-	-	Fractionated crystallization of PCL phase, acceleration of PLA cold-crystallization. The presence of copolymers causes an enhancement in the crystallization rate of both polymers	38
		Neat PCL		-	-	25.9		
		80/20		100.5/ 154	-	15.8/ 32.1		
		78.4/19.6/2		96.3/1 51.5	110.8	15.3/ 31.6		
PLA/PCL/ P(LA-ran-CL)HMw	2016	78.4/19.6/2		93.4/ 152.2	95.8	34.7		

PLA/PCL	2016	Neat PLA	DSC non-isothermal crystallization	129	-	-	Fractionated crystallization of PCL phase has been observed in 70/30 PLA/PCL. Pure PLA is amorphous and the addition of PCL results in an increase of the PLA cold crystallization and *Xc*.	64
		Neat PCL		-	-	-		
		70/30		125	-	-		
		50/50		124	-	-		
		30/70		122	-	-		
PLA/PCL	2016	0-100 wt% of PCL using three different PLA grade	DSC non-isothermal crystallization	-	-	-	Addition of PCL resulted in (i) large increase in the nucleation density and (ii) faster PLA cold crystallization kinetics. PCL crystallinity decreased with the increase in PLA content.	66
PLA/PCL/PLA-b-PC	2017	Neat PLA	Isothermal and non-isothermal DSC, PLOM isothermal analysis of PLA crystallization	129.1	-	-	Fractionated crystallization of PCL phase (20 wt%) during the cooling scan, and accelerated cold crystallization of PLA phase due to the nucleation effect of PCL (molten) droplets on glassy PLA.	16
		Neat PCL		110.8	-	28.8		
		80/20		-	-	21.7/ 31.8		
		80/20/2		-	119.2	4.6/ 23.1		
PLA/PCL/PC	2017	80/20/2		-	93 .1	12/ 19.7		
PLA/PCL	2018	0-50 wt% of PCL	DSC non-isothermal crystallization; DSC and PLOM isothermal crystallization of PCL	-	-	-	Overall isothermal crystallization kinetics revealed that the presence of 20-40 wt% of PLA enhances the crystallization ability of PCL. Growth rate of PCL found to be independent of PLA content.	65

The crystallization of PLA as a major component in PLA/PCL blends will be considered first. A clear acceleration of PLA overall crystallization rate in the presence of 20 wt% PCL has been reported [16]. For example, the time to complete crystallization at 120°C is 1.5 min in the blend, with respect to 8 minutes in the pure PLA. A faster overall crystallization is consistently found for neat and compatibilized blends in a wider temperature range, as shown in Figure 3.8 [38]. Considering the results of neat PLA and 80/20 uncompatibilized PLA/PCL blend, we can notice, beside the increase of the overall crystallization rate, a shift of the maximum rate towards lower crystallization temperature and a substantial narrowing of the bell-shaped curve.

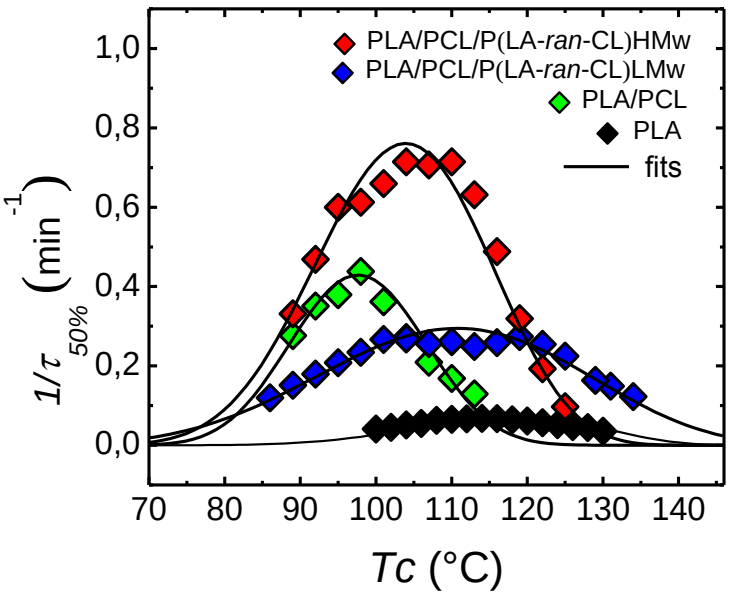

Figure 3.8. Overall crystallization rate ($1/\tau_{50\%}$) as a function of isothermal crystallization temperature T_c in neat PLA and blends with PCL 80/20. Results for blends compatibilized with Poly(lactide-ran-caprolactone) (P(LA-ran-CL)) of different molecular weights are also included. The solid lines represent a guide to the eye [38].

In order to account for the change in the temperature dependence of the overall crystallization rate (shape of the curve in Figure 3.8), the effect of PCL on the different stages of the crystallization process, i.e., primary nucleation and growth, should be considered.

Given the immiscibility of the polymers, a change in the growth rate of PLA by blending is not expected. In Figure 3.9, we can see optical micrographs of 80/20 PLLA/PCL blend at 125°C (Figure 3.9a), and in the molten state (Figure 3.9b) [59].

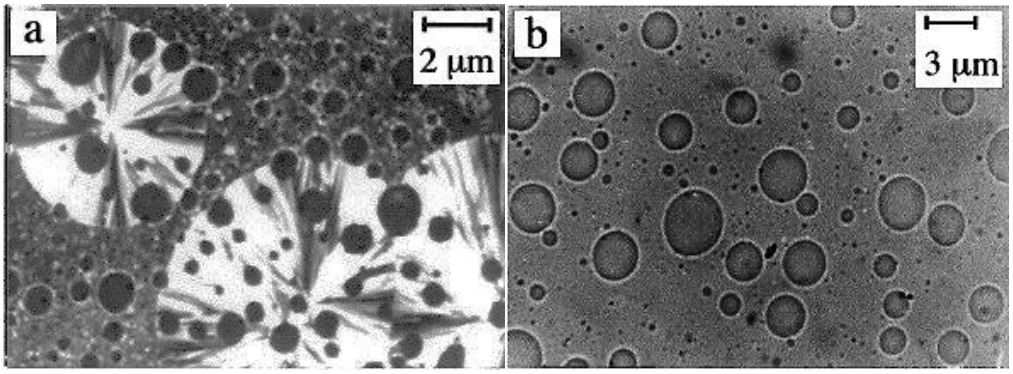

Figure 3.9. Optical micrographs of 80/20 PLLA/PCL blend (a) at 125°C and (b) in the melt state. Adapted from [59].

The phase separation is evident, and the PCL droplets, which are molten at 125°C, are not interfering with the growth of PLA spherulites, which simply proceed with their engulfment. The invariance of PLA growth rate between neat polymer and uncompatibilized PLA/PCL blend was quantitatively confirmed, as shown in Figure 3.10 [38]. No meaningful changes in the PLA spherulites growth rate (G) can be detected in the blend, in the whole crystallization temperature range, unless compatibilizing copolymers were added to the systems.

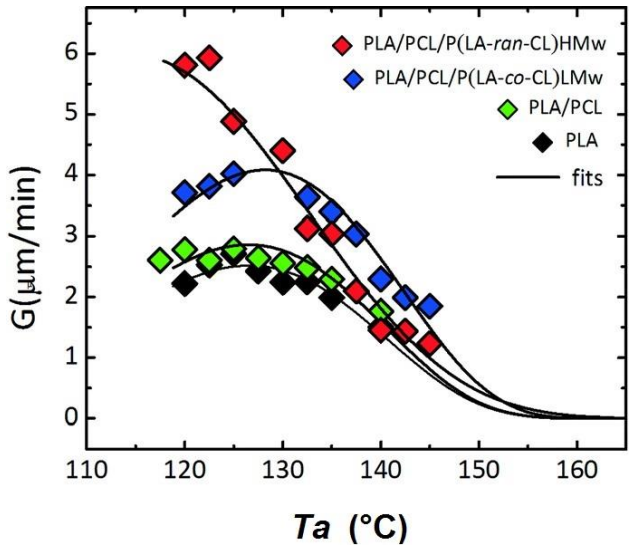

Figure 3.10. Spherulitic growth rate *G* as a function of isothermal crystallization temperature (T_c) for neat PLA and 80/20 PLA/PCL blends, with or without P(LA-ran-CL) copolymers as compatibilizing agents. The solid lines are a guide to the eye [38].

Therefore, it seems apparent that the increase in PLA overall crystallization rate with the presence of PCL (Figure 3.8) can be explained only as a nucleation effect, either by the interface between the molten polymers of by some heterogeneity transferred to the PLA phase from the PCL bulk during the mixing process.

Similarly, to the case of PLA/PBS blends, a distinct effect of PCL on the crystallization of PLA from the glassy state in their immiscible blend has also been extensively reported. [38,44,59,60,62,66,69-71]. A literature-based collection of PLA cold-crystallization temperatures as a function of PCL content is presented in Figure 3.11, according to the same normalization method employed in Figure 3.6. Despite differences among the systems are large, depending on the specific polymer grade, a clear reduction of ΔT_{cc} values is observed when PCL is added to PLA. While the trend as a function of composition is not so clear, the nucleating effect of the PCL component on PLA, for most values reported in the literature, is pronounced for most systems.

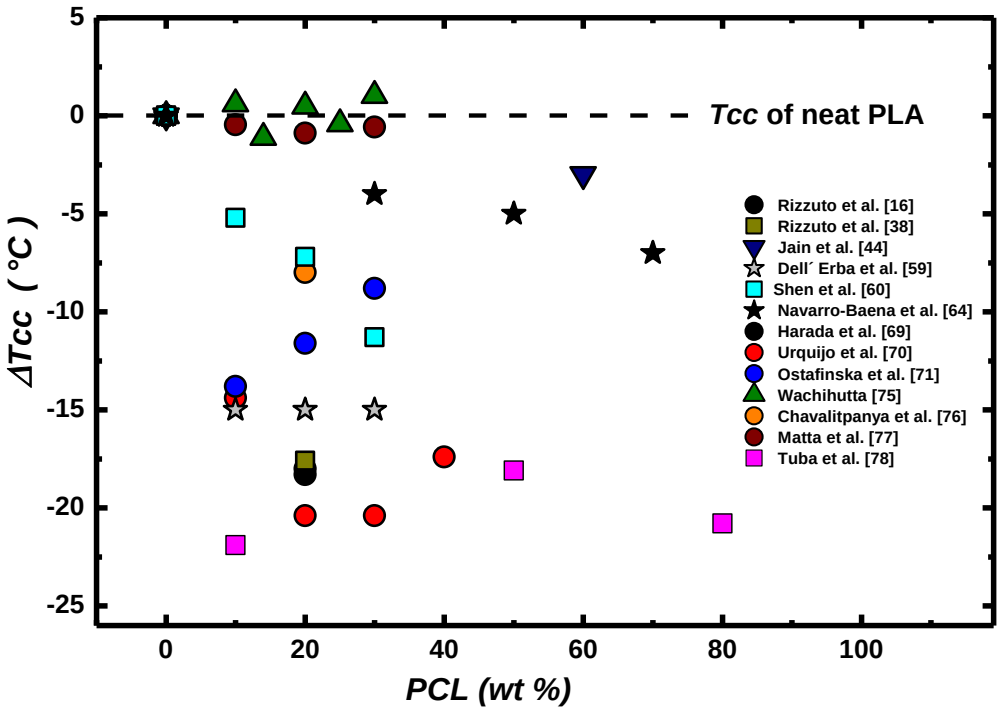

Figure 3.11. Difference in cold-crystallization temperature between neat PLA and blended sample (ΔT_{cc}) as a function of PCL content in different PLA/PCL blends reported in literature.

It should be noted, however, that a fundamental difference exists between PCL and PBS, at the typical temperatures of PLA cold-crystallization. Indeed, while in PLA/PBS immiscible blend the de-vitrified PLA is in contact with semicrystalline PBS droplets, in the case of PLA/PCL blend, the nucleating effect might originate from a molten PCL phase. Alternatively, it could be hypothesized that nucleation of PLA occurs during the cooling stage, upon PCL crystallization, even though the PLA matrix is already in the glassy state (at $T_{c,PCL}$). Note that this possibility is not contemplated for PLA/PBS blend, since poly(butylene succinate crystallizes above the glass transition of polylactide. In order to better understand the peculiar

nucleation mechanism upon cold-crystallization of PLA in its immiscible blend with PCL, a purposely designed thermal history has been applied by Müller et al. [16].

According to this protocol, the samples were quenched below $T_{g,PLA}$, and annealed at progressively lower temperatures for a fixed time, before re-heating to measure PLA cold-crystallization temperature and PCL crystallinity (by its melting enthalpy). The relevant results are reported in Figure 3.12 [16].

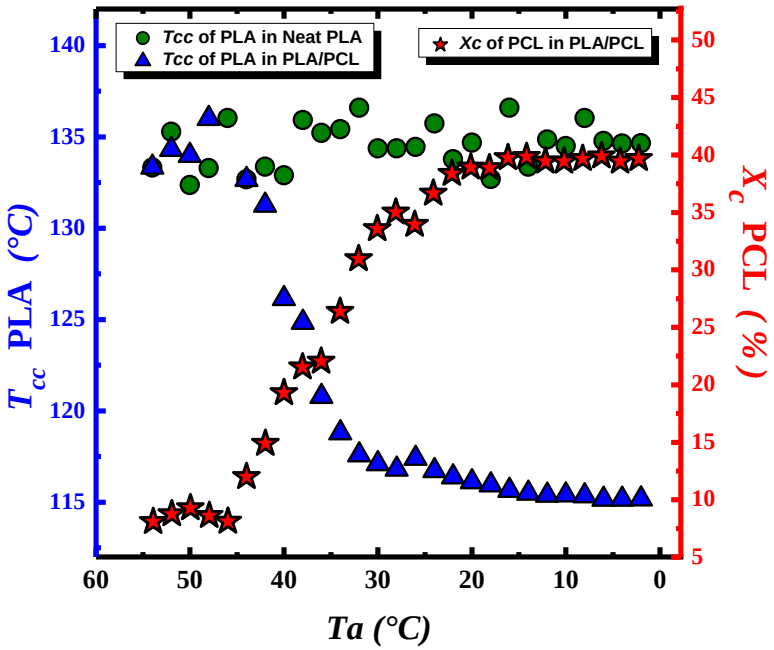

Figure 3.12. Cold-crystallization temperature of PLA (T_{cc}) and crystallinity degree of PCL (Xc) as a function the annealing temperature Ta. Data related to neat PLA and PLA/PCL 80/20 blend are shown [16].

Crystallization of PCL occurs in a rather broad temperature range, from about 45 to 20°C. Concomitantly with the increase of PCL crystallinity obtained by lowering the annealing temperature, the cold-crystallization temperature of PLA decreases smoothly from 135 to 115°C, indicating a nucleation effect of the developing PCL crystals on the glassy PLA matrix. It should be noted that a similar acceleration of PLA cold-crystallization is not observed in pure PLA, when annealed for the same time in the same temperature range (see Figure 3.12). If the blend is compatibilized, resulting in smaller PCL droplets and higher PLA/PCL interfacial area, a higher nucleating efficiency of PCL crystals on PLA cold-crystallization can be found [16]. Although is now well established that PLA can nucleate at temperatures below its glass transition [79,80], despite the extremely low mobility, the presence of PCL crystals seems to accelerate this process. The exact mechanism of nucleation in this peculiar situation has not

been established, but a role of the stresses developing at the interface between the two polymers, upon PCL crystallization, can be speculated.

The effect of the addition of a third polymeric component to PLA/PCL immiscible blend on the crystallization of PLA was reported in a number of works [16,38,59,75,76]. In general, an acceleration of PLA crystallization kinetics can be observed, although the exact origin of this effect depends on the balance between the miscibility of the additive with the PLA matrix and its compatibilizing action.

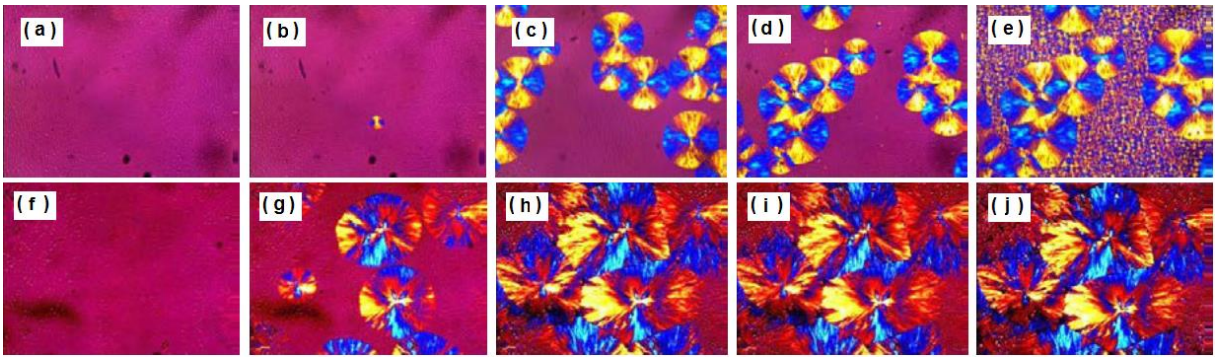

Figure 3.13. PLOM images during crystallization of 85/15 PLLA/PCL blends either neat (a-e) or with 5wt% Pluronic copolymer (f-j). Pictures are taken during stepwise crystallization at (a, f) 141°C, 0 min; (b,g) and (g) 141°C, 30 min; (c) and (h) 141°C, 90 min; (d,i) 127°C and (e,j) 37°C [75].

Rizzuto et al. [16] have investigated the crystallization behavior of PLA/PCL 80/20 wt% with the addition of 2 wt% of poly(L-lactide-*block*-carbonate) copolymers with different compositions. A large effect on the morphology, with the formation of sub-micron PCL droplets in the best case, was detected, together with a minor decrease in PLA glass transition temperature. Given that PLA spherulitic growth rate was not affected, the measured enhancement of overall crystallization kinetics with respect to the neat blend in the presence of the block copolymer was attributed to a nucleating effect of the PCL interfaces. On the other hand, when the added third polymer is partially miscible, plasticization effects can arise, causing higher PLA chain mobility and faster crystal growth rates. This is the case for instance of the already mentioned P(LA-ran-CL) copolymers [38] (see Figure 3.10) or Pluronic (PEG-PPG-PEG triblock copolymers) [75]. In this latter system, despite the block chain architecture, a partial miscibility exists, and it results in a faster PLA cold and melt-crystallization. Figure 3.13 indeed shows that, upon cooling a 85/15 PLA/PCL blend, larger spherulites develop when few percent of Pluronic block copolymer is added.

A relatively small number of works reported on the crystallization of the PCL components of immiscible PLLA/PCL blends. Opposite effects are observed, depending on the specific morphology. Few studies [38,44,65] have reported an enhancement of PCL crystallization during cooling upon the addition of PLA. This is a consequence of the nucleation at the interface with the previously crystallized PLA phase, as shown in the PLOM micrographs of Figure 3.14. A 32/68 PLLA/PCL immiscible blend is first crystallized at 120°C and subsequently cooled to 35°C. At 120°C (Figure 3.14a), only PLA is able to crystallize, whereas the PCL is molten and dispersed in between the PLA spherulites (see as an example the white oval marker in Figure 3.14a, where molten PCL is shown). By quenching to 35°C (Figure 3.14b), the PCL crystallization start clearly at the interface with crystalline PLA, developing a transcrystalline morphology clearly visible within the white oval region depicted [46].

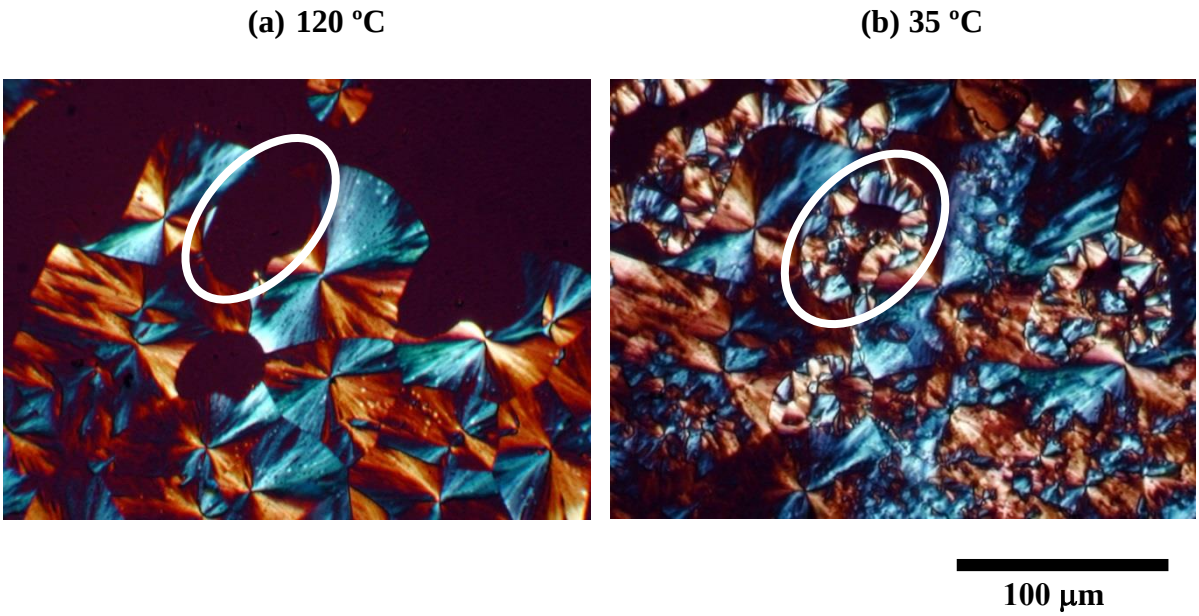

Figure 3.14. Optical micrographs of 32/68 PLLA/PCL immiscible blends during crystallization (a) at 120°C, and (b) at 35°C. Figure adapted from ref. [46].

On the other hand, when PCL is the minority phase dispersed in small domains within the PLA matrix, fractionated crystallization and a decrease in PCL crystallinity was found [16,38,61,64,78]. As an example, the DSC cooling traces of PLA, PCL and 80/20 PLLA/PCL blends containing different kind of compatibilizing agents poly(L-lactide-block-carbonate) (PLA-b-PC) are shown in Figure 3.15. In neat PLA/PCL blends, two different populations of droplets are present. The majority of them crystallize at the same temperature as bulk PCL (32°C), indicating that they still contain most of the heterogeneities present in the original PCL sample. A minority of PCL droplets contains less efficient nucleating impurities, and solidifies

about 10°C lower. Upon addition of PLA-b-PC compatibilizer, droplet size is decreased and the larger fraction of droplets crystallizes at even lower temperatures, possibly nucleated at the interface with glassy PLA [16].

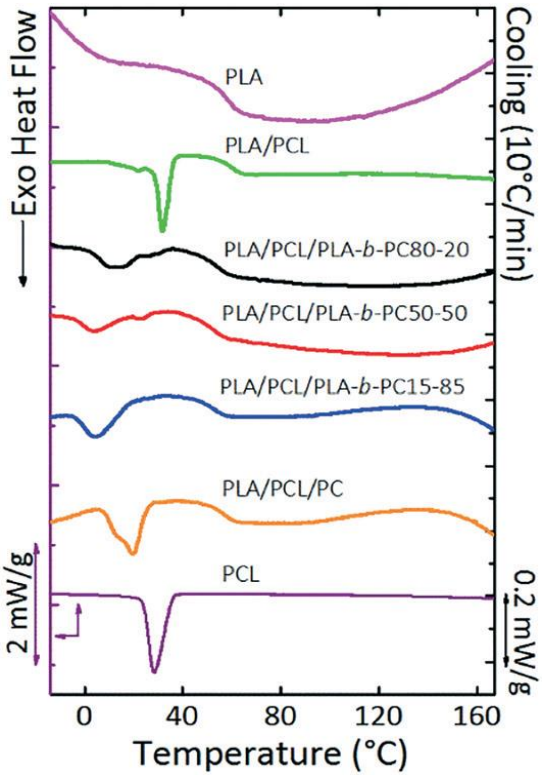

Figure 3.15. DSC cooling curves at 10°C/min, of neat PLA, neat PCL, PLA/PCL blends, and PLA/PCL/compatibilizer blends. Adapted from [16].

3.3.3 Poly (butylene succinate) / Poly (ε-caprolactone) immiscible blends

Blends of poly(butylene succinate) and poly(ε-caprolactone) are interesting because of the good mechanical properties shown by the two parent homopolymers, both of which are constituted by flexible chains. This notwithstanding, only very few works focused on the study of PBS/PCL blends, either neat or compatibilized. [81-83]

Qiu et al. [82] explored the effect of composition on crystallization and melting behavior of PBS/PCL blends. Figure 3.16 shows the DSC cooling curves of all samples at a cooling rate of 5°C/min.

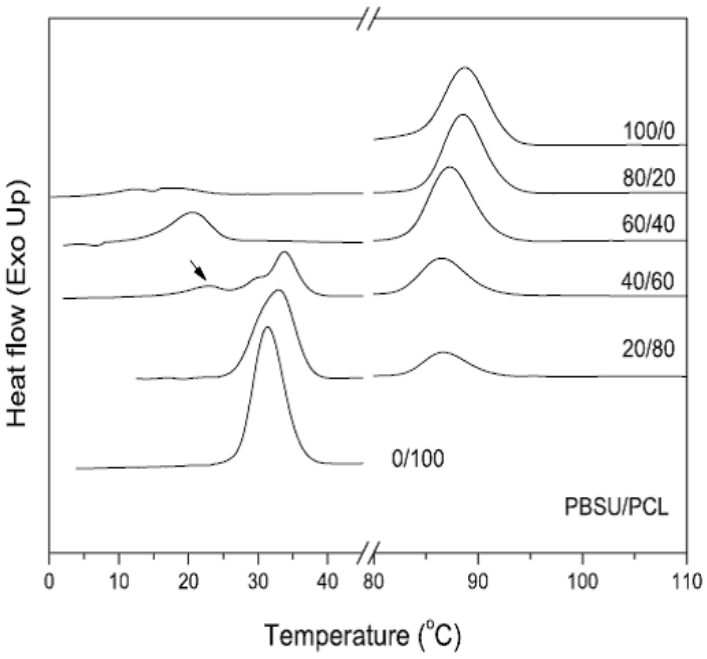

Figure 3.16. Non-isothermal crystallization from the melt of PBS/PCL blends with different compositions at a cooling rate of 5°C/min [82].

On the PBS-rich part of the composition range, no significant effect of PCL addition on the crystallization of the major component was noticed. On the other hand, a minor content (<40 wt%) of PBS causes at first the increase in PCL crystallization rate, i.e., an upward shift of the crystallization peak temperature. The same effect was reported for an 80/20 PBS/PCL blend, with an increase of $T_{c,PCL}$ of about 10°C and the invariance of $T_{c,PBS}$ [82]. The enhanced PCL crystallization was attributed to a nucleation effect of the interfaces with previously crystallized PBS. When PCL becomes the minority phase, a large depression of the crystallization temperature is observed and multiple crystallization events, i.e., fractionated crystallization, is also evident. Fractionated crystallization is particularly clear in the 60/40 PBS/PCL blend, [82] which is an unusual composition for the phenomenon. However, a detailed morphological analysis that could explain the observation has not been carried on.

Fractionated crystallization and finer dispersion of PCL phase at lower contents is also associated with a substantial decrease of its crystallinity, indicating a hindrance of the crystallized matrix on PCL structuring.

3.3.4 Poly(lactide) / poly (hydroxybutyrate) blends and other bio-based polyesters blends

Poly(3-hydroxybutyrate) (PHB) is a biodegradable thermoplastic polyester which can be obtained via a biotechnological process by means of selected bacteria. PHB is a highly crystalline polymer with high stiffness, and a melting and glass transition temperatures of around 170 and 5°C, respectively.

Blends of PHB with PLA have been investigated, with the aims of reducing PHB crystallinity (detrimental for some applications) on one side; and improve the properties of PLA (e.g., gas barrier properties for food packaging application) on the other side. The degree of compatibility between the PLA and PHB in their blends affects the crystallization behavior of the two components [43,62,84-97]. This section presents a summary of previous research on PLA/PHB blends in which the authors discussed, at least in part, the crystallization behavior. The results are summarized in Table 3.3.

It should be noted that PLA/PHB can be miscible in the melt state if PLA of low molecular weight is employed [87,97]. Crystallization from a miscible melt can give rise to concomitant formation of PHB and PLA crystals at the same isothermal crystallization temperature and with similar kinetics [87]. Each phase crystallizes in a distinct type of spherulite, which interpenetrate when their growth front meet, due to the continued growth of one kind of lamellae in the interlamellar region of the other spherulite [97].

Table 3.3. Main experimental works on PHB/PLA blends, with emphasis on nucleation and crystallization.

Sample	Publication year	Composition wt%	Crystallization/nucleation conditions and technics	T_{cc} of PLA (°C)	T_c of PLA (°C)	T_c of PHB (°C)	Crystallization/nucleation outcomes	Reference
PLA/PHB	2006	50/50	FTIR spectroscopy; stepwise isothermal crystallization of the two polymers	-	-	-	Crystallization mechanism of PLA not affected by PHB presence, but kinetics is retarded. Possible dilution effect. PHB crystallization rate after solidification of PLLA is depressed due to segregation/confinement of the polymer in the interfibrilar or interlamellar region of PLA spherulites.	84
PLA/PHB	2011	0-100 wt% of PHB	PLOM; DSC non-isothermal crystallization; WAXD; FTIR	-	-	-	PHB acts as a nucleating agent for PLA, leading to an enhancement in PLA cold-crystallization rate and crystallinity. The crystallization rate of PHB during cooling is also accelerated.	91
PLA/PHB/Lapol	2012	Neat PLA	DSC non-isothermal crystallization; XRD	115	-	-	No meaningful effect of PHB on the crystallization behavior of PLA. The addition of Lapol (plasticizer) increases PLA crystallinity.	96
		75/25		115	-	-		
		75/25/7		120	-	-		
PLA/PHB/talc	2013	90/10	DSC non-isothermal and isothermal crystallization; FT-IR; PLOM.	86.3	-	-	PHB acted as a nucleating agent for PLA. Further increases in PLA crystallization kinetics was found by addition of talc. PLOM revealed that addition of 10 wt% PHB resulted in large increase in PLA nucleation density. A further increase in PLA nucleation density was found with the addition of talc. PHB crystallization was inhibited by the presence of PLA and talc.	43
		90/10/0.5		86.2	-	-		
		90/10/1		76.5	-	-		
		90/10/2		83.3	-	-		
		90/10/5		76.6	-	-		

PLA/PHB/CNC	2014	Neat PLA	XRD F-TIR, DSC non-isothermal crystallization	82.5	-	-	Addition of PHB, CNC or CNCs resulted in a faster PLA cold crystallization rate. While addition of binary PHB/CNC or PHB/CNCs resulted in increase of T_{cc} of PLA due to lower chain mobility.	93
		75/25		66.4	-	-		
		71.25/23.75/5		70.9	-	-		
PLA/PHB/CNCs	2014	71.25/23.75/5		72.1	-	-		
PLA/PHB/ ATBC/CAT	2014	Neat PLA	DSC non-isothermal crystallization; XRD analysis.	118.1	-	-	Addition of PHB result in lowering the crystallization rate of PLA thus the PLA T_{cc} shifted to higher temperatures. PLA T_{cc} decreases upon addition of 15 wt% of ATBC due to its plasticizing effect. Presence of catechin increased PLA T_{cc}, due to specific intermolecular interactions.	94
		75/25/0/0		130	-	-		
		63.6/21.2/15/0		106.3	-	-		
		71.1/23.7/0/5		150	-	-		
		60/20/15/5		126	-	-		
PLA/PHB/LIM	2014	Neat PLA	DSC non-isothermal crystallization; PLOM; FT-IR	123.3	-	-	After blending, PHB play the role of nucleating agent for PLA. Further increase in PLA crystallinity was found in PLA/PHB/LIM blend due to the plasticizing effect of LIM.	95
		75/25		96.9	-	-		
		63.75/21.25/15		77.4	-	-		
PLA/PHBV/ TiO2	2015	30-70 wt% of PHBV with 1-5 wt% of TiO_2.	DSC non-isothermal crystallization	-	-	-	Addition of PHBV resulted in a faster cold crystallization of PLA due to a plasticizing effect, which provides more mobility to PLA.	62
PLA/PHB/ ATBC/ CNC	2015	Neat PLA	XRD; FT-IR; DSC non-isothermal crystallization	82.5	-	-	PHB works as a nucleating agent for the PLA phase. CNCs and ATBC have a synergic effect on PLA crystallization.	92
		75/25		66.4	-	-		
		63.75/21.25/15		75.5	-	-		
		60/20/15/5		67.2	-	-		
		60/20/15/5		95.8	-	-		

In the case of immiscible high-molecular weight polymer, the effect of PHB addition on PLA crystallization is not so well studied. Isothermal melt-crystallization of the PLA phase in a PLA/PHB 90/10 wt% shows a large acceleration effect, with half crystallization times decreasing more than twice with respect to neat PLA. By means of PLOM measurement, the enhanced crystallization rate was correlated with an increase in PLA nucleation density [43]. On the other hand, Zhang et al. studied the isothermal crystallization of PLLA in the immiscible 50/50 PLLA/PHB blend, and observed a substantial depression of the crystallization rate [87]. This decrease in crystallization rate was attributed to a dilution effect, i.e., the PHB melt lowers the PLLA growth rate by reducing the amount of PLA chains in the growth front of the spherulite. Similarly, opposite effects of PHB on PLA cold-crystallization have been found. Several researchers reported an enhancement of the cold crystallization rate of PLA upon addition of small amounts of PHB [43,62,91-93]. In analogy, with what has been already discussed for PLA/PBS blends, the decrease of PLA T_{cc} can be attributed to an interfacial nucleation effect on the crystalline PHB domains. On the contrary, Arrieta et al. [96] found that a 25 wt% of PHB in PLA/PHB blend caused a large increase in PLA cold-crystallization temperature from 118.1°C to 130°C. This peculiar effect was ascribed to the possible occurrence of transesterification reactions between PHB and PLA during the blending step.

Ternary systems containing immiscible PLA/PHB blend and various additives have also been investigated. Often, an acceleration in the crystallization rate of PLA is seen, typically due to (i) additional heterogeneous nucleation, for example from talc [43], cellulose nanocrystals (CNC) and surfactant modified cellulose nanocrystals (CNCs) [92,93]; and/or (ii) increase in the PLA chain mobility by a plasticizing effect of small soluble molecules such as acetyl (tributylcitrate) (ATBC) [92,94], and Limonene (LIM) [95]. Interestingly, a delayed cold-crystallization is observed for blends containing catechin, probably as a result of hydrogen bond formation with PLA chains [94].

Concerning the crystallization of the PHB phase in the presence of PLA as a major blend component, a strong depression of its kinetics - or even the complete suppression of crystallization in the adopted conditions - is always reported [43, 91]. These results have been generally interpreted as a confinement effect imposed by the crystalline PLA matrix, because upon PLA spherulitic crystallization at higher temperatures, the amorphous PHB chains are segregated to the interlamellar/interfibrilar regions of PLA superstructures [98,99]. Such intimate contact between the phases usually arises when some degree of partial miscibility exists between the chains in the melt state [100]

Few works have also investigated the phase behavior and crystallization of PHB blends with other biodegradable polymers, namely PBS and PCL [101-103]. Ma et al. [101] prepared PHB/PBS blends in the entire composition range, with the aim of improving the crystallizability of PHB by the addition of the second component. The blends were immiscible with typical sea-island morphology for asymmetric compositions and co-continuous PHB/PBS phases at 50/50 wt%. Non isothermal crystallization revealed a clear increase in $T_{c,PHB}$ of up to 30°C with PBS content. The crystallization of PBS is instead depressed when the polymer is the minor component. Ma et al. interpreted this result as a consequence of confinement by the crystalline PHB matrix, but it could also be due to changes in nucleation induced by impurity transfer phenomena. The increase of PHB crystallization rate in the presence of PBS was also noticeable in isothermal conditions, with half crystallization times which decreased more than 5 times in the blends with respect to the neat polymer, independently from the composition. This acceleration of crystallization kinetics was attributed to a nucleation effect of the interfaces with molten PBS domains, as supported by PLOM measurements during isothermal crystallization above the PBS melting point (Figure 3.17).

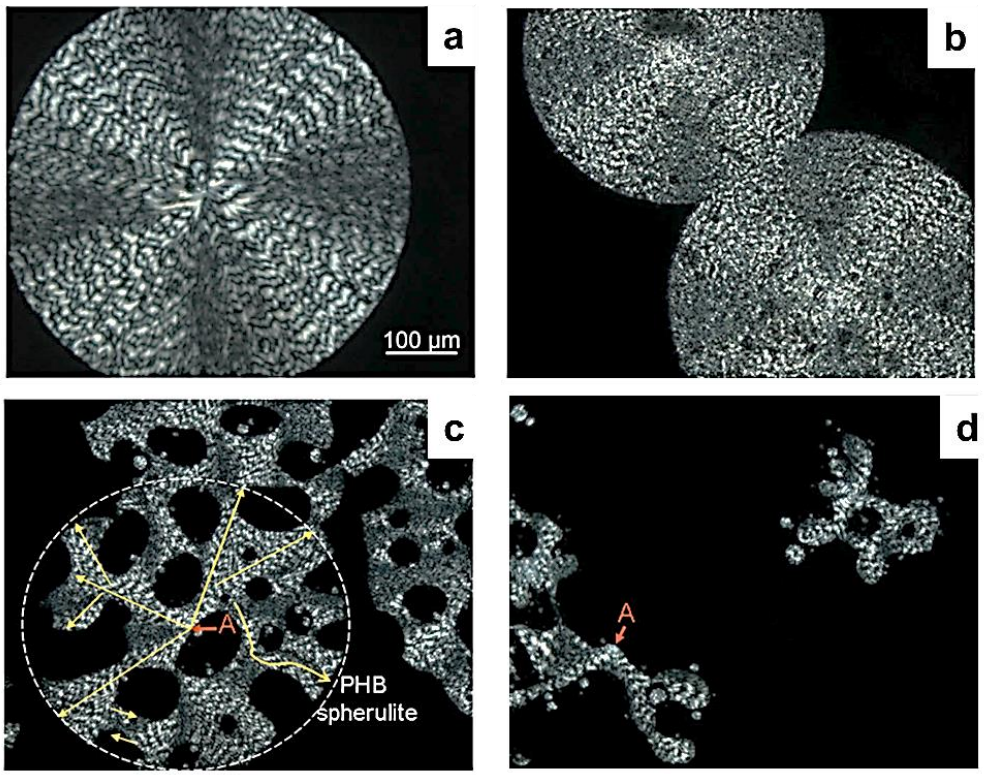

Figure 3.17. Polarized light optical microscopy during crystallization of PHB/PBS blends with various composition at 120°C. The PBS content in the blend is: a) 0 %; b) 30%; c) 50% and d) 70% by weight. The development of PHB spherulite in c) is indicated by the arrow and the nucleation point by the letter "A". Adapted from ref. [101].

It can be seen that neat PHB (Figure 3.17a) crystallized in banded spherulites with very low nucleation density. Upon addition of 30 wt% PBS, the morphology is still spherulitic with dark molten domains of PBS engulfed in it. When the PHB content in the blend becomes 50% or less, the crystals are forced to grow around the molten PBS domains, and the spherulitic structure becomes branched-like. However, the persistence of the banded motif allows one to identify the nucleation points (highlighted by the letter A in Figures 2.17 c,d), at the interface with molten PBS domains. Moreover, nucleation of smaller molten PHB domains by contact with crystallizing PHB in larger droplets was also observed. It should be noted that a small reduction of PHB growth rate is measured, and attributed to the hindrance of molten PBS to the crystal development, although a limited miscibility between PHB and PBS has also been suggested [102].

Polyhydroxybutyrate/poly(ε-caprolactone) exhibit a molecular weight dependent miscibility. Lovera et al. [103] investigated the crystallization, morphology, and degradation behavior of PHB/PCL blends upon varying PCL molecular weight.

PHB/high molecular weight PCL blend was found to be immiscible. Analysis of the crystallization behavior after blending revealed fractionated crystallization of the PCL minor phase, with a depression of crystallization temperature of around 30°C. Blends with low molecular weight PCL were also biphasic, but the PHB-rich phase exhibited a partial miscibility with PCL, as inferred by the measured depression in the PHB melting and glass transition temperatures and by the increase in the spherulitic growth rate close to T_g. A decrease of PHB nucleation density in the partially miscible blend has also been reported, probably caused by impurity transfer between the two phases during blending.

3.4 Conclusions of the bibliography research

The nucleation and crystallization of these polyesters components greatly depends on their morphology, as determined by their composition, processing conditions and thermal history. As far as the nucleation of double crystalline polyester blends is concerned, the component that crystallizes at higher temperatures can nucleate on: (a) existing heterogeneities which were either present in the parent homopolymer or transferred during melt blending from the second blend component or (b) on the interface between the two molten components. Notice that in the second case, or case (b) above, no epitaxial mechanism can be invoked to explain the heterogeneous nucleation that has been clearly documented by PLOM and DSC. Hence

other causes must be found that could be related to secondary interactions between the immiscible phases, interfacial free energy differences or other unknown factors that clearly need more future research.

If the blend above with two crystallizable components is further cooled, after the first blend component has already crystallized, then the second polymer can be nucleated by: (a) existing heterogeneities which were either present in the parent homopolymer or transferred during blending from the second melt component or (b) on the interface between the previously crystallized blend component and the melt of the second component. In this second case, epitaxial nucleation is a possibility.

In many cases, nucleation effects of the previously crystallized component on the second phase of the blend (that crystallizes at lower temperatures) have been reported. More peculiar effects like the nucleation of PCL droplets on glassy PLA matrices deserve more research in order to find how the nucleation can occur in the glassy state by interfacial contacts with crystalline polymeric droplets.

3.5 References

1. Utracki LA, Wilkie C (Eds) (2014) Polymer Blends Handbook. Springer, New York.
2. Utracki LA (Ed) (2002) Polymer Blends Handbook, vol 2. Kluwer Academic Publishers, Dordrecht, Netherlands
3. Paul DR, Barlow JW (1979) A Brief Review of Polymer Blend Technology. In: Cooper SL, Estes GM (eds) multiphase polymers. Advances in Chemistry, Washington, p 315-335
4. Paul DR, Barlow JW (1980) Polymer Blends (or Alloys). J. Macromol. Sci., Rev. Macromol. Chem. Phys. 18:109-168
5. Cor K, Martin VD, Christophe P, Robert J (1998) Strategies for compatibilization of polymer blends. Prog. Polym. Sci. 23:707-757
6. Supthanyakul R, Kaabbuathong N, Chirachanchai S (2016) Random poly(butylene succinate-co-lactic acid) as a multi-functional additive for miscibility, toughness, and clarity of PLA/PBS blends. Polymer 105:1-9
7. Dhibar AK, Kim JK, Khatua BB (2011) Cocontinuous Phase Morphology of Asymmetric Compositions of Polypropylene/High-density Polyethylene Blend by the Addition of Clay. J. Appl. Polym. Sci. 119:3080-3092

8. Tol RT, Mathot VBF, Reynaers H, Groeninckx G (2006) Relationship between Phase Morphology, Crystallization, and Semicrystalline Structure in Immiscible Polymer Blends. In: Harrats C, Thomas S, Droeninchx G (eds) Micro- and Nanostructured Multiphase Polymer Blend Systems Phase Morphology and Interfaces. Taylor & Francis, USA, p 391-420
9. Cordova ME, Lorenzo AT, Müller AJ, Gani L, Tence-Girault S, Leibler L (2011) The Influence of Blend Morphology (Co-Continuous or Sub-Micrometer Droplets Dispersions) on the Nucleation and Crystallization Kinetics of Double Crystalline Polyethylene/Polyamide Blends Prepared by Reactive Extrusion. Macromol. Chem. Phys. 212:1335-1350
10. Pracella M (2013) Crystallization of polymer blends. In: Piorkowska E, Rutledge GC (eds) handbook of polymer crystallization. Wiley, New Jersey, p 287-325
11. Jabarin SA, Ardakani KM, Lofgren EA (2016) Crystallization and Melting Behavior in Polymer Blends. In: Isayev AI (ed) Encyclopedia of Polymer Blends volume 3: Structure. Wiley-VCH Verlag GmbH & Co. KGaA, Weinheim, Germany, p 135-189
12. Michell RM, Müller AJ (2016) Confined crystallization of polymeric materials. Prog. Polym. Sci. 54-55, 183-213
13. Tien ND, Prud'homme RE (2017) Crystallization Behavior of Semicrystalline Immiscible Polymer Blends. In: Thomas S, Arif PM, Gowd B, Kalarikkal N (eds) Crystallization in Multiphase Polymer Systems. Elsevier, Amsterdam, p 181-212
14. Bartczak Z, Galeski A (1990) Homogeneous nucleation in polypropylene and its blends by small-angle light scattering. Polymer 31:2027-2038
15. Deng Y, Thomas NL (2015) Blending poly(butylene succinate) with poly(lactic acid): Ductility and phase inversion effects. Eur. Polym. J. 71:534-546
16. Rizzuto M, Marinetti L, Caretti D, Mugica A, Zubitur M, Müller AJ (2017) Can poly (ε-caprolactone) crystals nucleate glassy polylactide?. CrystEngComm 19:3178
17. Ma P, Cai X, Wang W, Duan F, Shi D, Lemstra PJ (2014) Crystallization Behavior of Partially Crosslinked Poly(b-hydroxyalkonates)/Poly(butylene succinate) Blends. J. Appl. Polym. Sci.131:41020
18. Frensch H, Harnischfeger P, Jungnickel BJ (1989) Fractionated Crystallization in Incompatible Polymer Blends. In: Utracky LA, Weiss RA (eds) Multiphase polymers: Blends and ionomers. American Chemical Society, Washington, pp 101-125

19. Müller AJ, Michell RM (2016) Differential Scanning Calorimetry of Polymers. In: Guo Q (ed) Polymer Morphology: Principles, Characterization, and Processing. John Wiley & Sons, Inc., New Jersey, p 72-99
20. Morales RA, Arnal ML, Müller AJ (1995) The evaluation of the state of dispersion in immiscible blends where the minor phase exhibits fractionated crystallization. Polym. Bull. 35:379-386
21. Arnal ML, Matos ME, Morales RA, Santana OO, Müller AJ (1998) Evaluation of the fractionated crystallization of dispersed polyolefins in a polystyrene matrix. Macromol. Chem. Phys. 199:2275-2288
22. Arnal ML, Müller AJ (1999) Fractionated crystallisation of polyethylene and ethylene/a-olefin copolymers dispersed in immiscible polystyrene matrices. Macromol. Chem. Phys. 200:2559-2576
23. Schick C, Androsch R, Schmelzer JWP (2017) Homogeneous crystal nucleation in polymers. J. Phys.: Condens. Matter 29:453002
24. Santana OO. Müller AJ (1994) Homogeneous nucleation of the dispersed crystallizable component of immiscible polymer blends. Polym. Bull.32:471-477
25. Michell RM, Blaszczyk-Lezak I, Mijangos C, Müller AJ (2013) Confinement effects on polymer crystallization: From droplets to alumina nanopores. Polymer 54:4059-4077
26. Tol RT, Mathot VBF, Groeninckx G (2005) Confined crystallization phenomena in immiscible polymer blends with dispersed micro- and nanometer sized PA6 droplets, part 2: reactively compatibilized PS/PA6 and (PPE/PS)/PA6 blends. Polymer 46:383-396
27. Tol RT, Mathot VBF, Groeninckx G (2005) Confined crystallization phenomena in immiscible polymer blends with dispersed micro- and nanometer sized PA6 droplets, part 3: crystallization kinetics and crystallinity of micro- and nanometer sized PA6 droplets crystallizing at high supercoolings. Polymer 46:2955-2965
28. Yordanov C, Minkova L (2005) Fractionated crystallization of compatibilized LDPE/PA6 blends. Eur. Polym. J. 41:527–534
29. Anstey A, Codou A, Misra M, Mohanty AK (2018) Novel Compatibilized Nylon-Based Ternary Blends with Polypropylene and Poly(lactic acid): Fractionated Crystallization Phenomena and Mechanical Performance. ACS Omega 3:2845-2854
30. Huo H, Guo C, Zhou J, Zhao X (2014) The combination of fluctuation-assisted crystallization and interface-assisted crystallization in a crystalline/crystalline blend of poly(ethylene oxide) and poly(ε-caprolactone). Colloid Polym. Sci. 292:971-983

31. Qiaolian Lv, Wu D, Xie H, Peng S, Chen Y, Xu C (2016) Crystallization of poly(ε-caprolactone) in its immiscible blend with polylactide: insight into the role of annealing histories. RSC Adv. 6:37721
32. Sakai F, Nishikawa K, Inoue Y, Yazawa K (2009) Nucleation Enhancement Effect in Poly(L-lactide) (PLLA)/Poly(ε-caprolactone) (PCL) Blend Induced by Locally Activated Chain Mobility Resulting from Limited Miscibility. Macromolecules 42:8335-8342
33. Pan P, Shan G, Bao Y (2014) Enhanced Nucleation and Crystallization of Poly(L-lactic acid) by Immiscible Blending with Poly(vinylidene fluoride). Ind. Eng. Chem. Res. 53:3148-3156
34. Kong Y, Ma Y, Lei L, Wang X, Wang H (2017) Crystallization of Poly(ϵ-caprolactone) in Poly(vinylidene fluoride)/Poly(ε -caprolactone) Blend. Polymers 9:42
35. Shi W, Chen F, Zhang Y, Han CC (2012) Viscoelastic Phase Separation and Interface Assisted Crystallization in a Highly Immiscible iPP/PMMA Blend. ACS Macro Lett. 1:1086-1089
36. Wu D, Lin D, Zhang J, Zhou W, Zhang M, Zhang Y, Wang D, Lin B (2011) Selective Localization of Nanofillers: Effect on Morphology and Crystallization of PLA/PCL Blends. Macromol. Chem. Phys. 212:613-626
37. Yu C, Han L, Bao J, Shan G, Bao Y, Pan P (2016) Polymorphic Crystallization and Crystalline Reorganization of Poly(L-lactic acid)/Poly(D-lactic acid) Racemic Mixture Influenced by Blending with Poly(vinylidene fluoride). J. Phys. Chem. B 120 (32):8046-8054
38. Rizzuto M, Mugica A, Zubitur M, Caretti D, Müller AJ (2016) Plasticization and anti-plasticization effects caused by poly(L-lactide-ran-caprolactone) addition to double crystalline poly(L-lactide)/poly(ε- caprolactone) blends. CrystEngComm 18:2014
39. Wei Q, Chionna D, Pracella M (2005) Reactive Compatibilization of PA6/LDPE Blends with Glycidyl Methacrylate Functionalized Polyolefins. Macromol. Chem. Phys. 206:777-786
40. Garcia-Garcia D, Rayon E, Carbonell-Verdu A, Lopez-Martinez J, Balart R (2017) Improvement of the compatibility between poly(3-hydroxybutyrate) and poly(ε-caprolactone) by reactive extrusion with dicumyl peroxide. Eur. Polym. J. 86:41-57
41. Wang R, Wang S, Zhang Y, Wan C, Ma P (209) Toughening Modification of PLLA/PBS Blends via In Situ Compatibilization. Polym. Eng. Sci. 49:26-33

42. Liu NC, Xie HQ, Baker WE (1993) Comparison of the effectiveness of different basic functional groups for the reactive compatibilization of polymer blends. Polymer 34 :4680-4687
43. Tri PN, Domenek S, Guinault A, Sollogoub C (2013) Crystallization Behavior of Poly(lactide)/Poly(β-hydroxybutyrate)/Talc Composites. J. Appl. Polym. Sci. 129:3355-3365
44. Jain S, Reddy MM, Mohanty AK, Misra M, Ghosh AK (2010) A New Biodegradable Flexible Composite Sheet from Poly(lactic acid)/Poly(ε-caprolactone) Blends and Micro-Talc. Macromol. Mater. Eng. 295:750-762
45. Monticelli O, Conzatti L, Stagnaro P, Cavallo D (2018) Correlating the morphology of poly(L-lactide)/poly(butylene succinate)/graphene oxide blends nanocomposites with their crystallization behavior. eXPRESS Polym. Lett. 12:58-70
46. Müller AJ, Avila M, Saenz G, Salazar J (2014) Crystallization of PLA-based Materials. In Jiménez A, Peltzer M, Ruseckaite R (eds) Poly(lactic acid) Science and Technology: Processing, Properties, Additives and Applications. The Royal Society of Chemistry, Cambridge, UK, p 66-98
47. Di Lorenzo MR, Androsch R (2015) Crystallization of Poly(lactic acid). In: *Fakirov S* (ed) Biodegradable Polyesters. Wiley-VCH Verlag GmbH & Co. KGaA, Weinheim, Germany, p 109-130
48. Androsch R, Schick C, Di Lorenzo ML (2017) Kinetics of Nucleation and Growth of Crystals of Poly(l-lactic acid). In: Advances in Polymer Science 279. Springer International, Basel, Switzerland, p – 235-272
49. Yokohara T, Yamaguchi M (2008) Structure and properties for biomass-based polyester blends of PLA and PBS. Eur. Polym. J. 44, 677-685
50. Supthanyakul R, Kaabbuathong N, Chirachanchai S (2016) Random poly(butylene succinate-co-lactic acid) as a multi-functional additive for miscibility, toughness, and clarity of PLA/PBS blends. Polymer 105:1-9
51. Shibata M, Inoue Y, Miyoshi M (2006) Mechanical properties, morphology, and crystallization behavior of blends of poly(L-lactide) with poly(butylene succinate-co-L-lactate) and poly(butylene succinate). Polymer 47:3557-3564
52. Wu D, Yuan L, Laredo E, Zhang M, Zhou W (202) Interfacial Properties, Viscoelasticity, and Thermal Behaviors of Poly(butylene succinate)/Polylactide Blend. Ind. Eng.Chem. Res. 51:2290-2298

53. Persenaire O, Quintana R, Lemmouchi Y, Sampson J, Martin S, Bonnaud L, Dubois P (2014) Reactive compatibilization of poly(L-lactide)/poly(butylene succinate) blends through polyester maleation: from materials to properties. Polym. Int. 63:1724-1731
54. Buasri A, Buranasing G, Piemjaiswang R, Yousatit S, Loryuenyong V (2014) Effect of titanium dioxide nanoparticles on mechanical and thermal properties of poly(lactic acid) and poly(butylene succinate) blends. Adv. Sci. Tech. 96:33-38
55. Zhang Z, Zhang Y (2016) Reinforcement effect of poly(butylene succinate) (PBS)-grafted cellulose nanocrystal on toughened PBS/polylactic acid blends. Carbohydr. Polym. 140:374-382
56. Harada M, Ohya T, Iida K, Hayashi H, Hirano K, Fukuda H (2007) Increased Impact Strength of Biodegradable Poly(lactic acid)/Poly(butylene succinate) blend Composites by using Isocyanate as a Reactive Processing Agent. J. Appl. Polym. Sci.106:1813-1820
57. Hassan E, Wei Y, Jiao H, Muhuo Y (2013) Dynamic Mechanical Properties and Thermal Stability of Poly(lactic acid) and Poly(butylene succinate) Blends Composites. J. Fiber Bioeng. Inf. 6:85-94
58. Luzi F, Fortunati E, Jiménez A, Pugliaa D, Pezzolla D, Gigliotti G, Kenny JM, Chiralt A, Torre L (2016) Production and characterization of PLA PBS biodegradable blends reinforced with cellulose nanocrystals extracted from hemp fibres. Ind. Crops Prod. 93:276-289
59. Dell'Erba R, Maglio G, Malinconico M, Migliozzi A (2001) Immiscible polymer blends of semicrystalline biocompatible components: thermal properties and phase morphology analysis of PLLA/PCL blends. Polymer 42:7831-7840
60. Shen T, Lu M, Liang L (2013) Modification of the Properties of Polylactide/ Polycaprolactone Blends by Incorporation of Blocked Polyisocyanate. J. Macromol. Sci. Part A Pure Appl. Chem. 50:547–554
61. Monticelli O, Calabrese M, Gardella L, Fina A, Gioffredi E (2014) Silsesquioxanes: Novel compatibilizing agents for tuning the microstructure and properties of PLA/PCL immiscible blends. Eur. Polym. J. 58:69-78
62. Mofokeng JP, Luyt AS (2015) Dynamic mechanical properties of PLA/PHBV, PLA/PCL, PHBV/PCL blends and their nanocomposites with TiO2 as nanofiller. Thermochim Acta 613:41-53
63. Lopez-Rodriguez N, Lopez-Arraiza A, Meaurio E, Sarasua JR (2006) Crystallization, Morphology, and Mechanical Behavior of Polylactide/Poly(ε-caprolactone) Blends. Polym. Eng. Sci. 46:1299-1308

64. Navarro-Baena I, Sessini V, Dominici F, Torre L, Kenny JM, Peponi L (2016) Design of biodegradable blends based on PLA and PCL: From morphological, thermal and mechanical studies to shape memory behavior. Polym. Degrad. Stab. 132:97-108
65. Han W, Liao X, He B, Yang Q, Li G (2018) Disclosing the crystallization behavior and morphology of poly(ε-caprolactone)/within poly(ε-caprolactone)/poly(L-lactide) blends. Polym. Int. 67:566-576
66. Derakhshandeh M, Noroozi N, Schafer LL, Vlassopoulos D, Hatzikiriakos SG (2016) Dynamics of partially miscible polylactide-poly(ε-caprolactone) blends in the presence of cold crystallization. Rheol. Acta 55:657-671
67. Cabedo L, Feijoo JL, Villanueva MP, Lagaron JM, Gimenez E (2006) Optimization of Biodegradable Nanocomposites Based on a PLA/PCL Blends for Food Packaging Applications. Macromol. Symp. 233:191-197
68. Bouakaz BS, Habi A, Grohens Y, Pillin I (2017) Organomontmorillonite/graphene-PLA/PCL nanofilled blends: New strategy to enhance the functional properties of PLA/PCL blend. Appl. Clay Sci. 139:81-91
69. Harada M, Iida K, Okamoto K, Hayashi H, Hirano K (2008) Reactive Compatibilization of Biodegradable Poly(lactic acid)/Poly(ε-caprolactone) Blends with Reactive Processing Agents. Polym. Eng. Sci. 48:1359-1368
70. Urquijo J, Guerrica-Echevarrıa G, Eguiazabal JI (2015) Melt processed PLA/PCL blends: Effect of processing method on phase structure, morphology, and mechanical properties. J. Appl. Polym. Sci. 42641:1-9
71. Ostafinska A, Fortelny I, Nevoralova M, Hodan J, Kredatusova J, Slouf M (2015) Synergistic effects in mechanical properties of PLA/PCL blends with optimized composition, processing, and morphology. RSC Adv. 5, 98971
72. Bai H, Huang C, Xiu H, Gao Y, Zhang Q, Fu Q (2013) Toughening of poly(L-lactide) with poly(ε-caprolactone): Combined effects of matrix crystallization and impact modifier particle size. Polymer 54:5257-5266
73. Bai H, Xiu H, Gao J, Deng H, Zhang Q, Yang M, Fu Q (2012) Tailoring Impact Toughness of Poly(L-lactide)/Poly(ε-caprolactone) (PLLA/PCL) Blends by Controlling Crystallization of PLLA Matrix. ACS Appl. Mater. Interfaces 4:897-905
74. Na YH, He Y, Shuai X, Kikkawa Y, Doi Y, Inoue Y (2002) Compatibilization Effect of Poly(ε-caprolactone)-b-poly(ethylene glycol) Block Copolymers and Phase Morphology Analysis in Immiscible Poly(lactide)/Poly(ε-caprolactone) Blends. Biomacromolecules 3:1179-1186

75. Wachirahuttapong S, Thongpin C, Sombatsompop N (2016) Effect of PCL and compatibility contents on the morphology, crystallization and mechanical properties of PLA/PCL blends. Energy Procedia 89:198-206
76. Chavalitpanya k, Phattanarudee S (2013) Poly(lactic acid)/Polycaprolactone Blends Compatibilized with Block Copolymer. Energy Procedia 34:542-548
77. Matta AK, Rao RU, Sumana KNS, Rambabuc V (2014) Preparation and Characterization of Biodegradable PLA/PCL Polymeric Blends. Procedia Mater. Sci. 6:1266-
78. Tuba F, Olah L, Nagy P (2011) Characterization of reactively compatibilized poly(D,L-lactide)/poly(ε-caprolactone) biodegradable blends by essential work of fracture method. Eng. Fract. Mech. 78:3123-3133
79. Androsch R, Di Lorenzo MR (2013) Kinetics of crystal nucleation of poly(L-lactic acid). Polymer 54:6882-6885
80. Di Lorenzo ML, Androsch R (2013) Crystal Nucleation in Glassy Poly(L-lactic acid). Macromolecules 46, 6048-6056
81. Liu Q, Zhou XM (2015) Preparation of Poly(butylene succinate)/poly(ε-caprolactone) Blends Compatibilized With Poly(butylene succinate-co-ε-caprolactone) Copolymer. J. Macromol. Sci. Part A Pure Appl. Chem. 52:625-629
82. Qiu Z, Komura M, Ikehara T, Nishi T (2003) Miscibility and crystallization behavior of biodegradable blends of two aliphatic polyesters. Poly(butylene succinate) and Poly(ε-caprolactone). Polymer 44:7749-7756
83. Gumede TP, Luyt AS, Müller AJ (2018) Review on PCL, PBS, and PCL/PBS blends containing carbon nanotubes. eXPRESS Polym. Lett. 12:505-529
84. Zhang J, Sato H, Furukawa T, Tsuji H, Noda I, Ozaki Y (2006) Crystallization Behaviors of Poly(3-hydroxybutyrate) and Poly(L-lactic acid) in Their Immiscible and Miscible Blends. J. Phys. Chem. B 110:24463-24471
85. Sato H, Nakamura M, Padermshoke A, Yamaguchi H, Terauchi H, Ekgasit S, Noda I, Ozaki Y (2004) Thermal Behavior and Molecular Interaction of Poly(3-hydroxybutyrate-co-3-hydroxyhexanoate) Studied by Wide-Angle X-ray Diffraction. Macromolecules 37:3763-3769
86. Sato H, Murakami R, Padermshoke A, Hirose F, Senda K, Noda I, Ozaki Y (2004) Infrared Spectroscopy Studies of CH···O Hydrogen Bondings and Thermal Behavior of Biodegradable Poly(hydroxyalkanoate). Macromolecules 37:7203-7213
87. Zhang L, Xiong C, Deng X (1996) Miscibility, crystallization and morphology of poly(P-hydroxybutyrate)/ poly(d,l-lactide) blends. Polymer 37:235-241

88. Arrieta MP, Samper MD, Aldas M, Lopez J (2017) On the Use of PLA-PHB Blends for Sustainable Food Packaging Applications. Materials 10, 1008
89. Arrieta MP, Lopez J, Rayon E, Jimenez A (2014) Disintegrability under composting conditions of plasticized PLA-PHB blends. Polym. Degrad. Stab. 108:307-318
90. Armentano I, Fortunati E, Burgos N, Dominici F, Luzi F, Fiori S, Jimenez A, Yoon K, Ahn J, Kang S, Kenny JM (2015) Processing and characterization of plasticized PLA/PHB blends for biodegradable multiphase systems. eXPRESS Polym. Lett. 9:583-596
91. Zhang M, Thomas NL (2011) Blending Polylactic Acid with Polyhydroxybutyrate: The Effect on Thermal, Mechanical, and Biodegradation Properties. Advances in Polymer Technology 30:67-79
92. Arrieta MP, Fortunati E, Dominici F, Lopez J, Kenny JM (2015) Bionanocomposite films based on plasticized PLA–PHB/cellulose nanocrystal blends. Carbohydr. Polym. 121:265-275
93. Arrieta MP, Fortunati E, Dominici F, Rayon E, Lopez J, Kenny JM (2014) Multifunctional PLA–PHB/cellulose nanocrystal films: Processing, structural and thermal properties. Carbohydr. Polym. 107:16-24
94. Arrieta MP, Castro-Lopez MDM, Rayon E, Barral-Losada LF, Lopez-Vilarino JM, Lopez J, Gonzalez-Rodriguez MV (2014) Plasticized Poly(lactic acid)−Poly(hydroxybutyrate) (PLA−PHB) Blends Incorporated with Catechin Intended for Active Food-Packaging Applications. J. Agric. Food Chem. 62:10170-10180
95. Arrieta MP, Lopez J, Hernandez A, Rayon E (2014) Ternary PLA–PHB–Limonene blends intended for biodegradable food packaging applications. Eur. Polym. J. 50:255-270
96. Abdelwahab MA, Flynn A, Chiou BS, Imam S, Orts W, Chiellini E (2012) Thermal, mechanical and morphological characterization of plasticized PLA-PHB blends. Polym. Degrad. Stab. 97:1822-1828
97. Blumm E, Owen AJ (195) Miscibility, crystallization and melting of poly(3-hydroxybutyrate)/poly(L-lactide) blends. Polymer 36:4077-4081
98. Xu J, Bao J, Guo BH, Ma H, Yun TL, Gao L, Chen GQ, Iwata T (2007) Imaging of nonlinear optical response in biopolyesters via second harmonic generation microscopy and its dependence on the crystalline structures. Polymer 48:348-355
99. Ohkoshia I, Abe H, Y, Doi Y (2000) Miscibility and solid-state structures for blends of poly[(S)-lactide] with atactic poly[(R,S)-3-hydroxybutyrate]. Polymer 41:5985-5992
100. Schultz JM (ed) (2001) Polymer Crystallization: The Development of Crystalline Order in Thermoplastic Polymers. American Chemical Society, New York

101. Ma P, Hristova-Bogaerds DG, Zhang Y, Lemstra PJ (2014) Enhancement in crystallization kinetics of the bacterially synthesized poly(β-hydroxybutyrate) by poly(butylene succinate). Polym. Bull. 71:907-923

102. Qiu Z, Ikehara T, Nishi T (2003) Poly(hydroxybutyrate)/poly(butylene succinate) blends: miscibility and nonisothermal crystallization. Polymer 44:2503-2508

103. Lovera D, Marquez L, Balsamo V, Taddei A, Castelli C, Müller AJ (2007) Crystallization, Morphology, and Enzymatic Degradation of Polyhydroxybutyrate/Polycaprolactone (PHB/PCL) Blends. Macromol. Chem. Phys. 208:924-937

PLLA/PBS/GO Blend nanocomposites

Partially reproduced from: S.E. Fenni et al. "Correlating the morphology of poly(l-lactide)/poly(butylene succinate)/graphene oxide blends nanocomposites with their crystallization behavior". eXPRESS Polymer Letters, 12:58-70 (**2018**).

Experimental work

Chapter IV

PLLA/PBS/GO blend nanocomposites: Morphology, Crystallization behavior, and Properties.

4.1 Introduction

Blends of PLLA with other bio-degradable polymers have been widely studied. For example, different flexible polymers, such as poly(hydroxybutyrate) (PHB), poly(ε-caprolactone) (PCL), poly(ethylene glycol) (PEG), and poly(butylene succinate) (PBS), have been used to toughen PLLA. In the present work we focused on PLLA/PBS blends, given the biodegradability and good processability of PBS [1-25].

A variety of compounds has been added to blends of these two polymers, with the aim of improving their physical properties. Chen et al. found that a reactive organoclay with glycidyl functionality acts as a compatibilizer for PLLA/PBS blends, improving the elongation at break and tensile modulus [2,4]. Homklin et al. clarified the effect of nucleating agents on the PLLA/PBS blend properties: adding nano-sized calcium carbonate or sodium benzoate improved mechanical properties, processability, and productivity in mold processing of the blend [8,26]. Luzi et al. reported that cellulose nanocrystals improved the barrier properties and increased the Young modulus of the blend [4]. Buasri et al. studied the effect of TiO_2 nanoparticles finding an enhancement of physical, mechanical and thermal behavior of the blend [11].

Recently, graphene oxide (GO) has been investigated as nano-compatibilizer and nano-reinforcement in polymer blends [14,15,27,28]. Cao et al. found that the addition of only 0.5 wt% of GO to the immiscible polyamide/poly(phenylene oxide) (PA/PPO) blend reduces the interfacial tension between the components, thanks to the amphiphilic nature of the graphene oxide. As such, the droplet size of the PPO minor phase decreases, thus improving the ductility and mechanical strength of the blend [15]. Yang et al. obtained similar results for nylon-6/poly(vinylidene fluoride) (PVDF) blends [14]. Moreover, graphene oxide has also revealed a good nucleating ability towards several semi-crystalline polymers, including for instance

isotactic polypropylene (iPP) [29-31], PVDF [32-34], PCL [35], and the two polymers object of the present study, PLLA and PBS [36,37].

As such, in the current part, the dual role of GO added in low amounts to PLLA/PBS blend is investigated. For a given phase composition of the blend (70/30 PLLA/PBS), different concentrations of GO (0.1 to 0.5 wt%) were introduced via melt-blending. Subsequently the polymer blend/GO nanocomposites were submitted to detailed characterization of their morphology and crystallization behavior, focusing in particular on the compatibilizing and nucleating effect of the graphene oxide additive.

4.2 Materials and methods

4.2.1. Materials

Poly(L-lactic acid) (PLLA) (Synterra 1010) was supplied by Synbra Technology bv (Etten-Leur, Netherlands). PLLA 1010 is a crystallizable grade of PLLA with a L-lactide content of about 99 wt. %. The melting point is in the range 175–180°C and the glass transition temperature (T_g) is located about 55-60°C. The polymer shows a melt flow rate (MFR) of about 12 g/10 min (190°C, 2.16 kg, ISO 1133) and a density of 1.25 g/cm3.

Poly(butylene succinate) (PBS) (PBI 003) was supplied by Natureplast (Caen, France). PBS (PBI 003) is a crystallizable polymer with a melting point in the range 110-115°C and a T_g of ca. -35°C. The MFR is about 15-25 g/10 min (190°C, 2.16 kg, ISO 1133) and its density is 1.26 g/cm3.

Graphene Oxide (GO) (796034) was purchased from Sigma-Aldrich. It consists of a powder of GO nanosheets (approximately15-20 sheets) with a degree of edge-oxidation of 4-10%. Acetone and anhydrous N,N-Dimethylformamide (DMF) (99.8% pure) were supplied by Sigma-Aldrich and used as received.

4.2.2 Preparation of PBS/GO masterbatches

PBS/GO masterbatches were prepared through a solution-mixing method, previously adopted for the preparation of PA/PPO/GO and nylon 6/PVDF/GO blend nanocomposites. At first, a suspension of GO in DMF was obtained by sonicating the mixture at 80°C for 1 h, in order to partially exfoliate the GOs into single-layer sheets [14,15,38]. The concentration of GO in the suspension was 1 mg/mL. Concomitantly, 15 g of PBS were dissolved in 50 mL of

DMF, by stirring at 100°C for 1 h. Subsequently, the GO suspension in DMF was added to the PBS solution and continuously stirred at 100°C for 10 min. Different amounts of suspension (50, 150 and 250 mL) were used, in order to obtain a final concentration in the blend of 0.1 wt%, 0.3 wt% and 0.5 wt%. The mixture was finally precipitated and coagulated by the addition of 400 mL of acetone. The precipitate was washed four times with acetone, filtered under vacuum overnight, and then dried at 60°C for 24 h, yielding PBS/GO masterbatches with the desired GO concentration [14,15].

4.2.3 Preparation of GO-Compatibilized PLLA/PBS blend nanocomposites

Before melt blending, the PLLA and PBS/GO masterbatches were dried at 60°C for 48 h. The PBS/GO masterbatches were melt blended with PLLA in different ratios, to obtain the following PLLA/PBS/GO compositions (70/30, 70/30/0.1, 70/30/0.3, 70/30/0.5 by weight). The melt blending was accomplished in a Plastograph Brabender internal mixer (W50 EHT, Brabender GmbH, Germany), at a temperature of 180°C with rotor speed of 60 rpm for 10 min, under continuous nitrogen flow.

4.2.4 Characterization

Field-emission Scanning electron microscopy: (FE-SEM)

The morphology of the fractured surface of blend nanocomposites was investigated using a Field-emission scanning electron microscope (Supra 40 VP model, Zeiss, Germany) at an accelerating voltage of1 kV. The specimens were submerged in liquid nitrogen for 30 min and fractured cryogenically. All samples were thinly sputter-coated with carbon using a Polaron E5100 sputter coater.

Transmission electron microscopy (TEM)

TEM analysis was performed by using a EM 900 microscope (Zeiss, Germany) operating at an accelerating voltage of 80 kV. Ultrathin sections (about 50 nm thick) were obtained using a EM FCS cryo-ultramicrotome (Leica Microsystems GmbH, Germany) equipped with a diamond knife. The sample was kept frozen at -80°C during sectioning.

Thermal analyses with Differential scanning calorimetry (DSC)

DSC was performed using a DSC1 STARe System (Mettler-Toledo, Switzerland). Several temperature protocols were employed in order to investigate in details the crystallization behavior of the PLLA/PBS blend and its nanocomposites with GO. All measurements were

performed using sample masses of between 3 and 5 mg and under a continuous nitrogen flow of 20 mL/min.

Non isothermal crystallization: The samples were molten at 200°C for 3 min and then cooled to -50°C at a rate of 10°C/min. After cooling, the polymer was subsequently heated to 200°C at 10°C/min.

Isothermal crystallization of neat PBS: The polymer was molten at 160°C for 3 min and subsequently cooled to the chosen isothermal crystallization temperature at 20°C/min and kept at the isothermal crystallization temperature for the required time. The isothermal temperatures were in the range 88-96°C.

Isothermal crystallization of PBS in blends: The minor component of the blend was crystallized isothermally after the crystallization of the PLLA matrix. To this aim, after the first non-isothermal run (see above), the sample was heated to 160°C at 10°C/min. This temperature is below the PLLA phase melting point, but high enough to completely melt the PBS domains. After 3 min at 160°C the blend sample was cooled to the chosen isothermal crystallization temperature in the range 98-105°C) at a rate of 20°C/min, and kept there for an adequate time.

Isothermal crystallization of PLLA: The PLLA component was molten at 200°C for 3 min and then cooled to the chosen isothermal crystallization temperature (in the range 115-140°C) at a rate of 20°C/min, and kept there for the required time.

Thermogravimetric analysis (TGA)

TGA was performed using a TGA Metller Toledo (STARe system Metllerthermobalance). The temperature was increased from 25 to 800°C with a heating rate of 10°C/min under a nitrogen flow of 80 mL/min.

4.3 Results and discussion

Morphological characterization

The morphology of neat PLLA/PBS blend and PLLA/PBS/GO blend nanocomposites was firstly observed by FE-SEM. Figure 4.1 reports the FE-SEM images of the fragile fracture surfaces of the neat PLLA/PBS blend (A,D) compared with those of the nanocomposites containing 0.3 and 0.5 wt% GO (B,E and C,F respectively). PLLA/PBS blends are known to be immiscible, with the two phases forming clearly separated domains [4,6]. As such, the

composition used in this study resulted in a typical sea-island morphology, in which PLLA constitutes the continuous matrix and the PBS minor phase is dispersed into spherical domains with an average diameter in the range of 1-2 μm (Figure 4.1). Slightly larger PBS domains are found in the blend nanocomposites, i.e., the size increases from around 1 μm in the neat PLLA/PBS blend to above 2 μm in PLLA/PBS blend containing 0.5 wt% GO.

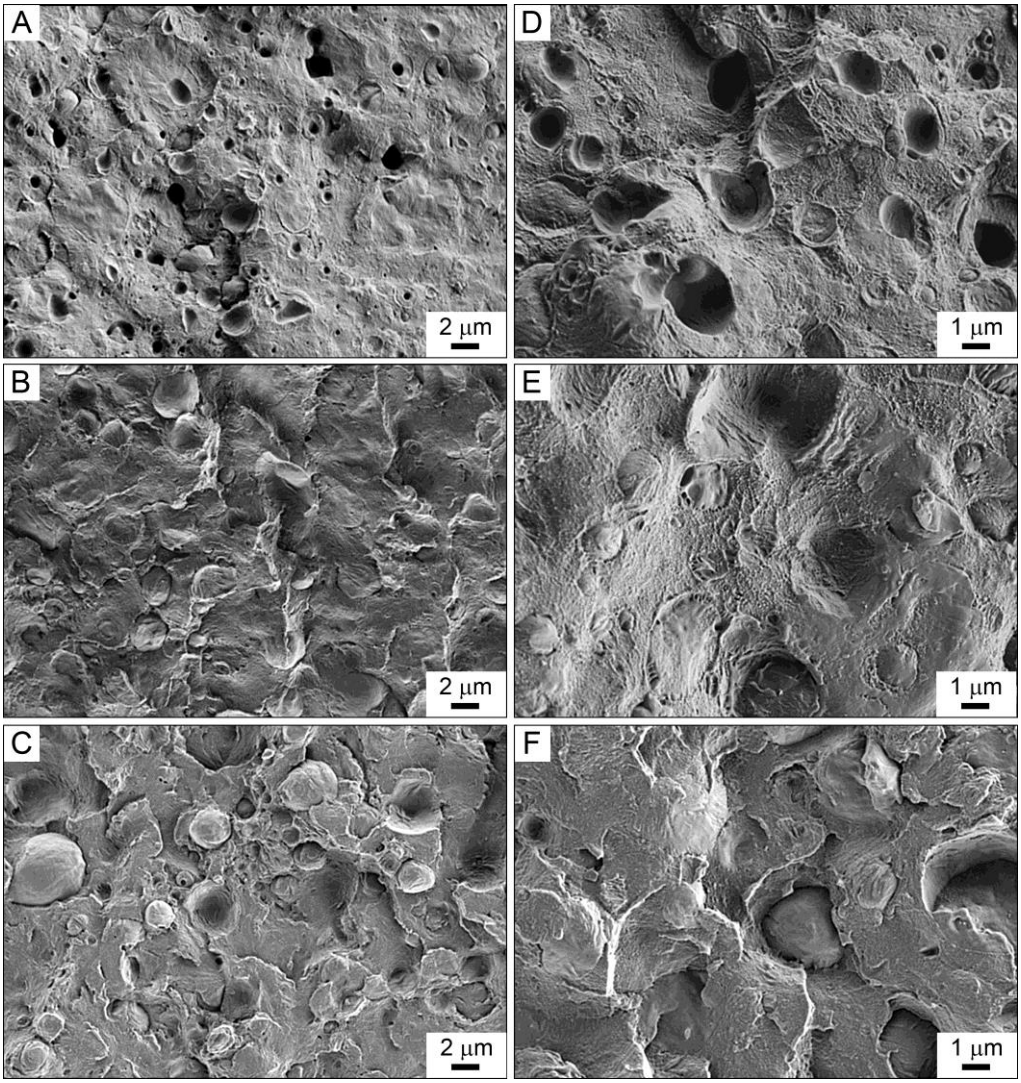

Figure 4.1. FE-SEM images of the PLLA/PBS/GO blend nanocomposites with different concentration of graphene oxide and at different magnifications (A, B and C 10.000 X; D, E and F 20.000 X). A and D (70/30/neat), B and E (70/30/0.3 wt%), C and F (70/30/0.5 wt%).

The fracture surface of the neat PLLA/PBS blend (Figure 4.1 A,D) shows a clear detachment of the PBS phase from the PLLA matrix: voids with a neat and smooth demarcation surface are in fact observed throughout the sample.

On the other hand, the morphology of fractured PLLA/PBS/GO blends nanocomposites (Figure 4.1 B-E, C-F) evidenced an improved adhesion between the two polymers. Indeed,

when GO is present: i) a considerably lower number of voids left by detached PBS droplets is observed; ii) an irregular surface appears in the cavities left by the detachment of the PBS domains. This fracture morphology is analogous to compatibilized immiscible polymer blends with or without graphene oxide [5,15]. Moreover, fibrillar structures localized at the interfaces between the two polymers are occasionally found (see Figure 4.1 E,F). Although the origin of this morphological entities is not clear, similar results were reported by Ye et al. by adding GO to PMMA/PS blends [27]. The observed morphological features indicate a higher interaction between PBS and PLLA, which could be induced by GO nanosheets located, at least in part, at the interface between the two polymers.

In order to investigate this hypothesis, TEM analysis of the blends nanocomposites has been performed; and some representative micrographs for PLLA/PBS/GO with 0.3 and 0.5 wt% GO additive are shown in Figure 4.2. The two different polyesters can be easily distinguished because of their difference in electron density that lead to sufficient contrast in the TEM image. The PBS domains appear darker than the PLLA matrix, with round/ellipsoidal shape and average sizes around 1-2 μm, in perfect agreement with the morphology disclosed by FE-SEM of fracture surfaces. Small stacks or aggregates of GO nanosheets can be easily recognized. The large majority of GO is located within the PBS phase, although occasionally some GO stacks are also found in the PLLA matrix. Figure 4.2 demonstrates that the dispersion of GO nanosheets is generally good, since also some isolated sheets are observed, together with the aggregate. Moreover, the extent of aggregation is minimal, since the observed lateral size of these aggregates is well below the micron: few hundreds nanometers, at most. The lower grey intensity of some areas of the aggregates indicates a lower number of GO nanosheets crossed by the electron beam, suggesting a good extent of exfoliation during the composite preparation. Although the TEM micrographs show that several GO nanosheets are located close to the phase boundary between the two immiscible polymers, an evident adsorption of the nanofiller at the interface could not be observed. Given that the TEM micrographs are a 2-D projection of the real 3-D bulk material, the possibility that GO stacks might in reality be at the boundaries between the two polymer phases at a different height of the PBS droplet, i.e., at the upper or lower interfaces, can not be ruled out. The enhanced adhesion between PLLA and PBS demonstrated with the FE-SEM could thus be due also to different reasons, such as the development of a transcrystalline layer at the polymer-polymer contact line.

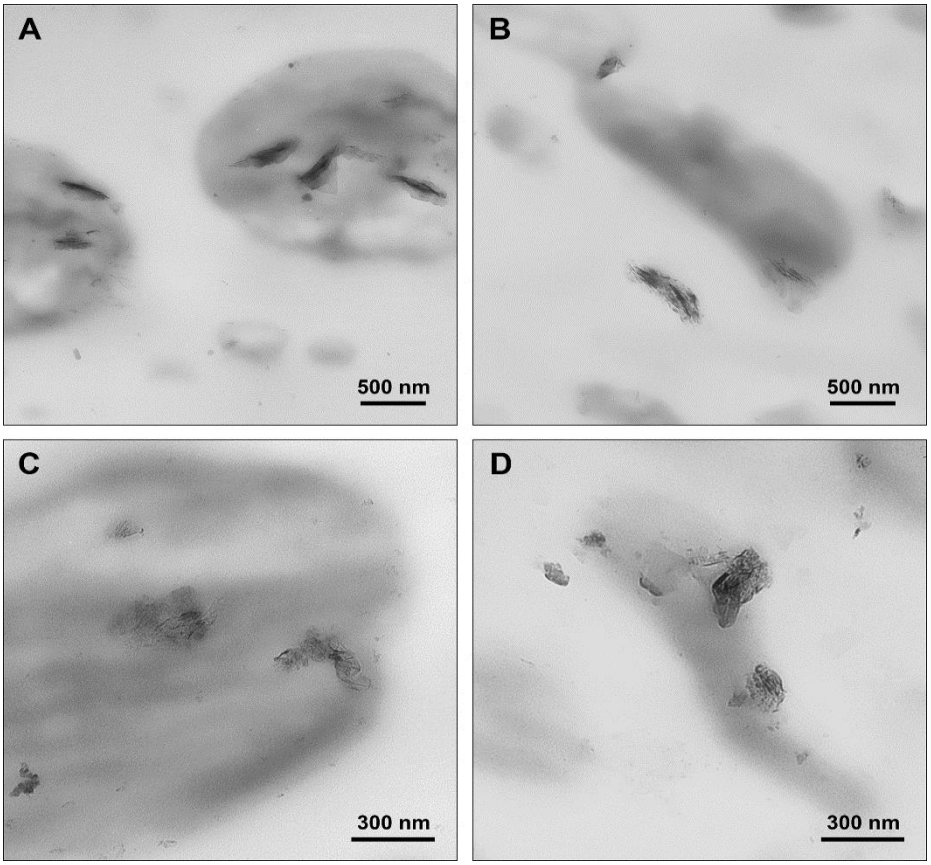

Figure 4.2. TEM micrographs at different magnifications of the PLLA/PBS/GO blend nanocomposites with different concentration of graphene oxide: 70/30/0.3 wt% GO (A,C), and 70/30/0.5 wt% GO (B,D).

Crystallization of PLLA/PBS/GO blend nanocomposites

The non-isothermal crystallization of the PLLA/PBS blend and nanocomposites with GO is investigated by differential scanning calorimetry, and the main results are reported in Figure 4.3. The investigated system being a double-crystalline polymer blend, it is possible to evaluate the effect of the nanofiller on the crystallization behavior of both polyesters.

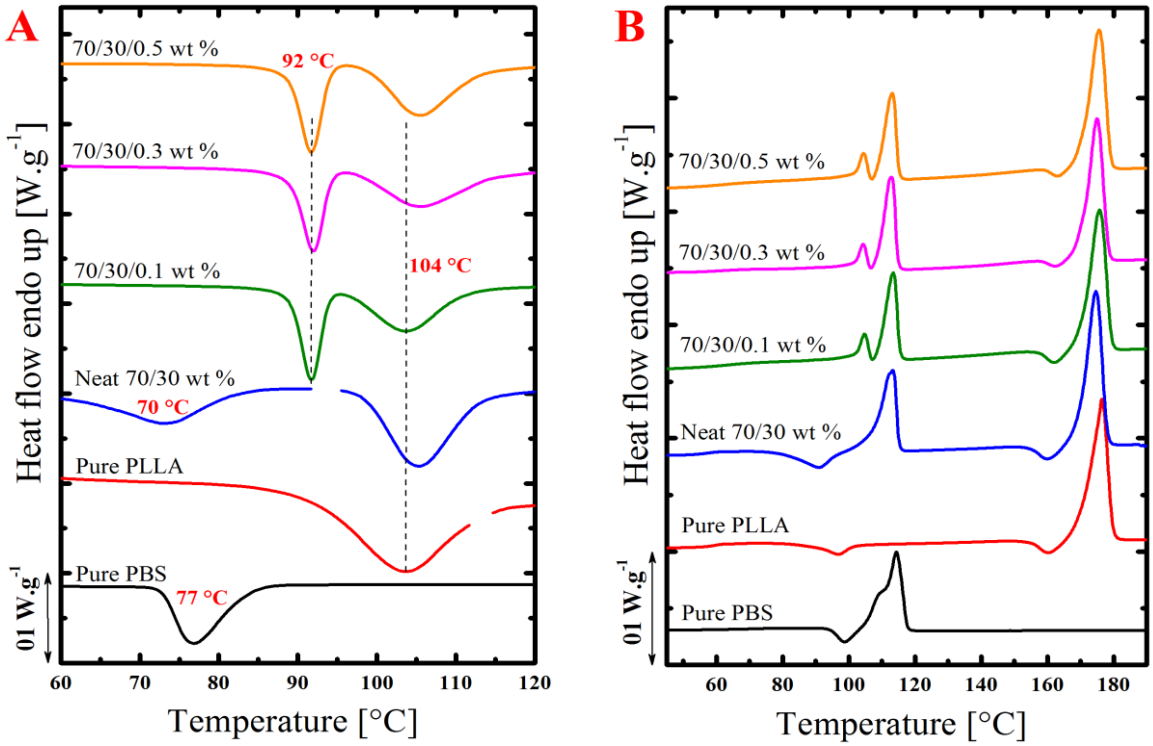

Figure 4.3. Cooling (A) and subsequent heating (B) DSC curves of the different PLLA/PBS/GO blend nanocomposites with various content of GO, compared to the neat 70/30 PLLA/PBS blend and the two pure polymers (scaled for their weight fraction in the blend).

At first, the crystallization behavior of the two components and of the neat 70/30 PLLA/PBS blend can be considered. PBS shows a crystallization exotherm around 77°C on cooling at 10°C/min, and the subsequent melting reveal a cold-crystallization of one of the polymers, followed by a broad melting characterized by re-crystallization phenomena. Pure PLLA partially crystallizes on cooling slightly above 100°C, and the crystallization process is completed during the heating scan. Just before melting the PLLA crystals, a slight exothermic event is observed, tentatively attributed to the reorganization of a disordered modification into the more stable α'-form [39,40]. Upon mixing the two polymers in a 70/30 PLLA/PBS weight ratio, the crystallization process is affected, while the melting curve is practically unaltered with respect to a combination of those of the pure components (Figure 4.3 B). When the PBS is the minor dispersed phase in the blend with PLLA, its crystallization temperature is decreased of about 5°C with respect to pure PBS (Figure 4.3 A). This effect is known to occur in immiscible blends: if the domain size of the minor component is small enough, fractionated crystallization can be observed, since most of the PBS droplets will be free of nucleating heterogeneities, and their crystallization takes place at higher undercooling. [41]. On the other hand, the crystallization of the PLLA component in the neat blend is slightly enhanced. This indicates a

weak nucleating activity of the PBS/PLLA interfaces. Although limited, this nucleating effect is rather interesting, because PBS droplets are still in the molten state, when the nucleation of the PLLA matrix on their surfaces occurs. Similar results have been previously reported, both for melt and cold-crystallization of PLLA in blends with PBS. [4,42]. The occurrence of this nucleation might be due to a low surface tension existing between PLLA lateral crystal surfaces and PBS melt. Nucleation at the interfaces between immiscible polymer components, during or after phase separation, has been predicted theoretically [43] and observed experimentally also in amorphous/semicrystalline polymer pairs [44].

The addition of relatively small quantities of graphene oxide has a large impact on the crystallization behavior of 70/30 PLLA/PBS blend. In particular, the crystallization temperature of the PBS dispersed phase in the nanocomposites shows a remarkable increase of about 20°C with respect to the one in the neat blend. The nucleating effect of GO on PBS is already observed at the lower loading of nanofiller, and practically does not depend on GO concentration. The measured change in crystallization temperature is remarkable, in comparison to previous literature results, where only a mild nucleation effect is observed, when a similar concentration of GO is added to PBS [37,45,46]. The difference with literature results can be attributed to a different degree of dispersion of the nanofiller, obtained thanks to the solution-assisted nanocomposite preparation method. Indeed, the TEM micrographs shown in Figure 4.2 demonstrate that the GO particles are partially exfoliated and the extent of aggregation is minor, as only aggregates with size of few hundreds nanometers are found. On the other hand, GO have only a small accelerating effect on PLLA crystallization, especially at the highest nanofiller concentrations. This result is in agreement with previous literature on PLLA/GO composites, which documented a limited nucleating effect of the nanofiller on polylactide. [47-49] Moreover, this modest effect observed in the PLLA/PBS blend nanocomposites could be ascribed to the particular morphology of the system. The GO might not efficiently be transferred from the PBS/GO masterbatch to the bulk of PLLA phase during the mixing stage. In fact, TEM results reported in Figure 4.2, indicate that graphene oxide are most frequently found inside the PBS domains. As such, nucleation of PLLA by the action of GO can occur mainly at the PBS/PLLA interfaces, or thanks to the few that moved to the bulk of PLLA matrix form the PBS droplets. The role of GO as heterogeneous nucleants for both crystalline polymers would be further explored in the following, with self-nucleation and isothermal crystallization experiments. We note that the melting behavior of PLLA/PBS blends (Figure 4.3 B) is not significantly affected by the addition of graphene oxide. The only

meaningful effect is the appearance of a more marked melting-recrystallization behavior of PBS, with evident double melting peaks for all the employed GO concentrations. The double melting peaks of PBS is widely discussed in the literature, and commonly interpreted as a melting-recrystallization phenomenon. Its occurrence in the present blend nanocomposite is related to the increase in the PBS phase crystallization temperature [50-53].

The relevant nucleating ability of GO on the PBS phase can be quantitatively described, by using the nucleation efficiently scale concept introduced by Lotz et al. in order to define a scale of nucleation efficiency, two reference values corresponding to a minimum and maximum in the crystallization rate should be chosen. When non-isothermal crystallization is considered, the minimum value obviously corresponds to the crystallization temperature of the neat, non-nucleated polymer. The maximum value is calculated by performing self-nucleation experiments. The polymer is submitted to a melting procedure at decreasing temperatures, until some crystalline seeds remain in the molten material and act as "self-nuclei" upon re-crystallization. The detailed procedure is described elsewhere. Self-nucleation allows obtaining a relevant increase of the crystallization temperature, typically of 20°C or more. The crystallization temperature of the polymer at the "optimal" self-nucleation temperature is taken as the 100% value of the nucleating efficiency scale. Any given nucleating agent can thus be quantitatively evaluated, by comparing the crystallization temperature increase of the nucleated sample with that provoked by self-nucleation [54].

The nucleating efficiency of various nucleants in different semicrystalline polymer matrices, rarely exceeds 60% [55-58], although exceptional cases of "supernucleation" (with nucleating efficiency above 100%) are reported in specially prepared polymer / carbon nanotubes composites [59]. In Figure (4.4 A), the crystallization temperature of the PBS phase in the neat 70/30 PLLA/PBS blend at different self-nucleation (SN) temperatures is compared with that of PLLA/PBS/GO blend nanocomposite (with 0.5 wt% GO). Note that the values for the non-self-nucleated blend and for the nanocomposite have actually been obtained by cooling from the melt at 200°C, but they are reported at an arbitrary SN temperature, for the sake of comparison. The PBS crystallization temperature remain constant and substantially equal to the one characteristic of non-self-nucleated melts (i.e. cooled from 200°C) for melt annealing temperatures between 160 and 130°C. Decreasing the self-nucleation temperature from 130°C to about 115°C results in a large increase of the PBS phase crystallization temperatures, of approximately 25°C. The crystallization temperature corresponding to a 100% nucleating efficiency value is thus about 97°C. The one obtained in PLLA/PBS/GO nanocomposites,

independently of the GO concentration is 92°C, resulting in a relative efficiency slightly higher than 80%. This value of nucleating efficiency, which is reached already at a concentration of 0.1 wt%, is surely among the highest ever reported in the literature for an additive which is dispersed in the polymer via common solution/melt routes. It should be noted that in nucleation efficiencies higher than 100% are sometime observed in nanocomposites with high degree of nanofiller dispersion [59]. As such, the proposed preparation method enhances the relatively mild nucleating efficiency of GO to the level of the best known nucleants for poly(butylene succinate), when used at comparable concentration. [60-62].

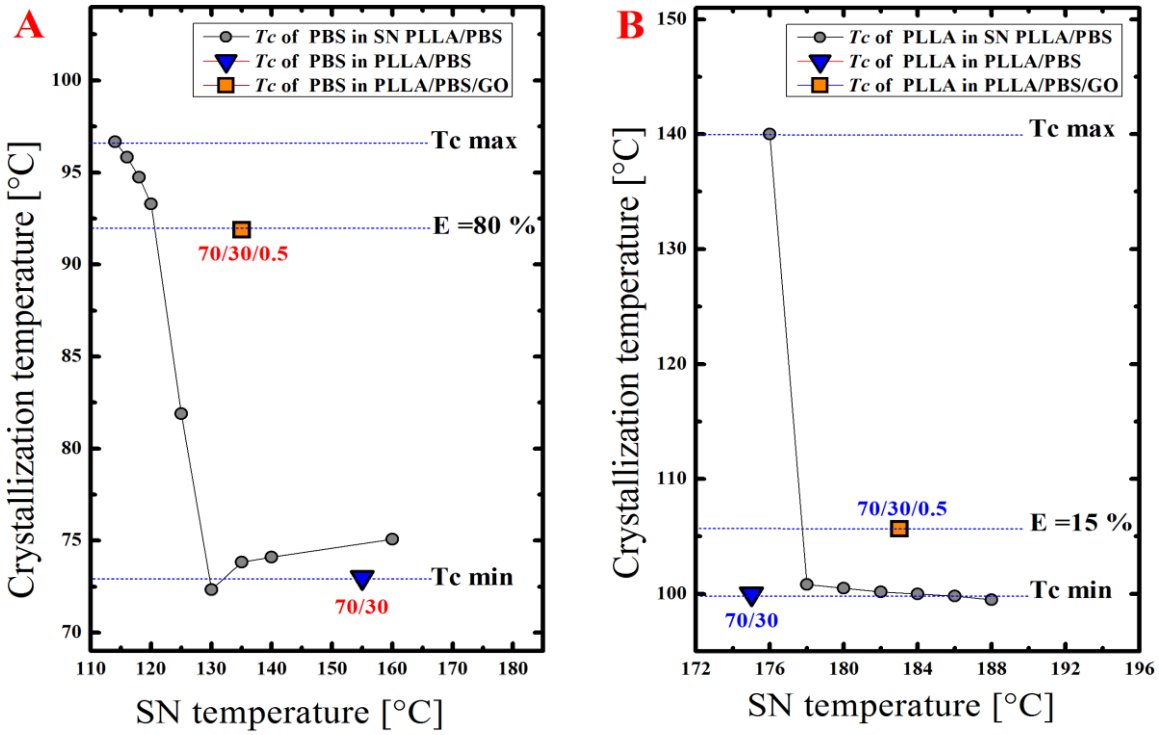

Figure 4.4. Crystallization temperature of the PBS (A) and PLLA (B) phases in PLLA/PBS neat blend as a function of the self-nucleation (SN) temperature. The data of the non-self-nucleated blend and of a PLLA/PBS/GO nanocomposite are added for comparison (see text).

In Figure (4.4 B) the nucleating efficiency of GO on the PLLA matrix is determined by comparison with self-nucleated PLLA. The self-nucleation behavior of PLLA in neat PLLA/PBS blend is analogous to the one of the PBS component: the crystallization temperature increase by more than 30°C for seeding temperatures lower than 175°C. On the other hand, the nucleation effect of GO nanosheets is much less marked with respect to the one measured for PBS, see Figure (4.4 A). In fact, an increase of crystallization temperature about 5°C only with respect to non-self-nucleated melt is observed. This shift corresponds to nucleating efficiency of 15%. The differences in nucleating ability of GO towards the two polymers is ascribed to

morphology of the blend nanocomposites, as previously discussed. Indeed, the majority of graphene oxide are located inside the PBS phase or at the phase boundaries (see Figure 4.1 and Figure 4.2).

The high nucleation density, naturally occurring in semicrystalline polymers when non-isothermally crystallized at relatively low temperatures, might effectively hide the effect of nucleating agents with low efficiency. In fact, the effect of an enhanced nucleation density on crystallization kinetics can be detected only if the number of extra-nuclei is at least comparable to the ”reference” concentration of nuclei of the neat system. Given that, this reference number is lower at higher crystallization temperature; isothermal crystallization experiments at the proper temperature could possibly highlight mild nucleating effects. Therefore, an isothermal crystallization protocol is separately applied to the two polyesters. Examples of typical DSC results are shown in Figure 4.5 for PBS (A) and PLLA (B), respectively. Figure (4.5 A) shows the comparison between neat PBS and PLLA/PBS/GO with different content of nanofiller. Due to the differences in crystallization kinetics, the neat PLLA/PBS blend could not be probed at similar temperatures. Also, neat PBS needs to be crystallized at 2°C higher undercooling with respect to the PLLA/PBS/GO nanocomposites to display a similar kinetics. Yet, crystallization is completed in about 200 seconds for the nanocomposites, while it requires more than 1000 seconds in the neat PBS homopolymer. No effect of GO concentration is observed, indicating that its nucleation activity on PBS saturates already at concentrations of 0.1 wt% or lower. Thus, a different nucleating effect and saturation concentration of the nanofiller exists, with respect to PBS, confirming the deductions of non-isothermal crystallization experiments. The crystallization of the PLLA phase in PLLA/PBS neat blend and in the blend with GO nanofiller at 124°C is shown as an example in Figure (4.5 B). In this case, a smaller accelerating effect is obtained: the overall crystallization rate, as evaluated form the peak-time, is about three time faster for 0.3 and 0.5 wt% GO, while it is only slightly faster for the 0.1 wt%.

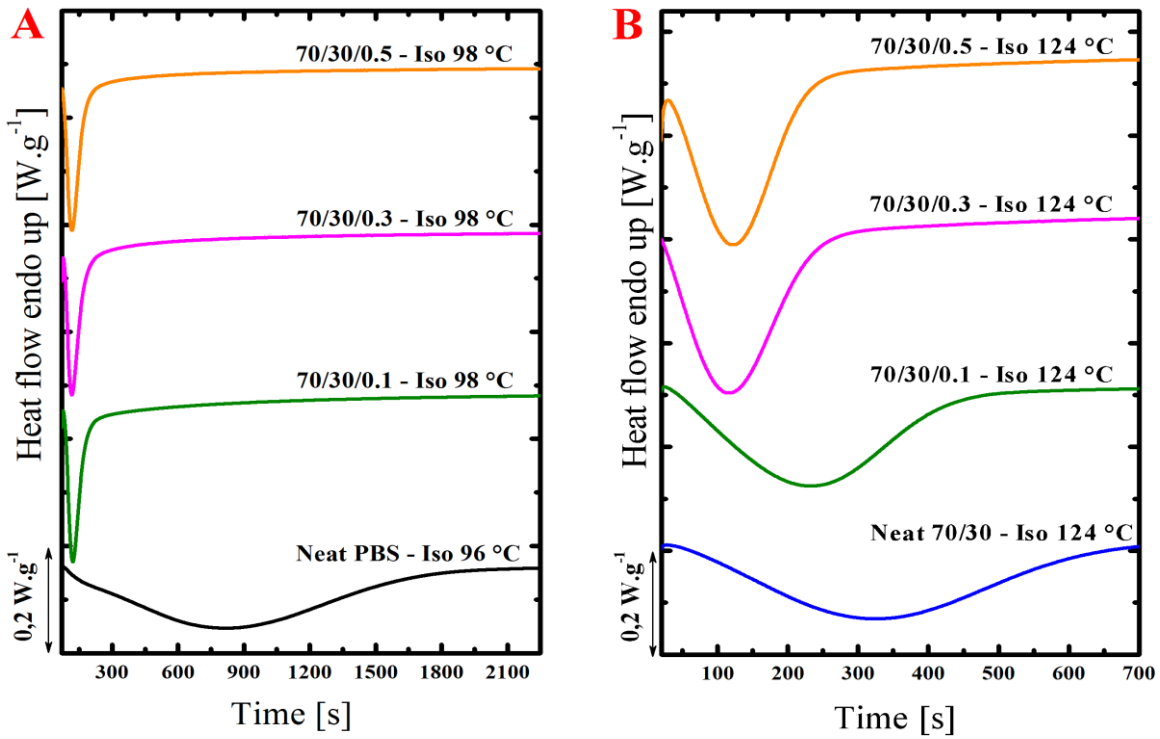

Figure 4.5. Heat flow as a function of time during the crystallization of PBS (A) and PLLA (B) phase in PLLA/PBS blend and PLLA/PBS/GO blend nanocomposites.

The results of overall crystallization kinetics of the two phases for the pure components, the 70/30 PLLA/PBS blend and the blend/GO nanocomposites are collected in a wider range of undercoolings and shown in Figure 4.6. The peak time of crystallization is chosen as a representative parameter to describe the overall isothermal crystallization kinetics. In Figure (4.6 A) the transformation of the PBS phase is considered. For all samples, the expected increasing trend with increasing crystallization temperature is observed, with an increase of the crystallization time of about one order of magnitude by decreasing the undercooling by less than 10°C. The nucleating effect of GO with respect to pure PBS and neat PLLA/PBS blend can be appreciated by considering the shift in undercooling required to obtain a comparable crystallization kinetics.

Indeed, the nanocomposites possess a kinetics comparable to that of the pure PBS at much lower undercoolings: the shift in temperature is around 10°C. This difference is even more important if one would consider the PLLA/PBS blend. Unfortunately, the slow crystallization kinetics of the neat blend prevents the direct measurement of latent heat evolution in isothermal conditions. The crystallization kinetics is practically independent of GO concentration, although small differences are observed between 0.1 and the higher concentrations at crystallization temperatures above 102°C.

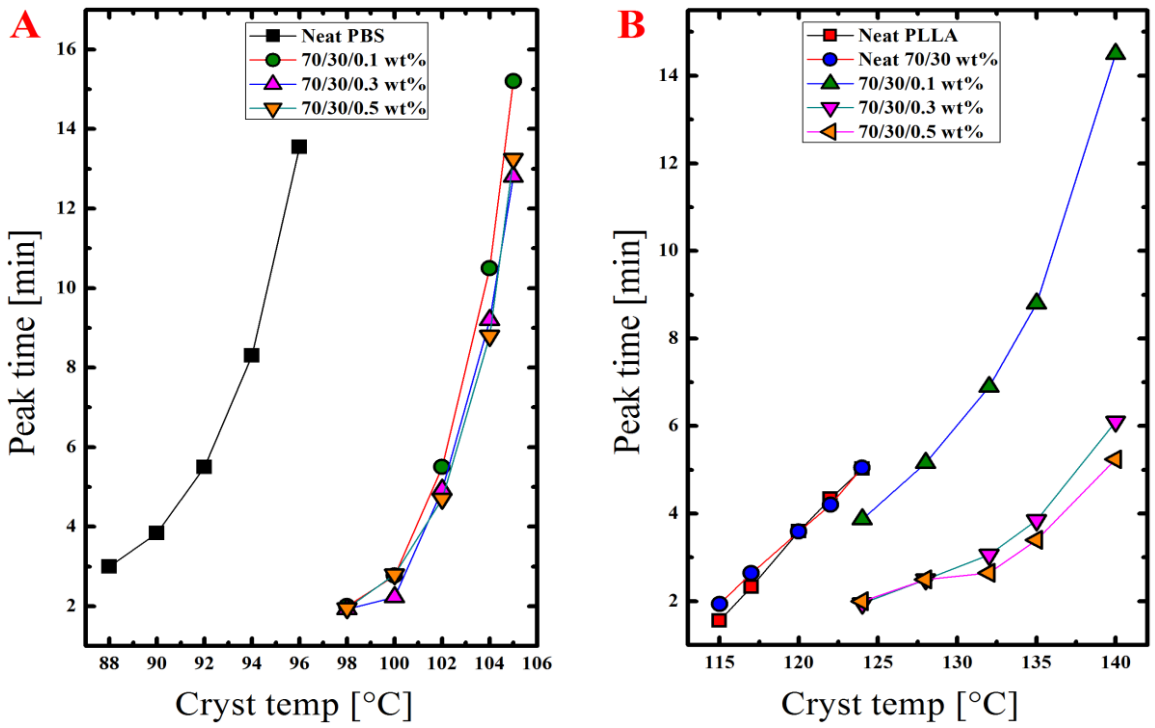

Figure 4.6. Crystallization peak time as a function of crystallization temperature for PBS (A) and PLLA (B) phase in PLLA/PBS blend and PLLA/PBS/GO blend nanocomposites.

Similarly, the crystallization kinetics data of the PLLA phase in the neat polymer, blend and nanocomposites are compared in Figure (4.6 B). It can be noted that, while the nucleating effect of GO was almost unnoticed in non-isothermal crystallization, by performing isothermal measurement at relatively high temperature it clearly shows up. In fact, adding 0.3-0.5 wt% of GO corresponds to a gain of 15°C in undercoolings in terms of crystallization kinetics. In other words, the nanocomposites should be crystallized at much higher temperatures to have a rate of crystallization similar to that of neat PLLA/PBS blend. Contrary to PBS, a concentration effect is found for the nucleating efficiency of PLLA: the efficiency increases going from 0.1 to 0.3 wt%, and seems to saturate at this concentration. Incidentally, the nucleation effect of PBS molten droplet on PLLA crystallization, which was deduced from non-isothermal crystallization experiments (see Figure 4.3 A) is not confirmed in isothermal experiment. We recall that surfaces with different nucleating ability become effective at different temperatures, the lower the efficiency of the nucleating surface, the higher the required undercooling to observe this effect. Therefore, the lack of nucleating effect of molten PBS on PLLA at high temperature might indicate a very low activity of this heterogeneity, which becomes effective only at much lower crystallization temperatures, such as those reached in non-isothermal crystallization.

Thermal stability of PLLA/PBS/GO blend nanocomposites

Figure 4.7 reports the weight loss of the neat PLLA/PBS and PLLA/PBS/GO blends and nanocomposites as a function of temperature. In all the cases, the separate thermal degradation of the PLLA and PBS components can be noticed. PLLA degradation occurs roughly between 300 and 360°C, while PBS is more thermally stable and decomposes between 370 and 430°C.

The addition of small amounts of GO nanosheets to PLLA/PBS blends does affect meaningfully the thermal degradation of the PBS phase. On the other hand, presence of GO nanosheets result in a clear enhancement of the thermal stability of the PLLA phase. Considering $T_{90\%}$ of PLLA (temperature in which PLLA reached 10% of the total weight loss), gradual increase by increasing the GOs content is observed and $T_{90\%}$ increased from 315°C for the neat 70/30 PLLA/PBS to 333°C for 70/30/0.5 PLLA/PBS/GO. A similar enhancement effect of graphene oxide on the polymer thermal stability has been observed in PLLA/GO nanocomposites [63,64], and PA/PPO immiscible blends [15].

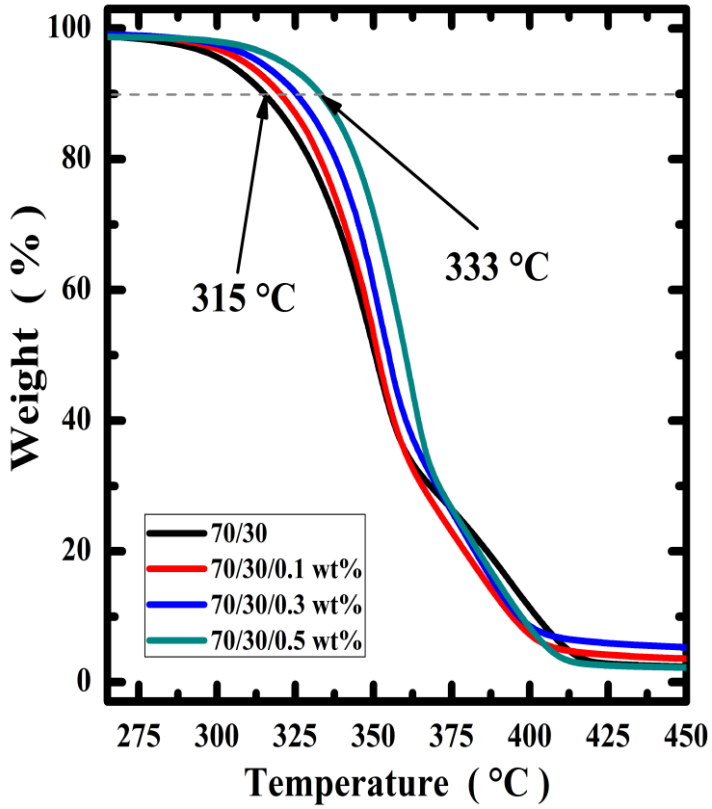

Figure 4.7. TGA curves (evaluation of weight loss as a function of temperature) of neat PLLA/PBS and PLLA/PBS/GO blend nanocomposites.

Such an enhancement in thermal stability is to be expected because GOs are proposed to act as barriers (thermal and gas) in polymer matrices to delay the permeation of oxygen and the escape of volatile degradation products, thus improving the thermal stability of the resulting polymer blends was obtained [15,63,64].

4.4 Conclusions

the interest of using graphene oxide to improve the properties of polymer nanocomposites is recently rising. Similarly, graphene, graphene oxide and other nanoparticles are frequently used to modify the interface between immiscible polymer blends (two-phases, three components systems). In this work, the relation between the obtained multiphase morphology of PLLA/PBS/GO blend nanocomposites was thoroughly investigated, with particular attention to the distribution of GO in the two polymers and at their interfaces.

The morphological information obtained with Scanning and Transmission Electron Microscopy is the basis to understand the role of GO in the nucleation process of the two crystalline blend components. GO improves the adhesion between the two polymers, improve slightly the thermal stability of the system, and have nucleation ability towards both PBS and PLLA. In particular, a remarkable effect is found on the minor PBS dispersed phase.

4.5 References

1. Wang R, Wang S, Zhang Y, Wan C, Ma P (2009) Toughening modification of PLLA/PBS blends via in situ compatibilization. Polym. Eng. Sci. 49:26-33
2. Chen G-X, Kim H-S, Kim E-S, Yoon J-S (2005) Compatibilization-like effect of reactive organoclay on the poly(l-lactide)/poly(butylene succinate) blends. Polymer. 46:11829-11836
3. Elwathig H, You W, He J. Yu M (2013) Dynamic mechanical properties and thermal stability of poly(lactic acid) and poly(butylene succinate) blends composites. J. Fiber Bioeng. Inf. 6:85-94
4. Yokohara T, Yamaguchi M (2008) Structure and properties for biomass-based polyester blends of PLA and PBS. Eur. Polym. J. 44:677-685

5. Nerkar M, Ramsay JA, Ramsay BA, Vasileiou AA, Kontopoulou M (2015) Improvements in the melt and solid-state properties of poly(lactic acid), poly-3-hydroxyoctanoate and their blends through reactive modification. Polymer. 64:51-61
6. Persenaire O, Quintana R, Lemmouchi Y, Sampson J, Martin S, Bonnaud L, Dubois P (2014) Reactive compatibilization of poly(l-lactide)/poly(butylene succinate) blends through polyester maleation: from materials to properties. Polym. Int. 63:1724-1731
7. Anderson KS, Schreck KM, Hillmyer MA (2008) Toughening Polylactide. Polym. Rev. 48:85-108
8. Homklin R, Hongsriphan N (2013) Mechanical and Thermal Properties of PLA/PBS Co-continuous Blends Adding Nucleating Agent. Energy Procedia. 34:871-879
9. Robeson L (2014) Historical Perspective of Advances in the Science and Technology of Polymer Blends. Polymers. 6:1251
10. Paul DR, Barlow JW (Eds) (1979) A Brief Review of Polymer Blend Technology. In: Cooper SL, Estes GM (Eds) Multiphase Polymers, vol 176. American Chemical Society, Washington, p 315-335
11. Buasri A, Buranasing G, Piemjaiswang R, Yousatit S, Loryuenyong V (2014) Effect of Titanium Dioxide Nanoparticles on Mechanical and Thermal Properties of Poly(Lactic Acid) and Poly(Butylene Succinate) Blends. Adv. Sci.Tech. 96:33-38
12. Mofokeng JP, Luyt AS (2015) Dynamic mechanical properties of PLA/PHBV, PLA/PCL, PHBV/PCL blends and their nanocomposites with TiO2 as nanofiller. Thermochimi. Acta. 613:41-53
13. Monticelli O, Calabrese M, Gardella L, Fina A, Gioffredi E (2014) Silsesquioxanes: Novel compatibilizing agents for tuning the microstructure and properties of PLA/PCL immiscible blends. Eur. Polym. J. 58:69-78
14. Yang J, Feng C, Dai J, Zhang N, Huang T, Wang Y (2013) Compatibilization of immiscible nylon 6/poly(vinylidene fluoride) blends using graphene oxides. Polym. Int. 62:1085-1093
15. Cao Y, Zhang J, Feng J, Wu P (2011) Compatibilization of Immiscible Polymer Blends Using Graphene Oxide Sheets. ACS Nano. 5:5920-5927
16. Ku KH, Yang H, Jang SG, Bang J, Kim BJ (2016) Tailoring block copolymer and polymer blend morphology using nanoparticle surfactants. J. Polym. Sci., Part A: Polym. Chem. 54:228-237
17. Jalali Dil E, Favis BD (2015) Localization of micro- and nano-silica particles in heterophase poly(lactic acid)/poly(butylene adipate-co-terephthalate) blends. Polymer. 76:295-306

18. Ock HG, Kim DH, Ahn KH, Lee SJ, Maia JM (2016) Effect of organoclay as a compatibilizer in poly(lactic acid) and natural rubber blends. Eur. Polym. J. 76:216-227
19. Vrsaljko D, Macut D, Kovačević V (2015) Potential role of nanofillers as compatibilizers in immiscible PLA/LDPE Blends. J. Appl. Polym. Sci. 132 :41414/1-41414/14
20. Arrieta MP, Fortunati E, Dominici F, López J, Kenny JM (2015) Bionanocomposite films based on plasticized PLA–PHB/cellulose nanocrystal blends. Carbohydr. Polym. 121:265-275
21. Noori FTM, Ali NA (2014) Study the mechanical and thermal properties of biodegradable polylactic acid / polyethylene glycol nanocomposites. IJAIEM. 3, 459-464
22. Shibata M, Inoue Y, Miyoshi M (2006) Mechanical properties, morphology, and crystallization behavior of blends of poly(l-lactide) with poly(butylene succinate-co-l-lactate) and poly(butylene succinate). Polymer. 47:3557-3564
23. Zhang X, Zhang Y (2016) Reinforcement effect of poly(butylene succinate) (PBS)-grafted cellulose nanocrystal on toughened PBS/polylactic acid blends. Carbohydr. Polym. 140:374-382
24. Luzi F, Fortunati E, Jiménez A, Puglia D, Pezzolla D, Gigliotti G, Kenny JM, Chiralt A, Torre L (2016) Production and characterization of PLLA_PBS biodegradable blends reinforced with cellulose nanocrystals extracted from hemp fibers. Ind. Crops Prod. 93, 276-289
25. Deng Y, Thomas NL (2015) Blending poly(butylene succinate) with poly(lactic acid): Ductility and phase inversion effects. Eur. Polym. J. 71:534-546
26. Kawamoto N, Sakai A, Horikoshi T, Urushihara T, Tobita E (2007) Physical and mechanical properties of poly(L-lactic acid) nucleated by dibenzoylhydrazide compound. J. Appl. Polym. Sci. 103:244-250
27. Ye S, Cao Y, Feng J, Wu P (2013) Temperature-dependent compatibilizing effect of graphene oxide as a compatibilizer for immiscible polymer blends. RSC Adv. 3:7987-7995
28. Cao Y, Feng J, Wu P (2012) Polypropylene-grafted graphene oxide sheets as multifunctional compatibilizers for polyolefin-based polymer blends. J. Mater. Chem. 22:14997-15005
29. Tong Y, Lin Y, Wang S, Song M (2015) A study of crystallisation of poly (ethylene oxide) and polypropylene on graphene surface. Polymer. 73:52-61
30. Yang S, Li Y, Liang Y-Y, Wang W-J, Luo Y, Xu J-Z, Li Z-M (2016) Graphene oxide induced isotactic polypropylene crystallization: role of structural reduction. RSC Adv. 6:23930-23941

31. Xu J-Z, Liang Y-Y, Huang H-D, Zhong G-J, Lei J, Chen C, Li Z-M (2012) Isothermal and nonisothermal crystallization of isotactic polypropylene/graphene oxide nanosheet nanocomposites. J. Polym. Res. 19:9975-9982
32. He L, Cui B, Jia N, Sun J, Xia G, Zhang H, Song R (2016) Enhanced β Crystalline Phase in Poly(vinylidene fluoride) via the Incorporation of Graphene Oxide Sheets assisted by Supercritical CO2 Treatment. J. Macromol. Sci. Part B Phys. 55:503-517
33. Tong J, Huang H-X, Wu M (2016) Structure and properties of pvdf/go nanocomposites prepared by water-assisted mixing extrusion. In: ANTEC Plastics Technology Conference, Indianapolis, USA, p 488-492
34. Hu Y-C, Hsu W-L, Wang Y-T, Ho C-T, Chang P-Z (2014) Enhance the Pyroelectricity of Polyvinylidene Fluoride by Graphene-Oxide Doping. Sensors. 14:6877
35. Wang B, Li Y, Weng G, Jiang Z, Chen P, Wang Z, Gu Q (2014) Reduced graphene oxide enhances the crystallization and orientation of poly(ε-caprolactone). Compos. Sci. Technol. 96:63-70
36. Zhao L, Liu X, Zhang R, He H, Jin T, Zhang J (2015) Unique Morphology in Polylactide/Graphene Oxide Nanocomposites. J. Macromol. Sci. Part B Phys. 54:45-57
37. Li Y-D, Li H, Du A-K, Wang M, Zeng J-B (2017) Morphology and isothermal crystallization of graphene oxide reinforced biodegradable poly(butylene succinate). Polym. Test. 59:1-9
38. Paredes JI, Villar-Rodil S, Martínez-Alonso A, Tascón JMD (2008) Graphene Oxide Dispersions in Organic Solvents. Langmuir. 24:10560-10564
39. Kawai T, Rahman N, Matsuba G, Nishida K, Kanaya T, Nakano M, Okamoto H, Kawada J, Usuki A, Honma N, Nakajima K, Matsuda M (2007) Crystallization and Melting Behavior of Poly (l-lactic Acid). Macromolecules. 40:9463-9469
40. Androsch R, Schick C, Di Lorenzo ML (2014) Melting of Conformationally Disordered Crystals (α′-Phase) of Poly(l-lactic acid). Macromol. Chem. Phys. 215:1134-1139
41. Santana OO, Müller AJ (1994) Homogeneous nucleation of the dispersed crystallisable component of immiscible polymer blends. Polym. Bull. 32:471-477
42. Wu D, Yuan L, Laredo E, Zhang M, Zhou W (2012) Interfacial Properties, Viscoelasticity, and Thermal Behaviors of Poly(butylene succinate)/Polylactide Blend. Ind. Eng. Chem. Res. 51:2290-2298
43. Mitra MK, Muthukumar M (2010) Theory of spinodal decomposition assisted crystallization in binary mixtures. J. Chem. Phys. 132:184908

44. Shi W, Chen F, Zhang Y, Han CC (2012) Viscoelastic Phase Separation and Interface Assisted Crystallization in a Highly Immiscible iPP/PMMA Blend. ACS Macro Lett. 1:1086-1089
45. Wang XW, Zhang C-A, Wang PL, Zhao J, Zhang W, Ji JH (2012) Enhanced Performance of Biodegradable Poly(butylene succinate)/Graphene Oxide Nanocomposites via in Situ Polymerization. Langmuir. 28:7091-7095
46. Wan C, Chen B (2013) Reinforcement of biodegradable poly(butylene succinate) with low loadings of graphene oxide. J. Appl. Polym. Sci. 127:5094-5099
47. Geng L-H, Peng X-F, Jing X, Li L-W, Huang A, Xu B-P, Chen B-Y, Mi H-Y (2016) Investigation of poly(l-lactic acid)/graphene oxide composites crystallization and nanopore foaming behaviors via supercritical carbon dioxide low temperature foaming. J. Mater. Res. 31:348-359
48. Chen Y, Yao X., Gu Q, Pan Z (2013) Non-isothermal crystallization kinetics of poly (lactic acid)/graphene nanocomposites. J. Polym. Eng. 33:163-171
49. Wu D, Cheng Y, Feng S, Yao Z, Zhang M (2013) Crystallization Behavior of Polylactide/Graphene Composites. Ind. Eng. Chem. Res. 52:6731-6739
50. Yoo ES, Im SS (1999) Melting behavior of poly(butylene succinate) during heating scan by DSC. J. Polym. Sci., Part B: Polym. Phys. 37:1357-1366
51. Wang X, Zhou J, Li L (2007) Multiple melting behavior of poly(butylene succinate). Eur. Polym. J. 43:3163-3170
52. Yasuniwa M, Satou T (2002) Multiple melting behavior of poly(butylene succinate). I. Thermal analysis of melt-crystallized samples. J. Polym. Sci., Part B: Polym. Phys. 40:2411-2420
53. Yasuniwa M, Tsubakihara S, Satou T, Iura K (2005) Multiple melting behavior of poly(butylene succinate). II. Thermal analysis of isothermal crystallization and melting process. J. Polym. Sci., Part B: Polym. Phys. 43:2039-2047
54. Fillon B, Thierry A, Lotz B, Wittmann JC (1994) Efficiency scale for polymer nucleating agents J. therm. Anal. 42:721-731
55. Sabino MA, Ronca G, Müller AJ (2000) Heterogeneous nucleation and self-nucleation of poly(p-dioxanone). J. Mater. Sci. 35:5071-5084
56. Yin H-Y, Wei X-F, Bao R-Y, Dong Q-X, Liu Z-Y, Yang W, Xie B-H, Yang M-B (2015) High-melting-point crystals of poly(l-lactic acid) (PLLA): the most efficient nucleating agent to enhance the crystallization of PLLA. CrystEngComm. 17:2310-2320

57. Schmidt SC, Hillmyer MA (2000) Polylactide stereocomplex crystallites as nucleating agents for isotactic polylactide. J. Polym. Sci., Part B: Polym. Phys. 39:300-313
58. Song P, Wei Z, Liang J, Chen G, Zhang W (2011) Crystallization behavior and nucleation analysis of poly(l-lactic acid) with a multiamide nucleating agent. Polym. Eng. Sci. 52:1058-1068
59. Müller AJ, Arnal ML, Trujillo M, Lorenzo AT (2011) Super-nucleation in nanocomposites and confinement effects on the crystallizable components within block copolymers, miktoarm star copolymers and nanocomposites. Eur. Polym. J. 47:614-629
60. Filizgok S, Kodal M, Ozkoc G (2016) Non-isothermal crystallization kinetics and dynamic mechanical properties of poly(Butylene succinate) nanocomposites with different type of carbonaceous nanoparticles. Polym. Compos. 39:2705-2721
61. Tang Y-R, Lin D-W, Gao Y, Xu J, Guo B-H (2014) Prominent Nucleating Effect of Finely Dispersed Hydroxyl-Functional Hexagonal Boron Nitride on Biodegradable Poly(butylene succinate). Ind. Eng. Chem. Res. 53:4689-4696
62. Ye H-M, Tang Y-R, Xu J, Guo B-H (2013) Role of Poly(butylene fumarate) on Crystallization Behavior of Poly(butylene succinate). Ind. Eng. Chem. Res. 52:10682-10689
63. Huang H-D, Ren P-G, Xu J-Z, Xu L, Zhong G-J, Hsiao BS, Li Z-M (2014) Improved barrier properties of poly(lactic acid) with randomly dispersed graphene oxide nanosheets. J. Membr. Sci. 464:110-118
64. Chieng WB, Ibrahim AN, Yunus MW, Hussein ZM, Then YY, Loo YY (2014) Effects of Graphene Nanoplatelets and Reduced Graphene Oxide on Poly(lactic acid) and Plasticized Poly(lactic acid): A Comparative Study. Polymers. 6 :2232-2246

Nucleation and crystallization in binary and ternary blends based on PLA, PCL, and PBS

Partially reproduced from: S.E. Fenni et al. "Morphology, nucleation and crystallization behavior of ternary blends based on PLA, PCL, and PBS with partial wetting morphology". **To be submitted soon.**

Chapter V

Nucleation and crystallization in binary and ternary blends based on PLA, PCL, and PBS

5.1 Introduction

Polymer blending is an extensively used method for tailoring and/or modifying the properties of polymers. Until recent years, mostly binary blends, composed of two components, have been mainly considered. The most encountered phase separated morphologies of immiscible binary blend are sea-island, double emulsion, fibers, co-continuous, laminar, and ordered microphases. Several parameters play a role in determining the obtained morphology, both related to the polymer themselves (composition, viscosity ratio, interfacial tension) or to processing (thermo-mechanical history of the sample) [1-8]. Recently, considerable attention has been drawn on multicomponent polymer blends, comprising at least three immiscible polymers. These efforts resulted from the commercial need for new materials, as well as from the possibility that multi-component commingled waste plastics can be recycled into useful products without extensive separation [9,10].

For immiscible ternary blends, a variety of phase morphologies can be obtained, which offers the possibility to tune the properties of the resulting blends [8-28]. In the case of ternary systems composed of one major continuous phase (which forms the matrix), and two other minor phases, three types of morphology were observed. Referring to the minor phases, there could be a total encapsulation of one phase into the other, with the formation of a core-shell morphology; a complete separation of the two, and an intermediate case (partial engulfing) where mixed phases of the two minor components are formed, without any preferred order or organization [8,29].

Ternary blends composed of two major phases and one minor phase, in turn can show a partial wetting or complete wetting behaviour. [9,11,14,18,20,25]. In case of complete wetting, the tricontinuous morphology, where a continuous phase A is located at the interface between another two continuous phases B and C, is the most encountered. Examples of such morphologies have been reported for instance in 33/33/33 PBAT/PHBV/PBS and 33/33/33

HDPE/PS/PCL ternary blends. [11,18] A partial wetting morphology is characterized by a minor phase, as a form of droplets, locates at the interface between both the two major components. Typical cases of partial wetting morphologies are found for 50/5/45 PCL/PBS/PLA and 45/10/45 PLA/EMA/PA11 ternary blends [11,14].

The understanding and control of ternary blend morphology is of importance, because the final mechanical performance of the material can be greatly affected [8,13,30,31]. For example, brittle binary polymer blends comprising PLA can be efficiently toughened by adding a suitable third component displaying partial wetting [14,15]. Several parameters, including polymers molecular weight, composition and viscosity have been found to affect the blend morphology, to some extent [9,28]. However, the dominant role is played by the interfacial tension and interfacial forces equilibrium between the phases, which are usually expressed by mean of the spreading coefficients [9,10,30-34]. The spreading coefficient (λ) of a given component in a ternary mixture gives the tendency of that component to spread at the interface of the other two. In general, three spreading coefficients for the immiscible blend can be calculated as follows:

$$\lambda_{A/B/C} = \sigma_{AC} - \sigma_{AB} - \sigma_{BC}$$

$$\lambda_{A/C/B} = \sigma_{AB} - \sigma_{AC} - \sigma_{CB}$$

$$\lambda_{B/A/C} = \sigma_{BC} - \sigma_{BA} - \sigma_{AC}$$

where σ_{AB} is the interfacial tension between components A and B and $\lambda_{A/B/C}$ is the spreading coefficient. $\lambda_{A/B/C}$ shows the tendency of phase B to locate at the interface A/C or to be encapsulated in one of these phases. The usage of spreading coefficients has shown high efficiency in predicting the position of each component between pairs of polymer phases in ternary blends [9,20,25,28]. When $\lambda_{A/B/C}$ is positive and the other two spreading coefficients are negative, a complete wetting morphology with phase A separating B and C is found (two-phase contact only). If all the spreading coefficients are lower than zero, a partial wetting situation is encountered and the minor phase will form droplets at the interface with the two major components, giving rise to a three-phase contact line [9,20,25,28]. examples of complete-wetting and partial-wetting morphology obtained from literature are shown in Figure 5.1 [22,26,35].

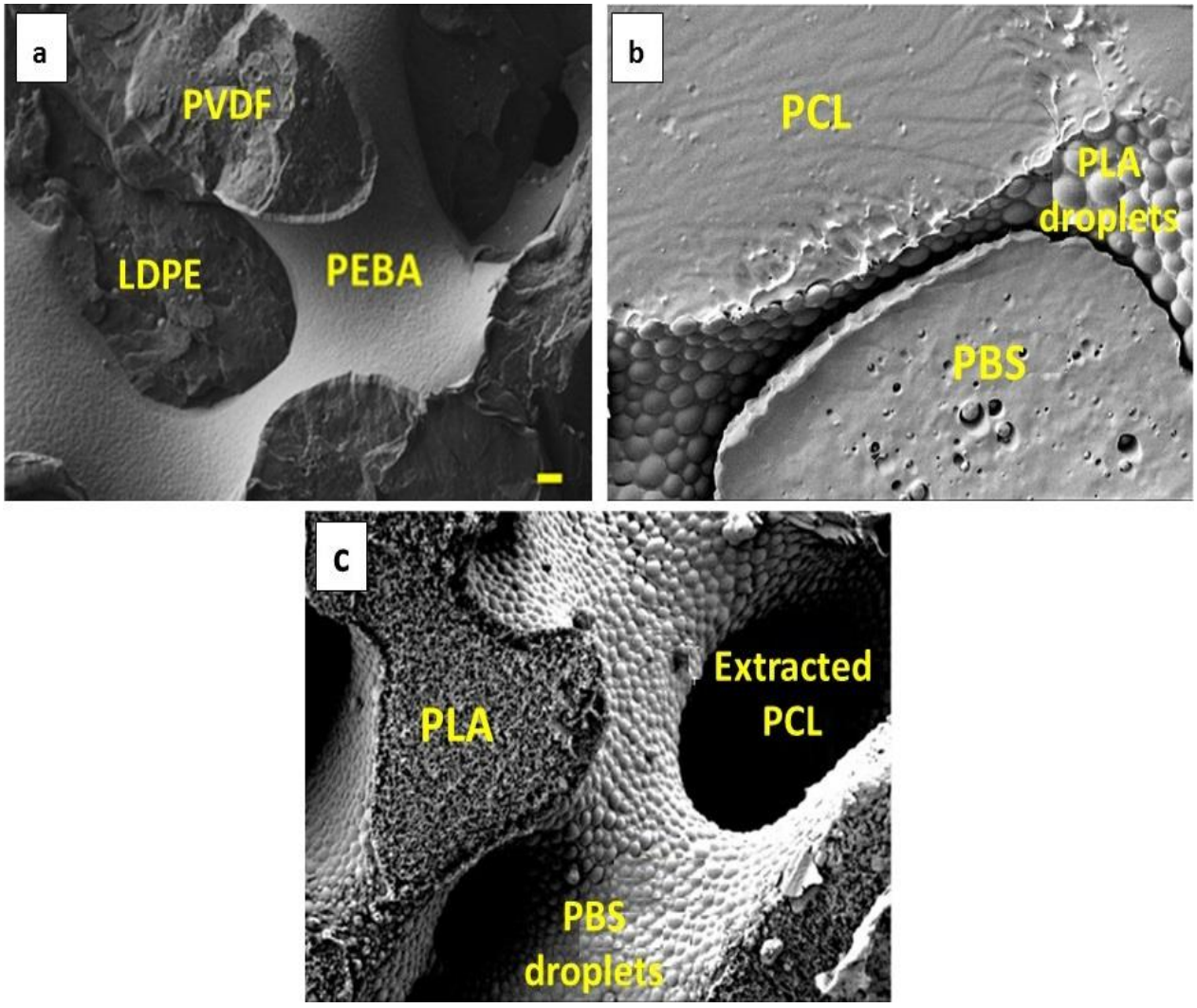

Figure 5.1. Selective SEM micrographs showing; (a) complete-wetting morphology of 50/3/47 LDPE/PEBA/PVDF, (b and c) partial-wetting morphology in 37.5/12.5/50 PBS/PLA/PCL and 45.5/4.5/50 PLA/PBS/PCL ternary blends, respectively [22,26,35]

As it was discussed in chapter III, the crystallization behaviour of a given polymer can be affected by blending. In particular, clear relationships have been found between blend morphology and crystallization of immiscible polymers, since the nucleation mechanism of both the major and (especially) the minor phase, can be affected. [36-40]. While several researchers have studied the effect of partial/complete wetting morphology in ternary blends on their mechanical and rheological performance, to the best of our knowledge detailed study on the crystallization behaviour of polymer in ternary blends are still missing.

Some sparse information on crystallization can be extracted from the literature. Ali et al. studied the compatibilization of PLA and PA11 using partially wetting droplets of ethylene methyl acrylate (EMA), poly(butylene adipate-co-terephthalate) (PBAT), ethylene methyl

acrylate–glycidyl methacrylate (EMA-EGMA), and PBS at the interface between the two. [14] DSC non-isothermal crystallization revealed a shift of cold crystallization temperature of PLA from 113°C in the neat polymer to 97°C when PLA was in contact with EMA and EMA-EGMA droplets. Consistently, the degree of crystallinity of PLA in these systems also increased (from 2 to above 11%). The faster cold crystallization rate and higher crystallinity degree can be due to an enhancement in the nucleation step at the interface via interface-induced nucleation, or to nucleating impurity transfer from one phase to the other. In another work, Ravati et al. studied binary and ternary blends based on PLA, PBS and PBAT. [20] The non-isothermal crystallization temperatures of neat PBAT and PBS were 52 and 78°C, respectively. DSC analysis of 50/50 PBS/PBAT binary blend showed that PBS and PBAT crystallized coincidentally at 65.6°C, revealing a nucleating effect of PBS on PBAT phase. More interestingly, in the 33/33/33 PBS/PLA/PBAT ternary blend displaying complete wetting morphology, all phase crystallized coincidentally at 93°C, suggesting an efficient nucleating effect of PLA on the other components. The authors attributed the enhancement of crystallization temperature to specific interactions between components and to the occurrence of transesterification reactions, later demonstrated by means of Time-of-Flight Secondary Ion Mass Spectrometry (ToF-SIMS) [26].

Chen et al. and Yang et al. studied PLLA/PVDF/PMMA ternary blends, in which the PMMA and PVDF components show a partial miscibility. [24,27] The authors reported a large depression of of both PLLA and PVDF crystallization. For PMMA concentration of 30-40 wt%, no crystallization of PVDF was observed anymore. It should be noted that due to the miscibility between PMMA and PVDF, the morphology in this blend is not complete nor partial wetting.

Ravati et al. examined the morphological state of ternary biodegradable polymer blends based on PLA, PCL, and PBS. [22] A partial wetting morphology was successfully produced in all the three types of ternary blends, i.e., PLA, PCL, and PBS droplets were located at PCL/PBS, PLA/PBS and PLLA/PCL interface, respectively, when present as minor component.

In this chapter, the nucleation and crystallization behavior of PLA, PCL, and PBS phases in their immiscible ternary and binary blends will be investigated in details, with emphasis on the nucleation and kinetics aspects. PLA, PCL, and PBS were chosen due to their different crystallization and melting ranges (T_c of PLA, PBS, and PBS are 101°C, 80°C, and 37°C, respectively. While T_m is 169°C, 116°C, and 59°C for PLA, PBS, and PBS,

respectively), which allow to study the crystallization of each phase separately. All binary blends exhibited sea-island morphology, while ternaries blends with partial wetting morphology were chosen. A significant number of work investigated the crystallization behavior of binary blends based on PLA, PCL, and PBS, while their crystallization behavior in ternary blends has not yet been explored. Hence the effect of blending, composition and morphology on the nucleation and crystallization behaviour of these systems will be discussed.

5.2 Materials and methods

5.2.1 Materials

Poly lactic acid (PLA) (Ingeo 3001D) was purchased from NatureWorks. PLA 3001D is a biodegradable and crystallizable grade of PLA with D isomer content of around 1.4 %. The melting point is in the range 170–180°C and the glass transition temperature (T_g) is located around 55-60°C. The polymer shows a melt flow rate (MFR) of about 22 g/10 min (210°C, 2.16 kg, D1238), a density of 1.24 g/cm^3 (D792) and an average molecular weight of 155,000 g/mol.

Poly(butylene succinate) (PBS) (1001MD) was purchased from Showa Denko. PBS (1001MD) is a crystallizable polymer with a melting point in the range 110-115°C and a T_g of ca. -32°C. The MFR is less than 3 g/10 min, its density is 1.26 g/cm^3, and its average molecular weight is 60,000 g/mol

Polycaprolactone (PCL) (Capa^{TM} 6800) was purchased from Perstorp. PCL Capa^{TM} 6800 is a biodegradable polymer of MFR of 2-4 g/ 10 min, with melting point of around 58°C and T_g of ca. -65°C, a density of 1.1 g/cm^3 and an average molecular weight of 87,000 g/mol.

5.2.2 Blend preparation

The polymers were dried at 50°C under vacuum for at least 24 h before melt processing. All the blends were prepared in a Brabender internal mixer with roller rotors. The mixing was performed at 190°C and 50 rpm for 8 min. Nitrogen flow was used to purge the blends during melt mixing to minimize thermal degradation. A total of 24 g material was inserted in the mixing chamber for each blend. The samples after processing were quickly taken from the mixer and quenched in ice water to freeze-in the morphology. After drying, the blends were annealed at 185°C for 20 min under a N_2 blanket, in order to stabilize the morphology. Table 1 summarizes the compositions of the different blends.

Table 5.1: Composition of the prepared binary and ternary blends.

Sample	PLA wt%	PCL wt%	PBS wt%
PLA	100	-	-
PCL	-	100	-
PBS	-	-	100
PLA/PCL	90	10	-
PLA/PBS	90	-	10
PCL/PLA	10	90	-
PCL/PBS	-	90	10
PBS/PLA	10	-	90
PBS/PCL	-	10	90
PLA/PCL/PBS	45	10	45
PLA/PBS/PCL	45	45	10
PCL/PLA/PBS	10	45	45

5.2.3 Blend characterization

SEM analysis

The blend samples were cryo-microtomed at -150°C using a Leica instrument (RM2165) equipped with an LN21 cooling system. A desktop SEM was used to characterize the morphology at 15kV. BSE mode (image with backscattered electrons) was employed. In some cases, the samples were stained by 2 wt % phosphotungstic acid or etched by a selective solvent to increase phase contrast. Gold coating on the microtomed surface is employed as needed.

Several micrographs of the most representative inner regions of the specimens were acquired. The diameters of the dispersed phases were then measured via image analysis. Number (*D*n) and volume (*D*v) were calculated using the following equations:

$$Dn = \sum n_i d_i / \sum n_i \qquad (1)$$

$$Dv = \sum n_i d_i^4 / \sum n_i d_i^3 \qquad (2)$$

where n_i is the number of droplets "i" of diameter D_i [41].

PLOM analysis

Polarized Light Microscopy (PLOM) was employed to observe the nucleation and morphology of different components in various blends. Film with a thickness of around 10μm was prepared and POM micrographs were recorded by a LEICA DC 420 camera. A METTLER FP35Hz hot stage was used to control the analysis temperature. The films were

firstly held at 200°C for 3 minutes to erase the effects of previous thermal histories, and then they were quenched to the crystallization temperature, where the nucleation was followed.

Stepwise crystallization of the different polymer components was performed according to the thermal protocol shown in Figure 5.2.

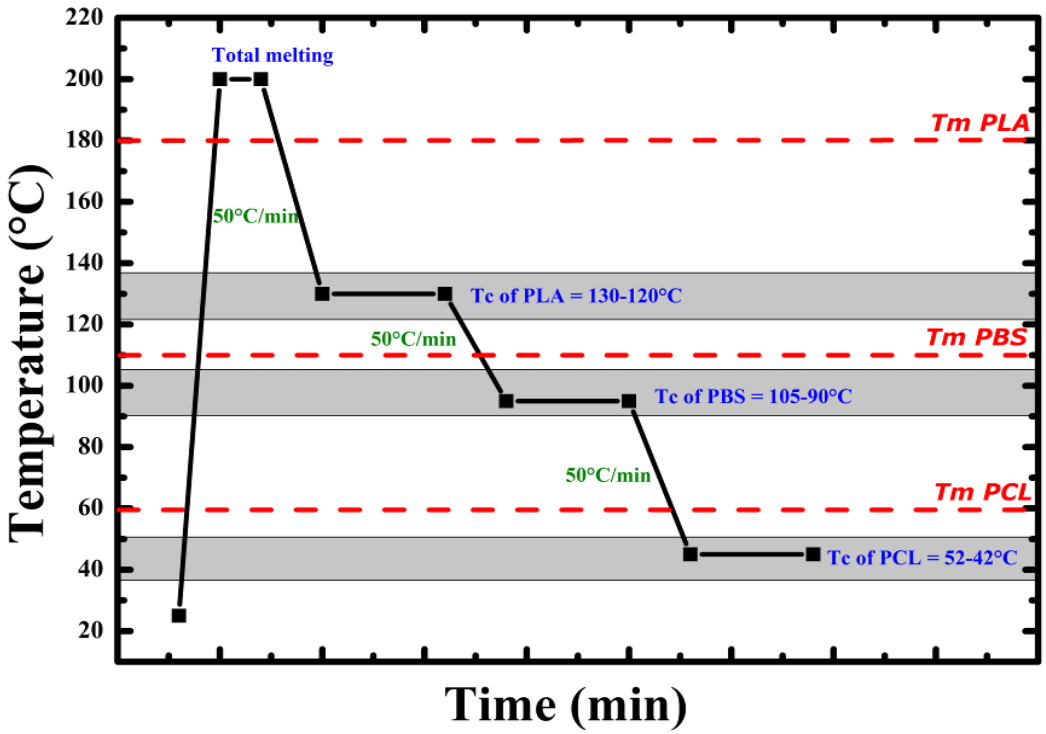

Figure 5.2. Thermal protocol employed during the stepwise crystallization of the different polymers with PLOM. The gray regions represent the crystallization temperature range chosen for each component.

Thermal behavior of the different blends with DSC

The thermal characterization of the blends was done by Differential Scanning Calorimetry (DSC) using a Perkin Elmer DSC Pyris 1 calorimeter, equipped with a refrigerated cooling system (Intracooler 2P).

Prior to the analysis, a calibration was done using indium and tin. All measurements were performed using sample masses of approximately 5 mg and under a continuous nitrogen flow.

Non-isothermal analysis: In these measurements, the samples were first heated from room temperature to 200°C at 10°C/min and held at 200°C for 3 minutes, to erase the thermal history of all the components. The samples were then cooled at a cooling rate of 5°C/min

from 200°C to −20°C, while the cooling scan was recorded. Finally, a second heating scan at a heating rate of 5°C/min was performed and acquired.

The crystallinity degree Xc (%) of each component in different blends was calculated using the following formula:

$$X_c(\%) = (\Delta H_m - \Delta H_{cc}) / (\Delta H_m^\circ * W_f) \qquad (3)$$

where ΔH_m and ΔH_{cc} are the corresponding measured enthalpies of melting and cold crystallization for each phase in the blends, ΔH_m° is the melting enthalpy of 100% crystalline polymer (93.7 J/g for PLA, 139.5 J/g for PCL, 110.3 J/g for PBS) and W_f is the weight fraction of the given polymer in the sample [42-44].

***I*sothermal analysis:** three thermal protocols were performed for the analysis of the isothermal crystallization

***Direct isothermal crystallization**:* was performed following the thermal protocol described by Lorenzo et al., [45] in which samples were firstly heated to 200°C and held at 200°C for 3 min to erase the thermal history of different components, followed by quenching the sample at a cooling rate of 60°C/min to the desired crystallization temperature (T_c). The isothermal scan was then recorded. Is worth to notice that a prior test was performed to detect the minimum T_c achievable without the occurrence of any crystallization during the cooling scan. Detection of the minimum T_c was performed by melting (heating) the sample immediately after chosen T_c was reached. If any sign of melting peak was observed, the experiment was repeated at a higher T_c, since the crystallization has taken place during the cooling process.

***Stepwise isothermal crystallization**:* in which the different components were separately crystallized in successive steps. After erasing the crystalline history of all components at 200°C for 3 min, we cooled the sample to the crystallization temperature of the selected polymer at a rate of 60°C/min. After completion of crystallization of the higher T_c component, the polymer is further cooled to the T_c of the second (and eventually third) component.

***Isothermal step crystallization**:* this analysis was used for studying the isothermal crystallization behavior of the components with the lower content (i.e., polymer droplets at10 wt% inside a matrix of the major component). This procedure was performed according to the following guidelines: (a) erasing the of crystalline history at 200°C for

3 min; (b) quenching the sample at 60°C/min to the chosen T_c; (c) hold the sample at T_c for a time tc; (d) subsequent melting at 10°C/min. The melting enthalpy recorded during the step (d) was evaluated and corresponds to the crystallization enthalpy of the crystals formed during step ‘‘c” at T_c for the specified crystallization time: (e) repetition of the steps (a–d) with an increase in tc at the employed T_c. Steps (a-e) were repeated until no increase in the melting enthalpy was observed with respect to the value measured at the previous time; (f) repetition of the whole previous steps applying different T_c [46].

5.3 Results and discussion

Morphological characterization with Scanning Electron Microscopy analysis

Figure 5.3 shows SEM micrographs of cryogenically fractured surfaces of PLA/PCL/PBS, PLA/PBS/PCL, and PCL/PLA/PBS blends. It is clear that all ternary blends exhibit a partial-wetting morphology, in which the phase with the lower content (10 wt%) self-assembles into droplets located at the interface of the co-continuous structure formed by the other two major components, with a content of 45 wt% each.

A clear phase separation was observed which confirm the immiscibility between all the components. The obtained morphology is mainly controlled by the spreading coefficient and the interfacial tension between polymer pairs. The spreading coefficient gives the tendency of one component to spread over another component or to locate at the interface between components. The shape of the droplets at the interface between components in different blends (45/10/45 PLA/PCL/PBS, 45/10/45 PLA/PBS/PCL, and 45/10/45 PCL/PLA/PBS) is controlled by the difference in the interfacial tension value between the middle phase and the other two surrounding components [22].

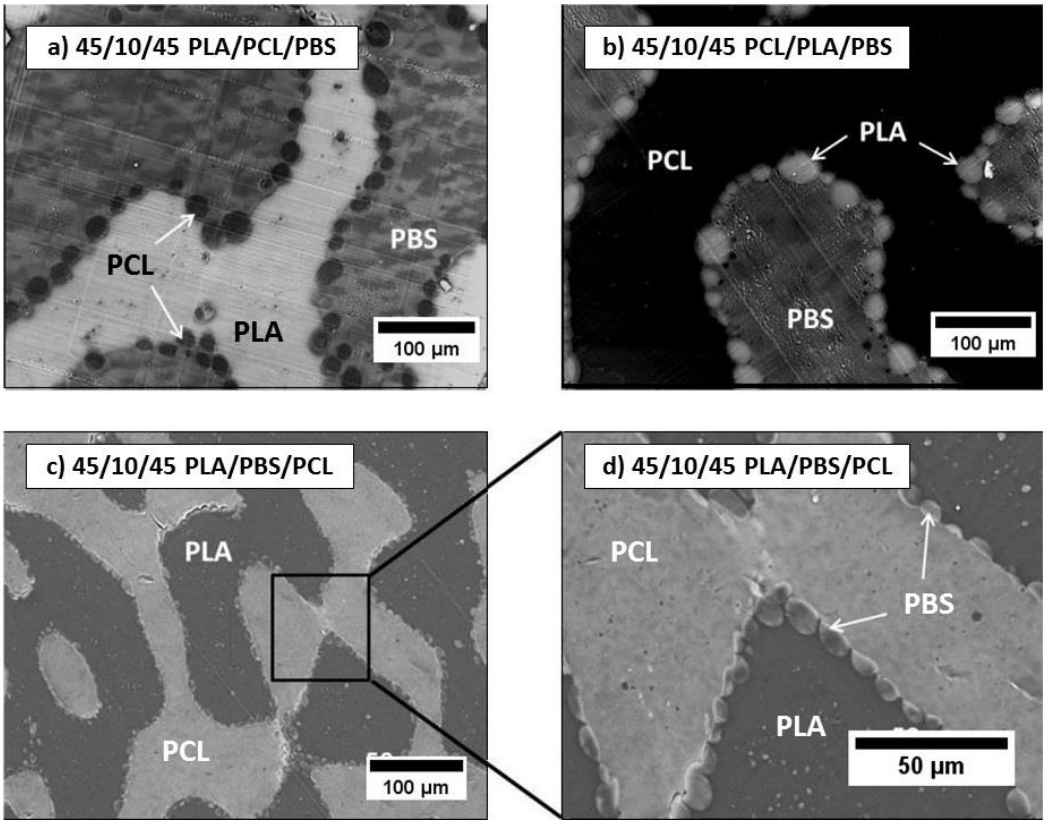

Figure 5.3. Morphologies of ternary blends PLA/PCL/PBS, PBS/PLA/PCL and PCL/PBS/PLA with a weight composition of 45/10/45 after annealing for 20 min at 185°C. a) and b) were directly imaged after cryo-microtoming; c) and d) were stained by tungstic acid followed by gold coating (~1 nm thickness) before SEM analysis.

Figure 5.4 shows that all binary blends exhibit sea-island morphology in which the minor phase is dispersed in form of droplets inside the matrix of the major phase. The droplets size range from 0.5 to around 2 µm. Similarly to the morphology observed in ternary blends, the sea-island morphology of binary blends revealed the immiscibility of the different polymer pairs. The cavities observed in different blends resulted either from the selective extraction of a given phase or from the debonding between the polymer phases during the cryogenic fracture (Figures 5.4c-5.4f). Complete debonding is a sign of immiscibility and poor adhesion between the different components in the binary blends.

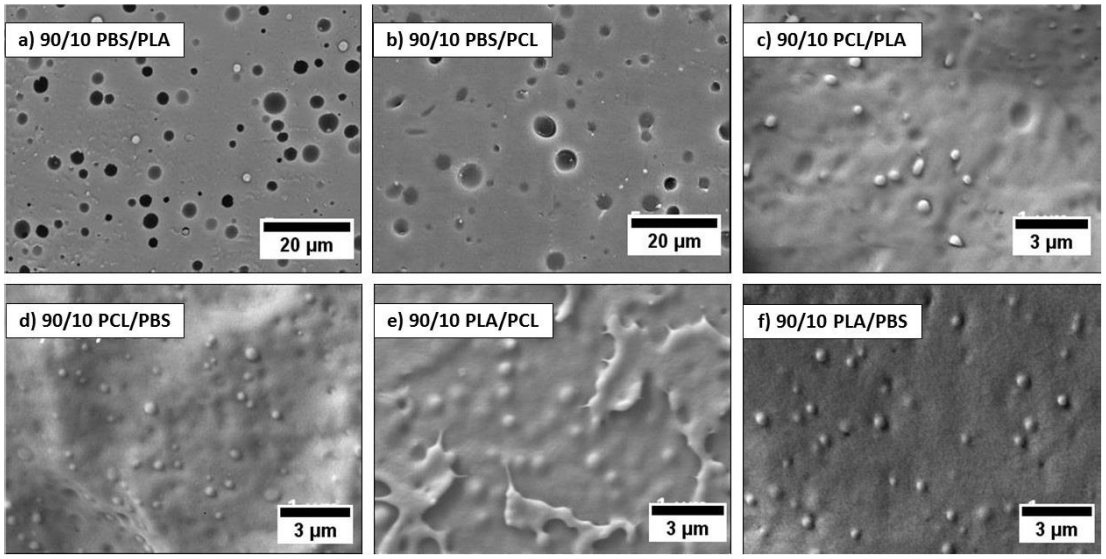

Figure 5.4. Morphologies of binary blends after annealing for 20 min at 185°C: a) 90/10 PBS/PLA, b) 90/10 PBS/PCL, c) PCL/PLA 90/10, d) 90/10 PCL/PBS, e) 90/10 PLA/PCL and f) 90/10 PLA/PBS. a) and b) are cryo-microtomed samples after extraction of PLA and PCL, respectively by THF. c)-f) are cryo-fractured images without extraction.

The droplets size in binary and ternary blends has a strong effect on the crystallization behavior (temperatures and enthalpies) of the minor phase component, which leads to the appearance of the fractionated crystallization with the decrease in the droplets size, and in some cases a meaningful effect on the crystallization of the matrix component as well [47-56].

Table 5.2 reports the average particle size of the different minor phases within the blends (measured by counting at least 100 micro-domains), and the percentage of the minor phases located at the interface in the different ternary blends.

Table 5.2. Composition (wt%) and phase size (Number average (D_n) and volume average (D_v) diameters) of the minority phase in binary and ternary blends.

Blends	Droplet size of the minor phase (D_n/D_v) (µm)	% of the minor phase at the interface
90/10 PLA/PCL	0.41/0.54	--
90/10 PLA/PBS	0.54/0.61	--
90/10 PCL/PLA	0.45/0.55	--
90/10 PCL/PBS	0.35/0.43	--
90/10 PBS/PLA	1.4/3.6	--
90/10 PBS/PCL	1.8/5.1	--
45/10/45 PLA/PCL/PBS	21.6/28.1	95 ± 1%
45/10/45 PLA/PBS/PCL	8.3/10.1	94 ± 2%
45/10/45 PCL/PLA/PBS	24.6/32.9	98 ± 1%

DSC non-isothermal analysis

Figures 5.5 & 5.6 show DSC cooling scans and subsequent heating scans at 5°C/min for all binary and ternary blends, respectively. Table 5.3 and 5.4 report the thermal properties obtained during the cooling (table 5.3) and heating (table 5.4) scans. The crystallization and melting enthalpies were normalized by the weight fraction of the respective component.

Table 5.3. Thermal properties obtained during the cooling scan at a rate of 5°C/min.

Sample & composition (wt%)	Tg (°C)	Tc PLA (°C)	Tc PCL (°C)	Tc PBS (°C)	DHc PLA (J/g)	DHc PCL (J/g)	DHc PBS (J/g)
Neat PLA	61	101	--	--	-8	--	--
Neat PCL	--	--	37.4	--	--	-54.5	--
Neat PBS	--	--	--	82.44	--	--	-69
90/10 PLA/PCL	59.5	100.2	15.3	--	-7.5	-36.5	--
90/10 PLA/PBS	58	99.1	--	*	-15.5	--	*
90/10 PCL/PLA	*	*	36.5	--	*	-53	--
90/10 PCL/PBS	--	--	36.5	*	--	-60	*
90/10 PBS/PLA	*	*	--	80	*	--	-65
90/10 PBS/PCL	--	--	24	80	--	-40	-67.5
45/10/45 PLA/PCL/PBS	57.5	*	37	82	*	-45	-61.5
45/10/45 PLA/PBS/PCL	*	100	36	85 & 75	×	-51	×
45/10/45 PCL/PLA/PBS	*	*	37	81.5	*	-54.5	-65.5

Table 5.4. Characteristic temperatures and enthalpies obtained during the heating scan at 5°C/min.

Sample & composition (wt%)	Tg (°C)	Tcc PLA (°C)	ΔHcc PLA (J/g)	Tm PLA (°C)	Tm PCL (°C)	Tm PBS (°C)	ΔHm PLA (J/g)	ΔHm PCL (J/g)	ΔHm PBS (J/g)	Xc PLA (%)	Xc PCL (%)	Xc PBS (%)
Neat PLA	63.2	97	-17.5	169.3	--	--	47	--	--	32	--	--
Neat PCL	--	--	--	--	9.2	--	--	61	--	--	44	--
Neat PBS	--	--	--	--	--	116	--	--	74	--	--	67
90/10 PLA/PCL	62.5	93	-17.5	168.5	57	--	47	34	--	32	24	--
90/10 PLA/PBS	60	91	-10	168	--	114	46	--	56	39	--	50
90/10 PCL/PLA	*	91	-1.4	166	59	--	37	54	--	38	38.5	--
90/10 PCL/PBS	--	--	--	--	59	114.5	--	56	73	--	40	66
90/10 PBS/PLA	*	*	*	167	--	115	44	--	72	47		65
90/10 PBS/PCL	--	--	--	--	57	115	--	43	74	--	31	67
45/10/45 PLA/PCL/PBS	64.5	94.5	×	167.5	60	115.5	47	40	66.5	×	28.5	60
45/10/45 PLA/PBS/PCL	65	96	×	169	60	115.5	44.5	48	65	20	34	59
45/10/45 PCL/PLA/PBS	*	*	*	168	60	115.5	48	54	73.5	51	38.5	66.5

* Undetectable transition or value.
× Overlapping effect

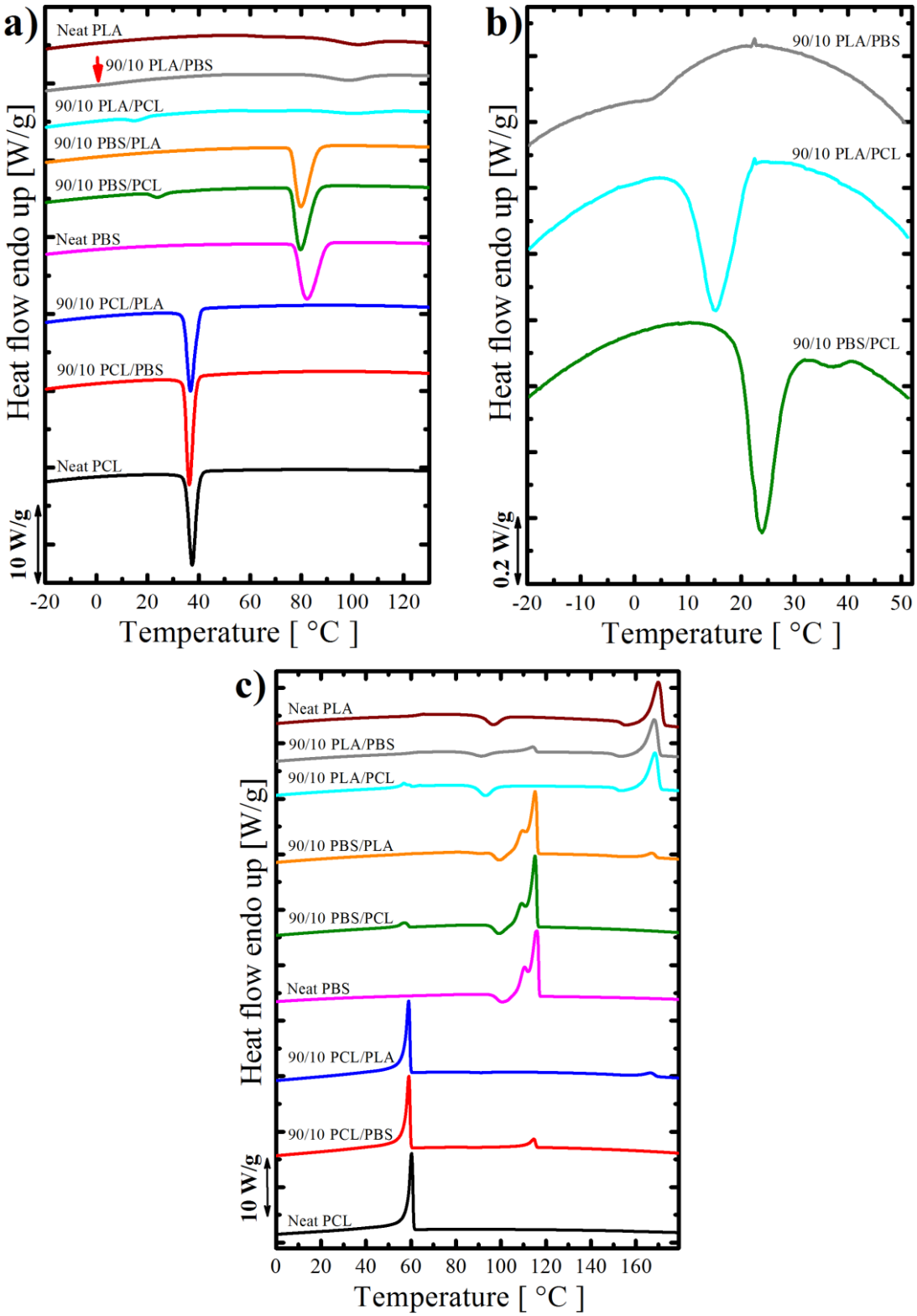

Figure 5.5. a) DSC cooling scans, b) zoom of the temperature region displaying weak thermal transitions upon cooling in selected samples, and c) subsequent DSC heating scans for the indicated binary blends at a cooling and heating rate of 5°C/min. The curves of neat polymers are added for the sake of comparison.

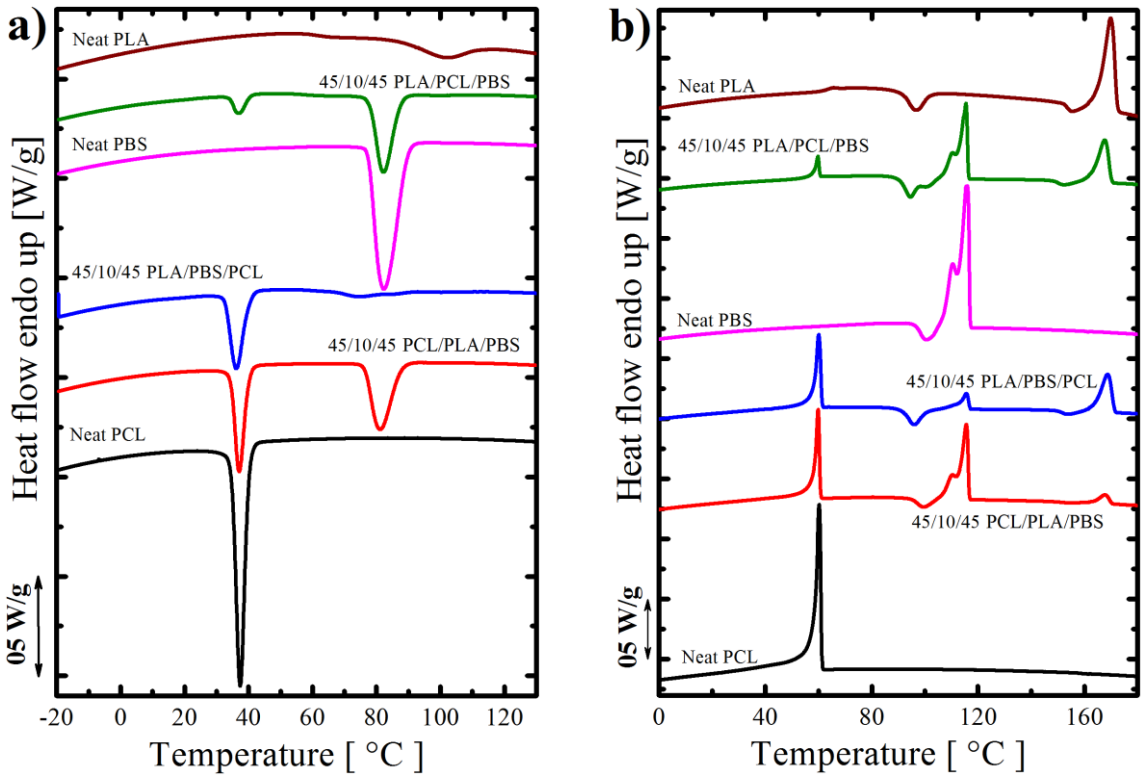

Figure 5.6. a) DSC cooling scans and b) subsequent DSC heating scans for the indicated ternary blends at a cooling and heating rate of 5°C/min. The curves of neat polymers are added for the sake of comparison.

At first the neat polymers are considered. Neat PBS crystallizes with a sharp peak at around 83°C, and on heating it exhibits a small cold crystallization exotherm at 100.5°C, and eventually melts at around 116°C (with a bimodal melting peak which, is probably a result of a reorganization process of the lamellae during the heating scan). PCL shows a crystallization peak at 37°C, and melts at around 61°C. Finally, PLA exhibits a broad crystallization event peaked around 101°C during cooling from the melt, a cold crystallization peak at around 97°C during heating, and a second exothermic event at about 155°C just before melting. On the basis of the literature, this peak can tentatively be attributed to the recrystallization of PLA mesophase into more stable α-crystals [57], PLA then melts at around 170°C.

Figure 5.5 shows that the melt blending process affects the crystallization behavior of the different systems. Considering the crystallization of the PLA phase, in samples where this polymer is the major component, we can find a negligible shift in the crystallization peak temperature, while the crystallization enthalpy is distinctly higher in the 90/10 PLA/PBS blend with respect to the 90/10 PLA/PCL blend. Accordingly, in the heating scans (Figure 5.5c) a reduced cold crystallization enthalpy of 17.5 J/g was obtained for PLA and 10 J/g in

the binary blend with PBS as minor component. We can thus deduce a mild nucleating effect of the PBS phase (during cooling from the melt), while the presence of PCL droplets does not significantly affect PLA major phase crystallization. The small nucleating effect can be attributed to impurity transfer from the PBS to the PLA phase, or to the effect of the PBS/PLA interfaces. Similar results of enhancement of the melt and cold crystallization rate of PLA in presence of PBS droplets were reported in literature [58-61]. Likewise, several papers reported the enhancement of the cold crystallization rate of PLA in contact with PCL droplets [62-72].

When PLA is the minority component of binary blends, i.e., is present as droplets in a PCL or PBS matrix, no trace of crystallization during cooling can be observed, while a small cold-crystallization exotherm is recorded on subsequent heating. It is deduced that the concentration of PLA droplets created by blending is larger than that of the nucleating heterogeneities existing in neat PLA. As such, the nucleation of crystals is delayed and does not occur on cooling before overcoming the glass transition [35,46,49,53,73-78].

Considering the crystallization of PCL, in 90/10 PCL/PLA and 90/10 PCL/PBS, the crystallization temperature keeps practically constant despite the addition of PLA or PBS. Instead, a clear reduction of the crystallization kinetics was observed for the PCL minor phase in 90/10 PLA/PCL and 90/10 PBS/PCL. The crystallization temperature of PCL decreased from 37 to around 15°C in 90/10 PLA/PCL, while 90/10 PBS/PCL blend exhibit fractionated crystallization, with a minor peak at the same value of the neat PCL and a second crystallization event around 24°C. The depression of crystallization temperature indicates that most of the droplets contain less-active heterogeneities, and thus require a larger undercooling to crystallize at detectable rates. It is worth noting that a minor fraction of PCL droplets nucleated by the same type of heterogeneities active in the neat polymer is still present in the PBS/PCL binary blend (see Figure 5.5b).

Fractionated crystallization of PCL droplets, as described above, is a common phenomenon that is frequently seen in immiscible blends [48-50,52-56]. This behavior occurs when the number of droplets is equal or higher than the number of highly active heterogeneities present in the bulk polymer. Such highly active heterogeneities are responsible for the heterogeneous nucleation of the bulk polymer at low supercoolings. When a population of droplets does not contain these highly effective heterogeneities, it can only crystallize at higher supercoolings by nucleating onto less active heterogeneities present, or at the interface with the matrix. Homogeneous nucleation can only occur when the number of

droplets exceeds by several orders of magnitude the number of all nucleating heterogeneities present in the bulk polymer and is not normally encountered in non-compatibilized polymer blends, as droplet sizes are too large [53].

In the binary blends 90/10 PBS/PLA and 90/10 PBS/PCL, the crystallization temperature of PBS was slightly decreased from 82.5°C to 80°C, possibly due to some impurity transfer from PBS to the other phases during melt processing. When PBS forms dispersed droplets, it exhibits slower crystallization. In 90/10 PLA/PBS the crystallization temperature decreased to around 3°C (see Figure 5.5b), while in 90/10 PCL/PBS, the crystallization of PBS droplets appeared to be concomitant with the crystallization of PCL matrix, peaked at 36.5°C. This deduction will be confirmed later on by applying the self-nucleation protocol (in chapter VI).

At this stage, the crystallization behavior of the various components in ternary blends is considered. Figure 5.6a shows the DSC cooling scan of neat components and ternary blends, it is clear that melt blending does not affect significantly the crystallization behavior of both PCL and PBS in all the ternary blends. On the other hand, no trace of PLA crystallization could be detected in 45/10/45 PLA/PCL/PBS and 45/10/45 PCL/PLA/PBS ternary blends, suggesting a possible transfer of nucleating impurities (highly active heterogeneities/impurities) from PLA to the other molten phases during mixing. Instead, PLA crystallizes on cooling to a certain extent in the ternary blend 45/10/45 PLA/PBS/PCL.

The DSC heating scans of the different homopolymers and ternary blends are reported in Figure 5.6b. No significant changes of the PCL and PBS melting temperatures and enthalpies was observed, while the cold crystallization temperature of the PLA component is slightly decreased in both blends with respect to the one of the homopolymer, suggesting a possible mild nucleating effect of PBS and/or PCL. We note that the cold crystallization enthalpy of PLA in the ternary blends is not measurable, due to the overlap with the PBS melting peak.

Contrary to what has been observed in binary blends, fractionated crystallization of the minor phases has not been observed in ternary blends. The different behavior can be attributed to the large droplet size difference, as highlighted in Table 2. In particular, the average size of the minor phase domains increased from around 1 µm in binary blends to around 20 µm in ternary blends, for all the considered polymers. The larger droplet size in ternary blends results in a higher opportunity of finding highly active nucleating heterogeneity inside the

minor phase, which in turns leads to its crystallization at supercoolings similar to those detected for the neat homopolymers.

The data presented in Figures 5.5 & 5.6, revealed that the variation in the droplets sizes (Table 5.2) of the different dispersed phase does not significantly affect the crystallization behavior of the various components.

DSC isothermal analysis

Isothermal crystallization of PLA phase in various blends

In order to better understand the crystallization kinetics and mechanism of the blended samples, the isothermal overall crystallization rate was studied. Two different thermal protocols were applied to study the overall crystallization rate; (i) direct isothermal crystallization from the melt was applied for components that have a content higher than 45 wt%) [45]. (ii) isothermal step crystallization was instead applied for components with a phase content of 10 wt% [46].

The inverse of the half-crystallization time determined by DSC gives an experimental indication and measure of the overall crystallization rate, including nucleation and growth rates [62,63].

The obtained isothermal crystallization data from DSC was then analyzed by Avrami equation. The fits to Avrami equation were performed using the Origin® plug-in developed by Lorenzo et al. [45] Avrami exponents "n" varies in general between 1 and 4. The exponent (or index) is related to both the dimensionality of the growing geometry (i.e., 3-D spherulites vs. 2-D lamellar aggregates) and to the nucleation mechanism (e.g., instantaneous vs. sporadic nucleation). For instance, n = 4 corresponds to 3-D spherulites that nucleate sporadically in time, while n = 3 might correspond to 3-D spherulites that nucleate instantaneously, or to 2D lamellar aggregates that nucleate sporadically. Value of the exponent close to 1 are usually found in confined or phase separated systems, where the overall crystallization kinetics is dominated by the nucleation step and growth is not relevant. [41,73,79].

Figures 5.7a, 5.7a, and 5.8a report the inverse of half-crystallization time ($1/\tau_{(50\%)}$) versus crystallization temperature (T_c) for the PLA, PCL, and PBS phases, respectively. Accordingly, Figures 5.7b, 5.7b, and 5.8b present the Avrami exponent (n) as a function of the applied crystallization temperature for the respective polymers.

Figure 5.7a shows the overall crystallization rate of neat PLA and PLA component in the different blends where PLA is either one the major or minor phase. With respect to neat PLA, the PLA component within all the different binary and ternary blends exhibits a somewhat lower crystallization rate. When PLA is the major component, the resulting decrease could be attributed to the transfer of impurities from PLA to the other phases during the melt processing step, which decreases the number of highly active heterogeneities and thus the nucleation density. A possible minor role of limited miscibility, leading to dilution effect on PLA crystallization kinetics, can also be hypothesized. [72-74,78-80].

For blends with PLA as minor component, the high number of droplet concentration with respect to active nucleating heterogeneities leads to the observed depression of overall crystallization rates ($1/\tau_{(50\%)}$), which is extremely large for binary blends due to the smaller droplet size (compared to PBS/PLA/PCL ternary blend). The lowest PLA droplets size was found in 90/10 PCL/PLA binary blend, which indeed requires the highest supercooling to obtain a measurable crystallization kinetics (i.e., the crystallization temperatures are 80-88°C vs. 120-130°C for 90/10 PBS/PCL blend, while the overall crystallization rate is comparable. Generally, the crystallization rate increases with decreasing T_c, for neat PLA and ternary blends. On the other hand, in the binary blends with dispersed PLA, no appreciable temperature dependence of the kinetics is revealed.

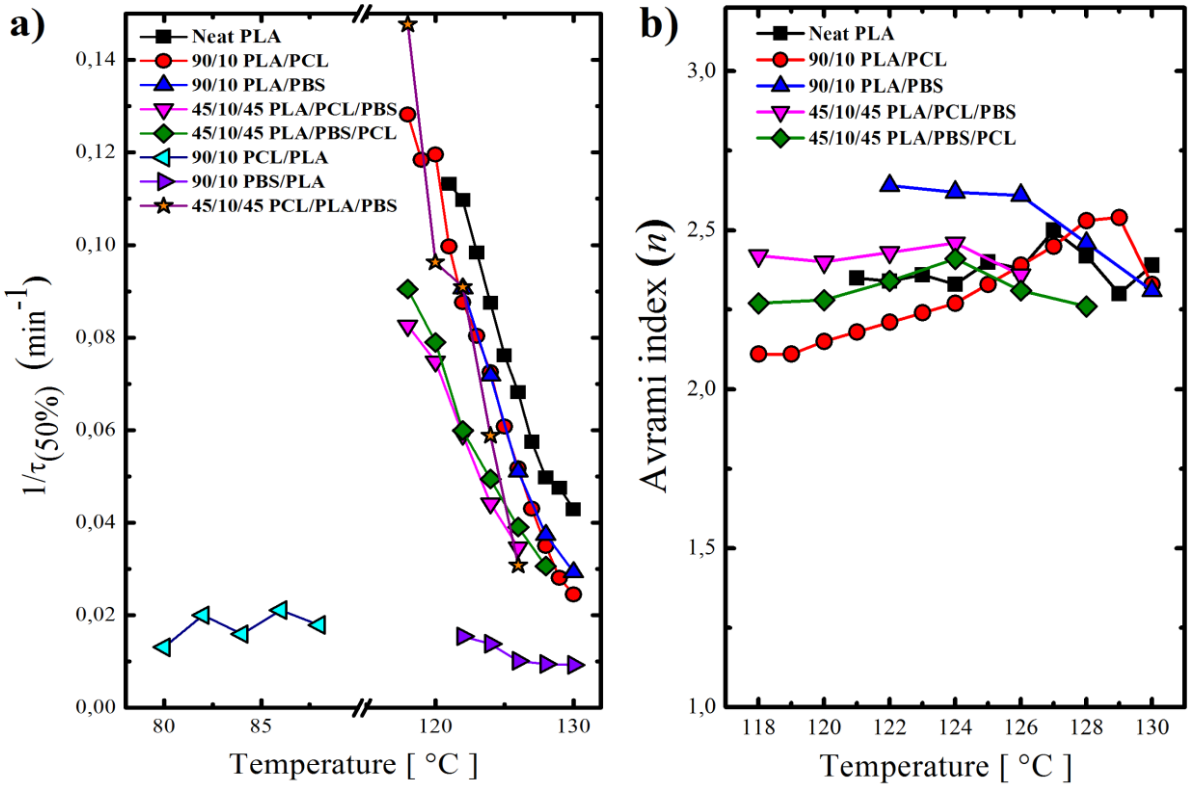

Figure 5.7. a) reciprocal of the half-crystallization time ($1/\tau_{(50\%)}$) and b) Avrami index (n) of PLA crystallization in the different blends.

Figure 5.7b presents the values of Avrami index for neat PLA and PLA within different blends, as a function of the applied isothermal crystallization temperature. The Avrami index is always found to lay between 2 and 3, regardless of the specific sample or crystallization temperature. The obtained results suggested that the nucleation mechanism of PLA in all studied blend can be well represented by an instantaneous nucleation of 3-D spherulites, or 2-D axialites when the nucleation density is higher ($n \approx 2$) [41,73,79].

Isothermal crystallization of PCL phase in various blends

Figure 5.8a shows the changes of the inverse of half-crystallization time ($1/\tau_{(50\%)}$) of neat PCL and PCL within different blends, as a function of the crystallization temperature T_c.

Samples with PCL as major component exhibit very similar crystallization kinetics in all the explored temperature range. In particular, the addition of PLA droplets or PBS droplets in the binary blends does not significantly affect the overall crystallization rate of the PCL matrix.

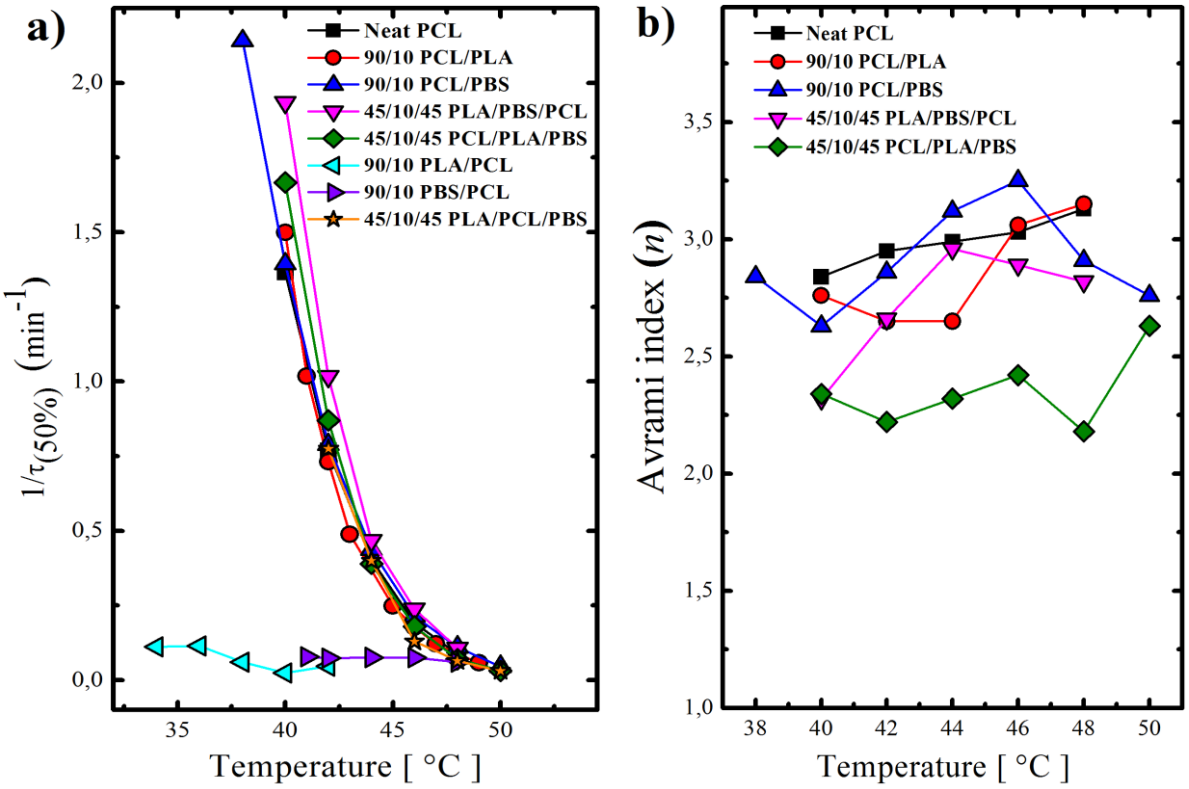

Figure 5.8. a) Reciprocal of the half-crystallization time ($1/\tau_{(50\%)}$); b) Avrami index (n) of PCL in different blends.

A slight increase in overall crystallization rate of PCL was observed for the ternary blends containing 45 wt% of PCL. This slight enhancement could be related to the nucleating effect of the previously crystallized PBS droplets or PLA droplets.

PCL droplets within 45/10/45 PLA/PCL/PBS ternary blend have similar overall crystallization rate of neat PCL, given the relatively large average size of PCL domains, which leads to a higher fraction of droplets containing highly active heterogeneities responsible for nucleation of bulk PCL.

The overall crystallization rate of PCL within 90/10 PLA/PCL and 90/10 PBS/PCL binary blends is much lower than the rest of the samples, and it remain constant with changing T_c. The larger observed reduction in the overall crystallization rate in 90/10 PLA/PCL blend with respect to 90/10 PBS/PCL blend can be attributed to the smaller droplets found in the former system (see Table 5.2).

The values of Avrami index (n) of PCL and PCL blends are close to 3 and almost independent of the crystallization temperature, suggesting a nucleation and growth mechanism based on the instantaneous growth of 3-D spherulites.

Isothermal crystallization of PBS phase in various blends

The results related to the crystallization of the PBS phase are similar to those obtained for PLA and PCL in the different blends (Figure 5.9a). In particular, the crystallization kinetics of PBS in all the systems where it is the majority phase, and in the ternary blend when PBS droplets are at the interface with PLA and PCL, are basically unchanged with respect to that of neat PBS. Therefore, even the PBS droplets in the ternary system are large enough to host some actively nucleating impurity, in addition to nucleation possibly occurring at the interface with PLA or PCL.

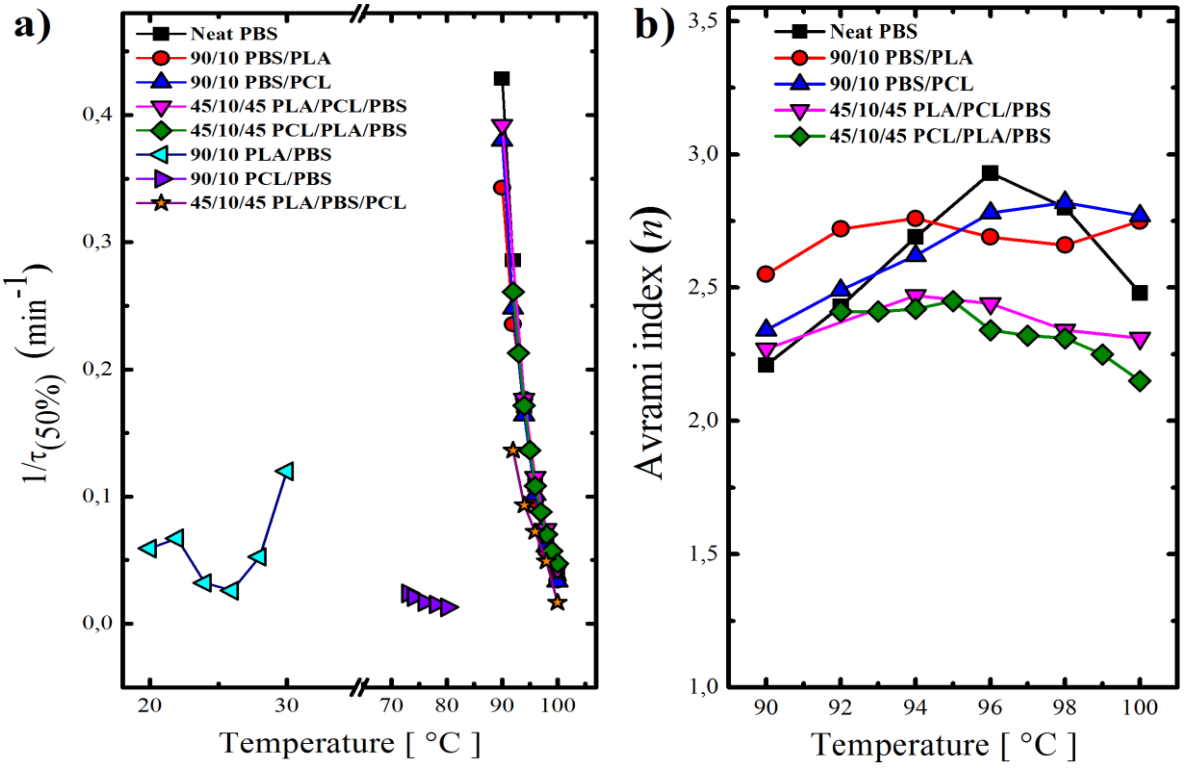

Figure 5.9. a) reciprocal of the half-crystallization time ($1/\tau_{(50\%)}$); b) Avrami index (n) of PBS in different blends.

On the other hand, small droplets in PLA and PCL matrices show strongly depressed crystallization kinetics, which is more severe when the majority phase is PLA. This effect would not be expected on the basis of morphological considerations alone, since the droplet size is comparable between the two systems. However, it is apparent that in the achieved crystallization temperature range, PBS droplet crystallization occurs either in a molten (in the case of PCL), or in a glassy (PLA) matrix. So a different hindering effect could be possibly expected in the two situations. This aspect might deserve more detailed investigation.

For what concerns the Avrami index, its value is constantly close to 3 (Figure 5.9b), as expected for the instantaneous growth of 3D spherulitic morphologies.

Isothermal crystallization studied by PLOM

Isothermal crystallization of PLA

Polarized light optical microscopy was employed to investigate the difference in PLA nucleation in contact with molten PBS droplets (in 45/10/45 PLA/PBS/PCL ternary blends) or molten PCL droplets (within the 45/10/45 PLA/PCL/PBS ternary blends).

Films of the material were prepared between two glass slides. The samples were firstly heated to 200°C for 3 min to erase the crystalline history, and then quenched at 50°C/min to the desired crystallization temperature.

Figure 5.10 shows PLOM micrographs taken during the isothermal crystallization of PLA component at 120°C. PLOM micrographs revealed that PLA can nucleate on both molten polymers: PBS and PCL.

It is clear that PLA nucleates mainly at the interface with molten PBS droplets in 45/10/45 PLA/PBS/PCL and at the interface with molten PCL droplets in 45/10/45 PLA/PCL/PBS, while few nuclei are formed in the bulk PLA phase. The presented nucleation phenomenon is commonly named as interface-induced nucleation or interface assisted-crystallization. Several results of interfacial-induced nucleation have been reported in literature such as in PVDF/PLLA, PVDF/PCL, iPP/PMMA, PEO/PCL, PLA/PCL blends [81-88].

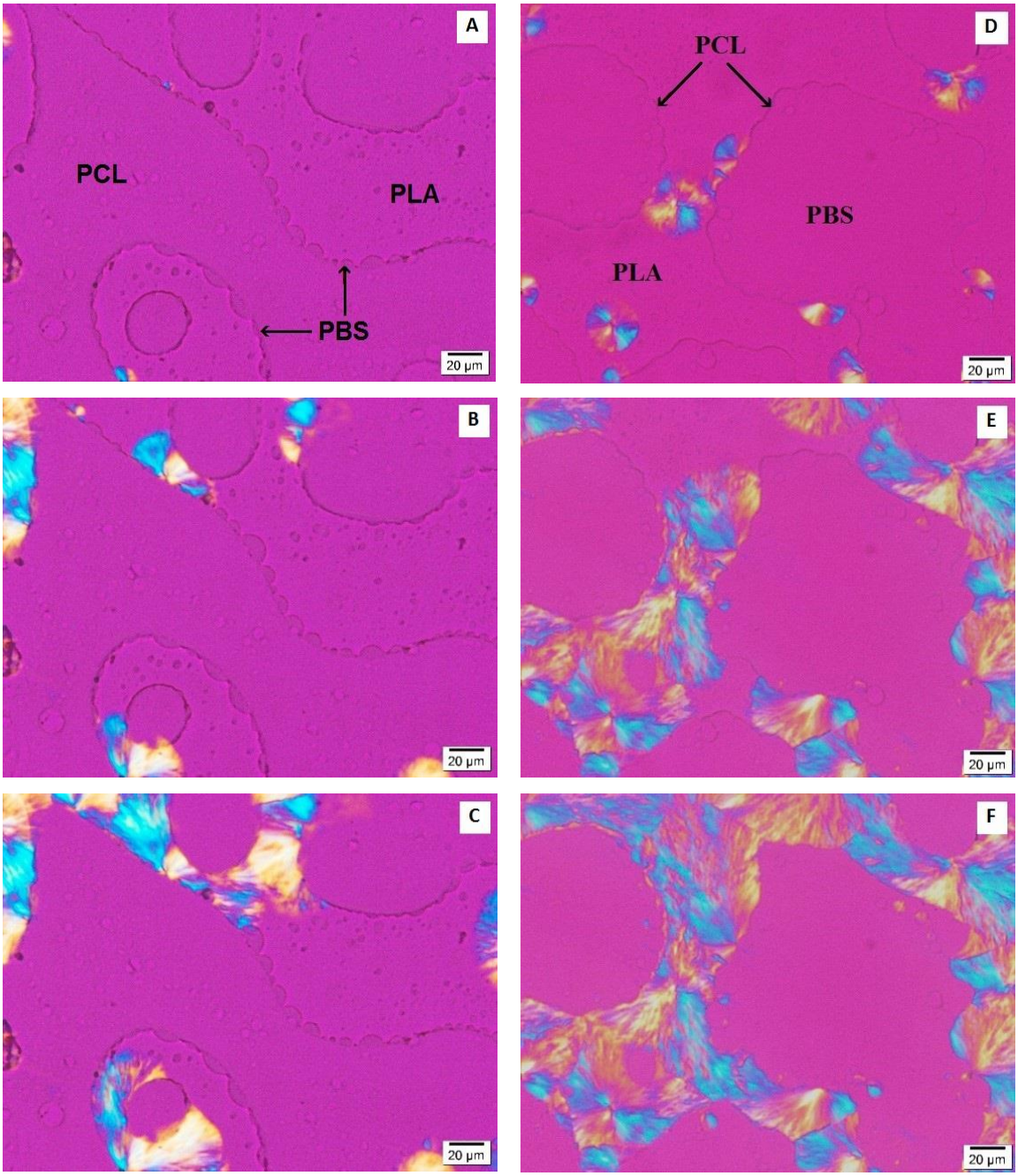

Figure 5.10. PLOM micrographs taken during the isothermal crystallization of PLA within 45/10/45 PLA/PBS/PCL (A-C) and 45/10/45 PLA/PCL/PBS (D-F) at 120°C. Micrographs (A, D) was taken after 5 min, (B, E) after 10 min, and (C, F) after 16 min.

We should note that at the same crystallization temperature and times, PLA nucleation is faster when it is in contact with molten PCL droplets, than when it is in contact with molten PBS. This is deduced by the fact that after equivalent crystallization time: (i) the number of PLA spherulites in contact with molten PCL droplets (in ternary 45/10/45 PLA/PCL/PBS blend) is higher than that in contact with molten PBS droplets (in ternary 45/10/45 PLA/PBS/PCL blend); (ii) the size of PLA spherulites after a given crystallization time is

larger when nucleation starts at the interphase with PCL droplets than when it starts at the interphase with PBS droplets, which means that PLA spherulites are born at earlier times in 45/10/45 PLA/PCL/PBS blend.

On the other hand, the surface area available for PLA nucleation in the two blends is similar but not equivalent, as revealed by Table 5.2. Therefore, Figure 5.11 shows an estimation of the nucleation efficiency of the two molten phases, expressed by the ratio of the number of PLA nuclei by the unit length of molten interface, at the different crystallization temperatures. It turns out that, regardless the crystallization temperature, the nucleation density of PLA in contact with molten PCL droplets is significantly higher than that in contact with molten PBS droplets, confirming the direct observation of Figure 5.10. However, these numbers should be considered just as an estimate, since a correct statistical analysis could not be afforded, due to the limited number of counted nuclei/repetition. In this respect, a more detailed data analysis will be provided further on.

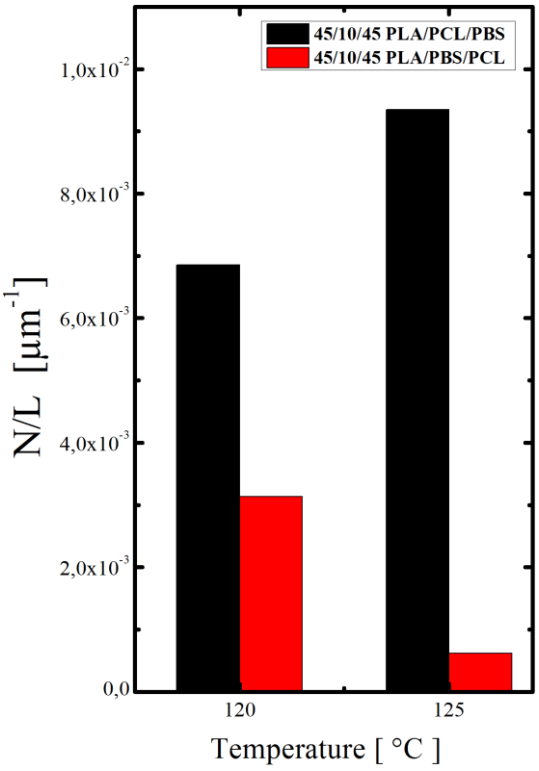

Figure 5.11. Linear nucleation density of PLA within 45/10/45 PLA/PBS/PCL and 45/10/45 PLA/PCL/PBS at two different crystallization temperatures.

A confirmation of the occurrence of PLA nucleation on the contact surface with molten PBS or PCL should be found also analyzing in-situ the crystallization of PLA droplets in binary blends with the two polymers via PLOM. Figure 5.12 shows some micrographs

taken during the crystallization of PLA droplet within 90/10 PBS/PLA blends at 120°C. We should note that the droplets have undergone a substantial coarsening during the melting process, reaching an average diameter larger than 10 micrometers, suitable for the optical microscopy observation.

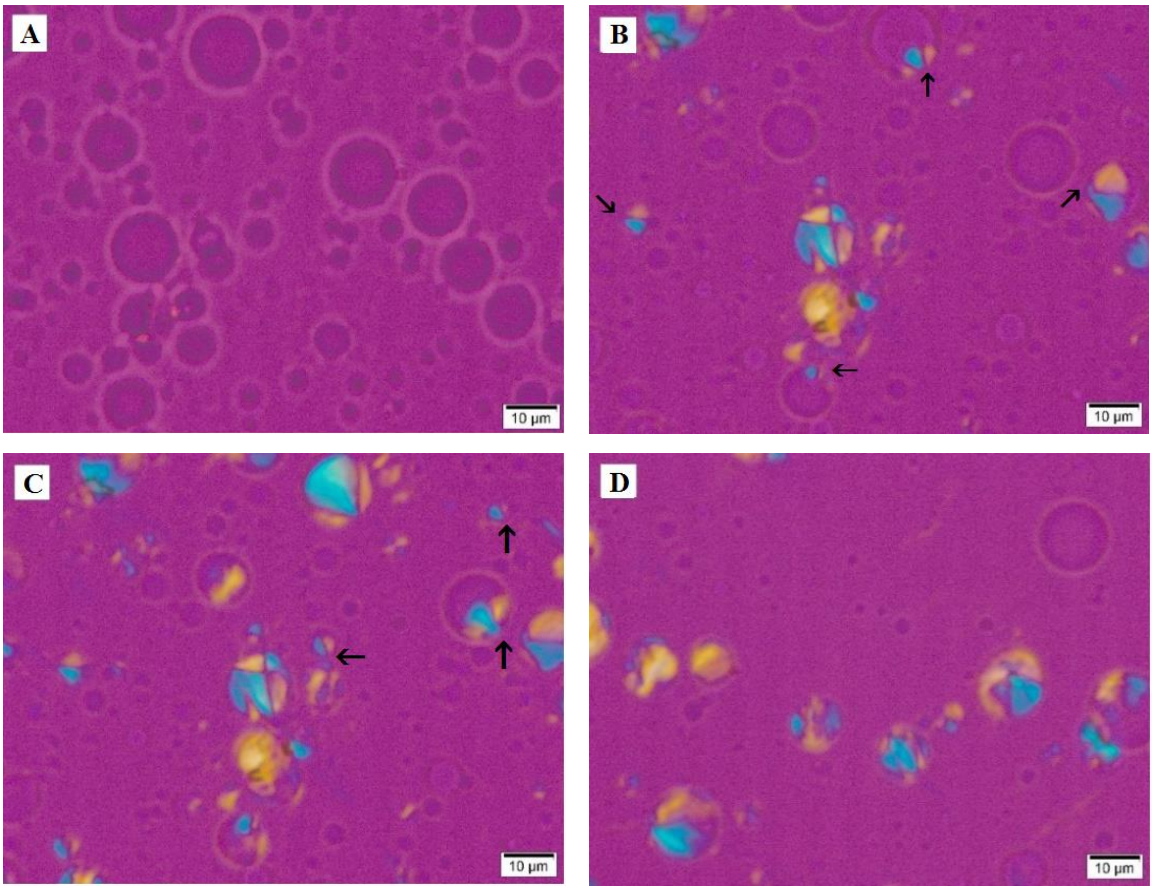

Figure 5.12. PLOM micrographs during the isothermal crystallization of PLA in 90/10 PBS/PLA binary blend at T_c = 120°C: A) 0 min, B) 10 min, C) 20 min and D) 30 min.

Several PLA spherulites are clearly seen to nucleate and grow in the separate PLA domains, until each droplet is completely crystallized. The point at which the nucleation occurred can be distinguished in most of the domains. Although a certain fraction of the PLA spherulites apparently originate from the bulk of the droplet, nucleation at the interface between molten PLA and PBS can be seen in multiple cases (highlighted by arrows). Unfortunately, a similar direct morphological observation cannot be carried out for 90/10 PCL/PLA blend, since the PLA droplet size is too small to be discernible, and we could not easily obtained an appropriate coarsening of the morphology with mild melt annealing treatments.

The 45/10/45 PCL/PLA/PBS ternary blend gave us the opportunity to compare the nucleation of PLA in contact with both molten PBS and PCL at the same time.

Figure 5.13 (A, B, and C) shows selected POM micrographs during the isothermal crystallization of PLA droplets at 125°C. PLA droplets are located between the molten polymers (molten PCL on one side and molten PBS on the other side). Micrographs B and C revealed that several PLA droplets nucleate at the interface with molten PCL, while only one started to grow from the PLA/PBS side. The nucleation is sporadic in time, but occurs mostly at the PLA/PCL interface. Another peculiar observation is the "sequential crystallization" or "contact nucleation" of PLA droplets: once that one droplet nucleates and crystallizes, the nucleation of the adjacent droplet occurs at the contact point with the former one.

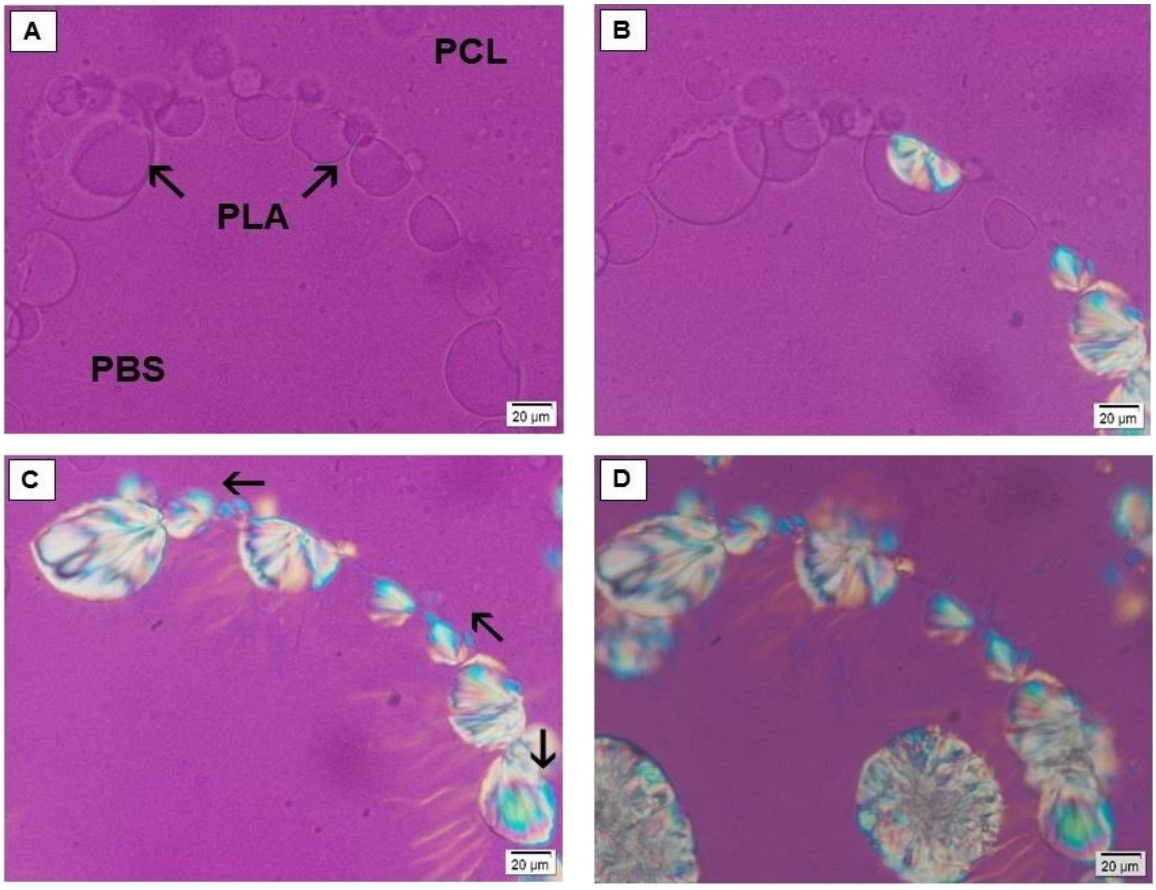

Figure 5.13. Selected POM micrographs during the stepwise isothermal crystallization of 45/10/45 PCL/PLA/PBS ternary blend. Micrograph (A) was taken after 1 min at 125°C, (B) after 20 min at 125°C, (C) after 45 min at 125°C, and (D) after 6 min at 98°C.

However, PLA droplets in 45/10/45 PCL/PLA/PBS found to nucleate through other different mechanisms such us nucleation from (i) PBS side, (ii) three phase contact line (point), and (iii) Bulk material. Figure 5.14 presents selective PLOM micrographs showing, as

it is indicated with arrows, cases of PLA droplets nucleation from three phase contact point (Figure 5.14A), from PBS side (Figure 5.14B), and from bulk phase (Figure 5.14C).

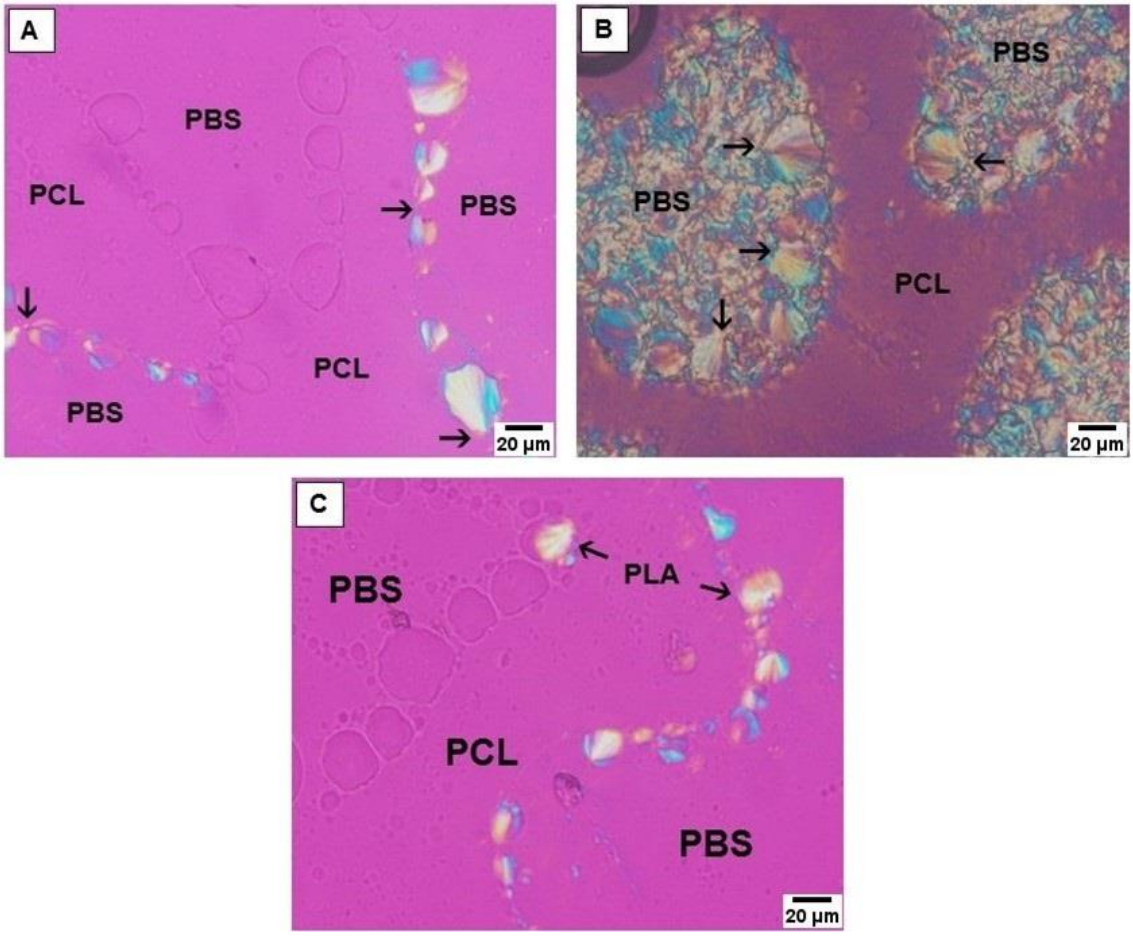

Figure 5.14. Selected POM micrographs during the stepwise isothermal crystallization of 45/10/45 PCL/PLA/PBS ternary blend. Micrograph (A) was taken at 130°C, (B,C) at 127.5°C.

The authors attributed this interface-induced nucleation to several reason:

1. phase separation effect: that the phase separation between the phases reduces the energy barrier needed for formation of nuclei [73,74,79,80,89].
2. Impurity and heterogeneities migration effect: heterogeneities migrate from one phase to the other phase and can be localized at the interface [74].
3. Interactions (chemical and/or physical) between the functional groups of the polymer chains at the interface during the melt processing, which leads to some local chain orientation, which will then facilitate the nucleation step [26,80,90].
4. Local miscibility between the phase separated components, which lower the energy barrier for the primary nucleation [72,91-95].

In Figure 5.15 we attempted a quantification of the number of PLA droplets that have been nucleated either from the bulk, from the molten PBS or PCL interfaces, or by contact with previously crystallized droplets (sequential crystallization). The analysis was performed at three different crystallization temperatures for a total number of more than 160 PLA droplets from multiple samples for each crystallization temperature (T_c).

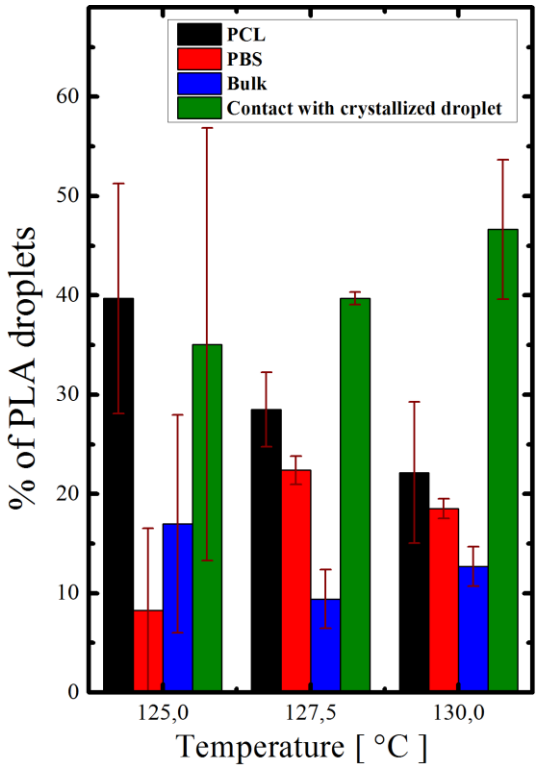

Figure 5.15. Percentage of PLA droplets that nucleate from the PCL side (black), PBS side (red), bulk PLA phase (blue), and by contact with previously crystallized droplets (green) for different crystallization temperatures (T_c).

It can be seen that, for all the investigated crystallization temperatures, PLA is found to nucelate predominantly by contact with crystallized droplet, or from the interface with molten PCL. Nucleation at the PBS interface or from the bulk of the PLA droplet is less common. This data only account for the number of droplet, without taking into account their relative size. By considering the specific length of each interface, we can obtain a meaningful comparison between the nucleating efficiency of PCL and PBS melts towards the PLA phase.

Figure 5.16 shows an estimation of the linear nucleation density of PLA droplets in contact with the two molten phases at the different crystallization temperatures.

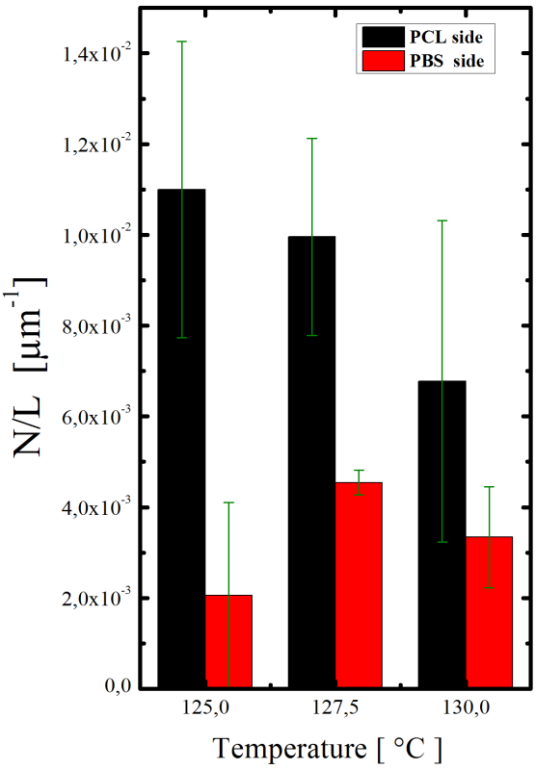

Figure 5.16. Linear nucleation density of PLA droplets in contact with molten PCL and molten PBS phases within 45/10/45 PCL/PLA/PBS as function of crystallization temperature.

The obtained results (Figure 5.13 & 5.16) are in agreement with those presented in Figure 5.10 and 5.11. Regardless of the applied T_c, the difference in the nucleating effect between PBS and PCL can be clearly grasped. The number of unit per length of PCL interface is always from 2 to 5 times larger than that on PBS. The applied crystallization temperatures have a small effect on the nucleation process occurring at the interfaces, i.e., a slight decrease in the nucleation density from PCL side with decreasing undercooling can be appreciated, while the differences between the two molten polymers is simultaneously reduced. It should be noted that from Figure 5.15, the amount of nuclei originating as an effect of the contact with crystallized droplets decreases by lowering the temperature, possibly due to the larger occurrence of other nucleation mechanism (bulk nucleation and nucleation from the molten surfaces) at larger undercoolings, and thus to the larger percentage of crystalline droplets at shorter times.

We could hypothesize that the higher nucleating effect of PCL on PLA, with respect to PBS originate from 1) the much higher interfacial tensions between the polymer pair, or 2) some local miscibility between PLA and0 PCL, which increases the mobility of PLA chains and lowers the energy barrier for the formation of nuclei [72,91-93]. We should note however

that several works reported a complete immiscibility between PLA and PCL [41,62]. As such, the hypothesis of a faster nucleation due to the local miscibility between the two polymers seems unlikely.

Isothermal crystallization of PBS in 45/10/45 PLA/PCL/PBS ternary blend

Stepwise crystallization of the 45/10/45 PLA/PCL/PBS ternary blend was studied. The PLA phase was firstly crystallized at 120°C for 20 min followed by quenching the sample at 50°C/min to the isothermal crystallization temperature of PBS (100°C for 25 min).

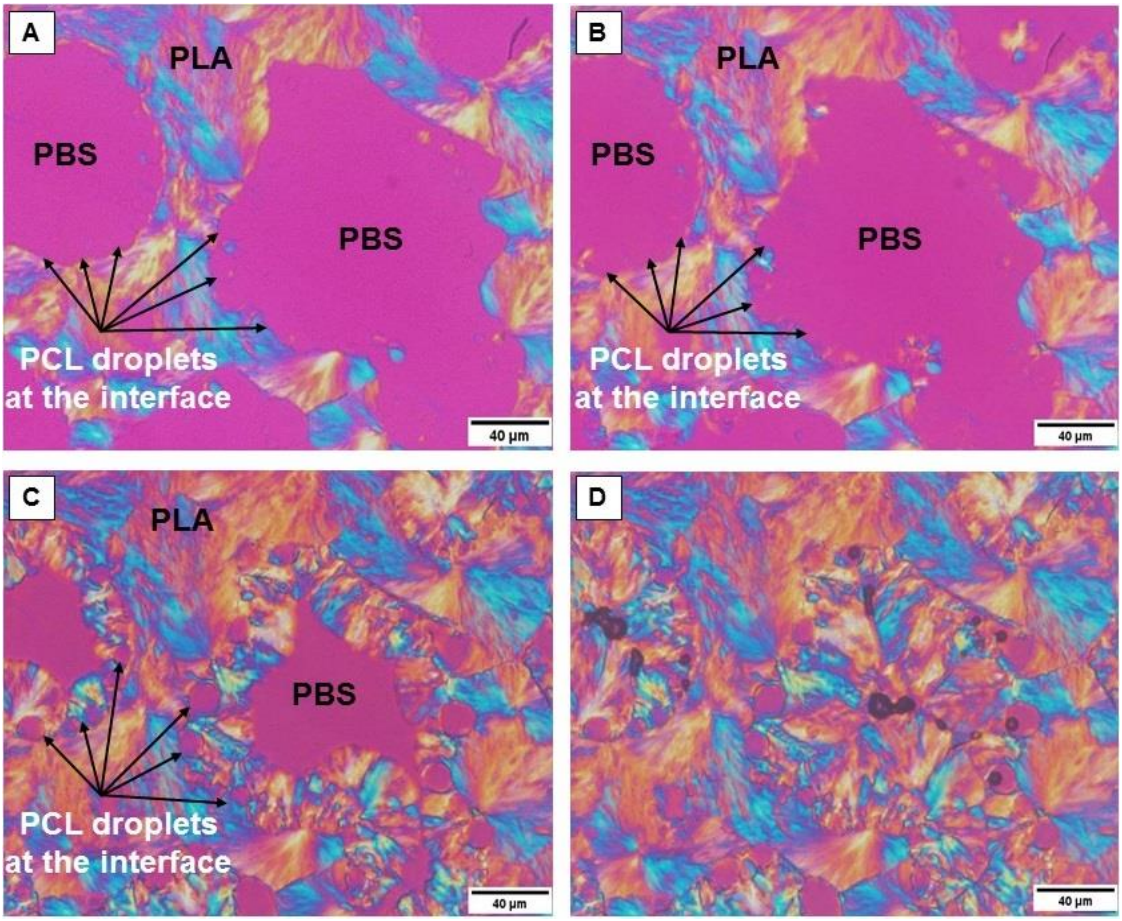

Figure 5.17. PLOM micrographs during the isothermal crystallization of PBS at T_c =100°C in the 45/10/45 PLA/PCL/PBS ternary blend. (A) after 0 min, (B) after 4 min, (C) after 12 min, and (D) after 25 min.

Figure 5.17 shows selected PLOM micrographs captured during the isothermal crystallization of PBS at 100°C (after the complete crystallization of the PLA phase at 120°C). The images revealed that the crystalline PLA phase plays the role of nucleating agent for PBS crystallization, as the PBS phase nucleation starts mainly at the interface with crystalline PLA. (The analysis of the obtained morphology shows the appearance of a

transcrystalline structure (Figure 5.17C and D). A transcrystalline structure is produced due to the high nucleation density at the interface PLA/PBS which leads to the growth of PBS spherulites perpendicular to the PLA/PBS interface. The observation in this particular system is in agreement with a previous investigation by Deng and Thomas [96] which reported the enhancement of PBS nucleation in in PLA/PBS blends.

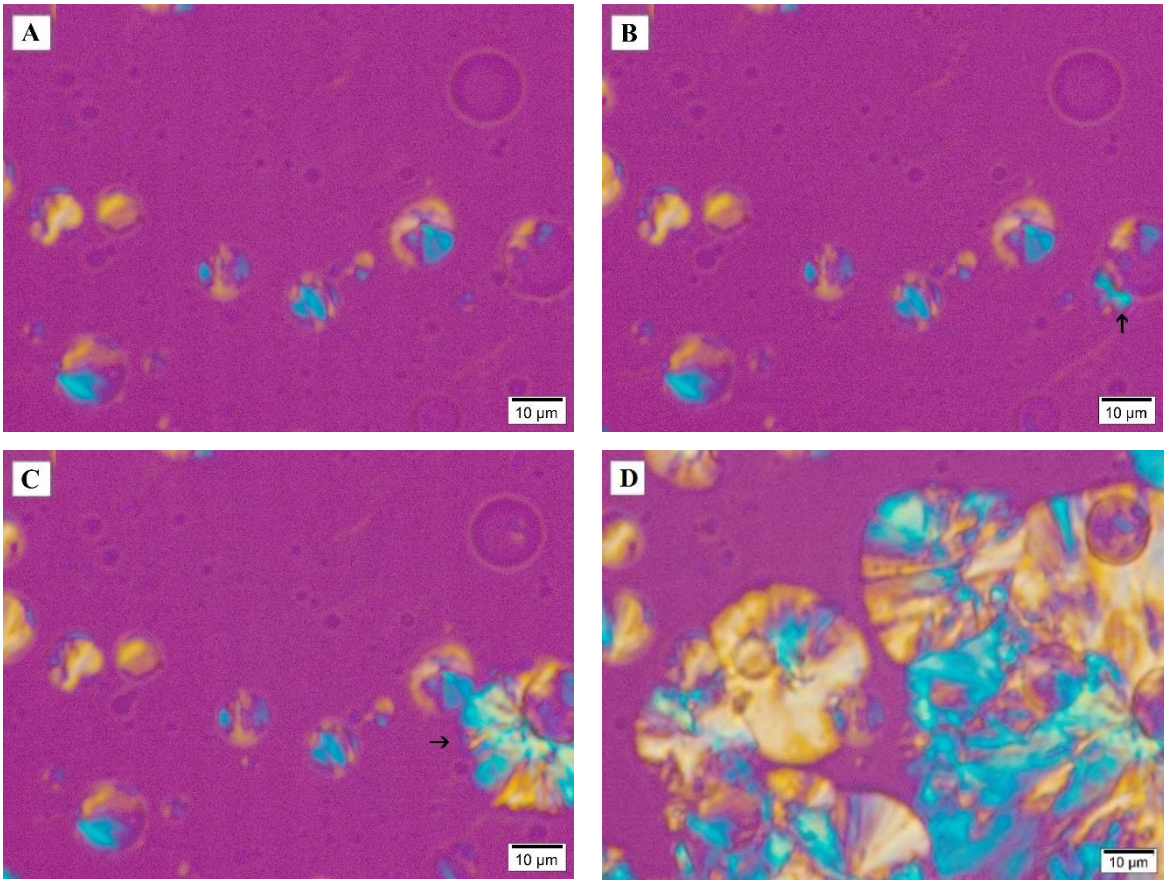

Figure 5.18. PLOM micrographs during the isothermal crystallization of the PBS phase in 90/10 PBS/PLA blend, in presence of PLA droplets previously crystallized at 120°C. Images were taken at 90°C after different crystallization times: A after 0 min, B after 2 min, C after 4 min, and D after 10 min.

The nucleating effect of crystalline PLA on PBS is also detectable in 90/10 PBS/PLA binary blend, upon stepwise crystallization. Figure 5.18 reports the isothermal crystallization of the PBS matrix, in presence of previously crystallized PLA droplets. The different frames capture the nucleation and growth of a PBS spherulite, starting at the interface with semicrystalline PLA (right side of the picture, see arrow). Given the fast PBS crystallization and relatively high bulk nucleation density of this polymer, it is not easy to distinguish other nucleation events at the polymer/polymer interface.

Sequential crystallization of droplets located at the interface between major phases in ternary blends

The case of nucleation of minor phase droplets at the interface between two major phases upon contact of previously crystallized droplets is further considered for both PBS and PLA phases. At first, the results of 45/10/45 PLA/PBS/PCL blends are shown. According to a stepwise crystallization protocol, PLA was firstly crystallized at 125°C for 45 min then the sample was quenched (at a rate of 50°C/min) to the crystallization temperature of PBS (100°C). Figure 5.19 shows PLOM micrographs at different times during the isothermal crystallization of PBS droplets.

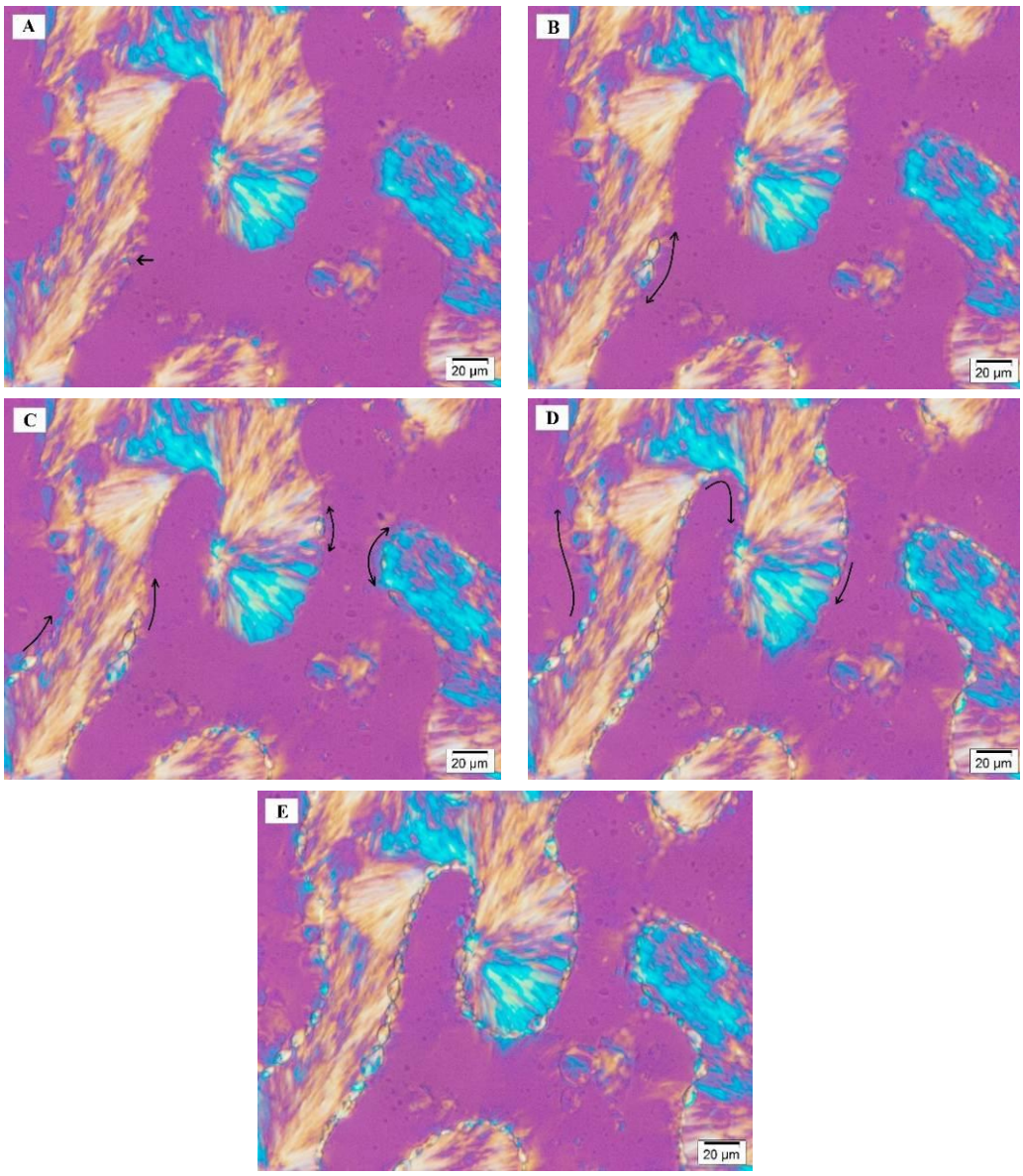

Figure 5.19. PLOM micrographs showing the sequential crystallization of PBS droplets in the 45/10/45 PLA/PBS/PCL ternary blend at 100°C, A) after 11 min, B) after 15 min, C) after 20 min, D) after 30 min, and E) after 50 min. The arrows indicate the direction of nucleation.

Although the PBS droplets are not easily distinguished before crystallization, they become birefringent upon solidification. In several locations, as indicated by the black arrows, it can be seen that the crystallization of PBS domains does not occur at random places, but rather initiate from one droplets, and then propagate to the adjacent one progressively, either in one or two directions. As such, nucleation spread from one droplet to another in a sequence, obviously when the crystalline domains come in contact with the yet amorphous PBS. A "pearl-necklace" morphology, constituted of PBS crystalline droplets around solidified PLA and molten PCL domains is formed at later stages.

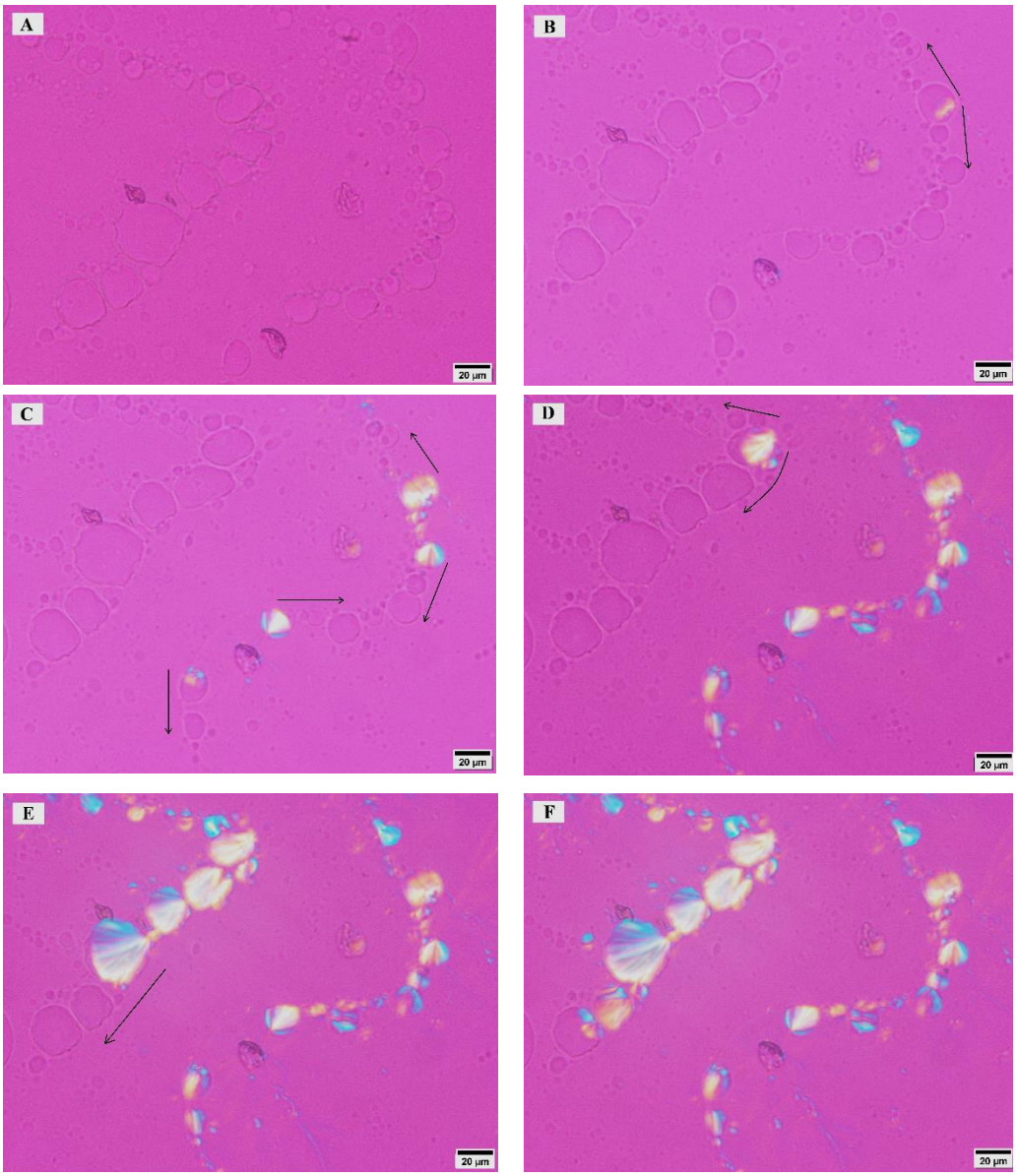

Figure 5.20. PLOM micrographs showing the sequential crystallization of PLA droplets in the 45/10/45 PCL/PLA/PBS ternary blend at 127.5°C, A) after 0 min, B) after 5 min, C) after 10 min, D) after 30 min, E) after 44 min, and F) after 50 min. The black arrows indicate the direction of sequential crystallization.

An analogous situation can be highlighted in 45/10/45 PBS/PLA/PCL blends, where PLA droplets can crystallize at the interface with two different molten phases. Figure 5.20 shows PLOM micrographs taken at different times during the isothermal crystallization of PLA droplet at 127.5°C.

Similarly to what observed for PBS droplets, it can be clearly seen that the crystallization of a given droplet can affect nucleation in adjacent molten domains, thus leading to droplet solidification in a sequential fashion. Moreover, when the droplets are large enough, the morphological signature of this sequential nucleation is retained by analyzing the growth direction of the spherulites. Once the nucleation point is identified, it can indeed be seen that adjacent droplets often show a related crystal growth direction, testifying that the nucleation occurs in a precise sequence from the contact point between the considered amorphous droplet and the previously crystallized one.

The reasons behind this phenomenon should be investigated in details, but it is believed that the sequential nucleation originates because of the high surface coverages realized for partial wetting morphology in these systems (see Table 5.2), which makes relatively unavoidable this "percolation" of the nuclei.

5.4 Conclusions

In this work, we mostly focused on triple crystalline thermoplastic polyester immiscible blends. The nucleation and crystallization of these complex materials greatly depends on their morphology, as determined by their composition and thermal history. Two different kinds of blend morphology were successfully produced, namely sea-island morphology in binary blends and partial-wetting morphology in the ternary blends.

For binary blends, the crystallization behavior was investigated by DSC, revealing enhanced or depressed crystallization of a given polymer in the different blends. In particular, a small acceleration of PLA cold-crystallization by both PCL and PBS phases was observed.

The different ternary blends were studied upon isothermal crystallization using PLOM. PLA was found to nucleate both on PCL and PBS phases, while these polymers were in the molten state. In particular, molten PCL exhibited a higher nucleating efficiency towards PLA, with respect to PBS. This could be tentatively attributed to the substantially higher interfacial tension between PLA/PCL in comparison with that of PLA/PBS. However, this

new intriguing mechanism of nucleation on a molten surface is worthwhile of further investigation.

In sequential crystallization, the lower melting temperature component can nucleate on the surface of the previously crystallized one) (with higher melting temperature). This is the case for instance of PBS which nucleate on crystalline PLA both in binary and ternary blends. The possible existence of epitaxial relationships between the two polymers could be explored in the future. Also, the peculiar nucleating effects of PCL and PBS droplets on glassy PLA matrices definitely deserve more research.

The achievable degree of morphological complexity, and the interplay between morphology and nucleation will require further studies, with the aim of eventually tailoring the properties of biodegradable polymer blends for substituting traditional non-degradable polymeric materials.

5.5 References

1. Utracki LA, Wilkie C (Eds) (2014) Polymer Blends Handbook. Springer, New York
2. Utracki LA (Ed) (2002) Polymer Blends Handbook, vol 2. Kluwer Academic Publishers, Dordrecht, Netherlands
3. Paul DR, Barlow JW (1979) A Brief Review of Polymer Blend Technology. In: Cooper SL, Estes GM (Eds) multiphase polymers. Advances in Chemistry, Washington, p 315-335
4. Paul DR, Barlow JW (1980) Polymer Blends (or Alloys). J. Macromol. Sci., Rev. Macromol. Chem. Phys. 18:109-168
5. Supthanyakul R, Kaabbuathong N, Chirachanchai S (2016) Random poly(butylene succinate-co-lactic acid) as a multi-functional additive for miscibility, toughness, and clarity of PLA/PBS blends. Polymer 105:1-9
6. Dhibar AK, Kim JK, Khatua BB (2011) Cocontinuous Phase Morphology of Asymmetric Compositions of Polypropylene/High-density Polyethylene Blend by the Addition of Clay. J. Appl. Polym. Sci. 119:3080-3092
7. Harrats C, Groeninckx G, Thomas S (Eds) (2005) Micro-and nanostructured multiphase polymer blend systems: phase morphology and interfaces. CRC press, Taylor & Francis, USA

8. Hemmati M, Nazokdast H, Shariat Panahi H (2001) Study on morphology of ternary polymer blends. I. Effects of melt viscosity and interfacial interaction. J. of Appl. Polym. Sci. 82:1129-1137
9. Le Corroller P, Favis BD (2011) Effect of viscosity in ternary polymer blends displaying partial wetting phenomena. Polymer. 52:3827-3834
10. Guo H, Packirisamy S, Gvozdic N, Meier D (1997) Prediction and manipulation of the phase morphologies of multiphase polymer blends: 1. Ternary systems. Polymer. 38:785-794
11. Zolali AM, Favis BD (2016) Partial and Complete Wetting in Ultralow Interfacial Tension Multiphase Blends with Polylactide. J. Phys. Chem. B. 120:12708-12719
12. Zolali AM, Favis BD (2017) Partial to complete wetting transitions in immiscible ternary blends with PLA: the influence of interfacial confinement. Soft Matter. 13:2844-2856
13. Virgilio N, Desjardins P, L'Espérance G, Favis BD (2009) In Situ Measure of Interfacial Tensions in Ternary and Quaternary Immiscible Polymer Blends Demonstrating Partial Wetting. Macromolecules. 42:7518-7529
14. Zolali AM, Favis BD (2017) Compatibilization and toughening of co-continuous ternary blends via partially wet droplets at the interface. Polymer 114:277-288
15. Zhang K, Nagarajan V, Misra M, Mohanty AK (2014) Supertoughened Renewable PLA Reactive Multiphase Blends System: Phase Morphology and Performance. ACS Appl. Mater. Interfaces. 6:12436-12448
16. Zhang K, Mohanty AK, Misra M (2012) Fully Biodegradable and Biorenewable Ternary Blends from Polylactide, Poly(3-hydroxybutyrate-co-hydroxyvalerate) and Poly(butylene succinate) with Balanced Properties. ACS Appl. Mater. Interfaces. 4:3091-3101
17. Fu Y, Fodorean G, Navard P, Peuvrel-Disdier E (2018) Study of the partial wetting morphology in polylactide/poly[(butylene adipate)-co-terephthalate]/polyamide ternary blends: case of composite droplets. Polym. Int. 67:1378-1385
18. Ravati S, Favis BD (2013) Interfacial coarsening of ternary polymer blends with partial and complete wetting structures. Polymer. 54:6739-6751
19. Jegat C, Virgilio N, Favis BD (2017) Self-assembly of oil microdroplets at the interface in co-continuous polymer blends. Eur. Polym. J. 93:259-271
20. Ravati S, Beaulieu C, Zolali AM, Favis BD (2014) High performance materials based on a self-assembled multiple-percolated ternary blend. AIChE J. 60:3005-3012
21. Virgilio N, Marc-Aurèle C, Favis BD (2009) Novel Self-Assembling Close-Packed Droplet Array at the Interface in Ternary Polymer Blends. Macromolecules. 42:3405-3416

22. Ravati S, Favis BD (2013) Tunable morphologies for ternary blends with poly(butylene succinate): Partial and complete wetting phenomena. Polymer. 54:3271-3281
23. Jalali Dil E, Carreau PJ, Favis BD (2015) Morphology, miscibility and continuity development in poly(lactic acid)/poly(butylene adipate-co-terephthalate) blends. Polymer. 68:202-212
24. Chen H-m, Wang X-f, Liu D, Wang Y-p, Yang J-h, Wang Y, Zhang C-l, Zhou Z-w (2014) Tuning the interaction of an immiscible poly(l-lactide)/poly(vinylidene fluoride) blend by adding poly(methyl methacrylate) via a competition mechanism and the resultant mechanical properties. RSC Adv. 4:40569-40579
25. Ravati S, Favis BD (2010) Morphological states for a ternary polymer blend demonstrating complete wetting. Polymer. 51:4547-4561
26. Ravati S, Poulin S, Piyakis K, Favis BD (2014) Phase identification and interfacial transitions in ternary polymer blends by ToF-SIMS. Polymer. 55:6110-6123
27. Yang J-h, Feng C-x, Chen H-m, Zhang N, Huang T, Wang Y (2016) Toughening effect of poly(methyl methacrylate) on an immiscible poly(vinylidene fluoride)/polylactide blend. Polym. Int. 65:675-682
28. Rezaei Kolahchi A, Ajji A, Carreau PJ (2014) Surface Morphology and Properties of Ternary Polymer Blends: Effect of the Migration of Minor Components. J. Phys. Chem. B. 118:6316-6323
29. Luzinov I, Xi K, Pagnoulle C, Huynh-Ba G, Jérôme R (1999) Composition effect on the core–shell morphology and mechanical properties of ternary polystyrene/styrene–butadiene rubber/polyethylene blends. Polymer. 40:2511-2520
30. Guo H-F, Gvozdic N, Meier D (1997) Prediction and manipulation of the phase morphologies of multiphase polymer blends: II. Quaternary systems. Polymer. 38:4915-4923
31. Luzinov I, Pagnoulle C, Jérôme R (2000) Ternary polymer blend with core–shell dispersed phases: effect of the core-forming polymer on phase morphology and mechanical properties. Polymer. 41:7099-7109
32. Nemirovski N, Siegmann A, Narkis M (1995) Morphology of ternary immiscible polymer blends J. Macromol. Sci. Part B phys. 34:459-475
33. Cerclé C, Favis BD (2012) Generalizing interfacial modification in polymer blends. Polymer. 53:4338-4343

34. Chen YC, Dimonie V, El-Aasser MS (1991) Effect of interfacial phenomena on the development of particle morphology in a polymer latex system. Macromolecules. 24:3779-3787
35. Wang J, Reyna-Valencia A, Favis BD (2016) Assembling Conductive PEBA Copolymer at the Continuous Interface in Ternary Polymer Systems: Morphology and Resistivity. Macromolecules. 49:5115-5125
36. Cordova ME, Lorenzo AT, Müller AJ, Gani L, Tence-Girault S, Leibler L (2011) The Influence of Blend Morphology (Co-Continuous or Sub-Micrometer Droplets Dispersions) on the Nucleation and Crystallization Kinetics of Double Crystalline Polyethylene/Polyamide Blends Prepared by Reactive Extrusion. Macromol. Chem. Phys. 212:1335-1350
37. Pracella M (2013) Crystallization of polymer blends. In: Piorkowska E, Rutledge GC (eds) handbook of polymer crystallization. Wiley, New Jersey, p 287-325
38. Jabarin SA, Ardakani KM, Lofgren EA (2016) Crystallization and Melting Behavior in Polymer Blends. In: Isayev AI (ed) Encyclopedia of Polymer Blends volume 3: Structure. Wiley-VCH Verlag GmbH & Co. KGaA, Weinheim, Germany, p 135-189
39. Michell RM, Müller AJ (2016) Confined crystallization of polymeric materials. Prog. Polym. Sci. 54-55, 183-213
40. Tien ND, Prud'homme RE (2017) Crystallization Behavior of Semicrystalline Immiscible Polymer Blends. In: Thomas S, Arif PM, Gowd B, Kalarikkal N (eds) Crystallization in Multiphase Polymer Systems. Elsevier, Amsterdam, p 181-212
41. Rizzuto M, Marinetti L, Caretti D, Mugica A, Zubitur M, Müller AJ (2017) Can poly (ε-caprolactone) crystals nucleate glassy polylactide?. CrystEngComm. 19:3178
42. Arrieta MP, Fortunati E, Dominici F, López J, Kenny JM (2015) Bionanocomposite films based on plasticized PLA–PHB/cellulose nanocrystal blends. Carbohydr. Polym. 121:265-275
43. Salehi S, Bahners T, Gutmann JS, Gao SL, Mäder E, Fuchsluger TA (2014) Characterization of structural, mechanical and nano-mechanical properties of electrospun PGS/PCL fibers. RSC Adv. 4:16951-16957
44. Phua YJ, Pegoretti A, Araujo TM, Ishak ZAM (2015) Mechanical and thermal properties of poly(butylene succinate)/poly(3-hydroxybutyrate-co-3-hydroxyvalerate) biodegradable blends. J. Appl. Polym. Sci. 132:42815/1-42815/10

45. Lorenzo AT, Arnal ML, Albuerne J, J. Müller AJ (2007) DSC isothermal polymer crystallization kinetics measurements and the use of the Avrami equation to fit the data: Guidelines to avoid common problems. Polym. Test. 26:222-231
46. Balsamo V, Urdaneta N, Perez L, Carrizales P,Abetz V, Müller AJ (2004) Effect of the polyethylene confinement and topology on its crystallization within semicrystalline ABC triblock copolymers. Eur. Polym. J. 40:1033-1049
47. Müller AJ, Michell RM (2016) Differential Scanning Calorimetry of Polymers. In: Guo Q (ed) Polymer Morphology: Principles, Characterization, and Processing. John Wiley & Sons, Inc., New Jersey, p 72-99
48. Morales RA, Arnal ML, Müller AJ (1995) The evaluation of the state of dispersion in immiscible blends where the minor phase exhibits fractionated crystallization. Polym. Bull. 35:379-386
49. Arnal ML, Matos ME, Morales RA, Santana OO, Müller AJ (1998) Evaluation of the fractionated crystallization of dispersed polyolefins in a polystyrene matrix. Macromol. Chem. Phys. 199:2275-2288
50. Arnal ML, Müller AJ (1999) Fractionated crystallisation of polyethylene and ethylene/a-olefin copolymers dispersed in immiscible polystyrene matrices. Macromol. Chem. Phys. 200:2559-2576
51. Schick C, Androsch R, Schmelzer JWP (2017) Homogeneous crystal nucleation in polymers. J. Phys.: Condens. Matter. 29:453002
52. Santana OO. Müller AJ (1994) Homogeneous nucleation of the dispersed crystallizable component of immiscible polymer blends. Polym. Bull. 32:471-477
53. Michell RM, Blaszczyk-Lezak I, Mijangos C, Müller AJ (2013) Confinement effects on polymer crystallization: From droplets to alumina nanopores. Polymer. 54:4059-4077
54. Tol RT, Mathot VBF, Groeninckx G (2005) Confined crystallization phenomena in immiscible polymer blends with dispersed micro- and nanometer sized PA6 droplets, part 2: reactively compatibilized PS/PA6 and (PPE/PS)/PA6 blends. Polymer. 46:383-396
55. Tol RT, Mathot VBF, Groeninckx G (2005) Confined crystallization phenomena in immiscible polymer blends with dispersed micro- and nanometer sized PA6 droplets, part 3: crystallization kinetics and crystallinity of micro- and nanometer sized PA6 droplets crystallizing at high supercoolings. Polymer. 46:2955-2965
56. Yordanov C, Minkova L (2005) Fractionated crystallization of compatibilized LDPE/PA6 blends. Eur. Polym. J. 41:527–534

57. Di Lorenzo ML, Androsch R (2018) Influence of α′-/α-crystal polymorphism on properties of poly(l-lactic acid). Polym. Int. 0:1-15
58. Yokohara T, Yamaguchi M (2008) Structure and properties for biomass-based polyester blends of PLA and PBS. Eur. Polym. J. 44, 677-685
59. Shibata M, Inoue Y, Miyoshi M (2006) Mechanical properties, morphology, and crystallization behavior of blends of poly(L-lactide) with poly(butylene succinate-co-L-lactate) and poly(butylene succinate). Polymer. 47:3557-3564
60. Wu D, Yuan L, Laredo E, Zhang M, Zhou W (202) Interfacial Properties, Viscoelasticity, and Thermal Behaviors of Poly(butylene succinate)/Polylactide Blend. Ind. Eng.Chem. Res. 51:2290-2298
61. Luzi F, Fortunati E, Jiménez A, Pugliaa D, Pezzolla D, Gigliotti G, Kenny JM, Chiralt A, Torre L (2016) Production and characterization of PLA/PBS biodegradable blends reinforced with cellulose nanocrystals extracted from hemp fibres. Ind. Crops Prod. 93:276-289
62. Rizzuto M, Mugica A, Zubitur M, Caretti D, Müller AJ (2016) Plasticization and anti-plasticization effects caused by poly(L-lactide-ran-caprolactone) addition to double crystalline poly(L-lactide)/poly(ε- caprolactone) blends. CrystEngComm. 18:2014
63. Jain S, Reddy MM, Mohanty AK, Misra M, Ghosh AK (2010) A New Biodegradable Flexible Composite Sheet from Poly(lactic acid)/Poly(e-caprolactone) Blends and Micro-Talc. Macromol. Mater. Eng. 295:750-762
64. Dell'Erba R, Maglio G, Malinconico M, Migliozzi A (2001) Immiscible polymer blends of semicrystalline biocompatible components: thermal properties and phase morphology analysis of PLLA/PCL blends. Polymer. 42:7831-7840
65. Shen T, Lu M, Liang L (2013) Modification of the Properties of Polylactide/ Polycaprolactone Blends by Incorporation of Blocked Polyisocyanate. J. Macromol. Sci. Part A Pure Appl. Chem. 50:547–554
66. Navarro-Baena I, Sessini V, Dominici F, Torre L, Kenny JM, Peponi L(2016) Design of biodegradable blends based on PLA and PCL: From morphological, thermal and mechanical studies to shape memory behavior. Polym. Degrad. Stab. 132:97-108
67. Harada M, Iida K, Okamoto K, Hayashi H, Hirano K (2008) Reactive Compatibilization of Biodegradable Poly(lactic acid)/Poly(ε-caprolactone) Blends with Reactive Processing Agents. Polym. Eng. Sci. 48:1359-1368

68. Urquijo J, Guerrica-Echevarrıa G, Eguiazabal JI (2015) Melt processed PLA/PCL blends: Effect of processing method on phase structure, morphology, and mechanical properties. J. Appl. Polym. Sci. 42641:1-9
69. Ostafinska A, Fortelny I, Nevoralova M, Hodan J, Kredatusova J, Slouf M (2015) Synergistic effects in mechanical properties of PLA/PCL blends with optimized composition, processing, and morphology. RSC Adv. 5, 98971-98982
70. Chavalitpanya k, Phattanarudee S (2013) Poly(lactic acid)/Polycaprolactone Blends Compatibilized with Block Copolymer. Energy Procedia. 34:542-548
71. Matta AK, Rao RU, Sumana KNS, Rambabuc V (2014) Preparation and Characterization of Biodegradable PLA/PCL Polymeric Blends. Procedia Mater. Sci. 6:1266-1270
72. Tuba F, Olah L, Nagy P (2011) Characterization of reactively compatibilized poly(D,L-lactide)/poly(ε-caprolactone) biodegradable blends by essential work of fracture method. Eng. Fract. Mech. 78:3123-3133
73. Di Lorenzo ML, Cimmino S, Silvestre C (2001) Nonisothermal Crystallization of Isotactic Polypropylene Blended with Poly(α-pinene). I. Bulk Crystallization. J. Appl. Polym. Sci. 82:358-367
74. Bartczak A, Galeski A, Krasnikova NP (1987) Primary nucleation and spherulite growth rate in isotactic polypropylene-polystyrene blends. Polymer. 28:1627-1634
75. Ma P, Hristova-Bogaerds DG, Zhang Y, Lemstra PJ (2014) Enhancement in crystallization kinetics of the bacterially synthesized poly(β-hydroxybutyrate) by poly(butylene succinate). Polym. Bull. 71:907-923
76. Lovera D, Marquez L, Balsamo V, Taddei A, Castelli C, Müller AJ (2007) Crystallization, Morphology, and Enzymatic Degradation of Polyhydroxybutyrate / Polycaprolactone (PHB/PCL) Blends. Macromol. Chem. Phys. 208:924-937
77. Müller AJ, Avila M, Saenz G, Salazar J (2014) Crystallization of PLA-based Materials. In Jiménez A, Peltzer M, Ruseckaite R (eds) Poly(lactic acid) Science and Technology: Processing, Properties, Additives and Applications. The Royal Society of Chemistry, Cambridge, UK, p 66-98
78. Di Lorenzo ML, Androsch R (2015) Crystallization of Poly(lactic acid). In: Fakirov S (ed) Biodegradable Polyesters. Wiley-VCH Verlag GmbH & Co. KGaA, Weinheim, Germany, p 109-130
79. Wenig W, Fiedel HW (1991) Dispersion of trans-polyoctenylene in isotactic poly(propylene), 2[a)] Crystallization behavior. Makromol. Chem. 192:191-199

80. Di Lorenzo ML, Rubino P, Cocca M (2014) Isothermal and Non-Isothermal Crystallization of Poly(L-lactic acid)/Poly(butylene terephthalate) Blends. J. Appl. Polym. Sci. 40372:1-8
81. Huo H, Guo C, Zhou J, Zhao X (2014) The combination of fluctuation-assisted crystallization and interface-assisted crystallization in a crystalline/crystalline blend of poly(ethylene oxide) and poly(ε-caprolactone). Colloid Polym. Sci. 292:971-983
82. Qiaolian Lv, Wu D, Xie H, Peng S, Chen Y, Xu C (2016) Crystallization of poly(3-caprolactone) in its immiscible blend with polylactide: insight into the role of annealing histories. RSC Adv. 6:37721
83. Sakai F, Nishikawa K, Inoue Y, Yazawa K (2009) Nucleation Enhancement Effect in Poly(L-lactide) (PLLA)/Poly(ε-caprolactone) (PCL) Blend Induced by Locally Activated Chain Mobility Resulting from Limited Miscibility. Macromolecules 42:8335-8342
84. Pan P, Shan G, Bao Y (2014) Enhanced Nucleation and Crystallization of Poly(L-lactic acid) by Immiscible Blending with Poly(vinylidene fluoride). Ind. Eng. Chem. Res. 53:3148-3156
85. Kong Y, Ma Y, Lei L, Wang X, Wang H (2017) Crystallization of Poly(ϵ-caprolactone) in Poly(vinylidene fluoride)/Poly(ε -caprolactone) Blend. Polymers 9:42
86. Shi W, Chen F, Zhang Y, Han CC (2012) Viscoelastic Phase Separation and Interface Assisted Crystallization in a Highly Immiscible iPP/PMMA Blend. ACS Macro Lett. 1:1086-1089
87. Wu D, Lin D, Zhang J, Zhou W, Zhang M, Zhang Y, Wang D, Lin B (2011) Selective Localization of Nanofillers: Effect on Morphology and Crystallization of PLA/PCL Blends. Macromol. Chem. Phys. 212:613-626
88. Yu C, Han L, Bao J, Shan G, Bao Y, Pan P (2016) Polymorphic Crystallization and Crystalline Reorganization of Poly(L-lactic acid)/Poly(D-lactic acid) Racemic Mixture Influenced by Blending with Poly(vinylidene fluoride). J. Phys. Chem. B 120 (32):8046-8054
89. Di Lorenzo ML, Rubino P, Cocca M (2013) Miscibility and properties of poly(L-lactic acid)/poly(butylene terephthalate) blends. Eur. Polym. J. 49:3309-3317
90. Tang YR, Li T, Ye HM, Xu J, Guo BH (2016) The Effect of Polymer-Substrate Interaction on the Nucleation Property: Comparing Study of Graphene and Hexagonal Boron Nitride Nanosheets. Chin. J. Polym. Sci. 34 :1021-1031

91. Sakai F, Nishikawa K, Inoue Y, Yazawa K (2009) Nucleation Enhancement Effect in Poly(L-lactide) (PLLA)/Poly(ε-caprolactone) (PCL) Blend Induced by Locally Activated Chain Mobility Resulting from Limited Miscibility. Macromolecules 42:8335-8342
92. Wachirahuttapong S, Thongpin C, Sombatsompop N (2016) Effect of PCL and compatibility contents on the morphology, crystallization and mechanical properties of PLA/PCL blends. Energy Procedia. 89:198-206
93. Wang L, Ma W, Gross RA, McCarthy SP (1998) Reactive compatibilization of biodegradable blends of poly(lactic acid) and poly(ε-caprolactone). Polym. Degrad. Stab. 59:161-168
94. Persenaire O, Quintana R, Lemmouchi Y, Sampson J, Martin S, Bonnaud L, Dubois P (2014) Reactive compatibilization of poly(L-lactide)/poly(butylene succinate) blends through polyester maleation: from materials to properties. Polym. Int. 63:1724-1731
95. Bhatia A, Gupta RK, Bhattacharya SN, Choi HJ (2010) Effect of Clay on Thermal, Mechanical and Gas Barrier Properties of Biodegradable Poly(lactic acid)/Poly(butylene succinate) (PLA/PBS) Nanocomposites. Int. Polym. Proc. 25:5-14
96. Deng Y, Thomas NL (2015) Blending poly(butylene succinate) with poly(lactic acid): Ductility and phase inversion effects. Eur. Polym. J. 71:534-546

Self-nucleation of PLA, PBS and PCL in their immiscible binary and ternary blends

Partialy reproduced from: S.E. Fenni et al. "Crystallization and self-nucleation of PLA, PBS and PCL in their immiscible binary and ternary blends". Thermochimica Acta. Accepted (**2019**).

Chapter VI

Self-nucleation of PLA, PBS and PCL in their immiscible binary and ternary blends

6.1 Introduction

Among the various possible nucleation mechanisms of semicrystalline polymers, the peculiar self-nucleation process remains the least understood. The self-nucleation (SN) protocol consists in melting the polymer under "mild" conditions, i.e., relatively low temperatures and/or short times, that leads to the production of self-nuclei within the polymer melt. As a result, a large increase in nucleation density and crystallization temperature during subsequent cooling from the melt is observed. The exact nature of the residual order in the melt which provides the nucleation effect is still elusive. Blundell, Keller and Kovacs were the first to apply a self-nucleation experimental protocol to the production of single crystals with identical sizes from solution, while its first extension to Differential Scanning Calorimetry was proposed by Fillon et al. [1,2]. Müller et al. have extensively investigated self-nucleation and recently they reviewed its application to polymers, polymer blends, block and random copolymers and nanocomposites [3].

Fillon et al. [2] divided the range of self-nucleation temperatures (T_s) in three *Domains*, depending on the measured effect on re-crystallization and subsequent melting:

- ***Domain I*** (or complete melting *Domain*) is encountered when the polymer is completely molten and the crystalline memory of the material is totally erased.

- ***Domain II*** (or self-nucleation *Domain*) is entered when the applied T_s is low enough to leave self-nuclei and high enough to avoid annealing of unmolten crystals. As a consequence, the crystallization temperature of the material will shift toward higher values during the cooling scan after self-nucleation, while no sign of melting from annealed (thickened) crystals will be observed in a subsequent heating run.

- ***Domain III*** (or self-nucleation and annealing *Domain*), the applied T_s is so low that only partial melting of the original crystals will result, and thus unmolten crystal fragments will

anneal during the holding time at the specific T_s. The melting endotherm after re-crystallization will thus exhibit a sharp peak at temperatures higher than those of the non-self-nucleated material.

Figure 6.1 provides a schematic diagram to illustrate at the molecular level the different self-nucleation domains.

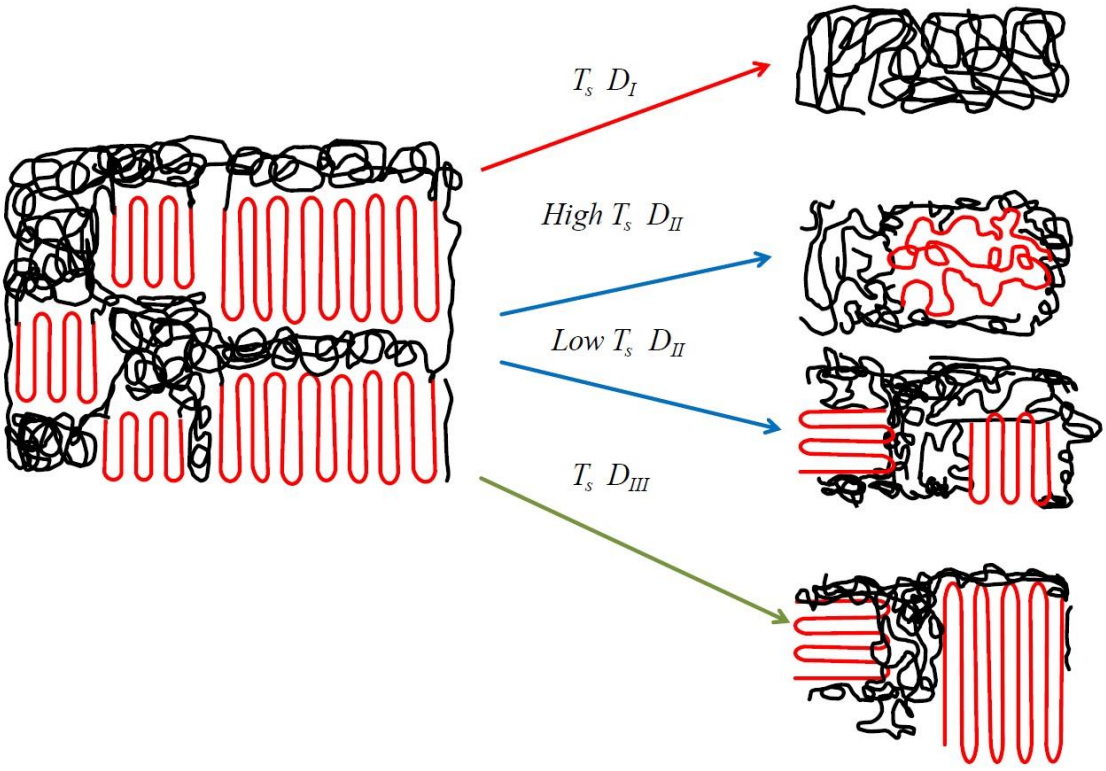

Figure 6.1. Schematic molecular representation of the different self-nucleation Domains [4].

The issue of polymer nucleation becomes of particular interest in immiscible polymer blends containing at least one semicrystalline component. In fact, it is well known that the nucleation behaviour can be greatly affected by the blend morphology. For example, in binary blends, when the crystallizable minor component is dispersed in the form of small droplets in the continuous matrix of the major phase, fractionated crystallization can be observed [5-15].

On the other hand, in blends with coarser morphologies, nucleation of a semicrystalline polymer at the interface with the second immiscible component is sometime reported. [16,17] Increasing the number of the blended polymers leads to an increased morphological complexity. For ternary blends, under particular conditions of polymer interfacial tension ratios, a partial-wetting morphology can be obtained [18-23]. This morphology consists of droplets of the minor phase which are assembled at the interface of the other two major phases and display three

phase contact. To date, little is known on the nucleation and crystallization of ternary blends containing one or more crystallizable component.

In fact, in addition to its large applications range as a tool to investigate: (i) the overall crystallization rate of low-crystallizing materials by accelerating the primary nucleation step, (ii) the crystalline memory, (iii) chain topology and their effect on the crystallization behavior, (iv) to trigger specific crystallization of a polymorphic polymer, (v) and to evaluate the nucleation efficiency of nucleating agents and fillers/nanofillers [3]. SN has been previously applied to several binary immiscible polymer blends characterized by a droplet-in-matrix morphology. It has been shown that self-nuclei can be injected in the polymer droplet, overcoming the effect of fractionated crystallization. For example, while an 80/20 PS/PP blend displayed four different crystallization exotherms at low temperatures when cooling from a melt in *Domain I*, a single peak at temperatures corresponding to those of the bulk self-nucleated samples was obtained upon cooling from the lowest T_s within *Domain II* [9]. Moreover, in case two semicrystalline components in an immiscible blend show a coincident crystallization, i.e., solidify upon cooling in the same temperature range, the self-nucleation of the high-melting temperature polymer can resolve the two distinct crystallization events [11]. A similar effect has been found in double crystalline block and random copolymers [24,25].

Despite these relevant studies, a comprehensive investigation of the effect of blend morphology on the self-nucleation behaviour of a certain semicrystalline polymer has not yet been reported. In this work, we investigated in detail immiscible ternary and binary blends of poly(lactide) (PLA), poly(ε-caprolactone) (PCL), and poly(butylene succinate) (PBS). PLA, PCL, and PBS were chosen due to their different crystallization and melting temperature ranges, this facilitates the study of the crystallization of each phase separately. All the binary blends exhibited sea-island morphology, and each polymer acted as continuous or dispersed phase in the various samples. Ternary blends showed a partial wetting morphology, with each of the three polyesters acting as minor component in the different cases. The effect of blending, composition and morphology (i.e., continuous matrix, dispersed droplets, or partially wet droplets) on the self-nucleation behaviour of these systems will be discussed.

6.2 Materials and methods

6.2.1 Materials and Blend preparation: Please see chapter V (same materials and blend preparation process as described in chapter V).

6.2.2 Blend characterization

The thermal characterization of the blends was done by Differential Scanning Calorimetry (DSC) using a Perkin Elmer DSC Pyris 1 calorimeter, equipped with a refrigerated cooling system (Intracooler 2P).

Prior to the analysis, a calibration was done using indium and tin. All measurements were performed using sample masses of approximately 5 mg and under a continuous nitrogen flow.

Self-nucleation experiments (SN): samples were analyzed using the self-nucleation procedure described hereinafter [2,3]:

1) Erasing the crystalline history by holding the sample in the melt at 200°C for 3 min (25°C above the melting point of the component with the higher crystallization and melting temperatures).

2) Creation of a standard crystalline state by cooling from 200°C to -20°C at a rate of 20°C/min.

3) Complete/partial melting of the sample by heating the sample at 20°C/min from -20°C to a selected temperature (T_s), where the sample was kept for 5 min. Depending on the value of T_s, during these 5 min the sample completely melts (*Domain I*), self-nucleates (*Domain II*) or self-nucleates and anneals (*Domain III*).

4) Crystallization of the samples, thermally treated in the preceding step 3, by cooling from T_s to -20°C at a rate of 20°C/min.

5) Subsequent melting of the re-crystallized sample by heating from -20°C to 200°C at a rate of 20°C/min.

For the self-nucleation study, each sample was used for three SN temperatures only, and subsequently replaced with a fresh sample, in order to avoid the effect of possible degradation of the polymer at high temperatures on its crystallization behavior. A faster heating/cooling rate with respect to the one adopted in the non-isothermal crystallization protocol has been employed for self-nucleation experiments, in order to reduce the analysis time.

6.3 Results and discussion

Self-nucleation of PLA in 90/10 PLA/PCL blend:

Figure 6.2 shows DSC cooling and heating runs after self-nucleation of the PLA phase at different T_s values. Under normal conditions, i.e., heating the sample into *Domain I*, PLA shows an almost negligible trace of crystallization trace during cooling (around 100°C), while it undergoes extensive cold crystallization upon subsequent heating. By applying SN, the crystallization rate of the self-nucleated PLA increases noticeably.

At temperatures higher than 170°C (*Domain I*), no changes in the cooling and/ melting behaviors of PLA can be observed. When the employed T_s is in the range 170-169°C (*Domain II*), a clear PLA crystallization exotherm appeared in the DSC cooling scan, and the subsequent cold-crystallization decreases accordingly. Within *Domain II*, the decrease in the employed T_s results in a large increase in the crystallization temperature and enthalpy (Figure 6.2a). Further decreases in T_s to temperatures lower than 168°C resulted in an additional enhancement in the crystallization behavior. In particular, two distinct crystallization events appear on cooling, with the relative fraction of the higher temperature one becoming larger with decreasing T_s (Figure 6.2a). In agreement with this enhanced crystallization, no cold-crystallization exotherm was observed on subsequent heating.

Moreover, the step increase in heat capacity associated with the glass transition of amorphous PLA, which in samples self-nucleated at higher temperatures occurred around 65°C, although partially superposed to the melting endotherm of the PCL minor phase, could not be clearly detected (Figure 6.2b) and is apparent on cooling only (Figure 6.2a). Finally, a sharp annealing peak at higher temperatures in the melting scan appears, allowing the detection of *Domain III*.

The three self-nucleation *Domains* of PLA within the 90/10 PLA/PCL binary blend are summarized in Figure 6.2c, where the crystallization temperature at the different T_s are superposed to a standard DSC melting endotherm of PLA. The transition between *Domain I* and *Domain II* is practically coincident with the melting endotherm endpoint.

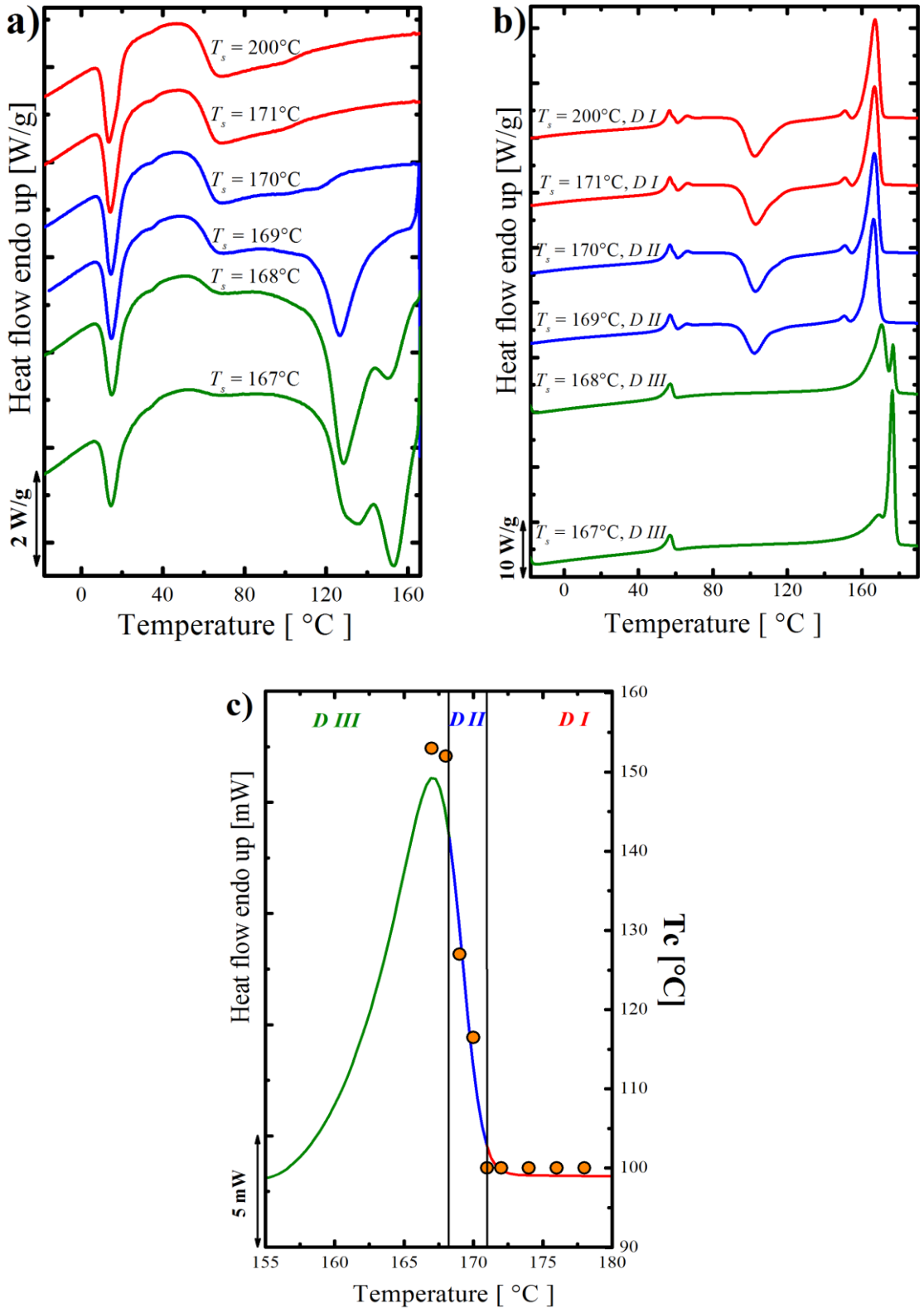

Figure 6.2. a) DSC cooling scans (at 20°C/min) for 90/10 PLA/PCL blend after 5 min at the indicated T_s. (b) Subsequent heating scans (at 20°C/min) after the cooling runs shown in (a). (c) Representation of the self-nucleation *domains* for PLA in 90/10 PLA/PCL blend: crystallization temperature vs. self-nucleation temperature, superimposed to the standard DSC melting trace of PLA.

Self-nucleation of PCL in 90/10 PBS/PCL blend:

Figure 6.3a shows the DSC cooling curves after self-nucleating the PCL minor phase at different T_s. It should be noted that due to the relatively small T_s values employed to SN the PCL phase, Figure 6.3 only plots a limited temperature range, hence the PBS phase melting cannot be observed when a T_s value of 140°C was employed.

As a consequence of melt blending, the PCL phase within 90/10 PBS/PCL undergoes fractionated crystallization showing two crystallization peaks (at around 31 and 22°C), corresponding to two populations of PCL droplets containing nucleating heterogeneities with different efficiencies. The SN protocol causes the injection of self-nuclei into PCL droplets. By decreasing T_s within *Domain II*, the enthalpy of the low-temperature crystallization peak decreases, while the opposite occurs to the high-temperature crystallization event. Also, a shift of the major crystallization peak towards higher temperature is observed. The annealing at T_s causes the appearance of a small endothermic signal above the melting point of PCL crystals, which is associated to an annealing peak of the PBS matrix. This can be confirmed in separate experiments, where the same annealing is applied, but avoiding the crystallization step of the PCL phase (Figure 6.4).

At temperatures equal to or lower than 58°C all the droplets are self-nucleated (as judged by the disappearance of the low-temperature exotherm), and *Domain III* is found. In fact, a sharp peak related to the high melting-temperature annealed PCL crystals is observed, although probably partially superposed with the PBS low-temperature endotherm. PCL displays a strong crystalline memory effect: *Domain II* extends to T_s = 71°C, i.e., 10°C above the standard melting endpoint (Figure 6.3c). The strong crystalline memory of PCL at temperatures distinctly higher than its melting point was recently investigated by means of rheological and dielectric spectroscopy measurements. [26,27]

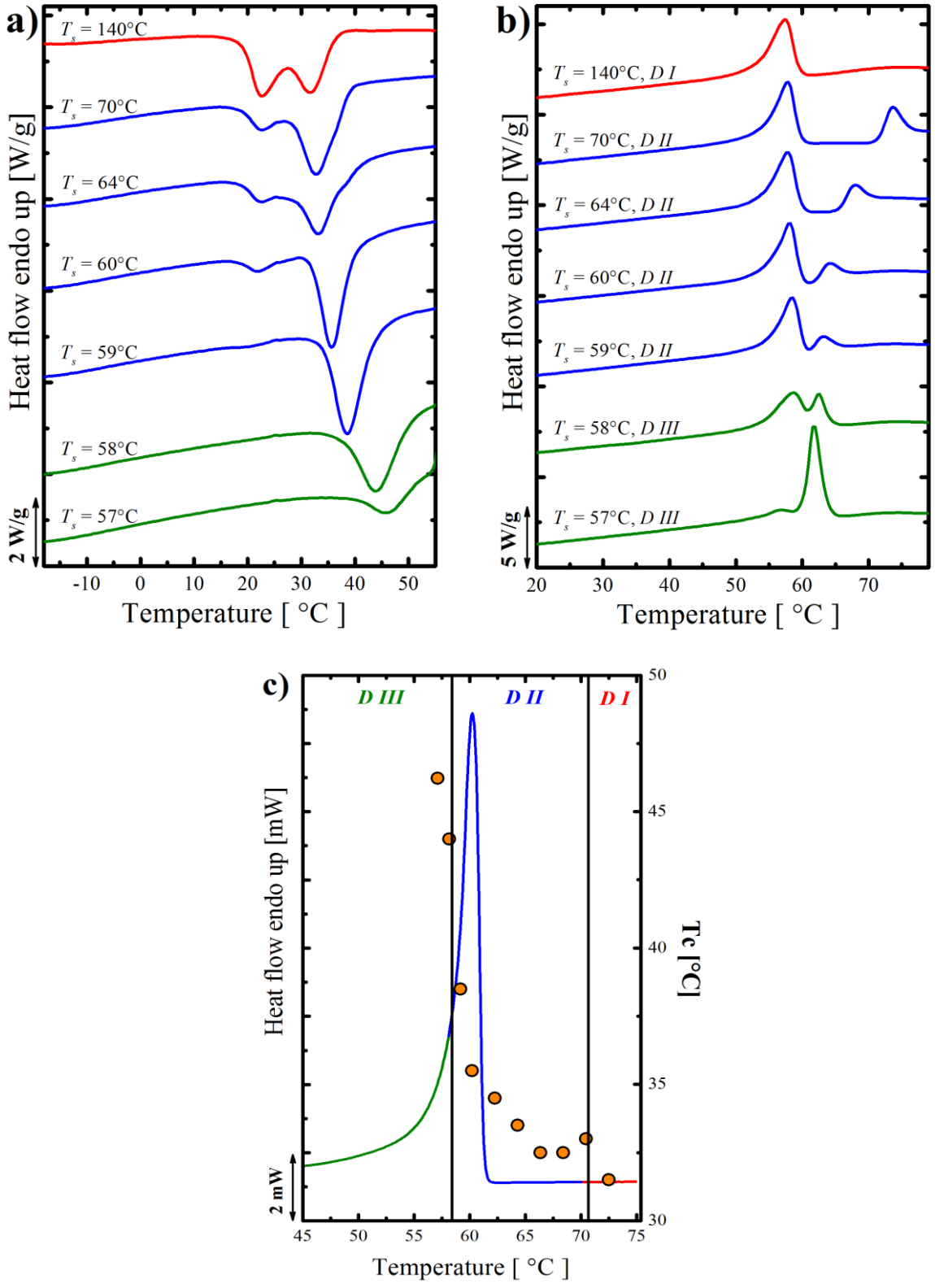

Figure 6.3. a) DSC cooling scans (at 20°C/min) of 90/10 PBS/PCL blend after 5 min at the indicated T_s. (b) Subsequent heating scans (at 20°C/min) after the cooling runs shown in (a). (c) Representation of the self-nucleation domains for PCL in 90/10 PBS/PCL blend; crystallization temperature vs. self-nucleation temperatures are superimposed to the standard DSC melting trace.

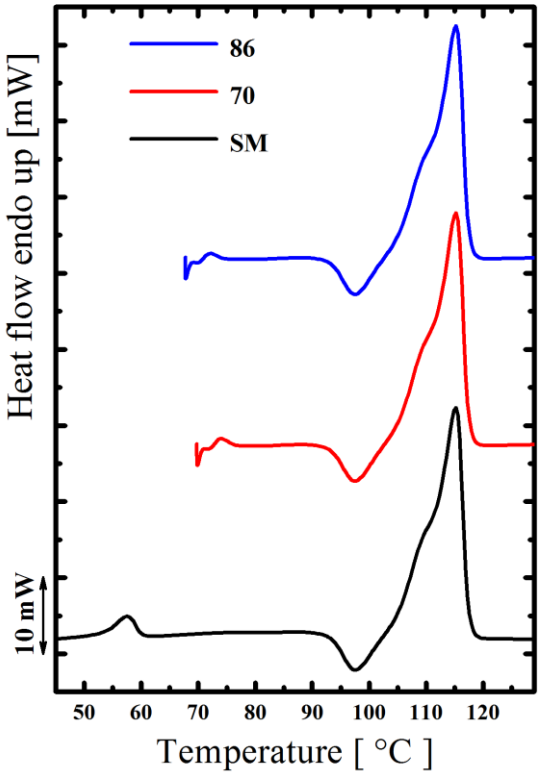

Figure 6.4. Heating scans after annealing of the partially crystallized 90/10 PBS/PCL binary blend. The sample has been cooled from the melt to the indicated temperature and annealed there for 5 minutes, reproducing one step of the SN protocol, but without allowing the crystallization of PCL phase. The heating runs are compared with the standard melting curve of a fully crystallized sample (standard melting, "SM" curve). Annealing peaks above 70 °C are well evident and thus associated to the PBS phase.

Self-nucleation of PBS in 90/10 PCL/PBS blend

Self-nucleation can also be used to separate the "coincident crystallization" of double crystalline polymer blends. Coincident crystallization occurs when the two crystalline components of a blend displaying sea-islands morphology crystallize concurrently in the same temperature range. Typically, once the crystallization of the matrix starts, it is quickly followed by the crystallization of the dispersed droplets, nucleated by the crystalline matrix. Therefore, DSC cooling scans shows a single crystallization peak, while two separate melting peaks associated with the melting of each component are observed in the subsequent heating scan. The presence of coincident crystallization phenomena can be revealed by WAXS and/or self-nucleation techniques [3,5,8,24,25,28-30].

Figure 6.5a and 6.5c show the DSC cooling and heating scans of 90/10 PCL/PBS self-nucleated at different T_s, between 140°C and 110°C, while Figures 6.5b and 6.5d show a close-up on PBS crystallization and melting temperature ranges.

At T_s higher than 118°C, a single crystallization peak around 35°C can be observed, but upon heating both PCL and PBS phase melting peaks are clearly revealed, indicating that coincident crystallization of both polymers took place during the cooling scan.

For lower self-nucleation temperatures, in the range 118-116°C, two crystallization peaks located between 65-100°C appear (see Figure 6.5b). These exothermic peaks can be related to the crystallization of different populations of PBS droplets. Simultaneously, the crystallization enthalpy of the main peak around 35°C decreases from 56 J/g at T_s = 140°C to 53 J/g at T_s 116°C (not shown). This small decrease is an indirect proof of the obtained separation between PBS and PCL crystallization events. Below T_s =116°C, PBS crosses into *Domain III*, and the further increase in the crystallization temperature is associated to the emergence of PBS annealing peaks with high melting temperature (see Figures 6.5c and 6.5d). We note that *Domain II* in this system starts only slightly above the end of the melting endotherm of PBS (Figure 6.5e), however, the self-nucleation effect is dramatic, since the crystallization temperature shifts from below 40°C (coincident with PCL major phase) for *Domain I*, to above 70 and 90°C. The obtained results demonstrate the efficiency of SN protocol in separating coincident crystallization phenomena.

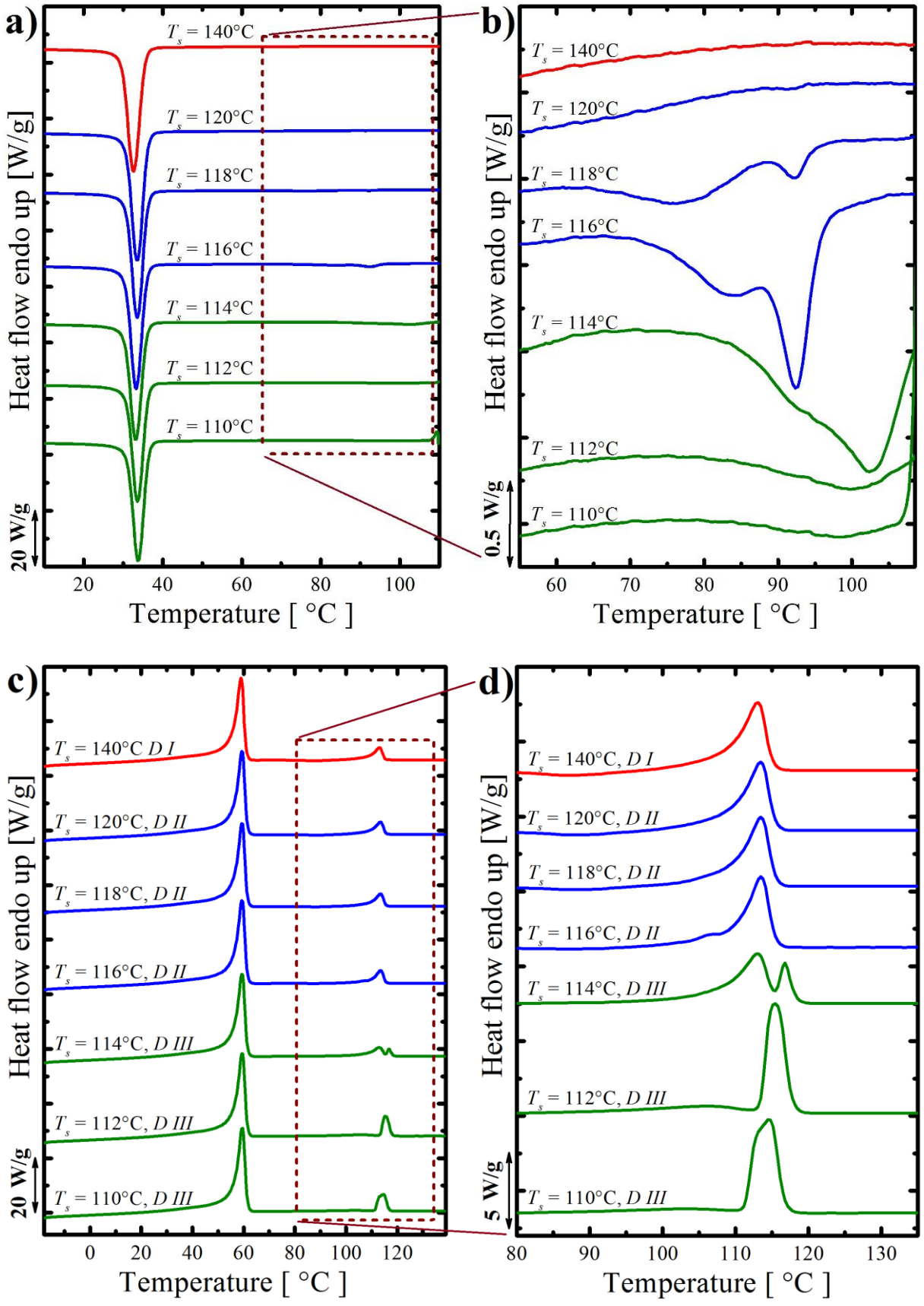
a)
b)
c)
d)
Heat flow endo up [W/g]
Temperature [°C]
T_s = 140°C
T_s = 120°C
T_s = 118°C
T_s = 116°C
T_s = 114°C
T_s = 112°C
T_s = 110°C
20 W/g
0.5 W/g
5 W/g
T_s = 140°C D I
T_s = 120°C, D II
T_s = 118°C, D II
T_s = 116°C, D II
T_s = 114°C, D III
T_s = 112°C, D III
T_s = 110°C, D III

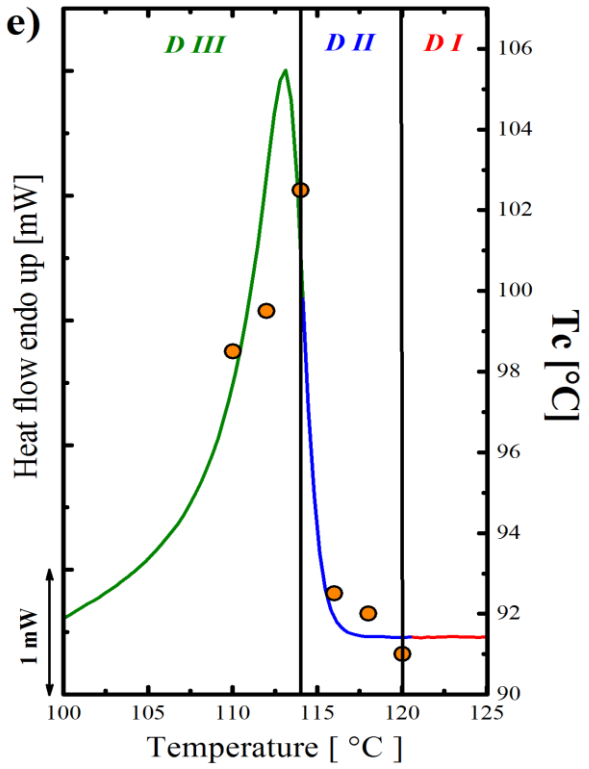

Figure 6.5. a) DSC cooling scans (at 20°C/min) of 90/10 PCL/PBS blend after 5 min at the indicated T_s; (b) is a close-up of the PBS crystallization temperature range; (c) Subsequent heating scans (at 20°C/min) after the cooling runs shown in (a); (d) is a close-up of the PBS melting temperature region. (e) Representation of the self-nucleation domains; crystallization temperature vs. Ts are superimposed to the standard DSC melting trace of PBS in 90/10 PCL/PBS blend.

In the following, the self-nucleation behavior of the minor components, located at the interface between the two major phases in the ternary blends, is analyzed and compared to that of binary blends and neat polymers.

Self-nucleation of PLA in 45/10/45 PCL/PLA/PBS blend

Figures 6.6a through 8d show the crystallization and melting behavior of 45/10/45 PCL/PLA/PBS ternary blends upon cooling and subsequent heating from different self-nucleation temperatures, with emphasis on the PLA phase. By employing self-nucleation temperatures higher than 170°C, no changes are found in the cooling or re-heating scans, a behavior characteristic of *Domain I*. Upon decreasing T_s, the crystallization process of PLA is enhanced, and *Domain II* is encountered. In particular, a small exothermic peak around 125°C can be found during cooling from T_s = 169°C, while the crystallization of PLA from T_s = 170°C cannot be directly detected. Nevertheless, the bimodal melting endotherm on subsequent

heating suggests a different crystallization process with respect to higher self-nucleation temperatures. Therefore, T_s = 170°C can be tentatively attributed to *Domain II*. *Domain III* is found for self-nucleation temperatures equal or lower than 168°C. Next to the main crystallization event, a second small exotherm at higher temperatures appears in the cooling scan, possibly related to the nucleation effect of annealed crystal fragments (Figure 6.6b). The presence of such crystals is detected on subsequent heating, as evidenced by a relatively sharp melting peak around 175°C. The width of *Domain II* for the PLA phase in the ternary blend is only about 2 Celsius degrees, partially superposed with the high temperature tail of the standard melting endotherm (Figure 6.6e).

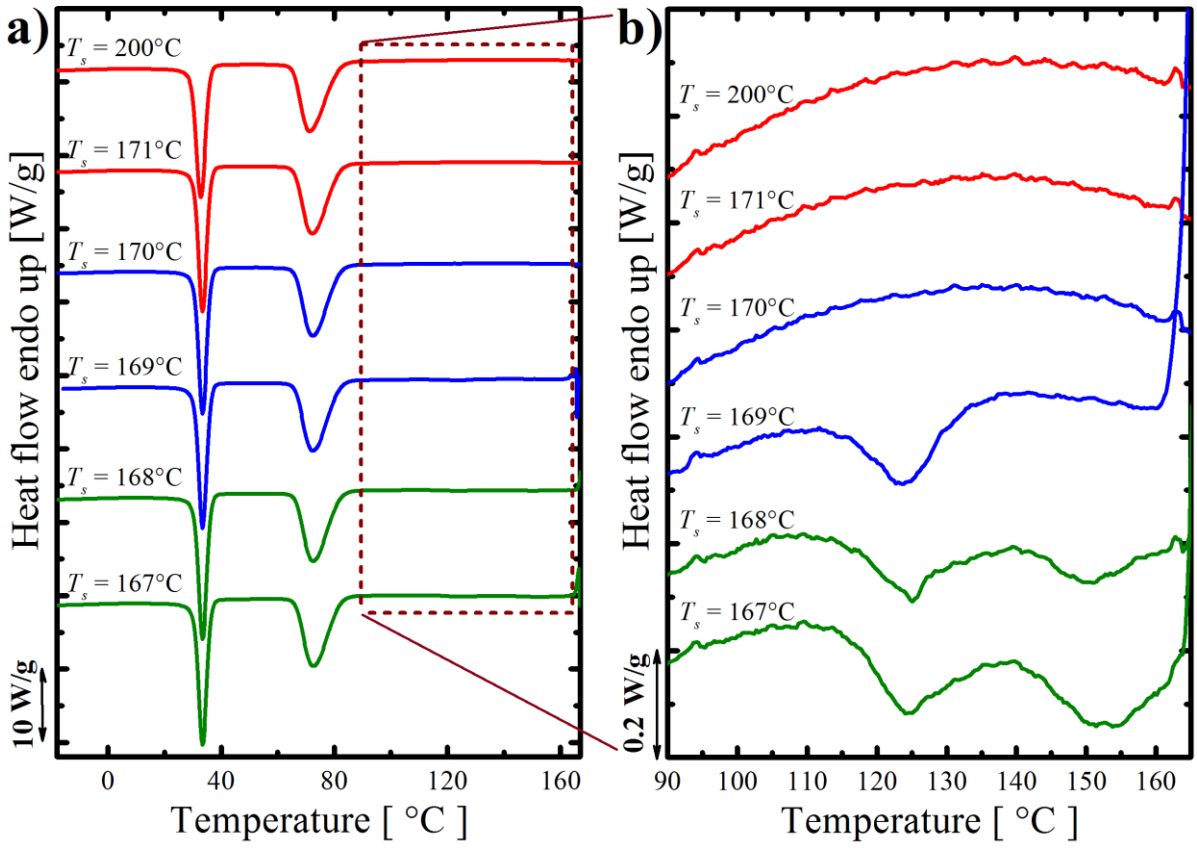

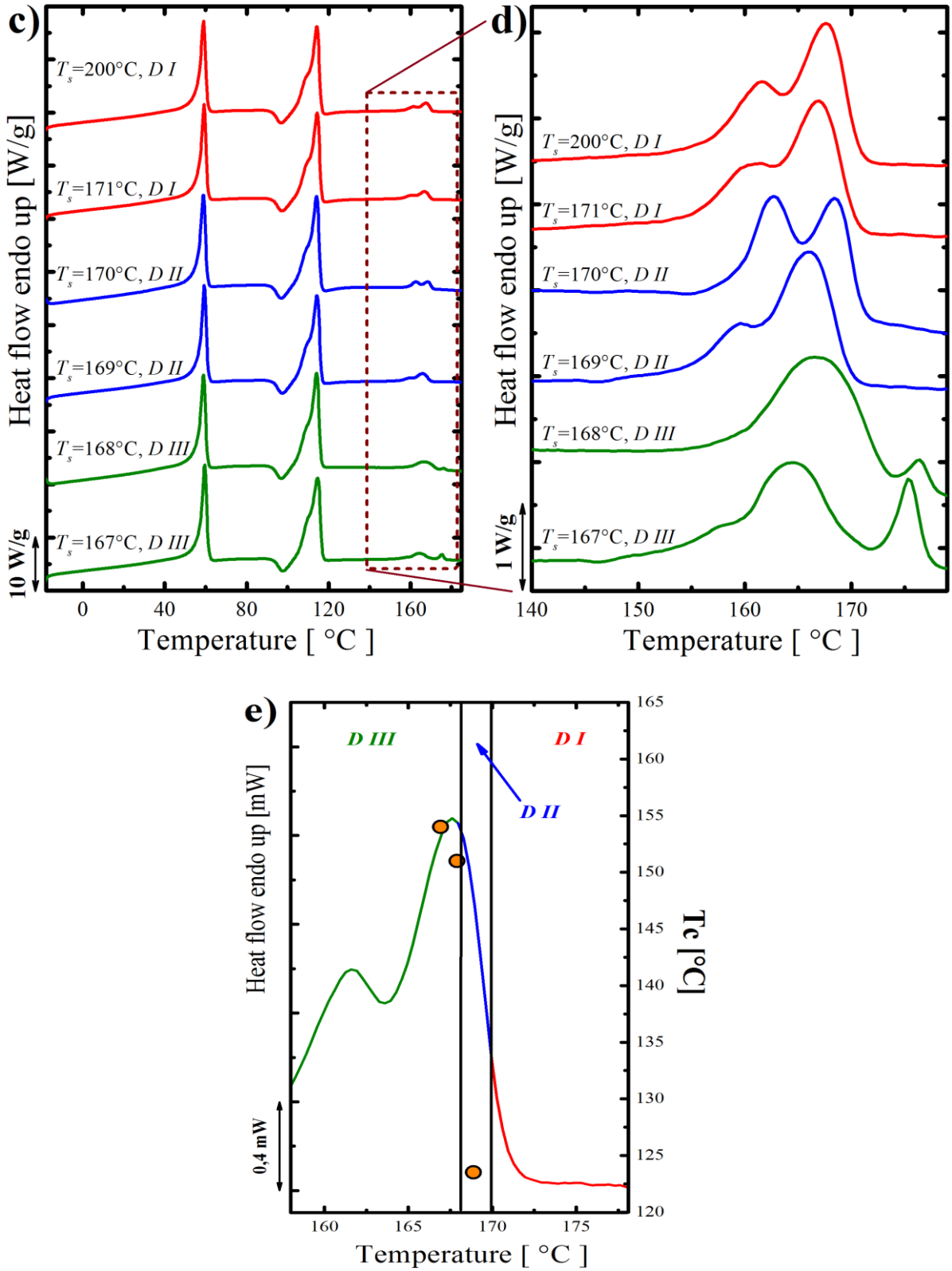

Figure 6.6. a) DSC cooling scans (at 20°C/min) for 45/10/45 PCL/PLA//PBS blend after 5 min at the indicated T_s; (b) Close-up of the PLA crystallization temperature region; (c) Subsequent heating scans (at 20°C/min) after the cooling runs shown in (a); (d) Close-up of the PLA melting temperature region. (e) Representation of the self-nucleation domains for PLA in 45/10/45 PCL/PLA/PBS blend: Crystallization temperature vs. seeding temperature superimposed to the standard DSC melting trace

Self-nucleation of PBS in 45/10/45 PLA/PBS/PCL

The results on the behavior of PBS droplets at the interface with PLA and PCL *Domains* are reported in Figure 6.7 for various self-nucleation temperatures.

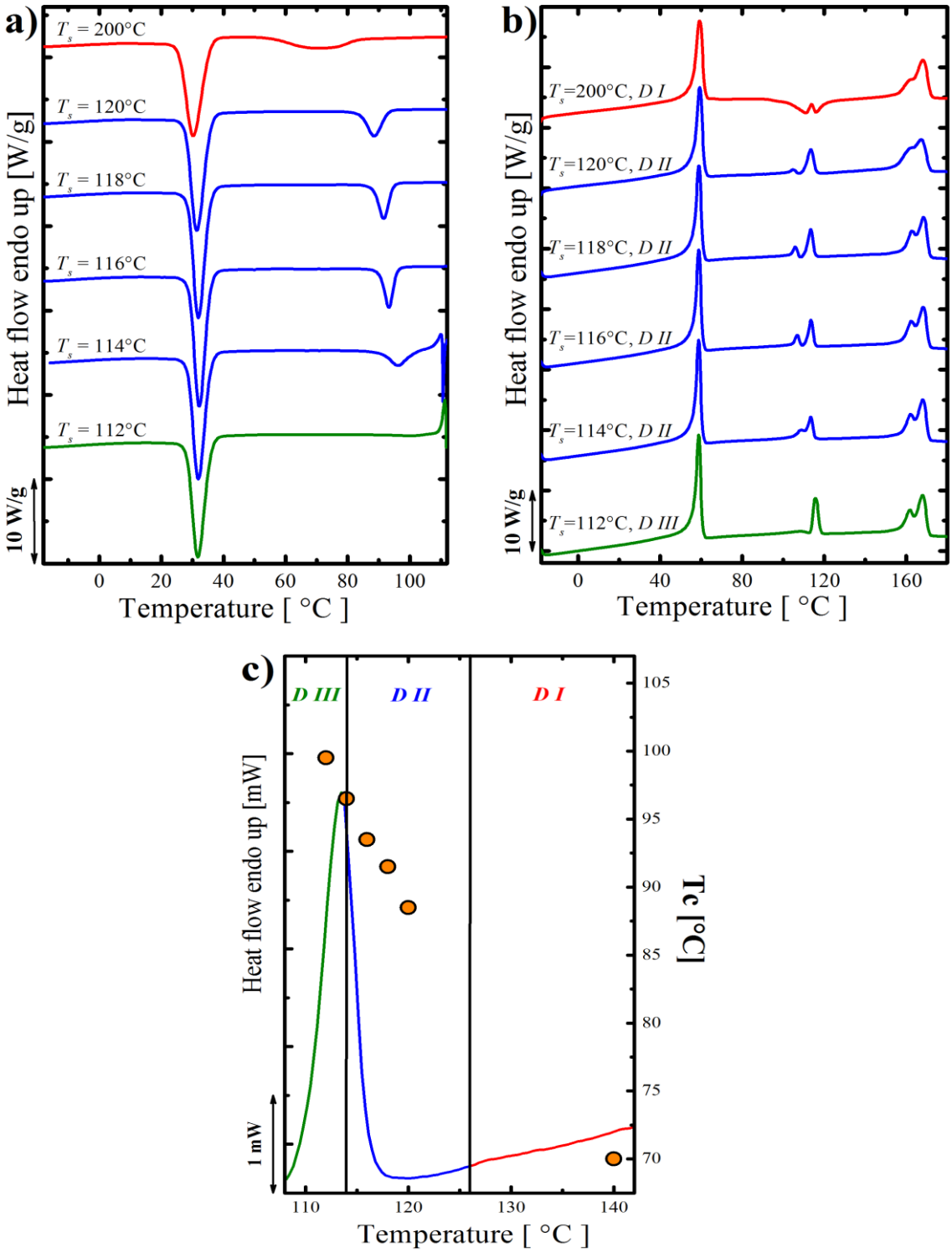

Figure 6.7. a) DSC cooling scans (at 20°C/min) for 45/10/45 PLA/PBS/PCL blend after 5 min at the indicated T_s; (b) Heating scans (at 20°C/min) after the cooling runs shown in (a). (c) Representation of the self-nucleation domains for PBS in 45/10/45 PLA/PBS/PCL blend: T_C vs. T_S superimposed to the standard DSC melting trace.

Crystallization of PBS occurs slowly during cooling from the melt (i.e., in *Domain I*, see Figure 6.7a, cooling DSC scan from T_s =140°C) resulting in a broad exotherm. Under this cooling condition, PLA crystallization is bypassed, and it can only crystallize upon subsequent heating, in a temperature range which is superposed on the melting of PBS crystals (Figure 6.7b). The lowest self-nucleation temperature (i.e., in *Domain II*) probed, T_s =120°C shows already a clear signature of enhanced PBS crystallization. The crystallization peak is shifted to temperatures higher than 15°C than those typical of *Domain I* crystallization, and displays a sharper appearance. In addition, no trace of PLA cold-crystallization is observed in the subsequent heating step.

The PBS crystallization temperature (Figure 6.7a) continues to increase upon lowering T_s, without apparent changes in the melting behavior, down to a self-nucleation temperature of 116°C (*Domain II*, see Figures 6.7a and 6.7b). For lower self-nucleation temperatures, *Domain III* is entered as judged by the reduction in crystallization enthalpy upon cooling and by the changes in the shape of the subsequent PBS melting endotherm. Although we did not investigate in detail the onset of the self-nucleation *Domain* (i.e., the *Domain I/Domain II* transition temperature), it is already clear that the crystalline memory effect extends well above the end of the melting endotherm (Figure 6.7c), similarly to what is typically found for the neat polymer [25]

Self-nucleation of PCL in 45/10/45 PLA/PCL/PBS

The self-nucleation of PCL droplets at the interface with solid PLA and PBS phases is analyzed in Figures 6.8a through 6.8d. The behavior is analogous to that previously shown in PBS/PCL binary blend. A distinct self-nucleation effect can be deduced for T_s lower than about 70°C (*Domain II*, see Figure 6.8a). The exact identification of *Domain III*, from the melting trace after re-crystallization (Figures 6.8b and 6.8c) is complicated by the concomitant occurrence of an endothermic effect (annealing peak or aging of the rigid amorphous fraction [31-33]) related to the PBS phase, just slightly above the melting peak of PCL (see also Figures 6.3 and 6.4). Tentatively, the melting of annealed PCL crystals can be distinguished from the PBS-related endotherm at T_s equal or lower than 58°C, when the PBS signal becomes weaker while the peak attributed to PCL gets sharper. The relatively strong memory effect of PCL is confirmed also for this blend, since the fully relaxed *Domain I* is obtained only at temperatures well above the end of the crystals melting endotherm (Figure 6.8d).

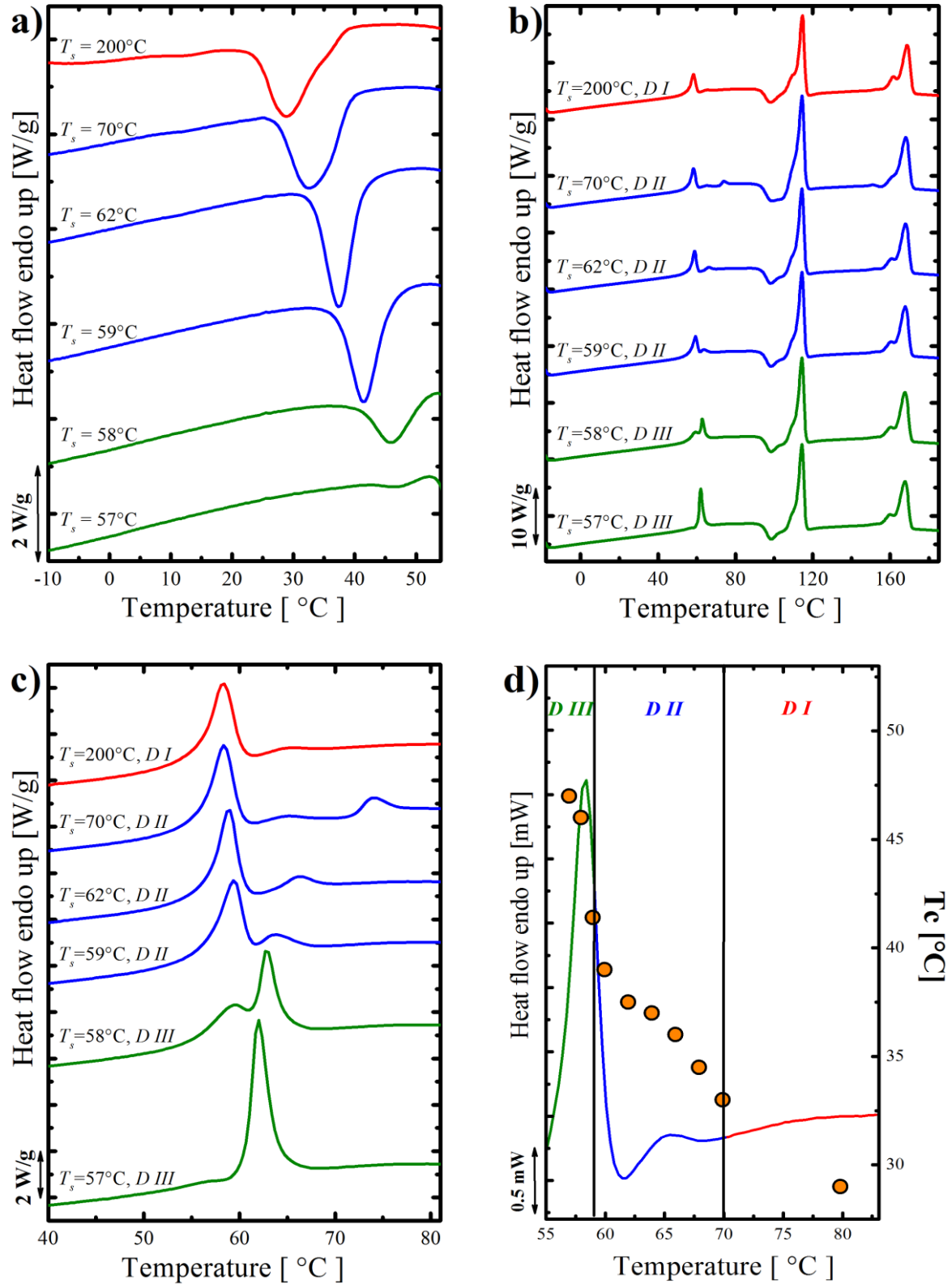

Figure 6.8. a) DSC cooling scans (at 20°C/min) for 45/10/45 PLA/PCL/PBS blend after 5 min at the indicated T_s; (b) Heating scans (at 20°C/min) after the cooling runs shown in (a); (c) Close-up of the PCL melting temperature region. (d) Representation of the self-nucleation domains for PCL in 45/10/45 PLA/PCL/PBS blend: T_C vs. T_S superimposed to the standard DSC melting trace.

Finally, the self-nucleation behavior of the different polymers in the various blends is compared in Figures 6.9a through 6.9c. As a general remark, we note that the boundaries between the self-nucleation *Domains* are basically unaffected by the blending process, or at most they vary by about 1 or 2 Celsius degrees. Moreover, the T_c values of self-nucleated samples at the same temperature within *Domain II* are remarkably similar, notwithstanding the phase content in the blend or the blend type (binary vs. ternary). This is true for all the three polymers, but is particularly evident for PLA and PBS phases.

We can deduce that the production of self-nuclei is mainly determined by the T_s temperature with no significant influence of blend morphology. This can be interpreted considering the exceedingly high number of self-nuclei that can be injected into the system, in comparison to the number of existing nucleating impurities or interfaces in the blend. Typically, the self-nucleation process is capable of introducing approximately 10^{12} to 10^{13} self-nuclei at the ideal self-nucleation temperature (i.e., the lowest temperature in *Domain II*, where the maximum number of self-nuclei are produced) [2,3]. PCL is the polymer with the highest heterogeneous nucleation density in the bulk, as compared to PBS and PLA, as judged by the typical spherulitic size upon cooling from the melt (data not shown). In the case of bulk PCL, the maximum heterogeneous nucleating density has been estimated by polarized optical microscopy to be of the order of 10^6-10^8 nuclei/cm^3. This means that SN of PCL can enhance its nucleation density by 4-7 orders of magnitude. In the cases of PBS and PLA the enhancement would be even larger [34,35].

On the other hand, self-nucleation temperatures within *Domain I* reveal morphology-related differences in T_c, since the intrinsic nucleation behavior of the particular blend is exposed. We note that the data reported in Figure 6.9 differ from those discussed in Tables 5.3 and Table 5.4 and Figures 5.5 and 5.6 (in chapter V), due to the different cooling rate employed (i.e., 20 vs. 5°C/min).

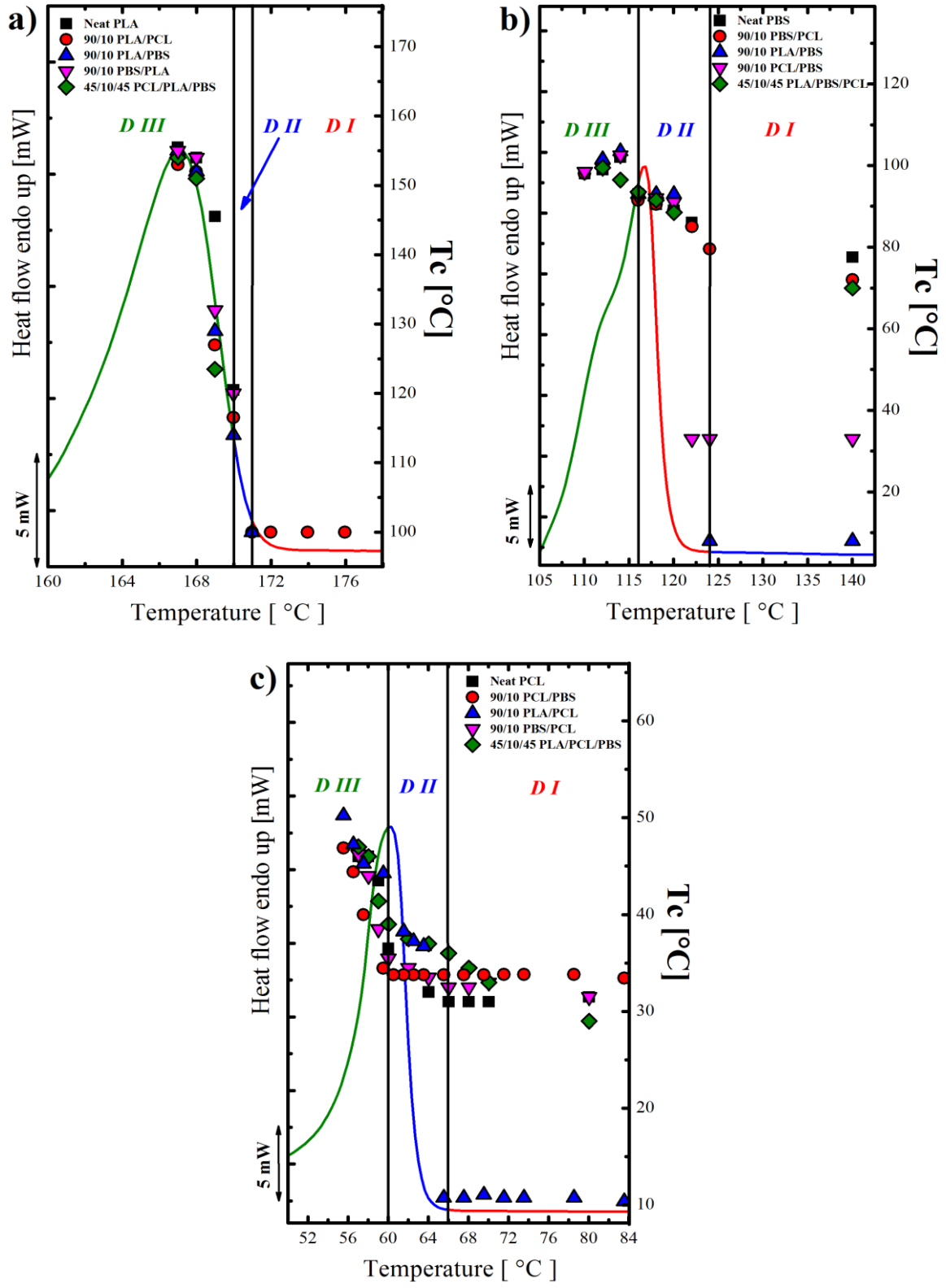

Figure 6.9. Collection of T_c as a function of the employed T_s for (a) PLA, (b) PBS and (c) PCL in different blends and neat components. The data are superposed to standard melting curves of the relative polymer and the boundaries between SN *Domains* in the neat polymer are also indicated.

For what concerns the PLA phase, crystallization can be inhibited at 20°C/min for the neat polymer, as well as for binary and ternary blends with a minor fraction of this component (see Figure 6.9a). Interestingly, for binary blends with PBS or PCL where PLA is the matrix, a different behavior is observed. The 90/10 PLA/PCL blend can crystallize to a certain extent upon cooling at 20°C/min, while the same does not occur in the 90/10 PLA/PBS blend. This enhanced crystallization can be due the different nucleating impurities that have been transferred to the PLA matrix in the two cases, or to a higher nucleation efficiency at the interface with molten PCL droplets, with respect to molten PBS. It should also be considered that PBS droplets in this blend have a high tendency to coalesce during melting, contrary to PCL ones. As such, the small differences in the nucleating effect towards PLA between the two molten polymers can be enhanced by the much higher amount of PCL surface per unit volume of blend, due to the smaller droplet size after melting for some time.

In the case of PBS, crystallization at temperatures equivalent to those of the neat polymer occurs in *Domain I* for binary blends where PBS is the major component, as well as in ternary blends where PBS forms (relatively large) droplets at the interface between PLA and PCL. However, crystallization is depressed in the binary blend with 10 wt% PBS (Figure 6.9b). Among the two blends (90/10 PLA/PBS and 90/10 PCL/PBS), the one with PCL as major phase shows the faster kinetics. This is attributed to differences in the transfer of nucleating impurities between the polymers during blending. Furthermore, the possible nucleating action of crystalline PLA on molten PBS, might be inactive given the fact that PLA is not able to crystallize at the applied cooling rates.

Finally, in the case of PCL, only minor differences between the crystallization of the neat polymer, the ternary blend with PCL concentration of 10% and the two binary blends (90/10 PBS/PCL and 90/10 PCL/PBS) could be observed (Figure 6.9c). In particular, by comparing neat PCL and 90/10 PCL/PBS blends, a small nucleating effect of PBS droplets on the PCL matrix can be noticed, and it can be attributed to the crystallization of PBS phase which induces the coincident crystallization of PCL matrix. On the other hand, PCL droplets in 90/10 PLA/PCL binary blend crystallize at much larger undercoolings with respect to those in 90/10 PBS/PCL blend. This difference of about 20 Celsius degrees can be tentatively ascribed to the nucleating effect of crystalline PBS or to the differences in droplet size between the two blends, given the much larger volume-averaged diameter of PCL domain size in the PBS/PCL blend (see Table 5.2 in chapter V).

6.4 Conclusions

In this work, we focused on the self-nucleation behavior of triple-crystalline thermoplastic polyester immiscible blends.

The self-nucleation behavior of the different polymers in the various binary and ternary blends was investigated taking into account the effect of different morphologies (sea-island and partial-wetting morphologies). It was found that the crystallization temperatures of samples self-nucleated at the same temperature are remarkably similar, notwithstanding the phase content in the blend or the morphology. As a consequence, the boundaries between different self-nucleation *Domains* are also basically unaffected by the blending process, or at most they vary by less than 2 Celsius degrees.

This is true for all the three polymers, allowing us to deduce that the production of self-nuclei is mainly determined by the self-nucleation temperature, with only a negligible influence of blend morphology and polymer content. This is attributed to the exceedingly high number of self-nuclei produced by SN, in comparison to the number of existing nucleating impurities or interface-induced nuclei. In fact, when T_s temperatures within *Domain I* are employed (i.e., no self-nucleation), the influence of heterogeneous nucleation is highlighted, in particular for minor components in blends with sea-island morphology.

6.5 References

1. Blundell DJ, Keller A, Kovacs AJ (1966) A new self-nucleation phenomenon and its application to the growing of polymer crystals from solution. J Polym Sci B Polym Lett. 4:481–486
2. Fillon B, Wittmann JC, Lotz B, Thierry A (1993) Self -Nucleation and Recrystallization of isotactic Polypropylene (α Phase) Investigated by Differential Scanning Calorimetry. J. Polym. Sci., Part B: Polym. Phys. 31:1383-1393
3. Michell RM, Mugica A, Zubitur M, Müller AJ (2017) Self-Nucleation of Crystalline Phases Within Homopolymers, Polymer Blends, Copolymers, and Nanocomposites. Adv Polym Sci. 276:215-256
4. Müller AJ, Michell RM, Pérez RA, Lorenzo AT (2015) Successive Self-nucleation and Annealing (SSA): Correct design of thermal protocol and applications. Eur. Polym. J. 65:132-154.

5. Müller AJ, Michell RM (2016) Differential Scanning Calorimetry of Polymers. In: Guo Q (ed) Polymer Morphology: Principles, Characterization, and Processing. John Wiley & Sons, Inc., New Jersey, p 72-99
6. Utracki LA, Wilkie C (Eds) (2014) Polymer Blends Handbook. Springer, New York
7. Paul DR, Barlow JW (1980) Polymer Blends (or Alloys). J. Macromol. Sci., Rev. Macromol. Chem. Phys. 18:109-168
8. Arnal ML, Matos ME, Morales RA, Santana OO, Müller AJ (1998) Evaluation of the fractionated crystallization of dispersed polyolefins in a polystyrene matrix. Macromol. Chem. Phys. 199:2275-2288
9. Arnal ML, Müller AJ (1999) Fractionated crystallisation of polyethylene and ethylene/a-olefin copolymers dispersed in immiscible polystyrene matrices. Macromol. Chem. Phys. 200:2559-2576
10. Santana OO. Müller AJ (1994) Homogeneous nucleation of the dispersed crystallizable component of immiscible polymer blends. Polym. Bull. 32:471-477
11. Morales RA, Arnal ML, Müller AJ (1995) The evaluation of the state of dispersion in immiscible blends where the minor phase exhibits fractionated crystallization. Polym. Bull. 35:379-386
12. Michell RM, Blaszczyk-Lezak I, Mijangos C, Müller AJ (2013) Confinement effects on polymer crystallization: From droplets to alumina nanopores. Polymer. 54:4059-4077
13. Tol RT, Mathot VBF, Groeninckx G (2005) Confined crystallization phenomena in immiscible polymer blends with dispersed micro- and nanometer sized PA6 droplets, part 2: reactively compatibilized PS/PA6 and (PPE/PS)/PA6 blends. Polymer. 46:383-396
14. Tol RT, Mathot VBF, Groeninckx G (2005) Confined crystallization phenomena in immiscible polymer blends with dispersed micro- and nanometer sized PA6 droplets, part 3: crystallization kinetics and crystallinity of micro- and nanometer sized PA6 droplets crystallizing at high supercoolings. Polymer. 46:2955-2965
15. Yordanov C, Minkova L (2005) Fractionated crystallization of compatibilized LDPE/PA6 blends. Eur. Polym. J. 41:527–534
16. Pan P, Shan G, Bao Y (2014) Enhanced Nucleation and Crystallization of Poly(L lactic acid) by Immiscible Blending with Poly(vinylidene fluoride). Ind. Eng. Chem. Res. 53:3148-3156
17. Kong Y, Ma Y, Lei L, Wang X, Wang H (2017) Crystallization of Poly(ϵ-caprolactone) in Poly(vinylidene fluoride)/Poly(ε -caprolactone) Blend. Polymers 9:42

18. Virgilio N, Marc-Aurèle C, Favis BD (2009) Novel Self-Assembling Close-Packed Droplet Array at the Interface in Ternary Polymer Blends. Macromolecules. 42:3405-3416
19. Ravati S, Favis BD (2013) Tunable morphologies for ternary blends with poly(butylene succinate): Partial and complete wetting phenomena. Polymer. 54:3271-3281
20. Zolali AM, Favis BD (2016) Partial and Complete Wetting in Ultralow Interfacial Tension Multiphase Blends with Polylactide. J. Phys. Chem. B. 120:12708-12719
21. Zolali AM, Favis BD (2017) Partial to complete wetting transitions in immiscible ternary blends with PLA: the influence of interfacial confinement. Soft Matter. 13:2844-2856
22. Virgilio N, Desjardins P, L'Espérance G, Favis BD (2009) In Situ Measure of Interfacial Tensions in Ternary and Quaternary Immiscible Polymer Blends Demonstrating Partial Wetting. Macromolecules. 42:7518-7529
23. Zolali AM, Favis BD (2017) Compatibilization and toughening of co-continuous ternary blends via partially wet droplets at the interface. Polymer 114:277-288
24. Müller AJ, Albuerne J, Márquez L, Raquez JM, Degée Ph, Dubois Ph, Hobbs J, Hamley IW (2005) Self-nucleation and crystallization kinetics of double crystalline poly(p-dioxanone)-b-poly(ε-caprolactone) diblock copolymers. Faraday Discuss. 128:231-252
25. Arandia I, Mugica A, Zubitur M, Arbe A, Liu G, Wang D, Mincheva R, Dubois Ph, Müller AJ (2015) How Composition Determines the Properties of Isodimorphic Poly(butylene succinate-ran-butylene azelate) Random Biobased Copolymers: From Single to Double Crystalline Random Copolymers. Macromolecules. 48:43-57
26. Sangroniz L, Barbieri F, Cavallo D, Santamaría A, Alamo RG, Müller AJ (2018) Rheology of self-nucleated poly(ε-caprolactone) melts. Eur. Polym. J. 99:495-503
27. Sangroniz L, Alamo RG, Cavallo D, Santamaría A, Müller AJ, Alegría A (2018) Differences between Isotropic and Self-Nucleated PCL Melts Detected by Dielectric Experiments. Macromolecules. 51:3663-3671
28. Müller AJ, Albuerne J, Esteves LM, Marquez L, Raquez JM, Degée Ph, Dubois Ph, Collins S, Hamley IW (2004) Confinement Effects on the Crystallization Kinetics and Self-Nucleation of Double Crystalline Poly(p-dioxanone)-b-poly(ϵ-caprolactone) Diblock Copolymers. Macromol. Symp. 215:369-382
29. Colonna S, Pérez-Camargo RA, Chen H, Liu G, Wang D, Müller AJ, Saracco G, Fina A (2017) Supernucleation and orientation of poly(butylene terephthalate) crystals in nanocomposites containing highly reduced Graphene Oxide. Macromolecules. 50:9380-9393

30. Pérez-Camargo RA, Fernández-d'Arlas B, Cavallo D, Debuissy T, Pollet E, Avérous L, Müller AJ (2017) Tailoring the Structure, Morphology, and Crystallization of Isodimorphic Poly(butylene succinate-ran-butylene adipate) Random Copolymers by Changing Composition and Thermal History. Macromolecules. 50:597-608
31. Righetti MC, Di Lorenzo ML, Tombari E, Angiuli M (2008) The low-temperature endotherm in poly(ethylene terephthalate): partial melting and rigid amorphous fraction mobilization. J. Phys. Chem. B. 112: 4233-4241
32. Righetti M C, Di Lorenzo ML (2016) Rigid amorphous fraction and multiple melting behavior in poly(butylene terephthalate) and isotactic polystyrene. J. Therm. Anal. Calorim. 126:521-530
33. Martin J, Stingelin N, Cangialosi D (2018) Direct calorimetric observation of the rigid amorphous fraction in a semiconducting polymer. J. Phys. Chem. Lett. 9: 990-995
34. Müller AJ, Balsamo V, Arnal ML, Jakob T, Schmalz H, Abetz V (2002) Homogeneous Nucleation and Fractionated Crystallization in Block Copolymers. Macromolecules. 35:3048-3058
35. Müller AJ, Balsamo V, Arnal ML (2005) Nucleation and Crystallization in Diblock and Triblock Copolymers. In: Abetz V (ed) Block Copolymers II. Springer Berlin Heidelberg, Berlin, p 1-63

Renewable and tough poly (L-lactic acid)/polyurethane blend prepared by dynamic vulcanization

Partially reproduced from: S.E. Fenni et al. "Renewable and toughened poly (L-lactic acid)/polyurethane blend prepared by dynamic vulcanization". **To be submitted soon**.

Chapter VII

Renewable and tough poly (L-lactic acid)/polyurethane blend prepared by dynamic vulcanization

7.1 Introduction

In recent years, biodegradable polymers, especially those derived from renewable resources, have attracted increasing interest to mitigate the negative effects and to alleviate the environmental concerns about the use of conventional petroleum-based polymers. Poly(L-lactic acid) (PLLA) is an excellent environmentally friendly plastic. It presents clear strength points, such as a high rigidity and mechanical strength, high melting point, excellent biocompatibility and biodegradability, and easy processability [1-8]. However, it also suffers from several drawbacks, which largely restricts its widespread application. In particular, the slow crystallization kinetics, low heat distortion temperatures, and high inherent brittleness. limits the application of PLA when ductility is required. Therefore, significant and increasing efforts have been devoted in the last decade to increase PLA toughness. Several strategies have been applied to overcome this brittleness such as plasticization, addition of fillers, and copolymerization. Chemical modification including grafting and reactive blending or dynamic vulcanization was found to be an efficient approach for PLA toughening [6-21].

Dynamic vulcanization and reactive blending represent a very powerful way to tailor the properties and produce polymer blends with high performance. The technique involves the *in-situ* reaction between PLA and added components during melt blending, with the formation of a cross-linked rubber phase inside the PLA matrix. Most often, the formed rubbery phase is a polyurethane (PU). PU is generally synthetized through a reaction of polyisocyanates (more than one –NCO group) with compounds possessing active hydrogen functional groups, such as polyamines, polycarbonates, polyethers, and polyols (−OH). The final polyurethane product will be composed of soft polymer segments (e.g., polyethers or polyols) and isocyanate-based hard/solid segments [5,12,14,21-29].

Several works reported the dynamic vulcanization of PLLA with different components, i.e., epoxidized synthetic elastomers, unsaturated polymers, and natural rubber, leading to the formation of supertough PLA materials with higher mechanical characteristics. The mechanism

of enhancement is related to two main factors which are the chemical modification of the molecular structure and the improved compatibility between the blend component [22,24-42].

Several examples of super-toughened PLA blends obtained by either reactive interfacial compatibilization, or dynamic vulcanization with the formation of a second component rubbery phase are reported. In order to prepare systems along the first strategy, several acrylate-glycicyl copolymers have been adopted, e.g, poly(ethylene-glycidyl methacrylate) (EGMA) and ethylene-co-acrylic ester-co-glycidyl methacrylate (E-AE-GMA) rubber [43,44]. The type of tested rubbers vulcanized in-situ in the PLA matrix are also various, including: i) nitrile rubber crosslinked with dicumyl peroxide [27]; ii) soybean oil vulcanized by free radical cross-linking agents [38]; iii) zinc ionomers of the ethylene methyacrylic acid copolymer (EMAA–Zn) and elastomeric ethylene-butyl acrylate–glycidyl methacrylate terpolymer (EBA–GMA) [30]; iv) poly(glycerol succinate-co-maleate) (PGSMA) [39] Besides the toughening effect, in some cases an increase of crystallization rate or nucleation density of the material was also reported [27,36,41].

The use of isocyanate based crosslinkers or chain extenders enable to obtain both the formation of a dynamically vulcanized rubber phase, when reactive oligomers with low T_g are added to PLA, and the simultaneous interfacial compatibilization of the resulting blend, thanks to the reaction with the terminal hydroxyl groups of the PLLA chains. Different "soft" building-blocks have been used to form in-situ the polyurethane, both oil-based, such as poly(ethylene glycol),[31] polyester-polyol, [42] and polyurethane elastomer pre-polymers [36]; or bio-renewable, e.g., based on castor-oil. [33,34,37,41] Largely enhanced ductility and impact behaviour were reported for PLA-based blends, as well faster cold-crystallization in most cases. Excellent compatibility of the formed rubber with PLA is generally expected, because of the reported miscibility of poly(lactide) with some polyethers and polyesters.

The development of bio-based rubbery materials remains an important research objective. Fatty acids based materials are promising candidates for this aim. In this work we aimed to toughen PLLA and prepare of a fully-biobased material by dynamic vulcanization with hexamethylene diisocyanate (HDI), using PLLA, glycerol and a polyester polyol derived from vegetable oils. This latter is produced by polymerization of fatty acid dimers containing 36 carbon atoms, and have the advantage of being commercially available. The morphology, thermal and crystallization behavior were investigated, and correlated with the measured mechanical properties.

7.2 Materials and methods

7.2.1 Materials

Poly(L-lactic acid) (PLLA) (Synterra 1010) was supplied by Synbra Technology (Etten-Leur, Netherlands). PLLA 1010 is a crystallizable grade of PLLA with a L-lactide content of about 99 wt%. The melting point is in the range 175–180°C, and the glass transition temperature (T_g) is around 55–60°C. The polymer shows a melt flow rate (MFR) of about 12 g/10 min (190°C, 2.16 kg, ISO 1133) and a density of 1.25 g/cm3. PLLA was dried at 60 C overnight prior to use.

Priplast™ 3196 is a dimerized fatty acid based polyester polyol with molecular weight of 3 Kg/mol. The polyol has been synthesized from C36 fatty acid dimers derivative, in turns obtained by dimerization of unsaturated C18 fatty acids (such as oleic, linoleic and linolenic acids). This material was kindly supplied by Croda Factory. Glycerol (99.5 %), hexamethylene diisocyanate (≥99%), Chloroform (99.5 %). were purchased from Sigma-Aldrich and used as received. Cellulose extraction thimbles (Grade 208) were purchased from AquaLab® technologies (USA).

7.2.2 Blend preparation

Dynamic vulcanization of the Priplast™ 3196 and glycerol in presence of HDI inside the PLLA matrix was performed in a Plastograph Brabender internal mixer (W50 EHT, Brabender GmbH, Germany), at 180°C, using a rotor speed of 60 rpm for around 18 min. PLLA and polyol and glycerol in predetermined amounts were firstly pre-mixed in the Brabender at 180°C and 60 rpm for 8 min to obtain a uniform melt. Then dynamic vulcanization of the polyol and glycerol was initiated by adding HDI under the same mixing conditions.

When the dynamic vulcanization occurred, the melt torque increased first and then levelled off (after approximately 10 min), which was interpreted as the end of the dynamic vulcanization process. The molar ratio of –NCO group (of HDI) to –OH group (of the polyol and glycerol) was fixed at 1:1. While the glycerol/polyol weight ratio was kept at about 10 %. Five samples with PLLA weight fraction of 100, 95, 90, 80 and 70 were prepared. The respective sample codes are reported in Table 7.1. For the sake of comparison, neat PLLA was also treated under the same processing conditions in the internal mixer.

Table 7.1. Composition of the prepared samples (in weight percentage, wt%).

Sample	PLLA (wt%)	Priplast™ 3196 (wt%)	Glycerol (wt%)	HDI (wt%)
Neat PLLA	100	0	0	0
PLLA/5PU	95	3,42	0,38	1,2
PLLA/10PU	90	6,84	0,76	2,4
PLLA/20PU	80	13,68	1,52	4,8
PLLA/30PU	70	20,52	2,28	7,2

7.2.3 Blend characterization

Determination of the cross-linked fraction

Samples with a predetermined weight ($m_i \approx 1$ g) were enclosed into cellulose extraction thimbles. The extraction was performed using a Soxhlet extractor for 3 days with an excess volume of boiling chloroform. The fraction of the sample which did not dissolve in chloroform but just swelled, was then weighted (m_f) after complete drying under vacuum at 50°C. The insoluble fraction must consist of the vulcanized PU and the PLLA chains which reacted with PU. The cross-linked fraction was calculated using the equation (1):

$$\text{Cross-linked fraction (\%)} = (m_f / m_i) \times 100 \qquad (1)$$

Where m_i is the initial sample weight and m_f is the weight of the insoluble part after extraction.

Fourier-transform infrared analysis (FTIR) spectra of PLLA/PU blends and insoluble sample fractions were recorded at room temperature, by means of a Bruker IFS66 spectrometer equipped with an attenuated total reflectance accessory (ATR). A total of 32 spectra with a resolution of 04 cm-1 were acquired for each sample, in the range 500–4000 cm^{-1}.

Scanning Electron Microscopy (SEM): The different PLLA/PU blends were cryogenically fractured after 3 hours of immersion in liquid nitrogen. Fracture surfaces were observed by SEM after gold coating under vacuum, using a Hitachi S-2700 electron microscope. Micrographs of the most representative inner regions of the specimens are reported.

Polarized light Optical Microscopy (PLOM) was employed to determine the morphology and measure the growth rate of PLA spherulites. The micrographs of blend films with a thickness of approximately 10 μm were recorded with a LEICA DC 420 camera. A METTLER FP35Hz hot stage was employed to impose the desired thermal history.

The isothermal spherulitic growth rate of neat PLLA and of the PLLA phase within the PLLA/PU blends was measured. The samples were first heated to 200°C for 3 minutes, to erase the previous thermal history, and then cooled to the chosen crystallization temperature, at which spherulitic growth was monitored in time by a suitable image acquisition.

Differential scanning calorimetry (DSC) was performed using a DSC1 STAR^e System (Mettler-Toledo, Switzerland). The samples were molten at 200°C for 3 min and then cooled to -50°C at a rate of 10°C/min. After cooling, the polymers were subsequently heated to 200°C at 10°C/min. During the DSC runs, a nitrogen flow at a rate of 20 mL/min was constantly applied.

The crystallinity degree Xc (%) of PLLA component in different blends was calculated

using the following formula:

$$Xc(\%) = (\Delta H_m - \Delta H_{cc}) / (\Delta H_m^\circ \times W_f) \qquad (2)$$

where ΔH_m and ΔH_{cc} are the measured enthalpies of melting and cold crystallization for PLLA phase in the blends, ΔH_m° is the melting enthalpy of 100% crystalline PLA (93.7 J/g) and Wf is the weight fraction of PLA in the blend, as determined from the preparation conditions [36].

Thermogravimetric analysis (TGA) was performed using a TGA Metller Toledo (STAR^e system Metller thermobalance). The temperature was increased from 25 to 800°C with a heating rate of 10°C/min under a nitrogen flow of 80 mL/min.

Tensile tests: The tensile properties of PLLA/PU blends were determined by an Instron mechanical tester (Instron 5565) using a crosshead speed of 05 mm/min and rectangular specimens with dimension of ASTM-D638 standard. The reported measured properties (Young's modulus, Strength and deformation at break) are average values from five different specimens.

Impact test: The impact strength of different PLLA/PU blends was tested using a Pendulum Impact Testing Machine (Charpy Zwick 5102). Specimens of 60×10×2 mm were cut from a compression molded plate, and a small notch was produced by means of a manual saw. The measured values are of significance for a relative comparison between the neat and blended PLLA materials only, given the customized (non-standard) sample preparation procedure and test. Five analyses were performed for each sample, and the average values are reported.

7.3 Results

Chemical analysis

Dynamic vulcanization was used to prepare PLLA/PU biobased blends in which the crosslinked PU was formed by the *in-situ* polymerization of polyester polyol oil, glycerol, and HDI. The reactive blending was performed in an internal mixer type Brabender. All blends were prepared at the same conditions, including neat PLLA, for a proper comparison. The interfacial compatibilization between the PLA matrix and PU phase can in principle take place thanks to the reaction of the terminal hydroxyl groups of PLA with −NCO groups of HDI. Figure 7.1 report the measured melt torque versus time during the dynamic vulcanization process. As judged from the instrumental response, dynamic vulcanization displays two steps. The first step is related to the melting of PLLA pellets and characterized by a sharp peak in the measured torque which decreases gradually with mixing time because of both the melting of PLLA pellets and the lubrication/plasticization effect of polyol and glycerol [31,41]. The second step starts with the addition of HDI: the torque increases gradually to a stable plateau, because the viscosity of the system increases during the occurrence of the vulcanization reaction. The time at which the torque remains constant indicates the end of the cross-linking process. It is worth noting that the measured torque decreases slightly when HDI is added. We hypothesize that this might be related to some extent of chain scission due to the high reactivity of the isocyanate.

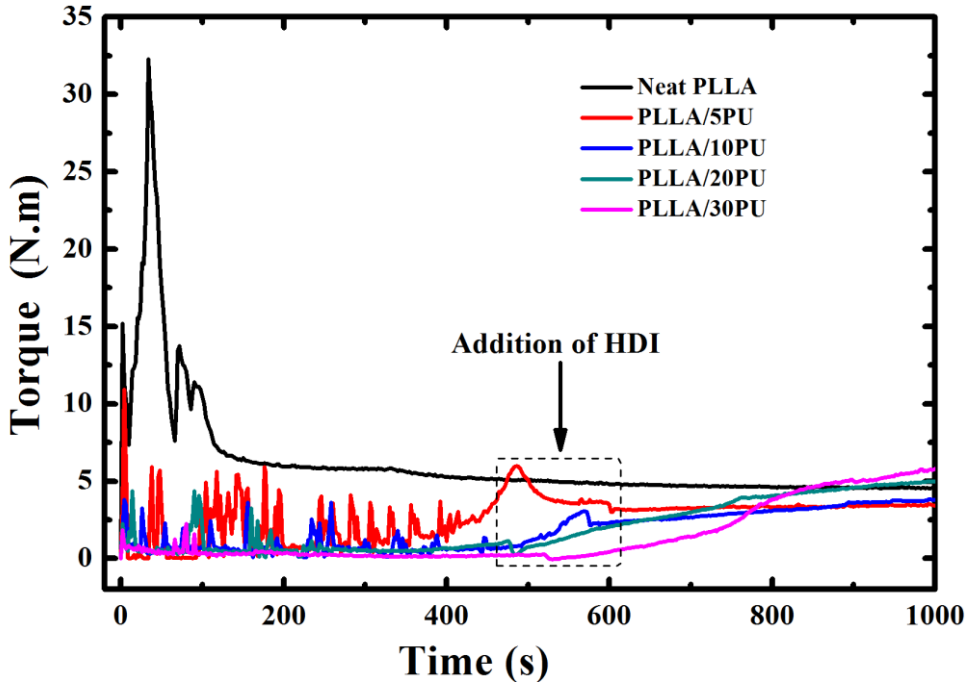

Figure 7.1. Torque versus time curves during the dynamic vulcanization of the different systems.

To confirm the presence of crosslinked PU network inside the PLLA matrix, we isolated a crosslinked fraction from samples extensively extracted with chloroform and carried on further analysis. Figure 7.2 shows the weight percentage of insoluble residues of the different PLLA/PU blends. The gel fraction increases gradually with the increase of the polyol content. However, in all cases, the vulcanized part weight was lower than the total content of added reactive mixture (polyester polyols oil, glycerol and HDI). This difference likely indicates that only a part of the polyol chains are effectively cross-linked, notwithstanding the stoichiometric ratios between isocyanate and hydroxyl groups. On the other hand, the presence of a non-negligible insoluble fraction confirms that the aim of producing a PLLA/rubber blend is achieved.

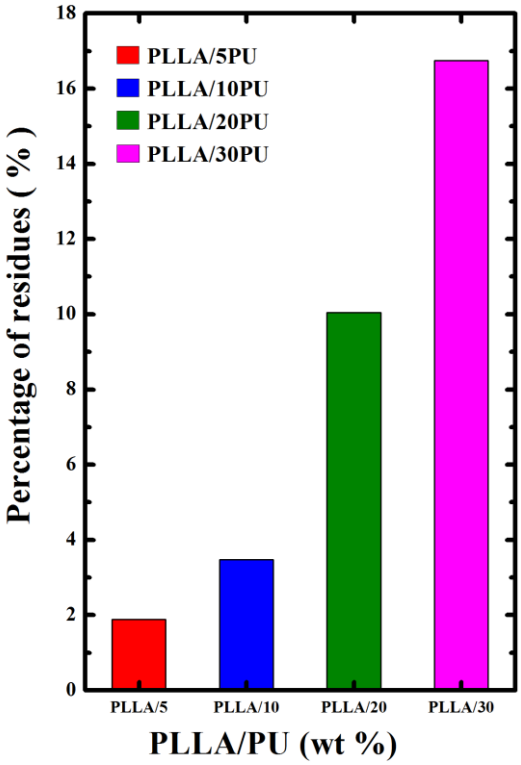

Figure 7.2. Percentage of the insoluble fraction (after Soxhlet extraction with chloroform) in different PLLA/PU blends.

FTIR was performed to confirm the occurrence of the reaction. The results related to the different as-prepared PLLA/PU blends and to the insoluble fractions are reported in Figure 7.3 and 7.4, respectively. All the characteristic absorption peaks of neat PLLA were also observed in PLLA/PU blends spectra. Moreover, distinct absorption bands are present in PLLA/PU samples. In particular, the peak at 1540 cm^{-1} which characterizes the urethane group is clearly evidenced and increases with the polyol concentration. Accordingly, no trace of the isocyanate

group peak of HDI (2200 cm^{-1}) could be detected in the reacted samples. Figure 7.4 shows the spectra of neat PLLA, and of the insoluble fraction of PLLA/10PU, PLLA/20PU, and PLLA/30PU blends. The bands at 1540 cm^{-1} and 3333 cm^{-1}, which represent the urethane groups, are distinctly evident in the vulcanized fractions. Figure 7.4 also revealed the appearance of an absorption band centred at 1758 cm^{-1} the insoluble fractions spectra. Such peak is related to the crystalline carbonyl vibration of PLLA unit, [3] and suggests the occurrence of the reaction between PLLA chains ends and HDI, to a certain extent. The obtained FTIR results confirm the successful dynamic vulcanization (of polyester polyol oil, glycerol, and HDI), and indicate that a certain degree of compatibilization between PLLA and PU through a chemical bond can also be expected. This chemical modification will strongly affect the morphology, mechanical properties, as well as thermal and crystallization behavior of the final blends, as it will be shown hereafter.

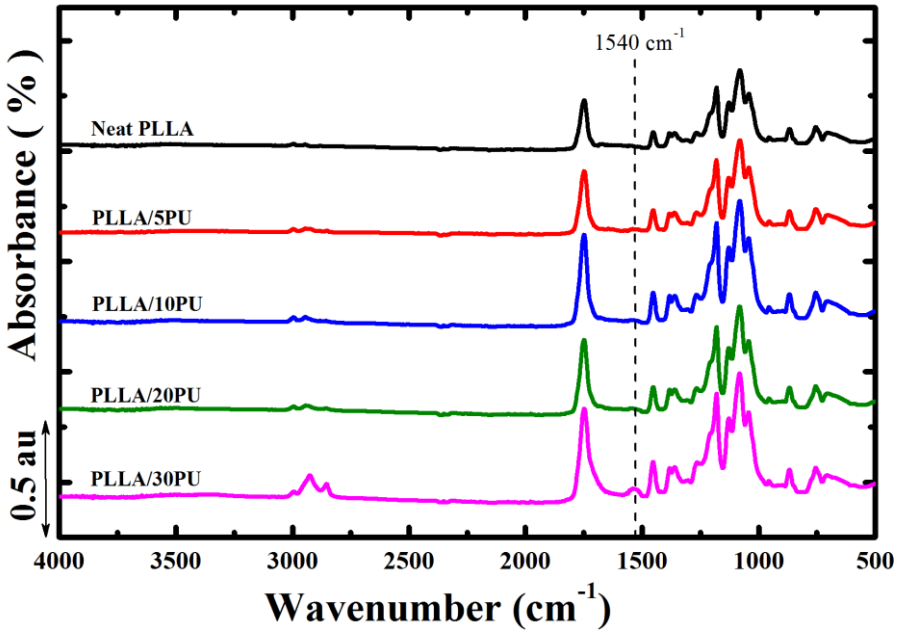

Figure 7.3. FTIR spectra of neat PLLA and PLLA/PU blends.

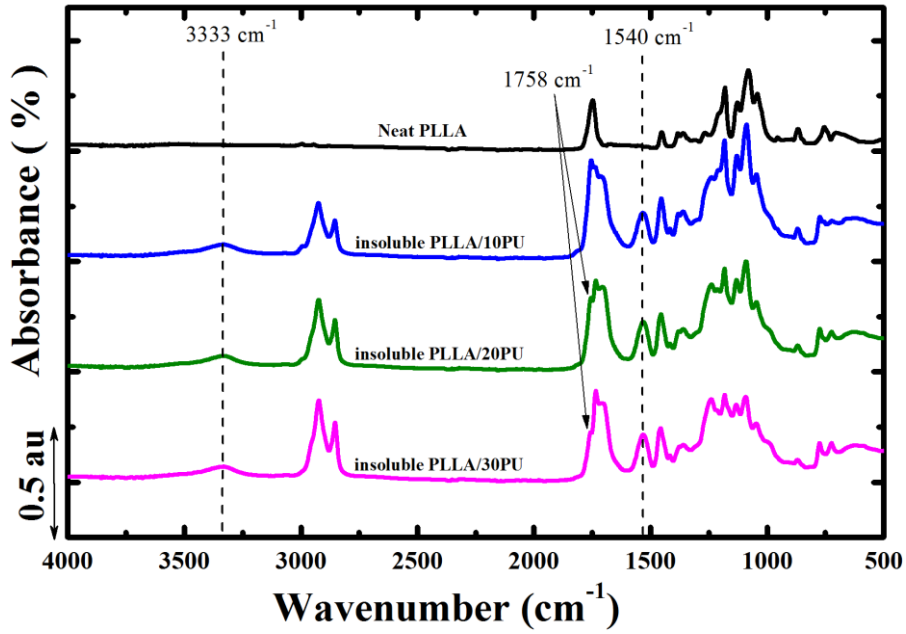

Figure 7.4. FTIR spectra of neat PLLA and insoluble fractions of different PLA/PU blends.

Scanning electron microscopy analysis

In Figure 7.5 some selected SEM micrographs of cryo-fractured surfaces for neat PLLA and PLLA/PU blends with different PU content are presented. Neat PLLA showed a typical brittle fracture characterized by smooth surface appearance. On the other hand, all the PLLA/PU vulcanized blends exhibit a rough surface featuring a phase-separated morphology with some evidence of deformed areas. Cryo-fractured surfaces of PLLA/5PU, display clear cavities and gaps due to the detachment of PU dispersed phases. This suggests the low interfacial adhesion between PLLA and PU for this blend composition. For PU content higher than 5 wt%, the PU droplets dispersed in the PLLA matrix possess an irregular shape.

A good adhesion is apparent in these systems, since no gaps were observed. This indicates the efficiency of the interfacial compatibilization between the two phases, as a consequence of the dynamic vulcanization process. In addition, plastic deformation occurred to a certain extent and the fibrils. The obtained results are in agreement with the chemical changes presented in Figures 7.2 and 7.4.

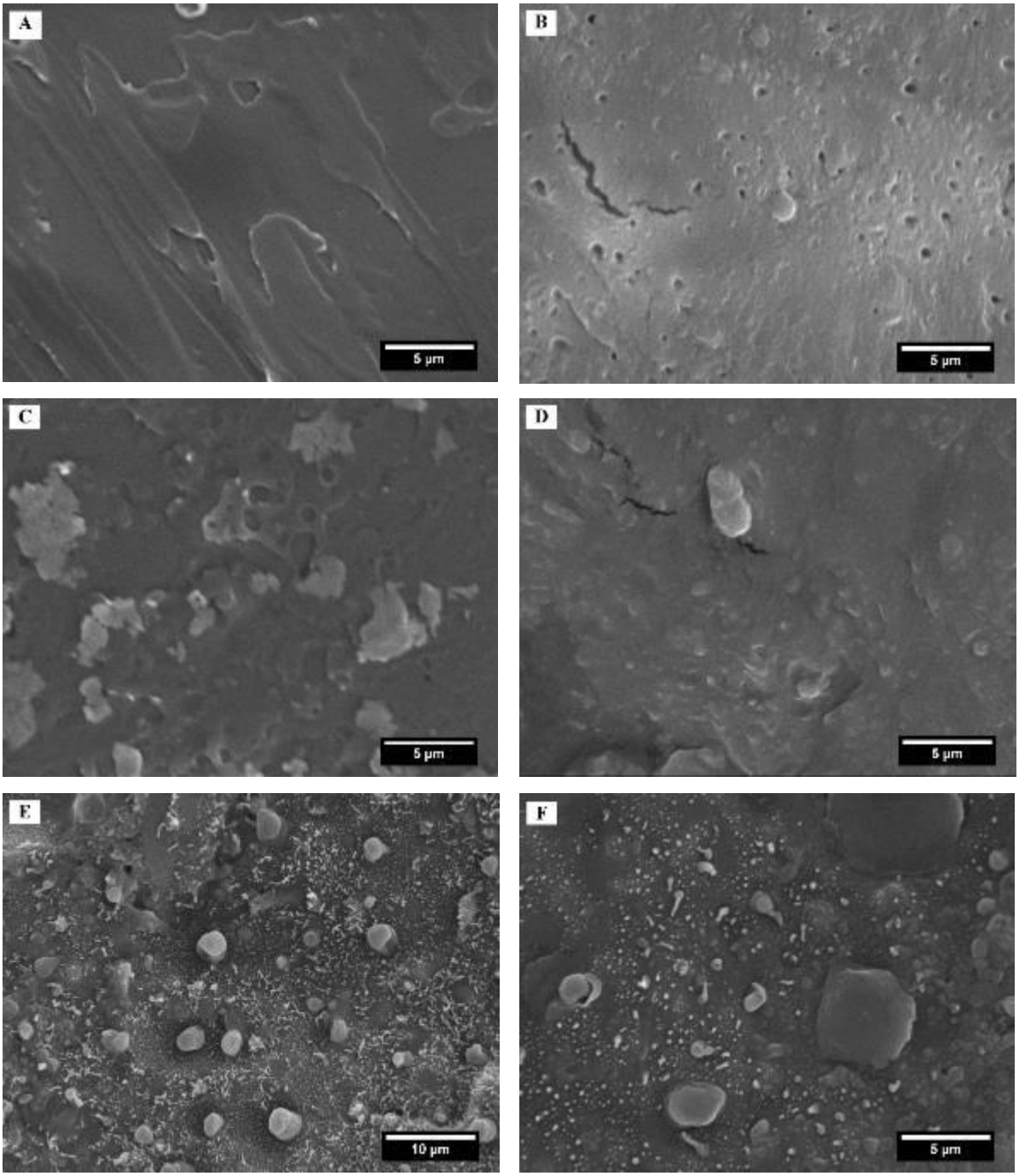

Figure 7.5. SEM images of different PLLA/PU blends with different concentration of PU phase A (neat PLLA), B (PLLA/5PU), C (PLLA/10PU), D (PLLA/20PU), E and F (PLA/30PU).

On the other hand, the size of the dispersed PU phase was found to increase with PU content, going from around 0.5-1 µm droplets in the PLLA/5PU to domains of the order of 5 µm in PLLA/30PU blend. The increase in PU domain size with the increase of PU content could result from the coalescence of PU phase, induced by its immiscibility with the PLLA matrix.

Polarized light optical microscopy analysis

PLOM was used to study the spherulitic morphology and the crystallization behaviour of the PLLA phase within the different blends. Figure 7.6 shows examples of PLOM micrographs obtained for the different samples after 10 min of isothermal crystallization at 140°C. Neat PLA (Figure 7.6A) showed regular spherulites with high degree of perfection and large diameters. The regularity and perfection of PLLA spherulites in PLLA/PU blends decreased with the increase of PU content, where small PU domains and particle-like impurities can be observed within the spherulite structure. In particular, at the highest content of PU, the characteristics radial fibrillary structure is not distinguishable anymore.

The decreased PLLA spherulites regularity and texture perfection could be attributed to the interlamellar segregation of the soft PU domains. In fact, the micrometer-sized crosslinked polyol phase cannot be easily excluded from the growth front of the PLLA spherulites, and thus strongly affect the lamellar arrangement. Similar results have been reported in literature for PLLA crystallizing from an immiscible blend showing a certain interaction with the matrix. [45].

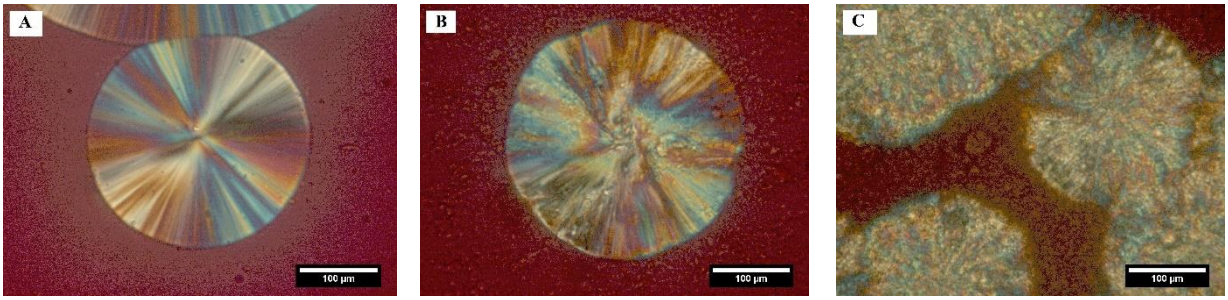

Figure 7.6. PLOM micrographs at a crystallization temperature of 140°C for neat PLLA (A), PLLA/10PU (B), and PLLA/30PU (C).

Beside the morphology, also the nucleation density of PLLA was affected by the dynamic vulcanization and presence of PU phase. Hence, number of PLA nuclei increase significantly with the increase of PU content, as shown in an enlarged view (Figure 7.7). The increase in PLLA nuclei concentration could be due to (i) some nucleating active impurities transferred from the different additives to PLLA matrix, (ii) an interface-induced nucleation mechanism due to PLLA/PU phase separation, perhaps ascribed to local order due to increased interactions between PLLA and PU.

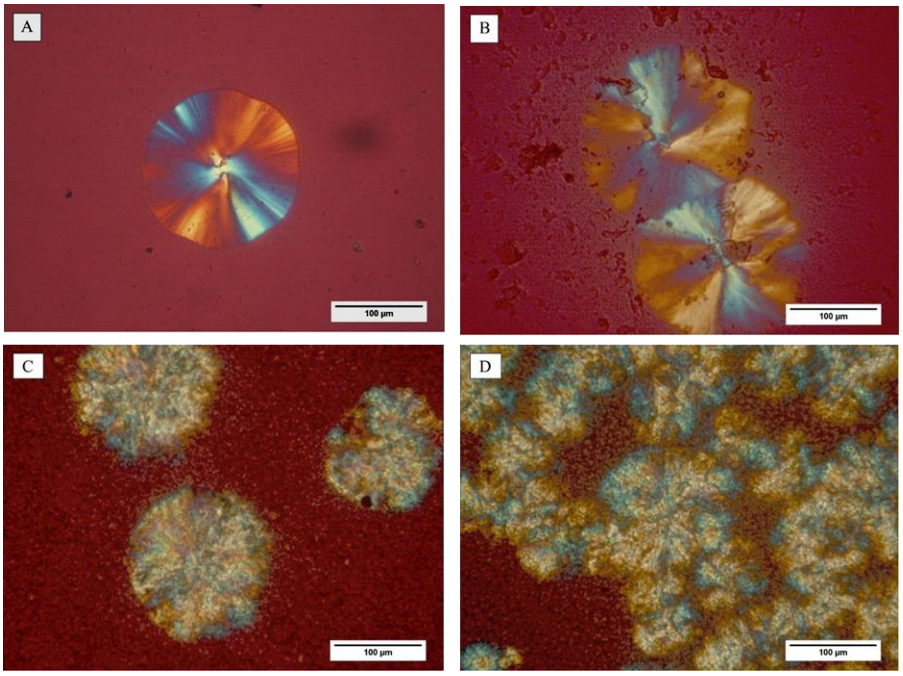

Figure 7.7. PLOM micrographs of PLLA/PU blends after 10 min at 138°C; A) neat blend, B) PLLA/5PU, C) PLLA/20PU, and D) PLLA/30PU.

Results of PLLA spherulites growth rates in the studied systems are shown in Figure 7.8, as a function of the chosen crystallization temperature. Overall, the effect of dynamic vulcanization on the growth rate is not striking. However, some small variations could be appreciated. In particular, we note that PLLA spherulitic growth rate of PLLA/5PU and PLLA/10PU was slightly higher than that of neat PLLA, which is tentatively explained by a slight decrease in the molecular weight, due to chain scission caused by HDI. Indeed, a lower molecular weight of these blends with respect to neat PLA could also be inferred by the lower torque value at the end of the vulcanization (Figure 7.1). The lower chain length would indeed lead to faster spherulitic growth. For PU contents higher of 30 wt%, the PLLA growth rate is instead slightly decreased, in comparison with the other samples. Possibly, this depression is related to the extent of chemical bonding between PLLA and PU phase, which hinders PLLA chains mobility, or to the disturbance brought by the rubber phase the growth front, since the PU must be segregated at the interfibrillar level. Due to the increased nucleation density with PU content, the minimum probed isothermal crystallization temperature, where we could clearly follow the growth rate, increased accordingly. Hence for neat PLLA, we were able to measure the growth rate starting from T_c of 130°C while for PLLA/30PU blend the minimum applied T_c was 138°C.

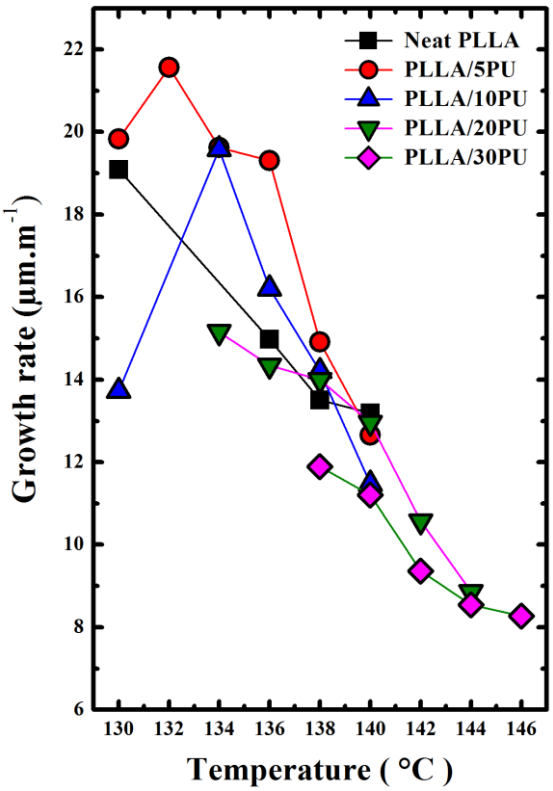

Figure 7.8. Growth rate of PLLA spherulites in the different PLLA/PU blends.

Crystallization behavior of PLLA/PU blends by DSC

DSC was employed to study the thermal transition of neat PLLA and PLLA/PU blends. The different temperature and enthalpies of the thermal events recorded during non-isothermal crystallization and melting at a scan rate of 10°C/min are summarized in Table 7.2, while Figure 7.9 shows the respective DSC cooling and heating scans.

Table 7.2: Transition temperatures and enthalpies of PLLA phase during the non-isothermal scans of the different blends different PLLA/PU blends at a cooling/heating rate of 10°C/min. The $\Delta H°_m$ of 100% crystalline PLA is 93.7 J/g.

PLA	**ΔHc**	**ΔHcc**	**ΔHm**	T_c	T_{cc}	T_m	X_c
wt%	(J/g)	(J/g)	(J/g)	**(°C)**	**(°C)**	**(°C)**	**(%)**
100	-20,7	-0,9	31,8	102,9	92,3	174,8	33
95	-5,8	-11,8	27,4	105,4	98,7	172,4	16,6
90	-3,6	-15,2	29,0	106,7	100	173,4	14,7
80	-4,2	-11,4	24,1	106,4	99,5	173,1	13,5
70	-4,5	-8,3	22,4	106,6	98,5	173,2	15

Neat PLLA partially crystallizes on cooling at around 103°C, and the crystallization process is completed during the heating scan via cold crystallization process at around 92°C (see figure 7.9a). Its endothermic melting peak was observed at 175°C, and just before melting the PLLA crystals, a slight exothermic event is observed, tentatively attributed to the reorganization of a disordered modification into the more stable α'-form. [46,47]. For PLLA/PU blends with different PU content, the DSC cooling scans show that PLLA phase exhibit a crystallization exotherm peaked at around 106°C for all the sample, and the partial vitrification is also observed during cooling at around 63°C, differently form the neat PLLA. No distinct transitions or peaks related to the PU phase and could be observed. The crystallization enthalpy on cooling decreases significantly in the dynamically vulcanized samples (see Table 7.2), testifying the hindered crystallization in the blend.

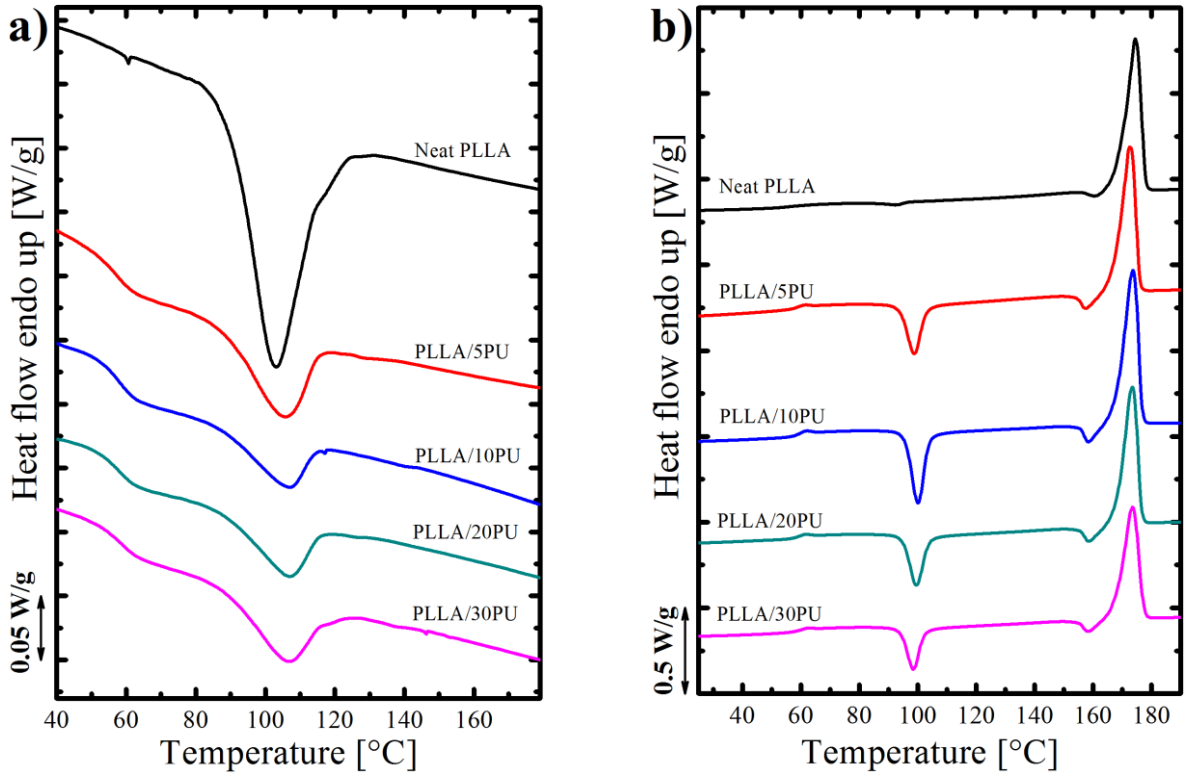

Figure 7.9. DSC cooling a) and heating b) curves recorded at a scan rate of 10°C/min for neat PLLA and PLA/PU blends.

The heating process is shown in Figure 7.9b. Neat PLLA displays an almost negligible cold crystallization at around 92°C, PLLA/PU blends all exhibit a large cold crystallization peak at about 99°C. The crystallinity degree (*Xc* %) of PLLA at the end of the temperature protocol, evaluated from the measured melting enthalpy after correction for PLLA weight fraction in the particular blend, dropped from 33 % for neat PLLA to around 15 % when the

vulcanized PU is added. We must deduce that a meaningful hindrance effect of the PU phase on crystallization is present, when the process occurs at temperatures lower than those probed by PLOM experiments. In fact, a significant decrease in the growth rate was only observed for PLLA/30PU sample, in the probed temperature range. This noticeable decrease in the crystallinity might be due to an higher viscosity of the blends compared to neat PLLA.

Thermal stability of PLLA/PU blends

Thermal stability of neat PLLA and PLLA/PU blends under non-oxidative conditions was investigated by TGA. The analysis was performed in the range 25-800°C at a heating rate of 10°C/min under a constant nitrogen gas flow. Figure 7.10 shows the TGA weight loss curves as a function of temperature. From these curves, we can identify the onset and end of the thermal decomposition, indicated with T5 (5% of mass loss) and Tend (100% of mass loss), respectively.

Neat PLLA displays single stage decomposition process, with T5 304 C° and Tmax around 374°C. On the other hand, all PLLA/PU blends show two-stage decomposition, obviously related to the presence of two chemically distinct units, the PLLA and polyol phases. In fact, the magnitude of mass lost at the different steps varies in agreement with the blend composition, i.e., the percentage of low-temperature decomposition event decreases with increasing PU fraction, and vice versa for the high-temperature event. An almost quantitative relation with the nominal content of PU is found.

For what concerns the degradation temperatures, the onset of PLLA degradation shifts to lower temperature after dynamic vulcanization and with increasing the PU phase content. In particular, T5 decreased from 304°C for neat PLLA to around 276°C for PLLA/30PU.

The decomposition stage with Tmax around 336°C observed in the blends was attributed to the urethane bonds breaking [41], while the decomposition event ending at around 485°C can be ascribed to the thermal degradation of the aliphatic segments of the polyester polyol.

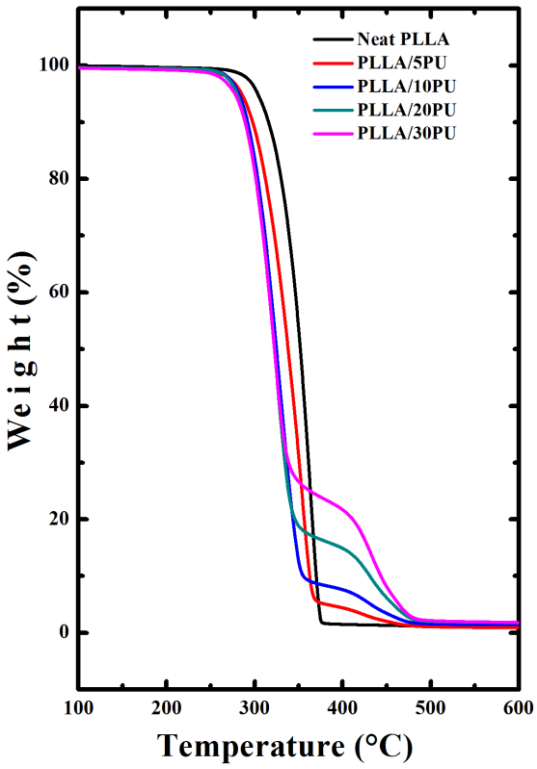

Figure 7.10. TGA (evaluation of weight loss as a function of temperature) curves of PLLA and PLA/PU blends.

Notwithstanding the slight decrease of the temperature of initial thermal degradation, a good thermal stability of different blends was observed overall, since the values of the decomposition temperatures are still at least 50°C above the commonly employed processing temperature.

Tensile and impact properties

Generally, the mechanical properties of interest for polymers are related to their strength and toughness. Tensile elongation at break and impact strength are considered as measures of material's toughness, whereas the flexural modulus and tensile strength at break are informative of material's strength [33,48]. Figures 7.11a-c) summarize the results of mechanical tensile test on the different systems. The inclusion of vulcanized PU phase affects the system strength and rigidity. In particular, the Young's modulus decreases steadily to about one third of its value in neat PLLA, when 30 wt% of PU blended. Similarly, the stress at break of the same blend is about two times lower than that of neat PLLA. However, this softening of the material is not accompanied by a very meaningful increase of the elongation at break, which is still very low, below 2% strain.

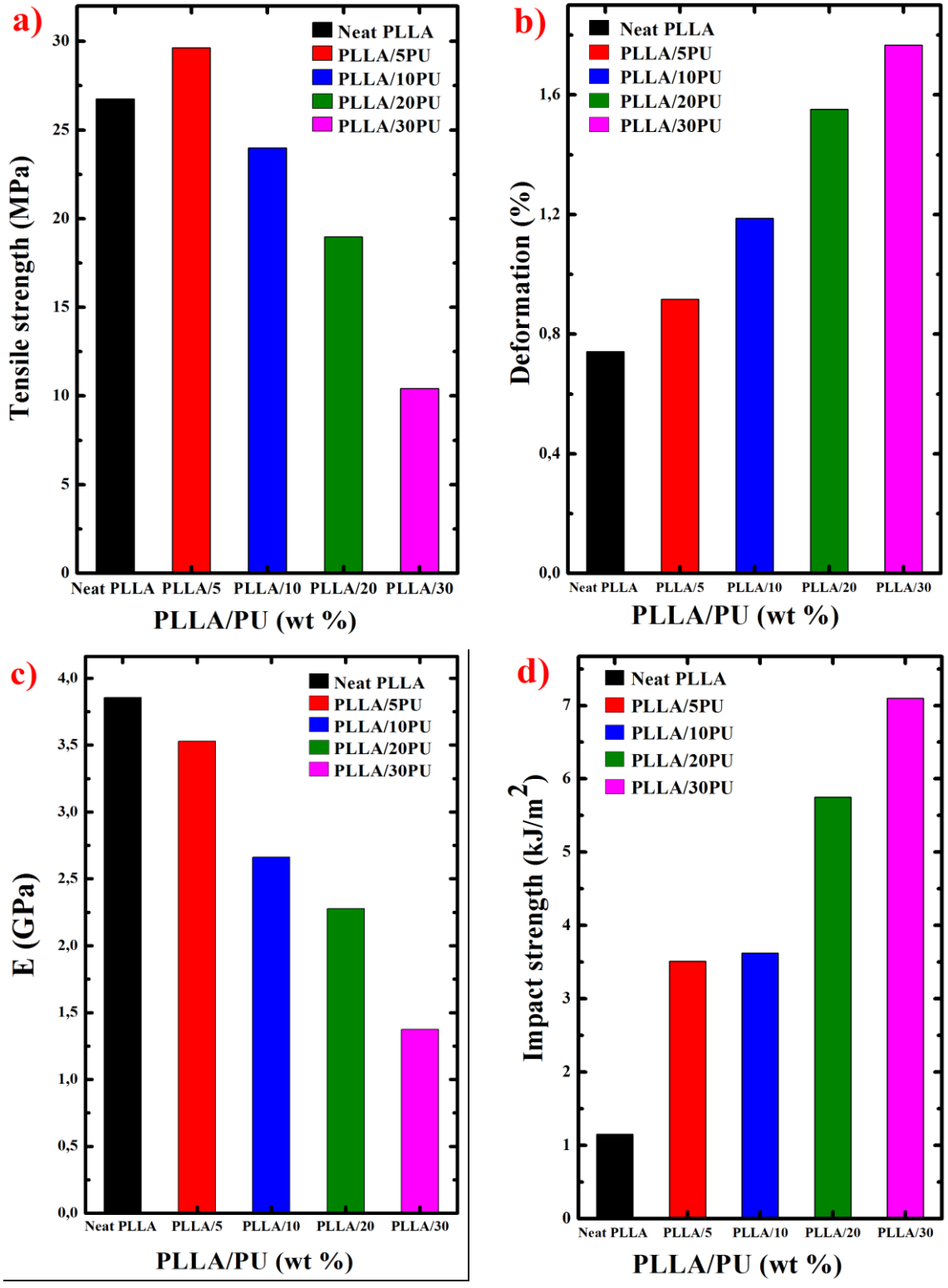

Figure 7.11. a) Tensile strength, b) deformation at break, c) Young's Modulus, and d) impact strength of PLLA and PLA/PU blends.

As such, the modified PLLA still behaves as a brittle material upon tensile deformation. The behaviour of the PLA matrix dominates the mechanical response of the blend; perhaps due

to an insufficient degree of molecular interactions between the two components, and the lack of any plasticization effects of the polyol segments on PLA.

On the other hand, the Charpy impact tests revealed a fairly good improvement in the impact strength values of PLLA/PU blends. In fact, the impact strength increase gradually with increasing the content of PU, reaching a value approximately 7 times higher than neat PLLA for the PLLA/30PU blend. It is deduced that the dispersed PU rubbery domains could absorb the energy released upon impact, and hinder the crack growth propagation in this fast loading mode [31,33,49]. However, in the tensile deformation mode, the failure of the sample is still dominated by the strong localization tendency of the PLA matrix, which easily develop crazes.

7.4 Conclusions

The present work discusses the efficiency of dynamic vulcanization reaction and formation of a PU phase on toughening the brittle PLLA. The dynamic vulcanization of PLLA, polyester polyol, glycerol, and HDI was successfully realized and fully biobased PLLA/PU blends were obtained. Analysis of FTIR spectra, extracted and insoluble fractions and the evolution of torque during sample preparation demonstrated the in-situ formation of a PU phase, thanks to the reaction between –NCO groups of HDI with the –OH groups of the polyester polyol, glycerol, and PLLA.

The partial reaction with PLLA chain give rise to some extent of interfacial compatibilization between PLLA and dispersed PU phase. The impact strength was significantly increased by the increase in PU content; however, the tensile properties were not largely enhanced.

For what concerns the thermal properties, DSC showed a depression in the crystallization rate the blends, as compared to neat PLLA. Thermogravimetric analysis demonstrated that all PLLA/PU blends were sufficiently stable at the typical processing temperatures of PLLA.

7.5 References

1. Yokohara T, Yamaguchi M (2008) Structure and properties for biomass-based polyester blends of PLA and PBS. Eur. Polym. J. 44:677-685

2. Cai Y, Lv J, Feng J (2013) Spectral Characterization of Four Kinds of Biodegradable Plastics: Poly (Lactic Acid), Poly (Butylenes Adipate-Co-Terephthalate), Poly (Hydroxybutyrate-Co-Hydroxyvalerate) and Poly (Butylenes Succinate) with FTIR and Raman Spectroscopy. J. Polym. Environ. 21:108-114
3. Di Lorenzo ML, Rubino P, Cocca M (2013) Miscibility and properties of poly(l-lactic acid)/poly(butylene terephthalate) blends. Eur. Polym. J. 49:3309-3317
4. Homklin R, Hongsriphan N (2013) Mechanical and Thermal Properties of PLA/PBS Co-continuous Blends Adding Nucleating Agent. Energy Procedia. 34:871-879
5. Wang R, Wang S, Zhang Y, Wan C, Ma P (2009) Toughening modification of PLLA/PBS blends via in situ compatibilization. Polym. Eng. Sci. 49:26-33
6. Bhardwaj R, Mohanty AK (2007) Modification of Brittle Polylactide by Novel Hyperbranched Polymer-Based Nanostructures. Biomacromolecules 8:2476-2484
7. Farah S, Anderson DG, Langer R (2016) Physical and mechanical properties of PLA, and their functions in widespread applications — A comprehensive review. Adv. Drug Delivery Rev. 107:367-392
8. Hamad K, Kaseem M, Yang HW, Deri F, Ko YG (2015) Properties and medical applications of polylactic acid: A review. eXPRESS Polym. Lett. 9:435-455
9. Jia S, Yu D, Zhu Y, Wang Z, Chen L, Fu L (2017) Morphology, Crystallization and Thermal Behaviors of PLA-Based Composites: Wonderful Effects of Hybrid GO/PEG via Dynamic Impregnating. Polymers. 9:528
10. Kamthai S, Magaraphan R (2015) Thermal and mechanical properties of polylactic acid (PLA) and bagasse carboxymethyl cellulose (CMCB) composite by adding isosorbide diesters. AIP Conference Proceedings. 1664:060006
11. Kobayashi J et al. (1995) Structural and optical properties of poly lactic acids. J. Appl. Phys. 77:2957-2973
12. Madhavan Nampoothiri K, Nair NR, John RP (2010) An overview of the recent developments in polylactide (PLA) research. Bioresour. Technol. 101:8493-8501
13. Mathew AP, Oksman K, Sain M (2005) Mechanical properties of biodegradable composites from poly lactic acid (PLA) and microcrystalline cellulose (MCC). J. Appl. Polym. Sci. 97:2014-2025

14. Nagarajan V, Mohanty AK, Misra M (2016) Perspective on Polylactic Acid (PLA) based Sustainable Materials for Durable Applications: Focus on Toughness and Heat Resistance. ACS Sustainable Chem. Eng. 4:2899-2916
15. Nakajima H, Dijkstra P, Loos K (2017) The Recent Developments in Biobased Polymers toward General and Engineering Applications: Polymers that are Upgraded from Biodegradable Polymers, Analogous to Petroleum-Derived Polymers, and Newly Developed. Polymers 9:523
16. Tawakkal ISMA, Cran MJ, Miltz J, Bigger SW (2014) A Review of Poly(Lactic Acid)-Based Materials for Antimicrobial Packaging. J. Food Sci. 79:1477-1490
17. Wang M, Wu Y, Li Y-D, Zeng J-B (2017) Progress in Toughening Poly(Lactic Acid) with Renewable Polymers. Polym. Rev. 57:557-593
18. Ock HG, Kim DH, Ahn KH, Lee SJ, Maia JM (2016) Effect of organoclay as a compatibilizer in poly(lactic acid) and natural rubber blends. Eur. Polym. J. 76:216-227
19. Paul DR, Barlow JW (1979) A Brief Review of Polymer Blend Technology. In: Cooper SL, Estes GM (eds) multiphase polymers. Advances in Chemistry, Washington, p 315-335
20. Robeson L (2014) Historical Perspective of Advances in the Science and Technology of Polymer Blends. Polymers 6:1251
21. Theryo G, Jing F, Pitet LM, Hillmyer MA (2010) Tough Polylactide Graft Copolymers. Macromolecules 43:7394-7397
22. Akrami M, Ghasemi I, Azizi H, Karrabi M, Seyedabadi M (2016) A new approach in compatibilization of the poly(lactic acid)/thermoplastic starch (PLA/TPS) blends. Carbohydr. Polym. 144:254-262
23. Anderson KS, Schreck KM, Hillmyer MA (2008) Toughening Polylactide. Polym. Rev. 48:85-108
24. Chen G-X, Kim H-S, Kim E-S, Yoon J-S (2005) Compatibilization-like effect of reactive organoclay on the poly(l-lactide)/poly(butylene succinate) blends. Polymer 46:11829-11836
25. Formela K, Zedler L, Hejna A, Tercjak A (2018) Reactive extrusion of bio-based polymer blends and composites – Current trends and future developments. eXPRESS Polym. Lett. 12:24-57

26. Hu X, Li Y, Li M, Kang H, Zhang L (2016) Renewable and Supertoughened Polylactide-Based Composites: Morphology, Interfacial Compatibilization, and Toughening Mechanism. Ind. Eng. Chem. Res. 55:9195-9204
27. Liu L, Hou J, Wang L, Zhang J, Duan Y (2016) Role of Dicumyl Peroxide on Toughening PLLA via Dynamic Vulcanization. Ind. Eng. Chem. Res. 55:9907-9914
28. Ma M, Zheng H, Chen S, Wu B, He H, Chen L, Wang X (2016) Super-toughened poly(l-lactic acid) fabricated via reactive blending and interfacial compatibilization. Polym. Int. 65:1187-1194
29. Nerkar M, Ramsay JA, Ramsay BA, Vasileiou AA, Kontopoulou M (2015) Improvements in the melt and solid-state properties of poly(lactic acid), poly-3-hydroxyoctanoate and their blends through reactive modification. Polymer 64:51-61
30. Liu H, Song W, Chen F, Guo L, Zhang J (2011) Interaction of Microstructure and Interfacial Adhesion on Impact Performance of Polylactide (PLA) Ternary Blends. Macromolecules. 44:1513-1522
31. Liu G-C, He Y-S, Zeng J-B, Xu Y, Wang Y-Z (2014) In situ formed crosslinked polyurethane toughened polylactide. Polym. Chem. 5:2530-2539
32. Das S, Pandey P, Mohanty S, Nayak SK (2017) Insight on Castor Oil Based Polyurethane and Nanocomposites: Recent Trends and Development. Polym.-Plast. Technol. Eng. 56:1556-1585
33. Gurunathan T, Chung JS, Nayak SK (2016) Reactive Compatibilization of Biobased Polyurethane Prepolymer Toughening Polylactide Prepared by Melt Blending. J. Polym. Environ. 24:287-297
34. Gurunathan T, Mohanty S, Nayak SK (2014) Preparation and performance evaluation of castor oil-based polyurethane prepolymer/polylactide blends. J. Mater. Sci. 49:8016-8030
35. Kunduru KR, Basu A, Haim Zada M, Domb AJ (2015) Castor Oil-Based Biodegradable Polyesters. Biomacromolecules 16:2572-2587
36. Lu X, Wei X, Huang J, Yang L, Zhang G, He G, Wang M, Qu J (2014) Supertoughened Poly(lactic acid)/Polyurethane Blend Material by in Situ Reactive Interfacial Compatibilization via Dynamic Vulcanization. Ind. Eng. Chem. Res. 53:17386-17393
37. Robertson ML, Paxton JM, Hillmyer MA (2011) Tough Blends of Polylactide and Castor Oil. ACS Appl. Mater. Interfaces. 3:3402-3410

38. Robertson ML, Chang K, Gramlich WM, Hillmyer MA (2010) Toughening of Polylactide with Polymerized Soybean Oil. Macromolecules. 43:1807-1814

39. Valerio O, Misra M, Mohanty AK (2017) Sustainable biobased blends of poly(lactic acid) (PLA) and poly(glycerol succinate-co-maleate) (PGSMA) with balanced performance prepared by dynamic vulcanization. RSC Adv. 7:38594-38603

40. Zhang K, Nagarajan V, Misra M, Mohanty AK (2014) Supertoughened Renewable PLA Reactive Multiphase Blends System: Phase Morphology and Performance. ACS Appl. Mater. Interfaces. 6:12436-12448

41. Zhao T-H, He Y, Li Y-D, Wang M, Zeng J-B (2016) Dynamic vulcanization of castor oil in a polylactide matrix for toughening. RSC Adv. 6:79542-79553

42. Zhao X, Ding Z, Lin Q, Peng S, Fang P (2017) Toughening of polylactide via in situ formation of polyurethane crosslinked elastomer during reactive blending. J. Appl. Polym. Sci. 134:44383

43. Oyama HT (2009) Super-tough poly(lactic acid) materials: Reactive blending with ethylene copolymer. Polymer. 50:747-751

44. Dong W, Jiang F, Zhao L, You J, Cao X, Li Y (2012) PLLA Microalloys Versus PLLA Nanoalloys: Preparation, Morphologies, and Properties. ACS Appl. Mater. Interfaces. 4:3667-3675

45. Park JW, Im SS (2003) Miscibility and morphology in blends of poly(l-lactic acid) and poly(vinyl acetate-co-vinyl alcohol). Polymer. 44:4341-4354

46. Androsch R, Schick C, Di Lorenzo ML (2014) Melting of Conformationally Disordered Crystals (α′-Phase) of Poly(l-lactic acid). Macromol. Chem. Phys. 215:1134-1139

47. Kawai T et al. (2007) Crystallization and Melting Behavior of Poly (L-lactic Acid). Macromolecules. 40:9463-9469

48. Tseng FP, Lin JJ, Tseng CR, Chang FC (2001) Poly(oxypropylene)-amide grafted polypropylene as novel compatibilizer for PP and PA6 blends. Polymer. 42:713-725

49. Lin Y, Zhang K-Y, Dong Z-M, Dong L-S, Li Y-S (2007) Study of Hydrogen-Bonded Blend of Polylactide with Biodegradable Hyperbranched Poly(ester amide). Macromolecules. 40:6257-6267

Conclusions and Perspectives

Chapter VII

8.1 Conclusions and perspectives

In this work, we focused on immiscible double and triple crystalline thermoplastic polyester blends. The nucleation and crystallization of these complex materials greatly depends on their morphology, as determined by their composition, processing conditions, thermal history, and presence of filler or compatibilizers.

On the basis of the obtained results, presented in the different sections of the thesis, we can draw several conclusions, as outlined below.

1. Recently, the use of graphene oxide to improve the properties of polymer blends and nanocomposites has attracted some attention. In this work, multiphase PLLA/PBS/GO blend nanocomposites were successfully prepared. GO nanofiller found to enhance the thermal stability of the system and ameliorate the adhesion between PLLA and PBS.

The nucleation and crystallization of PLLA/PBS system was largely affected by the addition of GO, thus a modest enhancement of PLLA nucleation and a large enhancement of the nucleation step of the PBS phase were observed.

The obtained results show a promising route to tune the crystallization and thus end-use properties of some biobased polymer blends, an issue of technological importance for the development of novel "green" materials.

2. Different ternary blends of PLA, PBS, and PCL were prepared, each containing one of the components as minor phase. A partial wetting morphology was produced and the nucleation of PLA on molten PCL or PBS was investigated.

PCL was found to have a higher nucleating effect on PLA with respect to PBS. This is likely due to the much higher interfacial tension between this polymers pair. The crystalline PLA in ternary blends was further found capable of nucleating PBS crystals upon cooling.

3. The self-nucleation protocol (SN) was extensively applied to the PLA/PCL/PBS binary and ternary blends, and proved to be a straightforward strategy to induce the crystallization of the different polymers. Results from SN revealed the strong dependence of

self-nuclei production on the applied melt temperature, with a small influence of the blend morphology and content of the polymers under study.

4. Finally, the efficiency of chemical modification of PLLA by dynamic vulcanization was investigated. Reaction between a polyester polyol from vegetable oil and glycerol in presence of hexamethylene diisocyanate was carried out, and the formation of PU rubbery phase inside PLLA was confirmed.

An interfacial compatibilization and good adhesion between PLLA and PU phases could be assessed. The variation of PU content within PLLA strongly affects the final properties of the resulting materials. In particular, PLLA crystallization rate and crystallinity significantly decrease, while the toughness of PLLA increases.

With this thesis, several gap of knowledge in the crystallization of immiscible blends were highlighted. In particular, the peculiar nucleating effect of molten polymer surfaces requires a much deeper investigation, for a better comprehension of the exact origin and to define the factors that control this nucleation mechanism. In the literature, exceedingly more studies are dealing with non-isothermal crystallization of immiscible polyester blend, with respect to the isothermal case. It should be noted that, since the spherulitic growth rates are clearly not affected by blending, unless compatibilizers or plasticizers are employed, further overall isothermal crystallization kinetics studies could provide information on the nucleation effect of one blend component on the other.

The importance of further research aimed at to the full comprehension of the solidification of these bio-based (and in many cases bio-degradable) materials, lays in the possibility of tailoring their properties, to enable the substitution of traditional non-biodegradable polymers in more advanced applications.

8.2 Publications made and prepared during the PhD period

8.2.1 Scientific publications

1- **S.E. Fenni**, O. Monticelli, L. Conzatti, R. Doufnoune, P. Stagnaro, N. Haddaoui, D. Cavallo (2018) Correlating the morphology of poly(l-lactide)/poly(butylene succinate)/graphene oxide blends nanocomposites with their crystallization behavior. *eXPRESS Polymer Letters*, 12:58-70.

2- **S.E. Fenni**, D. Cavallo, A.J Müller. Nucleation and crystallization in bio-based immiscible polyester blends. **Book chapter** in: Di Lorenzo ML, Androsch R (Eds) Advances in Polymer Sciences: Thermal Properties of Bio-based Polymers. Adv Polym Sci. Springer Nature Switzerland AG 2019. https://doi.org/10.1007/12_2019_48 (chapter 48).

3- **S.E. Fenni**, J. Wang, N. Haddaoui, B.D. Favis, A.J Müller, D. Cavallo (2019) Crystallization and self-nucleation of PLA, PBS and PCL in their immiscible binary and ternary blends. **Accepted in Thermochimica Acta Journal**.

4- **S.E. Fenni**, J. Wang, N. Haddaoui, B.D. Favis, A.J Müller, D. Cavallo. Morphology, nucleation and crystallization behavior of ternary blends based on PLA, PCL, and PBS with partial wetting morphology. **To be submitted soon**.

5- **S.E. Fenni**, O. Monticelli, D. Cavallo, N. Haddaoui. Renewable and toughened poly (L-lactic acid)/polyurethane blend prepared by dynamic vulcanization. **To be submitted soon**.

8.2.2 Communications at Conferences

1- **S.E. Fenni**, D. Cavallo and N. Haddaoui: Morphology and thermal properties of poly(l-lactide)/poly(butylene succinate) bioblend nanocomposites with graphene oxide nano-sheets. *Conférence Internationale sur les Matériaux Polymères et leurs Composites « CIMPC'17 »* (25 – 27 April 2017, University of Tlemcen - Algeria).

2- **S.E. Fenni**, D. Cavallo and N. Haddaoui: Study of the system nanocomposite Bio-blend PLLA / PBS using GO nanofiller: Compatibilization and crystallization behavior. *Ph.D. student Day*, (10 Mai 2017 University of Ferhat Abbes Setif-1 – Algeria).

3- **S.E. Fenni**, N. Haddaoui and D. Cavallo: Relations between morphology and crystallization behavior of poly(l-lactide)/poly(butylene succinate) bioblend nanocomposites with graphene oxide nano-sheets. *International Discussion Meeting on Polymer Crystallization 2017 «IDMPC 2017»* (17 – 20 September 2017, Martin Luther University Halle-Wittenberg – Germany).

4- **S.E. Fenni**, D. Cavallo and N. Haddaoui: Thermal analysis and crystallization behavior of poly(l-lactide)/poly(butylene succinate) / graphene oxide blend nanocomposites. *13th Mediterranean Conference on Calorimetry and Thermal Analysis «Medicta 2017» (*24 - 27 September 2017, Loano – Italy).

5- **S.E. Fenni**, N. Haddaoui, B.D. Favis, A.J Müller, and D. Cavallo: Crystallization behavior of binary and ternary blends based on PLA, PCL, and PBS. *Workshop on Polymer Crystallization*. (03 – 05 September 2018, Genoa, Italy).

Abstract

In this thesis, the morphology, crystallization behavior, thermal and mechanical properties of polymer blends and nanocomposites based on poly(L-lactide) (PLLA) were studied. With the aim of improving PLLA crystallization kinetics and mechanical properties (i.e., reducing PLLA brittleness), novel materials were prepared by the addition of other polymers immiscible with PLLA, or solid phase (nanoparticles).

Bio-based blend nanocomposites of poly(L-lactic acid) (PLLA) and poly(butylene succinate) (PBS), with different concentrations (from 0.1 to 0.5 wt%) of graphene oxide (GO), were prepared via solution dispersion of PBS/GO followed by melt blending with PLLA in a 70/30 PLLA/PBS weight ratio. Scanning and Transmission Electron Microscopy revealed micron-sized droplets of PBS in the PLLA matrix with the nanofillers preferentially found in the PBS phase, at least partially located at the interface with PLLA. The GOs acts as nucleating agent for both semicrystalline polymers. A value of nucleating efficiency (NE) of around 80% is determined for GO towards PBS, among the highest NEs ever reported for this polymer. On the other hand, the efficiency in nucleating PLLA is equal to a modest 15%, also due to the unequal distribution of the nanofiller in the two polymers. A close relationship between the nanocomposite complex morphology and crystallization behavior of the two different polymers is thus established.

A second part of the work, focused on the morphology, nucleation, and crystallization behavior of binary and ternary blends based on triple-crystalline polymers (PLLA, PBS and polycaprolactone (PCL)). Blends were prepared via melt-mixing, and morphological analysis revealed the occurrence of sea-island morphology in all the binary blends, while a "partial wetting" morphology was observed in all ternary blends. This morphology consists of droplets of the minor phase located and self-assembled at the interface between the other two major components. DSC analysis shows the occurrence of some common crystallization phenomena in immiscible polymer blends such us fractionated crystallization and coincident crystallization. DSC heating scans revealed the nucleating effect of crystalline PCL and PBS droplets on PLA from the glassy state during the heating process. PLOM analysis highlighted the existence of interface-induced nucleation phenomena: nucleating effect of (i) molten PCL and PBS on PLA phase and (ii) crystalline PLA on PBS phase were observed. In ternary blends, PCL was found to have a higher nucleating efficiency than PBS towards PLA.

Further investigation of binary and ternary blends based on PLA, PCL, and PBS was performed and the Self-nucleation analysis (SN) was investigated as a third part of the work. SN found to be a good way to induce the crystallization of different polymer and to overcome fractionated crystallization and coincident crystallization. Results from SN allows us to deduce that production of self-nuclei is mainly determined by the melt temperature with only a slight influence of the blend morphology and content of the polymers under study.

In the last part of the work, dynamic vulcanization of fatty acid based polyester polyol with glycerol and PLLA in the presence of hexamethylene diisocyanate (HDI) was performed, with the aim of sustainably toughen PLLA. The dynamic vulcanization took place in a Brabender internal mixer, leading to the formation of a PLLA/PU biobased blend. Melt torque, FTIR, and gel fraction analysis demonstrated the successful formation of vulcanized PU inside the PLLA matrix. SEM analysis shows that the PLLA/PU blends exhibit sea-island morphology. Solubility tests revealed the formation of a rubbery phase, insoluble in chloroform, inside the PLLA matrix. FTIR analysis of the insoluble part shows the appearance of absorption band centred at 1758 cm^{-1} related to the crystalline carbonyl vibration of PLLA units, thus suggesting the partial involvement of the PLLA chains in the reaction. The content of PU in the blends played an important influence on the mechanical properties, thermal stability, and crystallization behaviours of the formed PLLA/PU blends. The overall crystallization rate of PLA was noticeably decreased by incorporation of PU while PLOM analysis revealed that presence of PU network inside PLLA resulted in faster PLLA nucleation. The mechanical properties were enhanced after formation of PU network, leading to higher impact strength and lower Young's modulus. However, the thermal stability of the blends was slightly reduced compared to neat PLLA.

Abstract

In this thesis, the morphology, crystallization behavior, thermal and mechanical properties of polymer blends and nanocomposites based on Poly(L-lactide) (PLLA) were studied. Different multiphasic systems were studied, with the aim of improving PLLA crystallization kinetics and mechanical properties (i.e., reducing the PLLA brittleness). As such, the preparation of the novel material and the effect of the addition of other polymers, immiscible with PLLA, or solid phase (nanoparticles) was studied. Addition of PBS and GO found to have a strong effect on the final morphology and crystallization behavior. Binary and ternary blends revealed the enhanced nucleation and crystallization behavior of PLA by melt blending with small amount of PCL and PBS.

Résumé

Dans cette thèse, la morphologie, le comportement de cristallisation, les propriétés thermiques et mécaniques des mélanges des polymères et des nanocomposites à base de Poly (L-lactide) (PLLA) ont été étudiés. Différents systèmes multiphasiques ont été étudiés dans le but d'améliorer la cinétique de cristallisation du PLLA et ses propriétés mécaniques (c'est-à-dire de réduire la fragilité du PLLA). Ainsi, la préparation du nouveau matériau et l'effet de l'addition d'autres polymères, non miscibles au PLLA, ou des phases solides (nanoparticules) ont été étudiés. L'ajout de PBS et de GO a eu un effet important sur la morphologie finale et le comportement de cristallisation. Les mélanges binaires et ternaires ont révélé le comportement amélioré de la nucléation et de la cristallisation du PLA en mélangeant à l'état fondu avec une petite quantité de PCL et de PBS.

ملخص

في هذه الأطروحة ، تم دراسة مورفولوجيا ، سلوك التبلور ، والخصائص الحرارية والميكانيكية لخلطات البوليمر و المركبات الدقيقة على أساس بولي لكتيك أسيد (PLLA). أنظمة متعددة و مختلفة تمت دراستها بهدف تحسين حركية البلورة PLLA والخصائص الميكانيكية و تقليل هشاشة بولي لكتيك أسيد. على هذا النحو ، تم دراسة إعداد المواد الجديدة وتأثير إضافة البوليمرات الأخرى ، غير قابلة للامتزاج م بولي لكتيك أسيد، أو الصلبة (جسيمات متناهية الصغر). إضافة البولي بوتيلين سوكسينيت وأوكسيد الغرافين، وجدت أن يكون لها تأثير قوي على السلوك مورفولوجيا النهائية و البلورة. كشفت الخلطات الثنائية والثلاثية عن سلوك التنوي والبلورة المحسّن لبولي لكتيك أسيد بخلطه بكمية صغيرة من PCL وPBS.